Investigating the lipid profile of animal-microbe symbioses

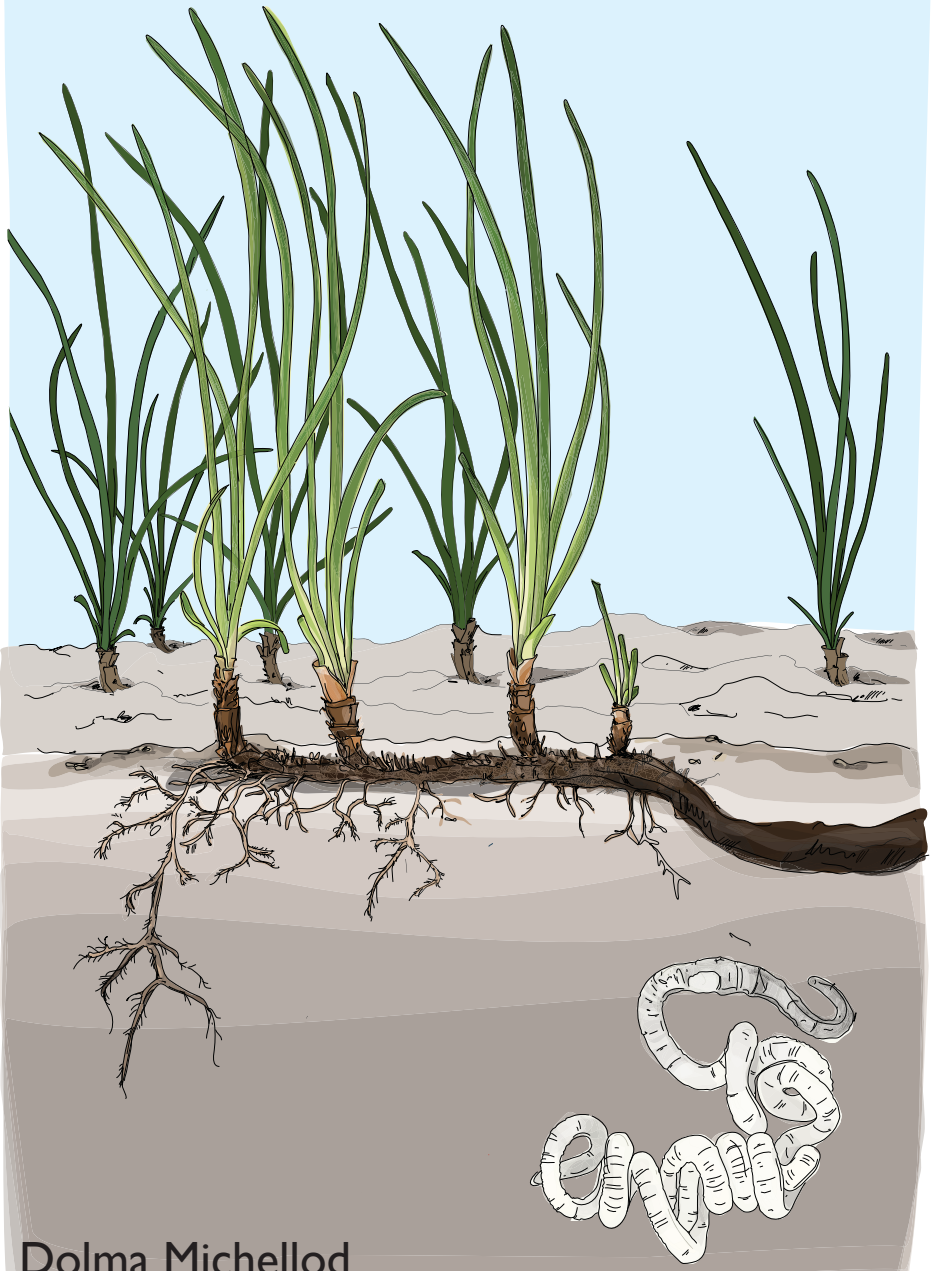

Dolma Michellod

Investigating the lipid profile of animal–microbe symbioses

Dissertation

zu Erlangung des Grades eines

Doktors der Naturwissenschaften

– Dr. rer. nat. –

dem Fachbereich Biologie/Chemie

der Universität Bremen

vorgelegt von

Dolma Michellod

Bremen

Juni 2021

Die Untersuchungen zur vorliegenden Arbeit wurden in der Abteilung Symbiose am Max-Planck-Institut für Marine Mikrobiologie unter der Leitung von Frau Prof. Dr. Nicole Dubilier und Dr. Manuel Liebeke als direktem Betreuer durchgeführt.

The research leading to the work presented in this thesis was conducted at the Max Planck Institute for Marine Microbiology under the direction of Prof. Nicole Dubilier and the direct supervision of Dr. Manuel Liebeke.

Gutachterinnen / Reviewers

Frau Prof. Dr. Nicole Dubilier

Frau Dr. Elizabeth Hambleton

Tag des Promotionskolloquium / Date of the doctoral defense

29th of July 2021

“Science is the belief in the ignorance of the experts”

Richard Feynman

Table of Contents

Summary

Lipids are important and understudied elements of host-bacteria interactions. Lipids play central roles in defining cellular membranes, they have a structural role but also influence the distribution and activity of transporters, enzymes and receptors. Aside of their functions in the membrane, they have important functions as signaling molecules, energy storages, coenzymes or toxins. In pathogenic interactions, lipids have been shown to participate to every stage of the interaction between the host and the bacteria. A few studies have focused on beneficial symbioses and we only start to discover the importance of lipids in those interactions. Much of the functional importance of the rich chemical diversity of lipids remains unknown.

In this study, I aimed to describe the chemical landscape of deep-sea mussels living in close association with chemoautotrophic bacteria (**Chapter I**) and determine the identity, distribution and potential functions of a metabolite group specific to the association between deep-sea mussels and methane-oxidizing symbionts (**Chapter II**). This research was expanded to shallow water symbioses formed by gutless annelids and chemoautotrophic bacteria. The study of their sterol pool revealed a new phytosterol synthesis pathway specific to animals (**Chapter III**).

The aim of my research presented in **Chapter I** was to study the lipid diversity and the impact the association with intracellular bacteria has on the lipid composition of symbiotic and non-symbiotic mussel tissues. The chemical profiles of five deep-sea mussel species were obtained using liquid chromatography tandem mass spectrometry. Molecular networking and similarity analyses were used to describe the chemical diversity present in deep-sea symbiotic mussels and identify compounds linked to the presence of the symbionts. This untargeted approach enabled us to detect and annotate compounds which had not been previously reported in those organisms and identify new groups of unknown compounds specific to the sulfur-oxidizing symbionts.

In **Chapter II**, I studied more in depth a specialized group of metabolites only present in the symbiotic organ and specific to methane-oxidizing bacteria and deep-sea mussel associations. Mass spectrometry enabled us to determine the structure of those specialized metabolites and identified them as a bacterial coenzyme, common in methylotrophic bacteria, as well as the esterified analogues of that coenzyme, described here for the first time. The distribution of those specialized metabolites led us to hypothesize potential functions for them in the symbiosis. The bacterial coenzymes is present in symbiotic and non-symbiotic tissues. This observation led us to speculate that the bacterial coenzyme is utilized by the host as an alternative to an essential coenzyme animals need to obtain from their diet. In an extreme environment as the deep-sea,

where resources are scarce, the host might need to adapt to the resources made available by its symbionts. The esterified analogues of the coenzyme co-localize with the methane-oxidizing symbionts and are likely to still be functional coenzymes. We hypothesized that the fatty acids anchor the coenzyme to the cytoplasmic membrane of the bacteria. It would allow the oxidation of formaldehyde, a toxic intermediate of methane oxidation, to take place at the membrane surface rather than freely diffuse in the cytoplasm. It would represent a new way for the symbiont to counteract the toxicity of formaldehyde.

Chapter III focused on the unusual presence of sitosterol, a plant sterol, in shallow water gutless oligochaetes. The gutless oligochaetes sterol pool is dominated by a plant sterol and not by cholesterol, as in nearly every other animals. A combination of isotopic and omics analyses revealed the ability of gutless oligochaetes to synthesize cholesterol but also sitosterol. It is the first group of animals able to synthesize plant sterol. Transcriptomic analysis revealed the existence of an animal sterol methyltransferase (SMT). This enzyme, widely present in plants and fungi but usually absent from animals, is essential to sitosterol synthesis. We identified SMT homologues in four animal phyla: in gutless oligochaetes as well as in other annelids, in a few rotifers and in one coral species, in addition of the sponges in which they were already described. Using heterologous gene expression and enzyme assay we could show that gutless oligochaetes' SMTs have a sterol methyl transferase activity. We described the first animal sitosterol biosynthesis pathway, which relies on an enzyme previously believed to be lost in animals.

Exploring the diversity and role of lipids in marine chemosymbioses revealed compounds specific to the symbioses which had not previously been described in animals. This study revealed new potential use of bacterial co-enzymes by invertebrate hosts and potential adaptation of the symbionts to burst of high methane concentration. It also revealed a novel animal sitosterol biosynthesis pathway that is unlike the plant pathways and represents a new, catalytically distinct type of SMT. My research identified gutless oligochaetes as an attractive novel system to study the impact of sterol composition on membrane properties in vivo and to expand our understanding of the many role sterols play in eukaryotic cells.

Zusammenfassung

Lipide sind ein wichtiger und wenig erforschter Bestandteil von Wirt-Bakterien-Interaktionen. Sie spielen eine zentrale Rolle in Zellmembranen, wo sie nicht nur strukturgebend sind, sondern auch die Verteilung und Aktivität von Transportern, Enzymen und Rezeptoren beeinflussen. Neben ihren Funktionen in der Membran dienen Lipide unter anderem als Signalmoleküle, Energiespeicher, Coenzyme und Toxine. Bei pathogenen Interaktionen zwischen Wirten und Bakterien ist gezeigt worden, dass Lipide in jeder Phase dieser Interaktion eine Rolle spielen. Bisher haben sich nur wenige Studien auf nutzbringende Symbiosen konzentriert, und wir beginnen erst jetzt, die Rolle von Lipiden in Interaktionen dieser Art zu verstehen. Viele wichtige Funktionen von Lipiden sind auf Grund ihrer großen chemischen Vielfalt weithin unbekannt.

In dieser Studie hatte ich zum Ziel, die Vielfältigkeit und Lokalisation von chemischen Molekülen in Tiefseemuscheln zu beschreiben, die in enger Assoziation mit chemoautotrophen Bakterien leben (**Kapitel I**). Zudem wollte ich die Identität, Verteilung und die potentiellen Funktionen einer Metabolitgruppe bestimmen, die spezifisch für die Assoziation zwischen Tiefseemuscheln und Methan-oxidierenden Symbionten ist (**Kapitel II**). Diese Analysen wurden im Weiteren auf Flachwasser-Symbiosen ausgeweitet, die von darmlosen Anneliden und chemoautotrophen Bakterien gebildet werden. Im Zuge der Untersuchung ihres Sterol-Pools wurde ein Phytosterol-Syntheseweg zum ersten Mal auch in Tieren nachgewiesen (**Kapitel III**).

Das Ziel meiner in **Kapitel I** vorgestellten Forschung war es, die Lipidvielfalt und den Einfluss der Interaktion zwischen Tiefseemuscheln und deren intrazellulären Bakterien auf die Lipidkomposition von symbiotischem und nicht-symbiotischem Muschelgewebe zu untersuchen. Das chemische Profil von fünf Tiefseemuschelarten wurde mittels Flüssigchromatographie-Tandem-Massenspektrometrie ermittelt. Es wurden molekulare Vernetzungs- und Ähnlichkeitsanalysen eingesetzt, um die chemische Vielfalt in den jeweiligen symbiotischen Tiefseemuschelarten zu beschreiben und Moleküle zu identifizieren, die mit den vorhandenen Symbionten zusammenhängen. Durch diese unspezifische Herangehensweise konnten wir Moleküle detektieren, die vorher in diesen Organismen noch nicht gefunden wurden und identifizierten neue Gruppen von bisher unbekannten Molekülen, spezifisch für schwefeloxidierende Symbionten.

In **Kapitel II** habe ich eingehender eine spezialisierte Gruppe von Metaboliten untersucht, die nur in symbiotischen Organen vorkommen und spezifisch für methanoxidierende Bakterien und Tiefseemuschel-Assoziationen sind. Mit Hilfe der Massenspektrometrie konnten wir die Struktur

dieser spezialisierten Metaboliten bestimmen und sie als ein bakterielles Coenzym identifizieren, das häufig in methylotrophen Bakterien vorkommt. Das veresterte Analog dieses Coenzyms wurde hier zum ersten Mal beschrieben. Die Verteilung dieser spezialisierten Metaboliten veranlasste uns zu Hypothesen über mögliche Funktionen in der Symbiose. Aufgrund der Häufigkeit des bakteriellen Coenzyms im Wirtsgewebe stellten wir die Hypothese auf, dass der Wirt dieses bakterielle Coenzym als Alternative zu einem essentiellen Coenzym verwenden könnte, welches Tiere normalerweise aus ihrer Nahrung beziehen müssen. In einer extremen Umgebung wie der Tiefsee, in der Ressourcen knapp sind, muss sich der Wirt möglicherweise an die von seinen Symbionten zur Verfügung gestellten Ressourcen anpassen. Die veresterten Analoga des Coenzyms, die mit den Methan-oxidierenden Symbionten ko-lokalisiert sind, sind wahrscheinlich nach wie vor funktionale Coenzyme. Wir stellten die Hypothese auf, dass die Fettsäure das Coenzym an der zytoplasmatischen Membran der Bakterien verankert. Dies würde es ermöglichen, dass die Oxidation von Formaldehyd, einem toxischen Zwischenprodukt der Methanoxidation, an der Membranoberfläche stattfindet, anstatt frei ins Zytoplasma zu diffundieren. Dies würde eine neue Möglichkeit für den Symbionten darstellen, der Toxizität von Formaldehyd entgegenzuwirken.

Der Fokus von **Kapitel III** war das ungewöhnliche Vorhandensein von Sitosterol, einem Pflanzensterol, in darmlosen Oligochaeten im Flachwasser. Der Sterol-Pool der darmlosen Oligochaeten wird von einem Pflanzensterol dominiert und nicht wie bei fast allen anderen Tieren von Cholesterin. Eine Kombination aus Isotopen- und Omics-Analysen zeigte die Fähigkeit der darmlosen Oligochaeten sowohl Cholesterin, als auch Sitosterin zu synthetisieren. Das macht darmlose Oligochaeten zur ersten Gruppe von Tieren, die in der Lage sind, pflanzliches Sterol zu synthetisieren. Transkriptomische Analysen zeigten die Existenz einer tierischen Sterol-Methyltransferase (SMT). Dieses in Pflanzen und Pilzen weit verbreitete Enzym ist für die Sitosterin-Synthese essentiell, fehlt aber gewöhnlich bei Tieren. Wir identifizierten SMT-Homologe in vier tierischen Phyla: in darmlosen Oligochaeten und anderen Anneliden, in einigen Rädertierchen, in einer Korallenart, sowie in Schwämmen, in denen sie bereits beschrieben wurden. Mittels heterologer Genexpression und Enzymassays konnten wir zeigen, dass die SMT der darmlosen Oligochaeten tatsächlich eine Sterol-Methyltransferase-Aktivität besitzt. Somit konnten wir den ersten tierischen Sitosterol-Biosyntheseweg beschrieben, der auf einem Enzym beruht, von dem man bisher annahm, dass es in Tieren verloren gegangen ist.

Die Erforschung der Diversität und Rolle von Lipiden in marinen Chemosymbiosen offenbarte symbiosespezifische Moleküle, die zuvor nicht in Tieren beschrieben wurden. Diese Studie

enthüllte eine neue potenzielle Nutzung bakterieller Co-Enzyme durch wirbellose Wirte und eine potenzielle Anpassung der Symbionten an plötzliche Anstiege der Methankonzentration. Außerdem wurde ein neuer tierischer Sitosterol-Biosyntheseweg entdeckt, der sich von den pflanzlichen Synthesewegen unterscheidet und einen neuen, katalytisch unterschiedlichen Typ der Sterol-Methyltransferase beinhaltet. Meine Forschung identifizierte darmlose Oligochaeten als ein potentielles Modelsystem um den Einfluss der Sterolzusammensetzung auf Membraneigenschaften *in vivo* zu untersuchen und unser Verständnis für die vielen Rollen, die Sterole in eukaryotischen Zellen spielen, zu erweitern.

Introduction

Introduction

Lipids' structural and functional diversity

Lipids display an incredible structural and functional diversity. A lipid bilayer delimits the cells of all living organisms, regardless of their environment, lifestyle or complexity. This lipid bilayer forms a membrane which serves as interface between the organisms and its environment. We tend to think of the lipid bilayer as an inert barrier forming a matrix for membrane proteins, while we should think of it as a dynamic, ever changing mosaic adapting to the conditions (pH, temperature, pressure) imposed on them by their habitat (Nicolson, 2013; Vereb et al., 2003). While one or two lipid species are enough to create a lipid bilayer *in vitro*, organisms in nature use tens to hundreds of different membrane lipids (Jeucken et al., 2019). One driving force behind lipid diversity is the environment; cells actively modify their lipid composition to protect their membrane integrity in changing environments. Additionally, lipid diversity is constrained by the cell's metabolic capacity to synthesize them and hence lipids are chemical markers that can be used to infer phylogeny. For example, membrane lipids are one of the main molecular features differentiating archaea from bacteria and eukaryotes (Koga, 2014; Koga & Morii, 2007; Sojo, 2019). Membrane lipids can also be used to tease apart plant from fungi and animals as their membranes are dominated by kingdom specific sterols, while bacteria host sterol analogues called hopanoids (Ourisson et al., 1987; Sáenz et al., 2015). However, lipids are not just structural elements of the cellular membrane; they have specific cellular functions for example, lipids are agents of biological information controlling the distribution and activity of transporters, enzymes and receptors (Burger et al., 2000; Paila & Chattopadhyay, 2010) . In addition, they play major roles as energy storages, signaling molecules, coenzymes or toxins to cite a few. Yet, the function of most lipids is hard to study and often remains unknown. Consequently, we still do not understand the biological relevance: how the lipid structural diversity relates to lipid function for the organism?

Why is there such a difference between our understanding of protein function and lipid function? There are several reasons. First, it is almost impossible to predict the

biological function of a lipid from its structure alone. You will find many examples of lipids with different structures which serve similar functions. Second, lipids often provide supporting role to proteins but do not function on their own. It is challenging to experimentally study lipid–protein interactions. Consequently the role of lipids often need to be assessed indirectly. For example, to study the role of cholesterol in cellular processes, membrane are often depleted of cholesterol by using methyl-β-cyclodextrin (Mahammad & Parmryd, 2015). Finally, even though most enzymes involved in lipid metabolic pathways have been identified, lipids cannot be easily manipulated thought mutational analysis. Lipid synthesis depends on metabolic pathways, which involve the step-wise activity of multiple enzymes. In addition, individual enzymes are often involved in the synthesis of multiple lipids. Changing the level of one lipid would require the manipulation of multiple enzymes, while modifying one enzyme could affect multiple lipids.

While the function of many lipids remain unknown we have more information on their molecular **structure**. Structural studies revealed an incredible diversity of lipids ranging from miniscule differences in fatty acid length and saturation to large swaps of entire backbones. Based on their structure, lipids are organized into **eight metabolic classes**: fatty acyls, prenols, glycerophospholipids, sphingolipids, glycerolipids, saccharolipids, sterols and polyketides (***Figure 1***). This classification reflects their biosynthetic pathways rather than their functions.

Fatty acyls and prenols, are hydrophobic molecules which together with small polar molecules such as ribitol, glycerol or oligosaccharides form the building blocks for the synthesis of membrane lipids. **Membrane lipids** include glycerophospholipids, sphingolipids, glycerolipids, saccharolipids and sterols. The last lipid class, the polyketides, are not found in the membrane and are the only lipid class which does not contribute to any constitutive membrane function. **Polyketides** are a diverse class of toxic compounds, which often have defensive roles. Some mimic signaling molecules and inhibit the function of ribosomes while other target the cell membrane (Dmitriev et al., 2020; Il et al., 2009; J. Dutton et al., 1995).

Free fatty acyls and prenols are not just building blocks for membrane lipids, they have functions on their own, inside and outside of the membrane environment. They can anchor proteins and enzymes in cellular membranes. In addition, fatty acyls participate to different signaling processes. As an examples, eicosanoids, derivatives of polyunsaturated fatty acids, function in diverse cellular processes such as: immune response and cell growth (Ferrer & Moreno, 2010; Stanley, 2011; Wang & DuBois, 2010). While prenols serve as precursor to many electron acceptors and coenzymes, critical to cell physiology.

Of all lipids, few play a role as important for the structure and function of the cell as **sterols**, a lipid class derived from prenols. When integrated in the phospholipid bilayer, sterols influence the biophysical properties of biological membranes (Bloch, 1983). They are central to the organization, dynamics, and function of the lipid bilayer. Together with sphingolipids, they are the main components of specialized membrane microdomains known as lipid rafts (Lingwood & Simons, 2010; Silvius, 2003; Sonnino & Prinetti, 2013). Those microdomains are enriched in cholesterol, sphingolipids and specific subsets of proteins involved in signaling and other fundamental cellular processes such as endocytosis, protein sorting and intracellular membrane trafficking. Outside of the membrane, sterols play important roles as precursors for steroid hormones and bile acids (Berg et al., 2002; Edwards & Ericsson, 1999).

Membrane lipids have long been considered only as structural molecules. However, they also act as signaling molecules in many cellular processes and play crucial roles in the regulation of pathogenic interactions. **Glycerophospholipids** for example, are the main structural component of all biological membranes, but also are the precursors of important signaling molecules like inositol triphosphate (IP3), an intracellular second messengers which trigger the activation of various calcium-regulated intracellular signals (Patterson et al., 2004).

Another important class of membrane lipids, especially in plants, are glycerolipids. **Glycerolipids** include membrane glycolipids and triacyglycerols. Glycolipids are major membrane lipids in photosynthetic organisms. In higher plant cells, chloroplast are enriched in glycolipids (Kobayashi, 2016). The second type of glycerolipids,

triacylglycerol, is present in all organisms. It is not integrated into cellular membrane but is used as energy storage often in the form of lipids droplets (Reue, 2011).

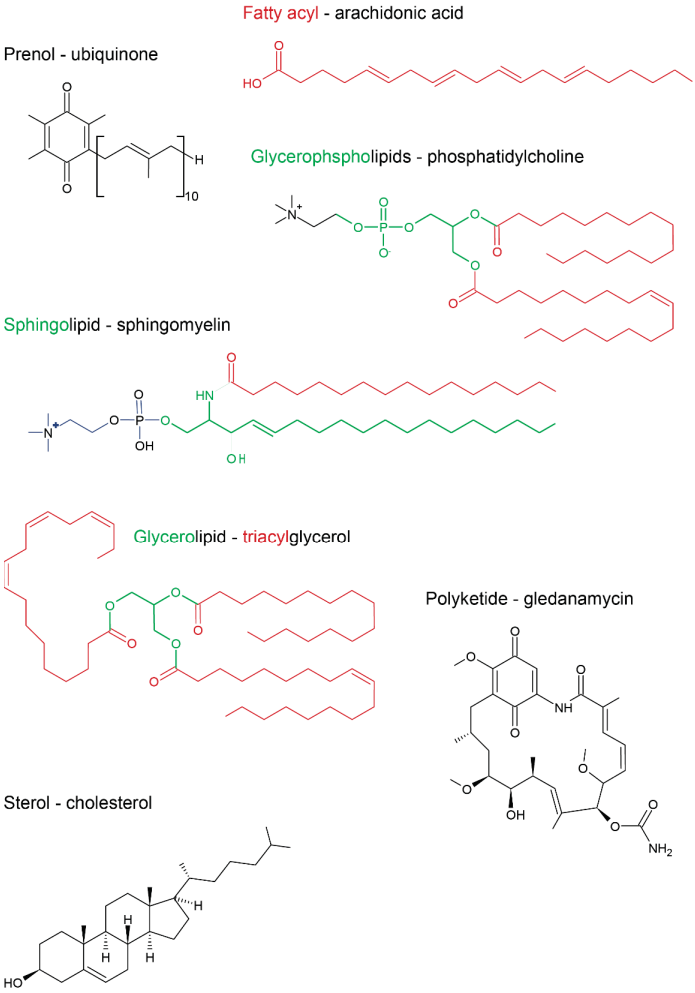

Figure 1 |Structural diversity of the lipid classes. Each class is represented by the structure of a well-known example. The fatty acids serve as building blocks for many membrane lipids and are highlighted in red. The backbones which give their name and usually define a class are highlighted in green. The structure of the eighth class, saccharolipid, is shown in Figure 2.

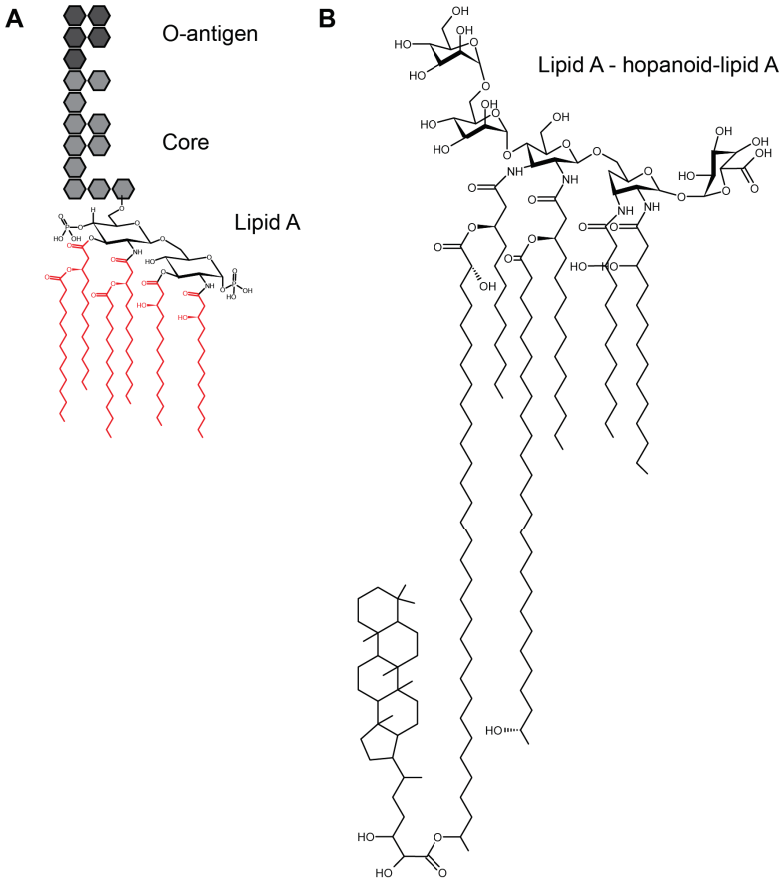

Figure 2 | Lipopolysaccharides, the eight lipid class, are the largest and most complex lipid. A, General structure of a lipopolysaccharide (LPS). LPS are composed of an O-antigen polysaccharide chain, a core oligosaccharide of 10 to 12 sugars and a membrane anchoring lipidA. **B,** An unusual lipid A: hopanoids-lipid A discovered in *Bradyrhizobium spp.* playing a role in the nitrogen-fixing root nodule symbioses (Belin et al., 2018).

Sphingolipids are abundant in the plasma membrane of eukaryotes and are one of the main components of specialized membrane microdomains. In addition, they modulates numerous cellular processes such as growth regulation, apoptosis, autophagy and immune responses (Hannun & Obeid, 2018). Most bacteria are unable to synthesize

sphingolipids but often use them to hijack the cellular machinery of eukaryotic host (Heaver et al., 2018; Heung et al., 2006).

Saccharolipids are present in the outer membrane of most gram-negative bacteria. The most studied saccharolipids are lipopolysaccharides (LPS) (**Figure 2**), they cover approximately 75% of the outer surface of the bacterial cell and thus are responsible for many biological interactions between the bacteria and its environment (Nikaido, 1996). LPS protect the bacteria by reducing the cell permeability and susceptibility to harsh environmental conditions. LPS are also called endotoxin due to their ability to trigger the immune system of the eukaryotic host. While they reflect the genetic lineage of the bacteria, they are highly diverse as a result of the host conditions (Silipo et al., 2010). They determine the specificity of interactions with its host organisms (Silipo et al., 2012).

Bacteria have developed a range of mechanisms to interfere with host lipids and exploit their functional diversity. Lipids are critical players at every stages of host-microbes interactions: recognition, entry, survival, multiplication and dissemination. The different strategies involving lipids used by bacteria in their interactions with eukaryotic host will be discussed in the second part of this introduction in relation to beneficial symbioses.

Interactions between microbes and eukaryotes

Symbiosis describes an intimate and long-lasting association between organisms of different species. Symbiotic associations involve different types of interactions: mutualistic, commensalism, and pathogenic. The symbiotic interaction are often hard to class in one of those three categories as temporal changes in the nature of the relationship and the numbers of partner further complicate the question (Mushegian & Ebert, 2016; Perez-Brocal et al., 2011).

While only a minority of microorganisms are pathogenic to eukaryotes, their impact on human health focused much attention to the identification and characterization of pathogenic interactions between microorganisms and eukaryotes. **The prevalence of non-pathogenic associations and their ecological and evolutionary importance only became apparent later**. Non-pathogenic symbioses are a source of novel

metabolic/physiological capabilities for the eukaryotic host. Nitrogen fixation, chemosynthesis, nitrate respiration and cellulose digestion are examples of novel metabolic capabilities acquired by multiple eukaryotic groups through bacterial symbionts (Brune & Ohkuma, 2011; Dubilier et al., 2008; Graf et al., 2021; Kneip et al., 2007). Those novel capabilities enable the host to adapt to new habitats and lifestyles and often participate to the evolutionary diversification of the host (Douglas, 2014). Beneficial symbiotic associations also have broader consequences and can directly impact ecosystem processes such as nitrogen cycling marine environment (Beinart, 2019; Martínez-Pérez et al., 2016). In addition to the nutritional aspect, symbioses can also impact defensive, reproductive or morphological aspects of the host biology.

Many of the same molecular mechanisms involving lipids underline pathogenic and non-pathogenic interactions. Environmentally acquired symbionts and pathogens overlap in their need to find and colonize specific hosts, and use very similar molecular mechanisms to do so (Gil et al., 2004; Goebel & Gross, 2001; Hentschel et al., 2000). Many of those mechanisms involved lipids which play key role in membrane trafficking, energy storage and cellular signaling: key processes the microbe need to hijack to be successful. As with other aspects of microorganism-eukaryote interactions, most of research focused on the mechanisms behind pathogenic interactions. Here, I will review some of the main roles played by lipids in pathogenic interactions (Allen & Martinez, 2020; Roingeard & Melo, 2017; Toledo & Benach, 2015; Wenk, 2006) and summarizing what is known for beneficial interactions.

Long distance delivery of chemical cues is possible via outer membrane vesicles.

Outer membrane vesicles (OMV) are vesicles of proteins and lipids secreted by gram-negative bacteria. OMVs have a broad range of activities. In pathogenic interactions they contribute to host colonisation, virulence and modulate the host immune system response (Kuehn & Kesty, 2005). Some pathogenic bacteria use OMVs to deliver **virulence effector** to the host cell and initiate the infection without cell-to-cell contact (Bomberger et al., 2009; Crowley et al., 2013; Lindmark et al., 2009). The role of OMV in beneficial interactions has been less well studied (Lynch & Alegado, 2017). OMVs have been proposed to be the main mode of carbon transfer between the host and the symbionts in

a flat worm symbiosis (Jäckle et al., 2019). In addition to their **nutritional role** they could participate to the delivery of chemical cues mediating the interactions between the host and the symbionts.

Host's membrane lipids are ideal targets for bacterial toxins mediating pathogenic and beneficial interactions.

The use of lipid receptors for bacterial toxins was one of the first lipid-mediated interaction studied. The toxins are pore-forming proteins that destabilize the vacuole and host cell membrane. The pore-forming toxins can target different lipid classes — cholesterol and sphingolipid — both lipid classes are usually absent from bacteria and therefor make for an ideal target.

Cholesterol-dependent cytolysins are the largest family of pore-forming toxins and are synthesized by many pathogenic gram-positive bacteria (Gonzalez et al., 2008; Tilley et al., 2005). One example of cholesterol-dependent cytolysins is listeriolysin O, a toxin produced by *Listeria sp.* which targets cholesterol-rich sites. Listeriolsin O, like most cholesterol-dependent cytolysins have several functions: they can participate to cell lysis, colonisation, phagosomal escape and survival by interfering with the host immune response (Gekara et al., 2005; Marriott et al., 2008; Nguyen et al., 2019; Tilley et al., 2005).

Toxin-producing bacteria also target host **sphingolipids**, leading to the modification of the host cytoskeleton and membrane damage. (Becker et al., 2018; Doery et al., 1963; Nagahama et al., 1996; Otto, 2014; Schwan et al., 2011). Other toxins, important for the pathogen's entry into the host cell, interact with both cholesterol and sphingolipids of the lipid rafts (Schraw et al., 2002).

In beneficial interactions, bacterial toxins such as **polyketides**, are usually used as defense mechanisms by the host. Lichen-forming fungi can synthesis a large repertoire of polyketides which protect the symbiosis from predation and parasitism (Stocker-Wörgötter, 2008). The polyketides produced by insect symbionts are also used to deter predators (Piel, 2002) or protect the eggs from fungal infection (Engl et al., 2018). Several marine invertebrates such as corals and sponges also form defensive symbiosis with polyketide-producing microorganism (Beedessee et al., 2019; Storey et al., 2020).

Lipopolysaccharides are a key players in pathogenic and beneficial interactions between bacteria and eukaryotes.

As a major surface component of gram-negative bacteria, LPSs are involved in interactions with the external environment, in particular in many aspects of host–bacterium interactions: recognition, adhesion, colonisation, and virulence (Silipo et al., 2010). LPS also called **endotoxins** are composed of three parts: O-antigen, core, and lipid A. **Lipid A** anchors LPS in the lipid membrane and once dissociated is recognized by the pattern-recognition receptor Toll-like receptor 4 (TLR4) and triggers the activation of the immune system. While the lipid A synthesis pathway is conserved, many bacteria are able to modify the lipid A structure to protect the pathogen from host antibacterial compounds such as cationic antimicrobial peptides or to evade recognition by TLR4 (Alexander & Rietschel, 2001; Trent et al., 2006).

LPS are were not lost in all beneficial symbionts. Many insects endosymbionts lost the enzymes required for lipopolysaccharide synthesis (Wu et al., 2004; Zientz et al., 2004). The author proposed that the establishment of a stable symbiosis required the detoxification of potentially dangerous compounds such as the LPS endotoxins. However, in some beneficial symbioses LPS became part of the cross-talk between host and their beneficial symbionts. A **Lipid A** derived from symbiotic LPS plays a key role in the establishment squid-vibrio symbiosis, participating to the morphogenesis of the light-organ (Koropatnick et al., 2004). At later stage of the symbiosis, the activity of the lipid A is modulated by the expression of a host enzyme (Rader et al., 2012). Interactions with LPS in the mammalian gut are essential not only to prevent infection by pathogenic bacteria but also for control of tissue homeostasis (Rakoff-Nahoum et al., 2004). In nitrogen-fixing root nodule symbioses, the presence of lipid A decorated with hopanoids increase the mechanical strength of the membrane and might play a role in the symbiosis (Belin et al., 2018).

Cholesterol-dependent association with the host membrane is often essential for activation of type three secretion systems (T3SS) and delivery of the virulence factor.

Lipids, especially the microdomains enriched in cholesterol and sphingolipids, play an important role in the delivery of virulence effector inside the host. **T3SS** participate to the

early stage of infection by many gram-negative intracellular pathogens (Tsai et al., 2019). T3SS are responsible for the translocation of effectors inside the host cell. The bacterial effectors activate cell-signaling cascades promoting the internalization and survival of the pathogen (Pinaud et al., 2018; Tosi et al., 2013). **Cholesterol**-rich sites serve as target for the T3SS and are central to the pathogen-host cross talk (Hayward et al., 2005; Kayath et al., 2010; van der Goot et al., 2004).

Genetic analyses of obligatory insect endosymbionts which underwent a dramatic genome size reduction reveal that they maintain genes encoding factors that are proposed to be virulence associated in pathogenic bacteria such as **T3SS** (Dale et al., 2001; Ffrench-Constant et al., 2000; Maezawa et al., 2006; Shigenobu et al., 2000). *Buchnersa aphidicola* encode and express a functional flagellar T3SS but no effector has been identified and the function of the T3SS in the symbiosis remain unknown (Maezawa et al., 2006; Schepers et al., 2021; G. M. Young et al., 1999). In the tse-tse fly endosymbionts, T3SS is proposed to participate to the entry of the symbionts in the host cell (Dale et al., 2002). In pathogenic bacteria, interactions of transcolon proteins with cholesterol-rich micro-domains are often necessary to trigger the T3SS and mediate infections (McShan & De Guzman, 2015). At the moment the importance of cholesterol for T3SS mediated-interactions in non-pathogenic symbioses is unknown.

Symbionts divert host second messenger to their own advantage.

Pathogens have evolved ingenious strategies to subvert the metabolism of lipids derived second messengers to affect the uptake process, interfere with the phagosomal maturation process and prevent host cell apoptosis (Grassmé & Becker, 2013; Hanada, 2005; S. A. Young et al., 2012) **Sphingolipid signaling** is a key signaling pathway in eukaryotic cells. Most viruses and bacteria cannot synthesize sphingolipids but many pathogenic bacteria are able to utilize or degrade eukaryotic sphingolipids to promote their virulence (Grassmé & Becker, 2013; Rolando & Buchrieser, 2019). Pathogenic bacteria use host sphingolipids during multiple steps of the infection process. One example is *M. tuberculosis* which block the calcium-signaling leading to phagosome maturation by inhibiting the synthesis of one sphingolipid (Malik et al., 2003). This strategy ensure the survival of the pathogen.

By acting as **apoptosis inhibitor**, sphingolipids signaling seems to play a regulatory role in coral symbiosis and in symbiont recognition in the early stages of the symbiosis (Kitchen et al., 2017). *Bacteriodetes* account for 30-40% of the gut microbiome and are one of the rare bacteria phylum able to synthesize sphingolipids (Heaver et al., 2018, 2018; Kato et al., 1995). The molecular signaling mediated by *Bacteriodetes*' sphingolipids is essential for their survival as well as the maintenance of the tissue homeostasis and symbiosis in the gut (An et al., 2011, 2014; Brown et al., 2019; Johnson et al., 2020).

The nutritional role of lipids in eukaryote-bacteria interactions

In order to thrive inside the host tissues, pathogens can use different host lipids as energy and carbon sources. They are often able to catabolize multiple carbon sources such as cholesterol, fatty acids from membrane lipids, sphingolipids and triacylglycerols (L. P. S. de Carvalho et al., 2010; Mali & Meena, 2018). *Mycobacterium tuberculosis,* for example, can use cholesterol as sole carbon source (Geize et al., 2007; Nesbitt et al., 2010). *M. tuberculosis* even develop different strategies to metabolize propionyl-coenzyme A, a toxic byproduct of cholesterol degradation, and use it as an energy source or as building block for cell synthesis (Griffin et al., 2012; Russell et al., 2010; Savvi et al., 2008).

Lipids play a key roles in arbuscular mycorrhizal symbiosis. Lipid transfer from plant to the arbuscular mycorrhizal fungi is essential for the establishment and the stability of the association (Feng et al., 2020). The fungi cannot synthesis lipid *de novo* and rely in transfer of lipids from the plant host for its nutrition (Jiang et al., 2017; Keymer et al., 2017). In *Drosophila melanogaster* symbiosis, endosymbionts proliferation is limited by the availability of host diacylglycerides (Herren et al., 2014). Lipids also play a role in energy and carbon exchange between anemone and its algal symbionts, the energy is stored and transferred under the form of lipid droplets (Kellogg & Patton, 1983). In coral-algal symbioses, sterol transfer participate to carbon acquisition. It allows the host, which cannot synthesis sterol *de novo*, to adapt to various ecological niches by efficiently exploiting limited resources (Hambleton et al., 2019). Sterols also play a key role in insect-fungi symbioses as insects cannot synthesize sterols de novo and rely on their symbionts as source of sterols (Six, 2012).

There are many unanswered questions on the role lipids are playing in the non-pathogenic symbioses (**Table 1**). It is no known yet if and how non-pathogenic bacteria modulate the membrane lipid of the host and if they exploit lipid rafts during the establishment of the symbiosis. The importance of lipid mimicry in beneficial interactions has not been studied neither.

Most of the lipid studies on non-pathogenic systems focused on terrestrial organisms: human microbiomes, plant, insect and lichen symbioses. The studies dedicated to marine interactions were limited to photosynthetic symbioses and very little attention was given to marine chemosynthetic interactions.

Marine Chemosynthetic Symbioses

Chemosynthetic symbioses were discovered at hydrothermal vent in the 1970s, since then many new associations were identified covering a wide range of habitats, host taxa, symbiont phylotypes and types of symbiotic interactions (Dubilier et al., 2008). Many invertebrates and some protist form a close, often obligatory nutritional symbiosis with chemosynthetic bacteria. The chemosynthetic symbionts are able to synthesize complex organic molecule from inorganic carbon by using chemical energy. Chemosynthetic symbionts can harvest chemical energy from wide range of energy source: reduced sulfur compounds, methane, hydrogen and carbon monoxide. The symbionts provide the host with new metabolic capabilities which enable the animal to access new ecological niches.

In this thesis we studied the lipids profile of on two beneficial marine chemosynthetic symbioses: deep-sea mussels and gutless oligochaetes.

Deep sea mussels

Deep-sea mussels (*Mytilidae, Bathymodiolinae*) inhabiting hydrothermal vents and cold seeps, form symbiotic association with chemosynthetic bacteria (reviewed in (Duperron, 2010). Deep-sea mussels of the family *Bathymodiolinae* are associated with gammaproteobacterial sulfur-oxidizing (SOX), methane-oxidizing (MOX) symbionts, or both (Duperron, 2010). The symbionts largely reside in specialized epithelial gill cells called bacteriocytes (**Figure 3**). They are intracellular symbionts and sit in vacuoles in the

cytosol of the bacteriocyte cells. The chemosynthetic symbionts enable the host to thrive in the nutrient-poor habitat of the deep sea. The symbionts of deep-sea mussel are acquired from the environment during the early developmental stages of the mussel (Franke et al., 2020; Wentrup et al., 2013).

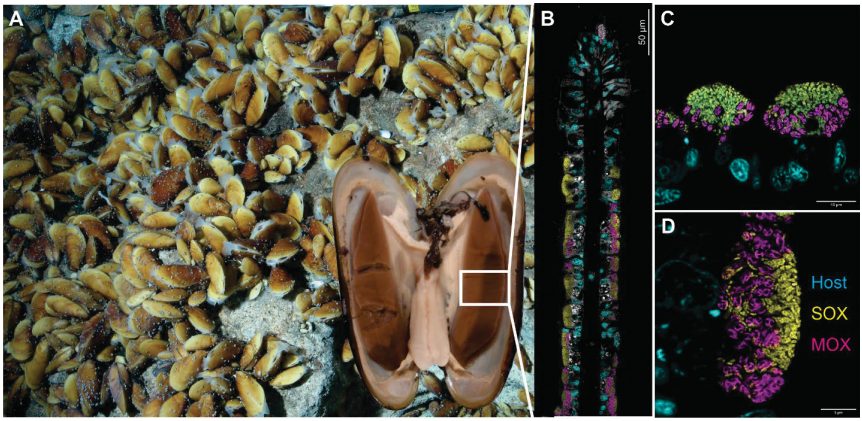

Figure 3 | Association with chemosynthetic bacteria enabled mussels to colonize deep-sea habitats. A, Deep-sea mussels thrive at hydrothermal vents and cold seeps; image courtesy of Marum. **B,** This is possible thanks to chemosynthetic symbionts, a methane-oxidizing (MOX) and a sulfur-oxidizing (SOX) bacteria, the mussels host in their gills. The FISH images show the distribution of SOX (in yellow) and MOX (in magenta) in a gill filament. The host nuclei is shown in cyan; image courtesy of M. Franke. **C and D,** The symbionts reside in specialized epithelial cells called bacteriocytes; images courtesy of M. Franke.

Interactions between bacteria and eukaryotes are mediated by chemical cues. Lipids are a good candidate for such chemical cues in deep-sea mussel symbiosis. They are involved in recognition, colonisation, long term maintenance of the interaction and nutritional exchanges. All those aspects are essential to the to the deep-sea mussel symbiosis: the juvenile host acquire its symbionts from the environment, internalized them by membrane rearrangements and form a nutritional symbiosis. Those processes suggest that the host and the symbionts developed a chemical language to recognize and interact with each other. Lipids are likely to be part of that language and to have play a role in the adaptation of the host to its unique lifestyle.

A few studies focused on the lipids in deep-sea mussels. A molecular isotopic study was conducted on three species of chemosynthetic mussels (Kellermann et al., 2012). They gave an overview of the fatty acids, membrane lipids and hopanoids composition of the

mussels and suggested lipids which could be used as symbionts biomarkers. A more recent study combined metabolic imaging and fluorescence in situ hybridization (FISH) microscopy to study the impact of the intracellular symbionts on the metabolites profile of the gill cells (Geier et al., 2020). We discovered a group of specialized metabolites at the host-microbe interface. The structural identity and function of those specialized metabolites is unknown.

Gutless oligochaetes

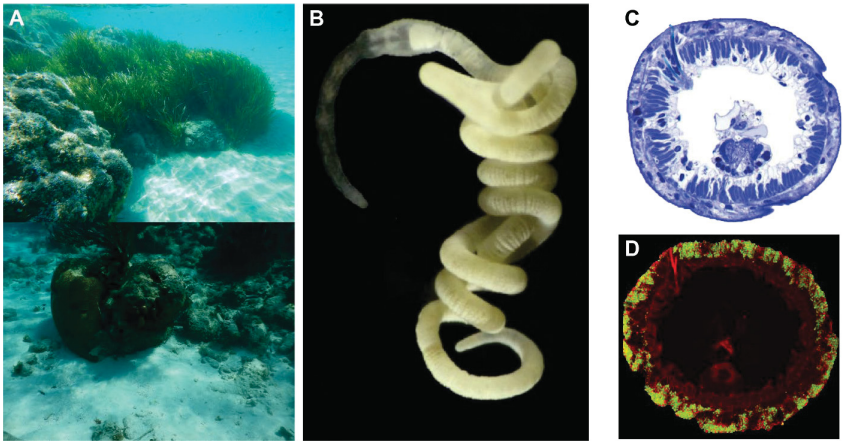

Figure 4 | Gutless oligochaetes live in shallow water sediment and gain their nutrition thanks to a thick coat of symbiotic bacteria sitting between their cuticule and epidermis. A, Gutless oligochaetes are often found at shallow water site in the vicinity of seagrass beds or coral reefs. **B,** Gutless oligochates are small marine annelids easily identified by their bright white color; image courtesy of A. Gruhl **C,** Toluene blue staining of a cross section of *O. algarvensis.* Gutless oligoachetes lack a digestive system; image courtesy of A. Gruhl. **D,** Cross section of *O. algarvensis* stained with fluorescent probes targeting the symbionts: gammaproteobacteria (green) and deltaproteobacteria (red). The image show the location of the dense bacterial layer between the epidermis and the cuticle; Adapted from *(Dubilier et al., 2001)*.

Gutless oligochaetes (**Figure 4**) are small marine annelids (0.1-0.2 mm × 20–40 mm) living in the interstitial pore water of marine sediments. They occur throughout the world in many tropical and subtropical sediments, where they are a significant part of the marine meiofauna (Dubilier et al., 2006). The highest diversity of gutless oligochaete species is found in warm shallow water coastal sediments.

Gutless oligochaetes form a monophyletic group within the Phallodrilinae (Clitellata) family (Nylander et al., 1999). The 100 species described so far belonged to two sister

genera *Olavius* and *Inanidrilus* (Erseus, 1984). Gutless oligochaetes are characterized by the absence of digestive tract and excretory organs, and by the thick multicellular layer of bacterial symbionts they host between their cuticle and epidermis (Giere, 1981). The bacterial symbionts are chemosynthetic providing the host with nutrition and participate to the recycling of host waste products (Kleiner et al., 2012; Woyke et al., 2006). The symbionts represent ~25% of the worm biomass (Giere et al., 1995). The host gain most if not all of his nutrition through its symbionts: together they form an obligate nutritional symbiosis. The symbionts are ingested by the host through phagocytic activity of the epidermal cells (Giere et al., 1995). The high percentage (8%-24%) of the bacterial cells in the process of being digested highlight the importance of symbiont lysis in the nutrition of the host (Giere et al., 1995). They The symbionts belongs to 33 different symbionts clades (Mankowski et al., 2021). The bacteria are extracellular endosymbionts, they sit between extensions of the epidermal cells under the cuticle of the host. The unusually thin cuticle of the worm is permeable to compounds as large as 70 kDa and allows the worm and the bacteria to access substrates and dissolved organic compounds present in the pore water (Dubilier et al., 2006; Giere et al., 1995).

Many aspects of the gutless oligochaete symbiosis were investigated in the last decades and we now have a good overview of the taxonomic and functional diversity of the symbiosis, the host and symbionts physiology as well as the interplay between the different partners. However, little is known on the lipid profile of those organisms or the role lipids might play in the host-symbionts interactions. Preliminary results showed that the sterol profile of *Olavius algarvensis* is dominated by sitosterol. This observation is very unusual, sitosterol is a plant sterol and the animal sterol profiles are usually dominated by cholesterol. The origin of the sitosterol in the worm is unclear as animal and bacteria are not able to synthesize plant stero

Table 1 | Processes mediated by lipids in symbiotic interactions

Mechanism	Role in beneficial interactions	References	Role in pathogenic interactions	References
Lipid-dependent toxins	Unknown		Colonisation Survival Phagosomal and/or cell Escape	(Becker et al., 2018; Doery et al., 1963; Gekara et al., 2005; Marriott et al., 2008; Nagahama et al., 1996; Nguyen et al., 2019; Otto, 2014; Schraw et al., 2002; Schwan et al., 2011; Tilley et al., 2005)
Lipid toxins (Polyketides)	Defense against predation and parasitism	(Beedessee et al., 2019; Engl et al., 2018; Piel, 2002; Stocker-Wörgötter, 2008; Storey et al., 2020)	Unknown	
Lipopolysaccharides	Establishment of the symbiosis Tissue homeostasis Maintenance of the association	(Belin et al., 2018; Koropatnick et al., 2004; Rakoff-Nahoum et al., 2004)	Recognition Adhesion Colonisation Virulence	Reviewed in: (Silipo et al., 2010; Steimle et al., 2016; Trent et al., 2006)
T3SS	Colonisation? Unknown	(Dale et al., 2001, 2002; Ffrench-Constant et al., 2000; Maezawa et al., 2006;	Colonisation Survival	(Hayward et al., 2005; Kayath et al., 2010; Pinaud et al.,

		Schepers et al., 2021; Shigenobu et al., 2000; G. M. Young et al., 1999)	Virulence	2018; Tosi et al., 2013; van der Goot et al., 2004)
Sphingolipid signaling	Symbiont recognition Survival Tissue homoeostasis Maintenance of the symbiosis	(An et al., 2011, 2014; Brown et al., 2019; Johnson et al., 2020; Kitchen et al., 2017)	Colonisation Phagosomal maturation Prevent host cell apoptosis Virulence	Reviewed in : (Grassmé & Becker, 2013; Hanada, 2005; Rolando & Buchrieser, 2019; S. A. Young et al., 2012)
Carbon and Energy transfer	Establishment of the symbiosis Stability of the symbiosis Proliferation control Sterol source C and E exchange	(Feng et al., 2020; Hambleton et al., 2019; Herren et al., 2014; Jiang et al., 2017; Kellogg & Patton, 1983; Keymer et al., 2017; Six, 2012)	Host lipid as carbon and/or energy source	(M. Carvalho et al., 2010; Geize et al., 2007; Griffin et al., 2012; Mali & Meena, 2018; Nesbitt et al., 2010; Russell et al., 2010; Savvi et al., 2008)
Lipid rafts hijacking	Unknown		Toxin binding Adhesion Entry	Reviewed in (Bagam et al., 2017; Bukrinsky et al., 2020; Mañes et al., 2003; van der Meer-Janssen et al., 2010)

			Phagosomal maturation Intracellular survival Signaling	
Lipid mimicry	Unknown		Resistance against defense mechanisms Evade recognition Entry	(Estabrook, Griffiss, and Jarvis 1997; Moran and Prendergast 2001; Moran 2008; Mercer and Helenius 2008; Amara and Mercer 2015)
Modification of the lipid membrane of the host	Unknown		Colonisation Survival Virulence C and E source Dispersion	(Chimalapati et al., 2020; Dorrell et al., 1999; Flieger et al., 2004; Hybiske & Stephens, 2008; Koo et al., 2007; O'Brien & Melville, 2004; Sitkiewicz et al., 2006, 2007; Walker et al., 2001)
Modification of the cholesterol homeostasis	Unknown		Survival and replication C and E source	(Gilk, 2012; Howe & Heinzen, 2006; Korhonen et al., 2013; Lin & Rikihisa, 2003; Samanta et al., 2017; Xiong et al., 2009)

Aims of this thesis

Little is known on the lipid composition of chemosynthetic symbiosis. Over the last decades evidence accumulated on the crucial roles lipids play in cell physiology. They were revealed to have diverse functions ranging from structural components of membrane to cell signaling molecules, energy storages, cell defenses and coenzymes. Despite their biological relevance, the study of lipids is still in its infancy and while their role in diseases and pathogenic infections has been well studied, less attention has been paid to their role in beneficial interactions. Evidence that lipids are also important player in beneficial interactions is accumulating and was briefly reviewed in the first part of this introduction. The aim of my thesis was to describe the lipid landscape present in deep-sea mussels and investigate the identity, origin and function of specialized lipids found in deep-sea mussels and gutless oligochaetes.

Investigation of the lipids landscape in deep-sea mussel symbiosis

Before looking at the role specific lipids species might play in symbiotic interactions it is important to have an overview of the lipid landscape of the system. The aim of this first chapter was to determine the general lipid composition of different species of deep-sea mussels using a state of the art ultra-high performance liquid chromatography tandem mass spectrometry (UHPLC-MS/MS) approach. Spectral library searches and unsupervised substructure predictions were used to unveil the identity of the lipids detected in this study. Comparisons between mussel species harboring different set of symbionts and between symbiotic and non-symbiotic tissues were performed to identify new compounds potentially involved in the cross-talk between the host and symbionts.

Structural identification of specialized metabolites at the host-microbe interface

A recent study combining metabolic imaging and fluorescence in situ hybridization (FISH) microscopy identified a new group of unknown metabolites at the host-symbiont interface in the gills of *Bathymodiolus puteoserpentis* (Geier et al., 2020). The aim of this chapter were to (1) resolve the structure of those compounds, (2) assess their prevalence and diversity in different species of deep-sea mussels and (3) infer their potential function in the symbiosis. I used a combination of mass spectrometry approaches to study their

identity, presence, diversity and distribution within the mussels. Based on their distribution in the host tissues, I hypothesized potential roles for those compounds in the host and in the symbionts.

Investigating the presence and the origin of sitosterol in gutless oligochaetes

In this chapter I studied the unusual presence of the phytosterol sitosterol in gutless oligochaetes. Unlike most animals, the sterol composition of *Olavius algarvensis* is dominated by sitosterol. I investigated the sterol composition of different species of gutless oligochaetes to confirm this first observation. I then set to identify the origin of sitosterol in gutless oligochaetes using combination of omics and isotopic analyses. This led to the discovery of an enzyme widespread in plant and fungi but described for the first time in eumetazoans. The activity of this enzyme was tested by heterologous gene expression and enzymatic assay. The results of those analyses are summarized in Chapter 3.

References

Alexander, C., & Rietschel, E. Th. (2001). Invited review: Bacterial lipopolysaccharides and innate immunity. *Journal of Endotoxin Research*, *7*(3), 167–202. https://doi.org/10.1177/09680519010070030101

Allen, P. E., & Martinez, J. J. (2020). Modulation of Host Lipid Pathways by Pathogenic Intracellular Bacteria. *Pathogens*, *9*(8), 614. https://doi.org/10.3390/pathogens9080614

Amara, A., & Mercer, J. (2015). Viral apoptotic mimicry. *Nature Reviews Microbiology*, *13*(8), 461–469. https://doi.org/10.1038/nrmicro3469

An, D., Na, C., Bielawski, J., Hannun, Y. A., & Kasper, D. L. (2011). Membrane sphingolipids as essential molecular signals for Bacteroides survival in the intestine. *Proceedings of the National Academy of Sciences*, *108*(Supplement 1), 4666–4671. https://doi.org/10.1073/pnas.1001501107

An, D., Oh, S. F., Olszak, T., Neves, J. F., Avci, F. Y., Erturk-Hasdemir, D., Lu, X., Zeissig, S., Blumberg, R. S., & Kasper, D. L. (2014). Sphingolipids from a Symbiotic Microbe Regulate Homeostasis of Host Intestinal Natural Killer T Cells. *Cell*, *156*(1), 123–133. https://doi.org/10.1016/j.cell.2013.11.042

Bagam, P., Singh, D. P., Inda, M. E., & Batra, S. (2017). Unraveling the role of membrane microdomains during microbial infections. *Cell Biology and Toxicology*, *33*(5), 429–455. https://doi.org/10.1007/s10565-017-9386-9

Becker, K. A., Fahsel, B., Kemper, H., Mayeres, J., Li, C., Wilker, B., Keitsch, S., Soddemann, M., Sehl, C., Kohnen, M., Edwards, M. J., Grassmé, H., Caldwell, C. C., Seitz, A., Fraunholz, M., & Gulbins, E. (2018). Staphylococcus aureus Alpha-Toxin Disrupts Endothelial-Cell Tight Junctions via Acid Sphingomyelinase and Ceramide. *Infection and Immunity*, *86*(1). https://doi.org/10.1128/IAI.00606-17

Beedessee, G., Hisata, K., Roy, M. C., Van Dolah, F. M., Satoh, N., & Shoguchi, E. (2019). Diversified secondary metabolite biosynthesis gene repertoire revealed in symbiotic dinoflagellates. *Scientific Reports*, *9*(1), 1204. https://doi.org/10.1038/s41598-018-37792-0

Beinart, R. A. (2019). The Significance of Microbial Symbionts in Ecosystem Processes. *MSystems*, *4*(3), Article 3. https://doi.org/10.1128/mSystems.00127-19

Belin, B. J., Busset, N., Giraud, E., Molinaro, A., Silipo, A., & Newman, D. K. (2018). Hopanoid lipids: From membranes to plant–bacteria interactions. *Nature Reviews. Microbiology*, *16*(5), 304–315. https://doi.org/10.1038/nrmicro.2017.173

Berg, J. M., Tymoczko, J. L., & Stryer, L. (2002). Important Derivatives of Cholesterol Include Bile Salts and Steroid Hormones. *Biochemistry. 5th Edition*. https://www.ncbi.nlm.nih.gov/books/NBK22339/

Bloch, K. E. (1983). Sterol structure and membrane function. *CRC Critical Reviews in Biochemistry*, *14*(1), 47–92. https://doi.org/10.3109/10409238309102790

Bomberger, J. M., MacEachran, D. P., Coutermarsh, B. A., Ye, S., O'Toole, G. A., & Stanton, B. A. (2009). Long-Distance Delivery of Bacterial Virulence Factors by Pseudomonas aeruginosa Outer Membrane Vesicles. *PLOS Pathogens*, *5*(4), e1000382. https://doi.org/10.1371/journal.ppat.1000382

Brown, E. M., Ke, X., Hitchcock, D., Jeanfavre, S., Avila-Pacheco, J., Nakata, T., Arthur, T. D., Fornelos, N., Heim, C., Franzosa, E. A., Watson, N., Huttenhower, C., Haiser, H. J., Dillow, G., Graham, D. B., Finlay, B. B., Kostic, A. D., Porter, J. A., Vlamakis, H., … Xavier, R. J. (2019). Bacteroides-Derived Sphingolipids Are Critical for Maintaining Intestinal Homeostasis and Symbiosis. *Cell Host & Microbe*, *25*(5), 668-680.e7. https://doi.org/10.1016/j.chom.2019.04.002

Brune, A., & Ohkuma, M. (2011). Role of the Termite Gut Microbiota in Symbiotic Digestion. In D. E. Bignell, Y. Roisin, & N. Lo (Eds.), *Biology of Termites: A Modern Synthesis* (pp. 439–475). Springer Netherlands. https://doi.org/10.1007/978-90-481-3977-4_16

Bukrinsky, M. I., Mukhamedova, N., & Sviridov, D. (2020). Lipid rafts and pathogens: The art of deception and exploitation: Thematic Review Series: Biology of Lipid Rafts. *Journal of Lipid Research*, *61*(5), 601–610. https://doi.org/10.1194/jlr.TR119000391

Burger, K., Gimpl, G., & Fahrenholz, F. (2000). Regulation of receptor function by cholesterol. *Cellular and Molecular Life Sciences: CMLS*, *57*(11), 1577–1592. https://doi.org/10.1007/pl00000643

Carvalho, M., Schwudke, D., Sampaio, J. L., Palm, W., Riezman, I., Dey, G., Gupta, G. D., Mayor, S., Riezman, H., Shevchenko, A., Kurzchalia, T. V., & Eaton, S. (2010). Survival strategies of a sterol auxotroph. *Development*, *137*(21), 3675–3685. https://doi.org/10.1242/dev.044560

Chimalapati, S., de Souza Santos, M., Lafrance, A. E., Ray, A., Lee, W.-R., Rivera-Cancel, G., Vale, G., Pawlowski, K., Mitsche, M. A., McDonald, J. G., Liou, J., & Orth, K. (2020). Vibrio deploys type 2 secreted lipase to esterify cholesterol with host fatty acids and mediate cell egress. *ELife*, *9*, e58057. https://doi.org/10.7554/eLife.58057

Crowley, J. T., Toledo, A. M., LaRocca, T. J., Coleman, J. L., London, E., & Benach, J. L. (2013). Lipid Exchange between Borrelia burgdorferi and Host Cells. *PLOS Pathogens*, *9*(1), e1003109. https://doi.org/10.1371/journal.ppat.1003109

Dale, C., Plague, G. R., Wang, B., Ochman, H., & Moran, N. A. (2002). Type III secretion systems and the evolution of mutualistic endosymbiosis. *Proceedings of the National Academy of Sciences*, *99*(19), 12397–12402. https://doi.org/10.1073/pnas.182213299

Dale, C., Young, S. A., Haydon, D. T., & Welburn, S. C. (2001). The insect endosymbiont Sodalis glossinidius utilizes a type III secretion system for cell invasion. *Proceedings of the National Academy of Sciences*, *98*(4), 1883–1888. https://doi.org/10.1073/pnas.98.4.1883

de Carvalho, L. P. S., Fischer, S. M., Marrero, J., Nathan, C., Ehrt, S., & Rhee, K. Y. (2010). Metabolomics of Mycobacterium tuberculosis Reveals Compartmentalized Co-Catabolism of Carbon Substrates. *Chemistry & Biology*, *17*(10), 1122–1131. https://doi.org/10.1016/j.chembiol.2010.08.009

Dmitriev, S. E., Vladimirov, D. O., & Lashkevich, K. A. (2020). A Quick Guide to Small-Molecule Inhibitors of Eukaryotic Protein Synthesis. *Biochemistry (Moscow)*, *85*(11), 1389–1421. https://doi.org/10.1134/S0006297920110097

Doery, H. M., Magnusson, B. J., Cheyne, I. M., & Gulasekharam, J. (1963). A Phospholipase in Staphylococcal Toxin which hydrolyses Sphingomyelin. *Nature*, *198*(4885), 1091–1092. https://doi.org/10.1038/1981091a0

Dorrell, N., Martino, M. C., Stabler, R. A., Ward, S. J., Zhang, Z. W., McColm, A. A., Farthing, M. J. G., & Wren, B. W. (1999). Characterization of Helicobacter pylori PldA, a phospholipase with a role in colonization of the gastric mucosa. *Gastroenterology*, *117*(5), 1098–1104. https://doi.org/10.1016/S0016-5085(99)70394-X

Douglas, A. E. (2014). The Molecular Basis of Bacterial–Insect Symbiosis. *Journal of Molecular Biology*, *426*(23), 3830–3837. https://doi.org/10.1016/j.jmb.2014.04.005

Dubilier, N., Bergin, C., & Lott, C. (2008). Symbiotic diversity in marine animals: The art of harnessing chemosynthesis. *Nature Reviews Microbiology*, *6*(10), 725–740. https://doi.org/10.1038/nrmicro1992

Dubilier, N., Blazejak, A., & Rühland, C. (2006). Symbioses between Bacteria and Gutless Marine Oligochaetes. In J. Overmann (Ed.), *Molecular Basis of Symbiosis* (pp. 251–275). Springer. https://doi.org/10.1007/3-540-28221-1_12

Dubilier, N., Mulders, C., Ferdelman, T., de Beer, D., Pernthaler, A., Klein, M., Wagner, M., Erseus, C., Thiermann, F., Krieger, J., Giere, O., & Amann, R. (2001). Endosymbiotic sulphate-reducing and

sulphide-oxidizing bacteria in an oligochaete worm. *Nature*, *411*(6835), 298–302. https://doi.org/10.1038/35077067

Duperron, S. (2010). The Diversity of Deep-Sea Mussels and Their Bacterial Symbioses. In S. Kiel (Ed.), *The Vent and Seep Biota: Aspects from Microbes to Ecosystems* (pp. 137–167). Springer Netherlands. https://doi.org/10.1007/978-90-481-9572-5_6

Edwards, P. A., & Ericsson, J. (1999). Sterols and Isoprenoids: Signaling Molecules Derived from the Cholesterol Biosynthetic Pathway. *Annual Review of Biochemistry*, *68*(1), 157–185. https://doi.org/10.1146/annurev.biochem.68.1.157

Engl, T., Kroiss, J., Kai, M., Nechitaylo, T. Y., Svatoš, A., & Kaltenpoth, M. (2018). Evolutionary stability of antibiotic protection in a defensive symbiosis. *Proceedings of the National Academy of Sciences*, *115*(9), E2020–E2029. https://doi.org/10.1073/pnas.1719797115

Erseus, C. (1984). Taxonomy and Phylogeny of the Gutless Phallodrilinae (Oligochaeta, Tubificidae), with Descriptions of One New Genus and 22 New Species. *Zoologica Scripta*, *13*(4), 239–272. https://doi.org/10.1111/j.1463-6409.1984.tb00041.x

Estabrook, M. M., Griffiss, J. M., & Jarvis, G. A. (1997). Sialylation of Neisseria meningitidis lipooligosaccharide inhibits serum bactericidal activity by masking lacto-N-neotetraose. *Infection and Immunity*, *65*(11), 4436–4444.

Feng, Z., Liu, X., Zhu, H., & Yao, Q. (2020). Responses of Arbuscular Mycorrhizal Symbiosis to Abiotic Stress: A Lipid-Centric Perspective. *Frontiers in Plant Science*, *11*. https://doi.org/10.3389/fpls.2020.578919

Ferrer, R., & Moreno, J. J. (2010). Role of eicosanoids on intestinal epithelial homeostasis. *Biochemical Pharmacology*, *80*(4), 431–438. https://doi.org/10.1016/j.bcp.2010.04.033

Ffrench-Constant, R. H., Waterfield, N., Burland, V., Perna, N. T., Daborn, P. J., Bowen, D., & Blattner, F. R. (2000). A Genomic Sample Sequence of the Entomopathogenic Bacterium Photorhabdus luminescens W14: Potential Implications for Virulence. *Applied and Environmental Microbiology*, *66*(8), 3310–3329. https://doi.org/10.1128/AEM.66.8.3310-3329.2000

Flieger, A., Rydzewski, K., Banerji, S., Broich, M., & Heuner, K. (2004). Cloning and Characterization of the Gene Encoding the Major Cell-Associated Phospholipase A of Legionella pneumophila, plaB, Exhibiting Hemolytic Activity. *Infection and Immunity*, *72*(5), 2648–2658. https://doi.org/10.1128/IAI.72.5.2648-2658.2004

Franke, M., Geier, B., Hammel, J. U., Dubilier, N., & Leisch, N. (2020). Becoming symbiotic – the symbiont acquisition and the early development of bathymodiolin mussels. *BioRxiv*, 2020.10.09.333211. https://doi.org/10.1101/2020.10.09.333211

Geier, B., Sogin, E. M., Michellod, D., Janda, M., Kompauer, M., Spengler, B., Dubilier, N., & Liebeke, M. (2020). Spatial metabolomics of in situ host–microbe interactions at the micrometre scale. *Nature Microbiology*, *5*(3), 498–510. https://doi.org/10.1038/s41564-019-0664-6

Geize, R. V. der, Yam, K., Heuser, T., Wilbrink, M. H., Hara, H., Anderton, M. C., Sim, E., Dijkhuizen, L., Davies, J. E., Mohn, W. W., & Eltis, L. D. (2007). A gene cluster encoding cholesterol catabolism in a soil actinomycete provides insight into Mycobacterium tuberculosis survival in macrophages. *Proceedings of the National Academy of Sciences*, *104*(6), 1947–1952. https://doi.org/10.1073/pnas.0605728104

Gekara, N. O., Jacobs, T., Chakraborty, T., & Weiss, S. (2005). The cholesterol-dependent cytolysin listeriolysin O aggregates rafts via oligomerization. *Cellular Microbiology*, *7*(9), 1345–1356. https://doi.org/10.1111/j.1462-5822.2005.00561.x

Giere, O. (1981). The Gutless Marine Oligochaete Phallodrilus-Leukodermatus—Structural Studies on an Aberrant Tubificid Associated with Bacteria. *Marine Ecology Progress Series*, *5*(3), 353–357. https://doi.org/10.3354/Meps005353

Giere, O., Nieser, C., Windoffer, R., & Erseus, C. (1995). A Comparative Structural Study on Bacterial Symbioses of Caribbean Gutless Tubificidae (Annelida, Oligochaeta). *Acta Zoologica*, *76*(4), 281–290.

Gil, R., Latorre, A., & Moya, A. (2004). Bacterial endosymbionts of insects: Insights from comparative genomics. *Environmental Microbiology*, *6*(11), 1109–1122. https://doi.org/10.1111/j.1462-2920.2004.00691.x

Gilk, S. D. (2012). Role of Lipids in Coxiella burnetii Infection. In R. Toman, R. A. Heinzen, J. E. Samuel, & J.-L. Mege (Eds.), *Coxiella burnetii: Recent Advances and New Perspectives in Research of the Q Fever Bacterium* (pp. 199–213). Springer Netherlands. https://doi.org/10.1007/978-94-007-4315-1_10

Goebel, W., & Gross, R. (2001). Intracellular survival strategies of mutualistic and parasitic prokaryotes. *Trends in Microbiology*, *9*(6), 267–273. https://doi.org/10.1016/S0966-842X(01)02040-6

Gonzalez, M. R., Bischofberger, M., Pernot, L., van der Goot, F. G., & Frêche, B. (2008). Bacterial pore-forming toxins: The (w)hole story? *Cellular and Molecular Life Sciences*, *65*(3), 493–507. https://doi.org/10.1007/s00018-007-7434-y

Graf, J. S., Schorn, S., Kitzinger, K., Ahmerkamp, S., Woehle, C., Huettel, B., Schubert, C. J., Kuypers, M. M. M., & Milucka, J. (2021). Anaerobic endosymbiont generates energy for ciliate host by denitrification. *Nature*, *591*(7850), 445–450. https://doi.org/10.1038/s41586-021-03297-6

Grassmé, H., & Becker, K. A. (2013). Bacterial Infections and Ceramide. In E. Gulbins & I. Petrache (Eds.), *Sphingolipids in Disease* (pp. 305–320). Springer. https://doi.org/10.1007/978-3-7091-1511-4_15

Griffin, J. E., Pandey, A. K., Gilmore, S. A., Mizrahi, V., Mckinney, J. D., Bertozzi, C. R., & Sassetti, C. M. (2012). Cholesterol Catabolism by Mycobacterium tuberculosis Requires Transcriptional and Metabolic Adaptations. *Chemistry & Biology*, *19*(2), 218–227. https://doi.org/10.1016/j.chembiol.2011.12.016

Hambleton, E. A., Jones, V. A. S., Maegele, I., Kvaskoff, D., Sachsenheimer, T., & Guse, A. (2019). Sterol transfer by atypical cholesterol-binding NPC2 proteins in coral-algal symbiosis. *ELife*, *8*, e43923. https://doi.org/10.7554/eLife.43923

Hanada, K. (2005). Sphingolipids in infectious diseases. *Japanese Journal of Infectious Diseases*, *58*(3), 131–148.

Hannun, Y. A., & Obeid, L. M. (2018). Sphingolipids and their metabolism in physiology and disease. *Nature Reviews Molecular Cell Biology*, *19*(3), 175–191. https://doi.org/10.1038/nrm.2017.107

Hayward, R. D., Cain, R. J., McGhie, E. J., Phillips, N., Garner, M. J., & Koronakis, V. (2005). Cholesterol binding by the bacterial type III translocon is essential for virulence effector delivery into mammalian cells. *Molecular Microbiology*, *56*(3), 590–603. https://doi.org/10.1111/j.1365-2958.2005.04568.x

Heaver, S. L., Johnson, E. L., & Ley, R. E. (2018). Sphingolipids in host-microbial interactions. *Current Opinion in Microbiology*, *43*, 92–99. https://doi.org/10.1016/j.mib.2017.12.011

Hentschel, U., Steinert, M., & Hacker, J. (2000). Common molecular mechanisms of symbiosis and pathogenesis. *Trends in Microbiology*, *8*(5), 226–231. https://doi.org/10.1016/S0966-842X(00)01758-3

Herren, J. K., Paredes, J. C., Schüpfer, F., Arafah, K., Bulet, P., & Lemaitre, B. (2014). Insect endosymbiont proliferation is limited by lipid availability. *ELife*, *3*, e02964. https://doi.org/10.7554/eLife.02964

Heung, L. J., Luberto, C., & Poeta, M. D. (2006). Role of Sphingolipids in Microbial Pathogenesis. *Infection and Immunity*, *74*(1), 28–39. https://doi.org/10.1128/IAI.74.1.28-39.2006

Howe, D., & Heinzen, R. A. (2006). Coxiella burnetii inhabits a cholesterol-rich vacuole and influences cellular cholesterol metabolism. *Cellular Microbiology*, *8*(3), 496–507. https://doi.org/10.1111/j.1462-5822.2005.00641.x

Hybiske, K., & Stephens, R. S. (2008). Exit strategies of intracellular pathogens. *Nature Reviews Microbiology*, *6*(2), 99–110. https://doi.org/10.1038/nrmicro1821

II, D. A. K., Meujo, D. A., & Hamann, M. T. (2009). Polyether ionophores: Broad-spectrum and promising biologically active molecules for the control of drug-resistant bacteria and parasites. *Expert Opinion on Drug Discovery*, *4*(2), 109–146. https://doi.org/10.1517/17460440802661443

Jäckle, O., Seah, B. K. B., Tietjen, M., Leisch, N., Liebeke, M., Kleiner, M., Berg, J. S., & Gruber-Vodicka, H. R. (2019). Chemosynthetic symbiont with a drastically reduced genome serves as primary energy storage in the marine flatworm Paracatenula. *Proceedings of the National Academy of Sciences of the United States of America*, *116*(17), 8505–8514. https://doi.org/10.1073/pnas.1818995116

J. Dutton, C., J. Banks, B., & B. Cooper, C. (1995). Polyether ionophores. *Natural Product Reports*, *12*(2), 165–181. https://doi.org/10.1039/NP9951200165

Jeucken, A., Molenaar, M. R., van de Lest, C. H. A., Jansen, J. W. A., Helms, J. B., & Brouwers, J. F. (2019). A Comprehensive Functional Characterization of Escherichia coli Lipid Genes. *Cell Reports*, *27*(5), 1597-1606.e2. https://doi.org/10.1016/j.celrep.2019.04.018

Jiang, Y., Wang, W., Xie, Q., Liu, N., Liu, L., Wang, D., Zhang, X., Yang, C., Chen, X., Tang, D., & Wang, E. (2017). Plants transfer lipids to sustain colonization by mutualistic mycorrhizal and parasitic fungi. *Science*, *356*(6343), 1172–1175. https://doi.org/10.1126/science.aam9970

Johnson, E. L., Heaver, S. L., Waters, J. L., Kim, B. I., Bretin, A., Goodman, A. L., Gewirtz, A. T., Worgall, T. S., & Ley, R. E. (2020). Sphingolipids produced by gut bacteria enter host metabolic pathways impacting ceramide levels. *Nature Communications*, *11*(1), 2471. https://doi.org/10.1038/s41467-020-16274-w

Kato, M., Muto, Y., Tanaka-Bandoh, K., Watanabe, K., & Ueno, K. (1995). Sphingolipid Composition in Bacteroides Species. *Anaerobe*, *1*(2), 135–139. https://doi.org/10.1006/anae.1995.1009

Kayath, C. A., Hussey, S., El hajjami, N., Nagra, K., Philpott, D., & Allaoui, A. (2010). Escape of intracellular Shigella from autophagy requires binding to cholesterol through the type III effector, IcsB. *Microbes and Infection*, *12*(12), 956–966. https://doi.org/10.1016/j.micinf.2010.06.006

Kellermann, M. Y., Schubotz, F., Elvert, M., Lipp, J. S., Birgel, D., Prieto-Mollar, X., Dubilier, N., & Hinrichs, K.-U. (2012). Symbiont–host relationships in chemosynthetic mussels: A comprehensive lipid biomarker study. *Organic Geochemistry*, *43*, 112–124. https://doi.org/10.1016/j.orggeochem.2011.10.005

Kellogg, R. B., & Patton, J. S. (1983). Lipid droplets, medium of energy exchange in the symbiotic anemone Condylactis gigantea: A model coral polyp. *Marine Biology*, *75*(2), 137–149. https://doi.org/10.1007/BF00405996

Keymer, A., Pimprikar, P., Wewer, V., Huber, C., Brands, M., Bucerius, S. L., Delaux, P.-M., Klingl, V., Röpenack-Lahaye, E. von, Wang, T. L., Eisenreich, W., Dörmann, P., Parniske, M., & Gutjahr, C. (2017). Lipid transfer from plants to arbuscular mycorrhiza fungi. *ELife*, *6*, e29107. https://doi.org/10.7554/eLife.29107

Kitchen, S. A., Poole, A. Z., & Weis, V. M. (2017). Sphingolipid Metabolism of a Sea Anemone Is Altered by the Presence of Dinoflagellate Symbionts. *The Biological Bulletin*, *233*(3), 242–254. https://doi.org/10.1086/695846

Kleiner, M., Wentrup, C., Lott, C., Teeling, H., Wetzel, S., Young, J., Chang, Y.-J., Shah, M., VerBerkmoes, N. C., Zarzycki, J., Fuchs, G., Markert, S., Hempel, K., Voigt, B., Becher, D., Liebeke, M., Lalk, M., Albrecht, D., Hecker, M., … Dubilier, N. (2012). Metaproteomics of a gutless marine worm and its symbiotic microbial community reveal unusual pathways for carbon and energy use. *Proceedings of the National Academy of Sciences*, *109*(19), E1173–E1182. https://doi.org/10.1073/pnas.1121198109

Kneip, C., Lockhart, P., Voß, C., & Maier, U.-G. (2007). Nitrogen fixation in eukaryotes – New models for symbiosis. *BMC Evolutionary Biology*, *7*(1), 55. https://doi.org/10.1186/1471-2148-7-55

Kobayashi, K. (2016). Role of membrane glycerolipids in photosynthesis, thylakoid biogenesis and chloroplast development. *Journal of Plant Research*, *129*(4), 565–580. https://doi.org/10.1007/s10265-016-0827-y

Koga, Y. (2014). From Promiscuity to the Lipid Divide: On the Evolution of Distinct Membranes in Archaea and Bacteria. *Journal of Molecular Evolution*, *78*(3), 234–242. https://doi.org/10.1007/s00239-014-9613-4

Koga, Y., & Morii, H. (2007). Biosynthesis of Ether-Type Polar Lipids in Archaea and Evolutionary Considerations. *Microbiology and Molecular Biology Reviews*, *71*(1), 97–120. https://doi.org/10.1128/MMBR.00033-06

Koo, B.-S., Lee, J.-H., Kim, S.-C., Yoon, H.-Y., Kim, K.-A., Kwon, K.-B., Kim, H.-R., Park, J.-W., & Park, B.-H. (2007). Phospholipase A as a potent virulence factor of Vibrio vulnificus. *International Journal of Molecular Medicine*, *20*(6), 913–918. https://doi.org/10.3892/ijmm.20.6.913

Korhonen, J. T., Olkkonen, V. M., Lahesmaa, R., & Puolakkainen, M. (2013). ABC-cassette transporter 1 (ABCA1) expression in epithelial cells in Chlamydia pneumoniae infection. *Microbial Pathogenesis*, *61–62*, 57–61. https://doi.org/10.1016/j.micpath.2013.05.006

Koropatnick, T. A., Engle, J. T., Apicella, M. A., Stabb, E. V., Goldman, W. E., & McFall-Ngai, M. J. (2004). Microbial Factor-Mediated Development in a Host-Bacterial Mutualism. *Science*, *306*(5699), 1186–1188. https://doi.org/10.1126/science.1102218

Kuehn, M. J., & Kesty, N. C. (2005). Bacterial outer membrane vesicles and the host–pathogen interaction. *Genes & Development*, *19*(22), 2645–2655. https://doi.org/10.1101/gad.1299905

Lin, M., & Rikihisa, Y. (2003). Ehrlichia chaffeensis and Anaplasma phagocytophilum Lack Genes for Lipid A Biosynthesis and Incorporate Cholesterol for Their Survival. *Infection and Immunity*, *71*(9), 5324–5331. https://doi.org/10.1128/IAI.71.9.5324-5331.2003

Lindmark, B., Rompikuntal, P. K., Vaitkevicius, K., Song, T., Mizunoe, Y., Uhlin, B. E., Guerry, P., & Wai, S. N. (2009). Outer membrane vesicle-mediated release of cytolethal distending toxin (CDT) from Campylobacter jejuni. *BMC Microbiology*, *9*(1), 220. https://doi.org/10.1186/1471-2180-9-220

Lingwood, D., & Simons, K. (2010). Lipid Rafts As a Membrane-Organizing Principle. *Science*, *327*(5961), 46–50. https://doi.org/10.1126/science.1174621

Lynch, J. B., & Alegado, R. A. (2017). Spheres of Hope, Packets of Doom: The Good and Bad of Outer Membrane Vesicles in Interspecies and Ecological Dynamics. *Journal of Bacteriology*, *199*(15). https://doi.org/10.1128/JB.00012-17

Maezawa, K., Shigenobu, S., Taniguchi, H., Kubo, T., Aizawa, S., & Morioka, M. (2006). Hundreds of Flagellar Basal Bodies Cover the Cell Surface of the Endosymbiotic Bacterium Buchnera aphidicola sp. Strain APS. *Journal of Bacteriology*, *188*(18), 6539–6543. https://doi.org/10.1128/JB.00561-06

Mahammad, S., & Parmryd, I. (2015). Cholesterol depletion using methyl-β-cyclodextrin. *Methods in Molecular Biology (Clifton, N.J.)*, *1232*, 91–102. https://doi.org/10.1007/978-1-4939-1752-5_8

Mali, P. C., & Meena, L. S. (2018). Triacylglycerol: Nourishing molecule in endurance of Mycobacterium tuberculosis. *Journal of Biosciences*, *43*(1), 149–154. https://doi.org/10.1007/s12038-018-9729-6

Malik, Z. A., Thompson, C. R., Hashimi, S., Porter, B., Iyer, S. S., & Kusner, D. J. (2003). Cutting Edge: Mycobacterium tuberculosis Blocks Ca2+ Signaling and Phagosome Maturation in Human Macrophages Via Specific Inhibition of Sphingosine Kinase. *The Journal of Immunology*, *170*(6), 2811–2815. https://doi.org/10.4049/jimmunol.170.6.2811

Mañes, S., del Real, G., & Martínez-A, C. (2003). Pathogens: Raft hijackers. *Nature Reviews Immunology*, *3*(7), 557–568. https://doi.org/10.1038/nri1129

Mankowski, A., Kleiner, M., Erséus, C., Leisch, N., Sato, Y., Volland, J.-M., Hüttel, B., Wentrup, C., Woyke, T., Wippler, J., Dubilier, N., & Gruber-Vodicka, H. (2021). Highly variable fidelity drives symbiont

community composition in an obligate symbiosis. *BioRxiv*, 2021.04.28.441735. https://doi.org/10.1101/2021.04.28.441735

Marriott, H., Mitchell, T., & Dockrell, D. (2008). Pneumolysin: A Double-Edged Sword During the Host-Pathogen Interaction. *Current Molecular Medicine*, *8*, 497–509. https://doi.org/10.2174/156652408785747924

Martínez-Pérez, C., Mohr, W., Löscher, C. R., Dekaezemacker, J., Littmann, S., Yilmaz, P., Lehnen, N., Fuchs, B. M., Lavik, G., Schmitz, R. A., LaRoche, J., & Kuypers, M. M. M. (2016). The small unicellular diazotrophic symbiont, UCYN-A, is a key player in the marine nitrogen cycle. *Nature Microbiology*, *1*(11), 1–7. https://doi.org/10.1038/nmicrobiol.2016.163

McShan, A. C., & De Guzman, R. N. (2015). The Bacterial Type III Secretion System as a Target for Developing New Antibiotics. *Chemical Biology & Drug Design*, *85*(1), 30–42. https://doi.org/10.1111/cbdd.12422

Mercer, J., & Helenius, A. (2008). Vaccinia Virus Uses Macropinocytosis and Apoptotic Mimicry to Enter Host Cells. *Science*, *320*(5875), 531–535. https://doi.org/10.1126/science.1155164

Moran, A. P, & Prendergast, M. M. (2001). Molecular Mimicry in Campylobacter jejuni and Helicobacter pylori Lipopolysaccharides: Contribution of Gastrointestinal Infections to Autoimmunity. *Journal of Autoimmunity*, *16*(3), 241–256. https://doi.org/10.1006/jaut.2000.0490

Moran, Anthony P. (2008). Relevance of fucosylation and Lewis antigen expression in the bacterial gastroduodenal pathogen Helicobacter pylori. *Carbohydrate Research*, *343*(12), 1952–1965. https://doi.org/10.1016/j.carres.2007.12.012

Mushegian, A. A., & Ebert, D. (2016). Rethinking "mutualism" in diverse host-symbiont communities. *BioEssays*, *38*(1), 100–108. https://doi.org/10.1002/bies.201500074

Nagahama, M., Michiue, K., & Sakurai, J. (1996). Membrane-damaging action of Clostridium perfringens alpha-toxin on phospholipid liposomes. *Biochimica et Biophysica Acta (BBA) - Biomembranes*, *1280*(1), 120–126. https://doi.org/10.1016/0005-2736(95)00288-X

Nesbitt, N. M., Yang, X., Fontán, P., Kolesnikova, I., Smith, I., Sampson, N. S., & Dubnau, E. (2010). A Thiolase of Mycobacterium tuberculosis Is Required for Virulence and Production of Androstenedione and Androstadienedione from Cholesterol. *Infection and Immunity*, *78*(1), 275–282. https://doi.org/10.1128/IAI.00893-09

Nguyen, B. N., Peterson, B. N., & Portnoy, D. A. (2019). Listeriolysin O: A phagosome-specific cytolysin revisited. *Cellular Microbiology*, *21*(3), e12988. https://doi.org/10.1111/cmi.12988

Nicolson, G. L. (2013). Update of the 1972 Singer-Nicolson Fluid-Mosaic Model of Membrane Structure. *Discoveries (Craiova, Romania)*, *1*(1), e3. https://doi.org/10.15190/d.2013.3

Nikaido, H. (1996). Outer membrane. *Escherichia Coli and Salmonella. Cellular and Molecular Biology*, 29–47.

Nylander, J. A. A., Erseus, C., & Kallersjo, M. (1999). A test of monophyly of the gutless Phallodrilinae (Oligochaeta, Tubificidae) and the use of a 573-bp region of the mitochondrial cytochrome oxidase I gene in analysis of annelid phylogeny. *Zoologica Scripta*, *28*(3–4), 305–313. https://doi.org/10.1046/j.1463-6409.1999.00001.x

O'Brien, D. K., & Melville, S. B. (2004). Effects of Clostridium perfringens alpha-toxin (PLC) and perfringolysin O (PFO) on cytotoxicity to macrophages, on escape from the phagosomes of macrophages, and on persistence of C. perfringens in host tissues. *Infection and Immunity*, *72*(9), 5204–5215. https://doi.org/10.1128/IAI.72.9.5204-5215.2004

Otto, M. (2014). Staphylococcus aureus toxins. *Current Opinion in Microbiology*, *17*, 32–37. https://doi.org/10.1016/j.mib.2013.11.004

Ourisson, G., Rohmer, M., & Poralla, K. (1987). Prokaryotic hopanoids and other polyterpenoid sterol surrogates. *Annual Review of Microbiology*, *41*, 301–333. https://doi.org/10.1146/annurev.mi.41.100187.001505

Paila, Y. D., & Chattopadhyay, A. (2010). Membrane cholesterol in the function and organization of G-protein coupled receptors. *Sub-Cellular Biochemistry*, *51*, 439–466. https://doi.org/10.1007/978-90-481-8622-8_16

Patterson, R. L., Boehning, D., & Snyder, S. H. (2004). Inositol 1,4,5-Trisphosphate Receptors as Signal Integrators. *Annual Review of Biochemistry*, *73*(1), 437–465. https://doi.org/10.1146/annurev.biochem.73.071403.161303

Perez-Brocal, V., Latorre, A., & Moya, A. (2011). Symbionts and Pathogens: What is the Difference? *Current Topics in Microbiology and Immunology*, *358*. https://doi.org/10.1007/82_2011_190

Piel, J. (2002). A polyketide synthase-peptide synthetase gene cluster from an uncultured bacterial symbiont of Paederus beetles. *Proceedings of the National Academy of Sciences*, *99*(22), 14002–14007. https://doi.org/10.1073/pnas.222481399

Pinaud, L., Sansonetti, P. J., & Phalipon, A. (2018). Host Cell Targeting by Enteropathogenic Bacteria T3SS Effectors. *Trends in Microbiology*, *26*(4), 266–283. https://doi.org/10.1016/j.tim.2018.01.010

Rader, B. A., Kremer, N., Apicella, M. A., Goldman, W. E., & McFall-Ngai, M. J. (2012). Modulation of Symbiont Lipid A Signaling by Host Alkaline Phosphatases in the Squid-Vibrio Symbiosis. *MBio*, *3*(3). https://doi.org/10.1128/mBio.00093-12

Rakoff-Nahoum, S., Paglino, J., Eslami-Varzaneh, F., Edberg, S., & Medzhitov, R. (2004). Recognition of Commensal Microflora by Toll-Like Receptors Is Required for Intestinal Homeostasis. *Cell*, *118*(2), 229–241. https://doi.org/10.1016/j.cell.2004.07.002

Reue, K. (2011). A Thematic Review Series: Lipid droplet storage and metabolism: from yeast to man. *Journal of Lipid Research*, *52*(11), 1865–1868. https://doi.org/10.1194/jlr.E020602

Roingeard, P., & Melo, R. C. N. (2017). Lipid droplet hijacking by intracellular pathogens. *Cellular Microbiology*, *19*(1). https://doi.org/10.1111/cmi.12688

Rolando, M., & Buchrieser, C. (2019). A Comprehensive Review on the Manipulation of the Sphingolipid Pathway by Pathogenic Bacteria. *Frontiers in Cell and Developmental Biology*, *7*. https://doi.org/10.3389/fcell.2019.00168

Russell, D. G., VanderVen, B. C., Lee, W., Abramovitch, R. B., Kim, M., Homolka, S., Niemann, S., & Rohde, K. H. (2010). Mycobacterium tuberculosis Wears What It Eats. *Cell Host & Microbe*, *8*(1), 68–76. https://doi.org/10.1016/j.chom.2010.06.002

Sáenz, J. P., Grosser, D., Bradley, A. S., Lagny, T. J., Lavrynenko, O., Broda, M., & Simons, K. (2015). Hopanoids as functional analogues of cholesterol in bacterial membranes. *Proceedings of the National Academy of Sciences*, *112*(38), 11971–11976. https://doi.org/10.1073/pnas.1515607112

Samanta, D., Mulye, M., Clemente, T. M., Justis, A. V., & Gilk, S. D. (2017). Manipulation of Host Cholesterol by Obligate Intracellular Bacteria. *Frontiers in Cellular and Infection Microbiology*, *7*. https://doi.org/10.3389/fcimb.2017.00165

Savvi, S., Warner, D. F., Kana, B. D., McKinney, J. D., Mizrahi, V., & Dawes, S. S. (2008). Functional Characterization of a Vitamin B12-Dependent Methylmalonyl Pathway in Mycobacterium tuberculosis: Implications for Propionate Metabolism during Growth on Fatty Acids. *Journal of Bacteriology*, *190*(11), 3886–3895. https://doi.org/10.1128/JB.01767-07

Schepers, M. J., Yelland, J. N., Moran, N. A., & Taylor, D. W. (2021). Isolation of the Buchnera aphidicola flagellum basal body complexes from the Buchnera membrane. *PLOS ONE*, *16*(5), e0245710. https://doi.org/10.1371/journal.pone.0245710

Schraw, W., Li, Y., McClain, M. S., van der Goot, F. G., & Cover, T. L. (2002). Association of Helicobacter pylori Vacuolating Toxin (VacA) with Lipid Rafts*. *Journal of Biological Chemistry*, *277*(37), 34642–34650. https://doi.org/10.1074/jbc.M203466200

Schwan, C., Nölke, T., Kruppke, A. S., Schubert, D. M., Lang, A. E., & Aktories, K. (2011). Cholesterol- and Sphingolipid-rich Microdomains Are Essential for Microtubule-based Membrane Protrusions

Induced by Clostridium difficile Transferase (CDT)*. *Journal of Biological Chemistry*, *286*(33), 29356–29365. https://doi.org/10.1074/jbc.M111.261925

Shigenobu, S., Watanabe, H., Hattori, M., Sakaki, Y., & Ishikawa, H. (2000). Genome sequence of the endocellular bacterial symbiont of aphids Buchnera sp. APS. *Nature*, *407*(6800), 81–86. https://doi.org/10.1038/35024074

Silipo, A., De Castro, C., Lanzetta, R., Parrilli, M., & Molinaro, A. (2010). Lipopolysaccharides. In H. König, H. Claus, & A. Varma (Eds.), *Prokaryotic Cell Wall Compounds: Structure and Biochemistry* (pp. 133–153). Springer. https://doi.org/10.1007/978-3-642-05062-6_4

Silipo, A., Leone, M. R., Lanzetta, R., Parrilli, M., Lackner, G., Busch, B., Hertweck, C., & Molinaro, A. (2012). Structural characterization of two lipopolysaccharide O-antigens produced by the endofungal bacterium Burkholderia sp. HKI-402 (B4). *Carbohydrate Research*, *347*(1), 95–98. https://doi.org/10.1016/j.carres.2011.10.038

Silvius, J. R. (2003). Role of cholesterol in lipid raft formation: Lessons from lipid model systems. *Biochimica et Biophysica Acta (BBA) - Biomembranes*, *1610*(2), 174–183. https://doi.org/10.1016/S0005-2736(03)00016-6

Sitkiewicz, I., Nagiec, M. J., Sumby, P., Butler, S. D., Cywes-Bentley, C., & Musser, J. M. (2006). Emergence of a bacterial clone with enhanced virulence by acquisition of a phage encoding a secreted phospholipase A2. *Proceedings of the National Academy of Sciences*, *103*(43), 16009–16014. https://doi.org/10.1073/pnas.0607669103

Sitkiewicz, I., Stockbauer, K. E., & Musser, J. M. (2007). Secreted bacterial phospholipase A2 enzymes: Better living through phospholipolysis. *Trends in Microbiology*, *15*(2), 63–69. https://doi.org/10.1016/j.tim.2006.12.003

Six, D. L. (2012). Ecological and Evolutionary Determinants of Bark Beetle—Fungus Symbioses. *Insects*, *3*(1), 339–366. https://doi.org/10.3390/insects3010339

Sojo, V. (2019). Why the Lipid Divide? Membrane Proteins as Drivers of the Split between the Lipids of the Three Domains of Life. *BioEssays*, *41*(5), 1800251. https://doi.org/10.1002/bies.201800251

Sonnino, S., & Prinetti, A. (2013). Membrane Domains and the "Lipid Raft" Concept. *Current Medicinal Chemistry*, *20*(1), 4–21.

Stanley, D. (2011). Eicosanoids: Progress towards manipulating insect immunity. *Journal of Applied Entomology*, *135*(7), 534–545. https://doi.org/10.1111/j.1439-0418.2010.01612.x

Steimle, A., Autenrieth, I. B., & Frick, J.-S. (2016). Structure and function: Lipid A modifications in commensals and pathogens. *International Journal of Medical Microbiology*, *306*(5), 290–301. https://doi.org/10.1016/j.ijmm.2016.03.001

Stocker-Wörgötter, E. (2008). Metabolic diversity of lichen-forming ascomycetous fungi: Culturing, polyketide and shikimate metabolite production, and PKS genes. *Natural Product Reports*, *25*(1), 188–200. https://doi.org/10.1039/B606983P

Storey, M. A., Andreassend, S. K., Bracegirdle, J., Brown, A., Keyzers, R. A., Ackerley, D. F., Northcote, P. T., & Owen, J. G. (2020). Metagenomic Exploration of the Marine Sponge Mycale hentscheli Uncovers Multiple Polyketide-Producing Bacterial Symbionts. *MBio*, *11*(2). https://doi.org/10.1128/mBio.02997-19

Tilley, S. J., Orlova, E. V., Gilbert, R. J. C., Andrew, P. W., & Saibil, H. R. (2005). Structural Basis of Pore Formation by the Bacterial Toxin Pneumolysin. *Cell*, *121*(2), 247–256. https://doi.org/10.1016/j.cell.2005.02.033

Toledo, A., & Benach, J. L. (2015). Hijacking and Use of Host Lipids by Intracellular Pathogens. *Microbiology Spectrum*, *3*(6). https://doi.org/10.1128/microbiolspec.VMBF-0001-2014

Tosi, T., Pflug, A., Discola, K. F., Neves, D., & Dessen, A. (2013). Structural basis of eukaryotic cell targeting by type III secretion system (T3SS) effectors. *Research in Microbiology*, *164*(6), 605–619. https://doi.org/10.1016/j.resmic.2013.03.019

Trent, M. S., Stead, C. M., Tran, A. X., & Hankins, J. V. (2006). Invited review: Diversity of endotoxin and its impact on pathogenesis. *Journal of Endotoxin Research*, *12*(4), 205–223. https://doi.org/10.1177/09680519060120040201

Tsai, A. Y., English, B. C., & Tsolis, R. M. (2019). Hostile Takeover: Hijacking of Endoplasmic Reticulum Function by T4SS and T3SS Effectors Creates a Niche for Intracellular Pathogens. *Microbiology Spectrum*, *7*(3). https://doi.org/10.1128/microbiolspec.PSIB-0027-2019

van der Goot, F. G., van Nhieu, G. T., Allaoui, A., Sansonetti, P., & Lafont, F. (2004). Rafts Can Trigger Contact-mediated Secretion of Bacterial Effectors via a Lipid-based Mechanism*. *Journal of Biological Chemistry*, *279*(46), 47792–47798. https://doi.org/10.1074/jbc.M406824200

van der Meer-Janssen, Y. P. M., van Galen, J., Batenburg, J. J., & Helms, J. B. (2010). Lipids in host–pathogen interactions: Pathogens exploit the complexity of the host cell lipidome. *Progress in Lipid Research*, *49*(1), 1–26. https://doi.org/10.1016/j.plipres.2009.07.003

Vereb, G., Szöllősi, J., Matkó, J., Nagy, P., Farkas, T., Vígh, L., Mátyus, L., Waldmann, T. A., & Damjanovich, S. (2003). Dynamic, yet structured: The cell membrane three decades after the Singer–Nicolson model. *Proceedings of the National Academy of Sciences of the United States of America*, *100*(14), 8053–8058. https://doi.org/10.1073/pnas.1332550100

Walker, D. H., Feng, H. M., & Popov, V. L. (2001). Rickettsial phospholipase A2 as a pathogenic mechanism in a model of cell injury by typhus and spotted fever group rickettsiae. *The American Journal of Tropical Medicine and Hygiene*, *65*(6), 936–942. https://doi.org/10.4269/ajtmh.2001.65.936

Wang, D., & DuBois, R. N. (2010). Eicosanoids and cancer. *Nature Reviews Cancer*, *10*(3), 181–193. https://doi.org/10.1038/nrc2809

Wenk, M. R. (2006). Lipidomics of host–pathogen interactions. *FEBS Letters*, *580*(23), 5541–5551. https://doi.org/10.1016/j.febslet.2006.07.007

Wentrup, C., Wendeberg, A., Huang, J. Y., Borowski, C., & Dubilier, N. (2013). Shift from widespread symbiont infection of host tissues to specific colonization of gills in juvenile deep-sea mussels. *The ISME Journal*, *7*(6), 1244–1247. https://doi.org/10.1038/ismej.2013.5

Woyke, T., Teeling, H., Ivanova, N. N., Huntemann, M., Richter, M., Gloeckner, F. O., Boeffelli, D., Barry, K. W., Shapiro, H. J., Anderson, I. J., Szeto, E., Kyrpides, N. C., Mussmann, M., Amann, R., Bergin, C., Ruehland, C., Rubin, E. M., & Dubilier, N. (2006). Metagenomic Analysis of Microbial Symbionts in a Gutless Worm. *Nature*, Article LBNL-2723E. https://doi.org/10.1038/nature05192

Wu, M., Sun, L. V., Vamathevan, J., Riegler, M., Deboy, R., Brownlie, J. C., McGraw, E. A., Martin, W., Esser, C., Ahmadinejad, N., Wiegand, C., Madupu, R., Beanan, M. J., Brinkac, L. M., Daugherty, S. C., Durkin, A. S., Kolonay, J. F., Nelson, W. C., Mohamoud, Y., … Eisen, J. A. (2004). Phylogenomics of the Reproductive Parasite Wolbachia pipientis wMel: A Streamlined Genome Overrun by Mobile Genetic Elements. *PLOS Biology*, *2*(3), e69. https://doi.org/10.1371/journal.pbio.0020069

Xiong, Q., Lin, M., & Rikihisa, Y. (2009). Cholesterol-Dependent Anaplasma phagocytophilum Exploits the Low-Density Lipoprotein Uptake Pathway. *PLOS Pathogens*, *5*(3), e1000329. https://doi.org/10.1371/journal.ppat.1000329

Young, G. M., Schmiel, D. H., & Miller, V. L. (1999). A new pathway for the secretion of virulence factors by bacteria: The flagellar export apparatus functions as a protein-secretion system. *Proceedings of the National Academy of Sciences*, *96*(11), 6456–6461. https://doi.org/10.1073/pnas.96.11.6456

Young, S. A., Mina, J. G., Denny, P. W., & Smith, T. K. (2012). Sphingolipid and Ceramide Homeostasis: Potential Therapeutic Targets. *Biochemistry Research International*, *2012*, e248135. https://doi.org/10.1155/2012/248135

Zientz, E., Dandekar, T., & Gross, R. (2004). Metabolic Interdependence of Obligate Intracellular Bacteria and Their Insect Hosts. *Microbiology and Molecular Biology Reviews*, *68*(4), 745–770. https://doi.org/10.1128/MMBR.68.4.745-770.2004

Chapter I

Investigating the lipid landscape of deep-sea mussel symbioses

Investigating the lipid landscape of deep-sea mussel symbioses

Dolma Michellod[1], Nicole Dubilier[1,2], Manuel Liebeke[1]

[1] Max Planck Institute for Marine Microbiology, Celsiusstraße 1, 28359 Bremen, Germany

[2] MARUM, Center for Marine Environmental Sciences, University of Bremen, 28359 Bremen, Germany

* *The manuscript is a draft and has not been revised by all authors.*

* Author contribution: D.M and M.L conceived the study. D.M prepared the mussel samples, run the LC-MS/MS measurements and analyzed the data. D.M drafted the manuscript, with support from M.L.

Abstract

The high structural and functional diversity of lipids make them a challenging subject to study, especially in non-model organisms. Recent analytical advances made the study and the interpretation of complex environmental samples possible. In this study we investigated the lipid diversity and the impact the association with intracellular bacteria has on the lipid composition of symbiotic and non-symbiotic deep-sea mussel tissues. We used a state of the art ultra-high performance liquid chromatography tandem mass spectrometry (UHPLC-MS/MS) approach to determine the lipid landscape of different species of deep-sea mussels. Molecular networking, similarity analyses and unsupervised substructure prediction were used to describe the chemical diversity present in deep-sea symbiotic mussels and identify compounds linked to the presence of the symbionts. This untargeted approach enabled the detection and annotation of compounds which had not been previously reported in deep-sea mussels. It also allowed the identification of new groups of related compounds which are specific to sulfur-oxidizing symbionts. This untargeted approach offered a more comprehensive overview of the lipid diversity in deep-sea mussels.

Introduction

Associations of deep-sea mussels with chemosynthetic bacteria enable the eukaryotic hosts to thrive around deep-sea hydrothermal vents (Duperron, 2010). The interactions between eukaryotic hosts and bacteria are mediated by chemical cues. Lipids' functional diversity, their involvement in many essential cellular processes and their location at the interface between the organisms make them good candidates to act as chemical cues mediating symbiotic associations. Lipids have been shown to be key players in pathogenic interactions (P. E. Allen & Martinez, 2020; Roingeard & Melo, 2017; Toledo & Benach, 2015; Wenk, 2006). As pathogenic and beneficial symbionts use very similar molecular mechanisms in their interactions with the host, lipids are likely to play an important role in beneficial symbioses as well (Gil et al., 2004; Goebel & Gross, 2001; Hentschel et al., 2000).

Before one can identify the specific lipids species involved in a symbiosis, an overview of the overall lipids composition of the system is needed. In the same way we moved away from 16S amplicons to embrace metagenomes, the lipidomics field is moving from targeted approach to an untargeted approach. This change was made possible by technological advances on the mass spectrometry side (Murphy et al., 2001; Soltwisch et al., 2020). However, the absence of a public

spectral libraries and of the tools needed to identify unknown lipids automatically meant that lipidomics focused heavily on model organisms and their well-studied lipids repertoire. Today, new tools based on collaborative spectral libraries or *in silico* fragmentation databases are supporting the identification of unknown lipids from environmental samples (Fahy et al., 2007; Koelmel et al., 2017; Rogers et al., 2019; Wang et al., 2016). Those analytical advances open the door to the study of lipids in beneficial symbioses, as most of the symbiotic partners cannot be cultivated in a lab. The deep-sea mussels are a good example of an environmental, non-culturable system that could not have been studied a few years ago.

Deep-sea mussels (*Mytilidae, Bathymodiolinae*) inhabiting hydrothermal vents and cold seeps form symbiotic associations with chemosynthetic bacteria (reviewed in (Duperron, 2010). Deep-sea mussels of the family *Bathymodiolinae* are associated with gammaproteobacterial sulfur-oxidizing (SOX), methane-oxidizing (MOX) symbionts, or both (Duperron, 2010). The chemosynthetic symbionts enable the host to thrive in the nutrient-poor habitat of the deep sea. The symbionts largely reside in specialized epithelial gill cells called bacteriocytes (**Figure 1**). Despite their functioning digestive system, these mussels depend on their chemosynthetic bacteria for nutrition (Reviewed in (DeChaine & Cavanaugh, 2006; Duperron, 2010). This nutritional dependence is reflected in the fatty acid profile as well as in the fatty acids' isotopic signature of deep-sea mussels, inside and outside of the symbiotic organ (Abrajano et al., 1994; Fang et al., 1993; Jahnke et al., 1995; Kellermann et al., 2012; Pond et al., 1998). The analysis of the fatty acid composition of the deep-sea mussels led to more general lipid studies. Their sterol and polar membrane lipid profiles were obtained using a targeted approach in order to identify symbionts biomarkers (Kellermann et al., 2012). More recently, the spatial distribution of the lipids in the gills of one species of deep-sea mussels was imaged using metabolite imaging combined with fluorescent labelling of the symbionts (Geier et al., 2020). This approach revealed a new class of compounds specific to MOX symbionts and a local lipids composition modified by the presence of the symbionts. The metabolite imaging was combined with liquid chromatography tandem mass spectrometry (LC-MS/MS) to identify the observed compounds and enable the interpretation of the results.

In this study we analyzed the lipid landscape of deep-sea mussels using an untargeted approach. We determined the lipid composition of the foot, gill and mantel of five deep-sea mussel species belonging to three different genera. The mussels were collected along the Mid-Atlantic ridge, the East pacific rise, the Tonga-Kermadec ridge and in the Gulf of Mexico (**Figure 1**). For details on the different species and sampling sites, see **Supplementary Table 1**. We performed this

untargeted lipidomics study acquiring LC-MS/MS data in positive and negative mode. The fragmentation patterns were then searched against spectral libraries and their substructure was predicted based on ~~*in*~~ *silico* fragmentation databases.

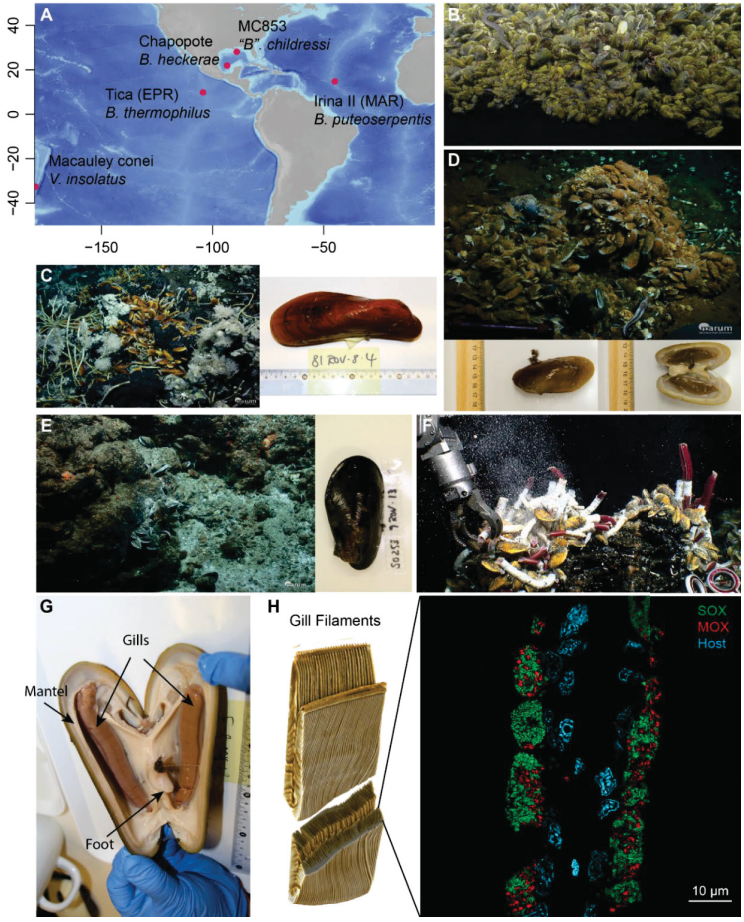

Figure 1 | Deep-sea mussels host chemosynthetic bacterial symbionts in their gills which enable them to thrive at deep-sea hydrothermal vents and cold seeps. A, Location of the hydrothermal sites at which the different mussel species were sampled. **B,** *"Bathymodiolus" childressi* specimens were sampled in the Gulf of Mexico at the MC583 site; image courtesy of MARUM. **C,** *Bathymdiolus heckerae* were also collected in the Gulf of Mexico at the Chapopote site; image courtesy of MARUM. **D,** *Bathymodiolus puteoserpentis* individuals were retrieved in the Mid-Atlantic Ridge, at the Irina II vent site; image courtesy of MARUM. **E,** *Vulcanidas insolatus* were sampled along the

Tonga-Kermadec Ridge at Macauley cone; image courtesy of MARUM. **F,** *Bathymodiolus thermophilus* were collected at the vent site TICA in the East Pacific Rise (EPR); image Dive and Discover™. **G,** Deep-sea mussels have enlarged gills in which they host methane-oxidizing (MOX) and sulfur-oxidizing (SOX) symbionts. **H,** Fluorescent in situ hybridization image of one gill filament showing MOX in red, SOX in green and a DNA stain for host nuclei in cyan; images courtesy of B. Geier and M.A. Gonzalez Porras.

Results and Discussion

Visualization of the lipid landscape of deep-sea mussels using molecular networking, library search and unsupervised sub-structure prediction.

The high functional diversity of lipids is reflected in their structural diversity (Dowhan, 1997). There are several million possible lipid structures and one single eukaryotic cell contains thousands of different lipid species (Koelmel et al., 2017). While one LC-MS/MS experiment does not cover the whole diversity of lipids, it still produces a wealth of data difficult to apprehend.

Molecular networks are needed to decrease the complexity of the data and apprehend its diversity. Molecular networks are visual representations of the chemical space described by tandem mass spectrometry (MS/MS) data. Based on their fragmentation pattern, related molecules are identified and linked together. Even in the absence of library hits, the related molecules are grouped together. This approach allowed us to visualize the thousands of compounds represented in our MS/MS experiment. This is especially useful as most compounds still resist identification and interpretation. Methods and tools to identify this large pool of unknown compounds are essential to gain a better understanding of their structure and function.

Global Natural Products Social (GNPS) molecular networking project offers new tools to help identify and discover new compounds (Wang et al., 2016). GNPS enables to search MS/MS spectra against their large spectral library of natural products which contains several thousand compounds. After a general search, the annotations were expanded using DEREPLICATOR+ (Mohimani et al., 2018).

In addition to the library searches, we used MS2LDA_MOTIFDB to identify more lipids. MS2LDA is a tool which performs unsupervised substructure discovery (Rogers et al., 2019; van der Hooft et al., 2016, 2017; Wandy et al., 2018). Finally, we used the MOLNETENHANCER workflow (Ernst et al., 2019) which combined the outputs from molecular networking, Dereplicator+ and MS2LDA. The integration of those different tools offers a more comprehensive chemical overview (***Figure 2*** and ***Figure 3***).

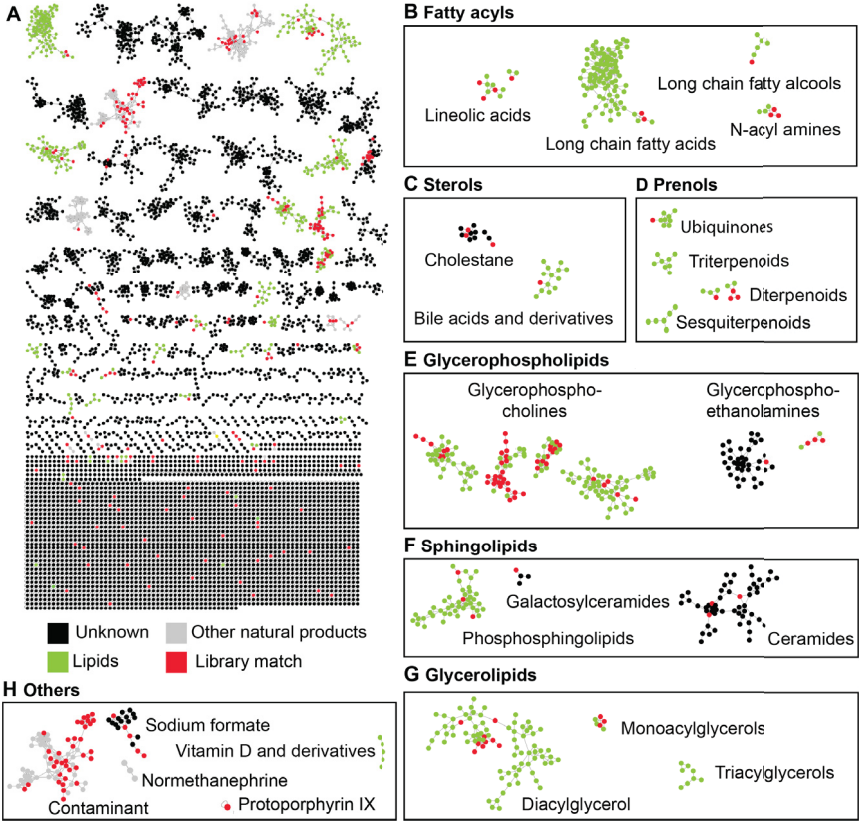

Figure 2 | Representation of the chemical landscape of deep-sea mussels represented in the MS/MS dataset acquired in positive mode. A, Molecular network, each node represents a compound. The compounds structurally related are linked together by an edge (cosine ≥ 0.7). The compounds identified by library search are highlighted in red. The compounds class identified by substructure search are highlighted in green (lipids) and in grey (other natural compounds). **B – H,** The identified compounds were grouped by lipid classes.

Library search and compound identification

In positive mode, the spectral library search yielded 159 unique library hits, 28 of which were high quality hits. The 28 compounds included: sphingolipids (two ceramides, one galactosylceramide and one sphingomyelin), membrane lipids (16 phosphatidylcholines and 4 phosphoethanolamines), one triacylglycerol and one prenol (***Supplementary Table 2***). In addition it identified *Protoporphyrin IX,* a metabolic precursor for hemes, cytochrome c and

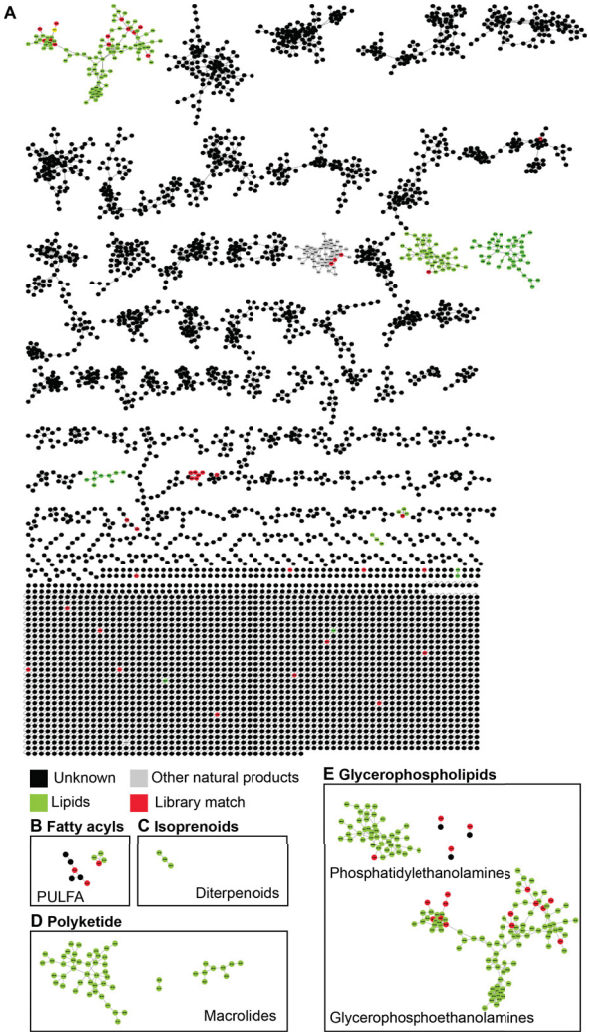

Figure 3 | Representation of the chemical landscape of deep-sea mussels represented in the MS/MS dataset acquired in negative mode. A, Molecular network: each node represents a compound and the compounds structurally related are linked together by an edge (cosine ≥ 0.7). The compounds identified by library search are highlighted in red. The compounds class identified by substructure search are highlighted in green (lipids) and in grey (other natural compounds). **B – E,** The identified compounds were grouped by lipid classes.

chlorophyll (Sachar et al., 2016). It also included normetanephrine, a derivative of octopamin which is an important hormone and neurotransmitter often present in invertebrates (Roeder, 1999). DEREPLICATOR+ (Mohimani et al., 2018) yielded another 36 metabolites identifications including the coenzyme ubiquinone and triacylglycerols as well as diacylglycerols and sterols ***Supplementary Table 3***.

The library search against the data acquired in negative mode yielded fewer identifications. Out of the thousands of compounds present in the data, only 31 unique library compounds were identified, and only eight with high confidence. Those eight compounds were seven phosphoethanolamines and one fatty acid: arachidonics acid (***Supplementary Table 4***). The expansion of the annotation yielded 19 unique metabolites (***Supplementary Table 5***).

General description

Species from seven out of the eight lipid classes were covered and identified by our analysis. The analysis also enabled us to identify contaminants (**Figure 2G**). We detected several bioactive molecules such as ubiquinones, heme precursor, vitamin D precursors and hormones. Other hits were more puzzling such as the Alstrosine B, an unusual monoterpenoid alkaloid–recently discovered in plants (Cai et al., 2011; Mohammed et al., 2021; Schinnerl et al., 2012).

Membrane lipids form the structural basis of the cellular membrane. They include glycerophospholipids, sphingolipids, glycerolipids and sterols. Glycerophospholipids are the building blocks of the lipid bilayer and are the most common membrane lipids in bacteria and eukaryotes (Dowhan, 1997; Zhang & Rock, 2008). They also are the precursors of important signaling molecules such as inositol triphosphate (IP3), an intracellular second messenger which triggers the activation of various calcium-regulated intracellular signals (Patterson et al., 2004). They have been well described and numerous phospholipids standards are commercially available, which explains the high number of phospholipids hits.

Sphingolipids are abundant in the membrane of eukaryotes and they modulate numerous cellular processes (Hannun & Obeid, 2018). They are likely to be of host origin as bacteria are usually not able to synthesize them. However, they might have been modified by the symbionts as many pathogenic bacteria use them to hijack the cellular machinery of eukaryotic hosts (Heaver et al., 2018; Heung et al., 2006).

Gylcerolipids have a dual function: they are membrane lipids but also serve as energy storage under the form of triacylglycerol. Triacylglycerols are present in all organisms and are often

abundant in the symbiotic tissues of deep-sea mollusks (C. E. Allen et al., 2001; Kellermann et al., 2012; Pranal et al., 1997). They are not integrated into the cellular membrane but are used as energy storage often in the form of lipids droplets (Reue, 2011). They have been shown to participate in the carbon and energy exchange in beneficial symbioses (Feng et al., 2020; Jiang et al., 2017; Kellogg & Patton, 1983; Keymer et al., 2017).

In eukaryotes, sterols influence the biophysical properties of biological membranes. They are central to the organization, dynamics, and function of the lipid bilayer. Bacteria have sterol analogues called hopanoids, which fulfill a function similar to sterols' (Ourisson et al., 1987; Sáenz et al., 2015). Hopanoids and C_4-methyl-sterols have been used as biomarkers for the presence of MOX symbionts in deep-sea mussels (Fang et al., 1993; Geier et al., 2020; Jahnke et al., 1995; Kellermann et al., 2012). C_4-methyl-sterols and steryl-glycosides were identified by DEREPLICATOR+. Steryl-glycosides have not been reported in deep-sea mussels before. They are usually found in plants, fungi and algae but are rarely present in bacteria and animals (Grille et al., 2010; Shimamura, 2020). Their function in animals and bacteria is still being investigated; they seem to be involved in pathogenic interactions (Grille et al., 2010; Shimamura, 2020). Hopanoids were not identified by our search. They were present in the MS spectra but in too low quantity to be selected for fragmentation. Outside of the membrane, sterols play important roles as precursors for steroid hormones and bile acids, which is reflected in the annotation obtained.

Fatty acyls and prenols, together with small polar molecules such as ribitol, glycerol or oligosaccharides form the building blocks for the synthesis of membrane lipids. Bacteria are usually enriched in glycerol-based phospholipids with short fatty acids (C_{14} to C_{20}) (Zhang & Rock, 2008). Interestingly, most of the TG identified had a combination of short monounsaturated and saturated fatty acids common in bacteria, and of polyunsaturated long chain fatty acids (PUFA) such as 18:3, 18:4, 20:3, 20:4, 20:5, 22:1, 22:5. A similar trend can be observed in the phospholipids. This suggest that those lipids are derived from the host as PUFA, while common in vent mussels, are rarely found in bacteria (Colaço et al., 2009; Fang et al., 1993; Pond et al., 1998; Pranal et al., 1997).

Free fatty acyls and prenols are not just building blocks for membrane lipids, they have functions of their own inside and outside of the membrane environment. Fatty acyls, for example, participate in different signaling processes. When released from their membrane lipids, PUFAs such as archidonic acid (20:4) serve as precursors to eicosanoids, a group of signaling molecules involved in diverse cellular processes such as tissue homeostasis and immune response (Buczynski et al., 2009; Ferrer & Moreno, 2010; Stanley, 2011).

Prenols serve as precursors to many electron acceptors and coenzymes critical to cell physiology such as ubiquinone. It is also a precursor to terpenoids, bioactive molecules often used as defense metabolites and abundant in marine invertebrates (Hegazy et al., 2015).

Polyketide, the seventh class of lipids, also often plays a defensive role. Macrolides are one type of polyketide from bacterial origin. They mimic signaling molecules and inhibit the function of ribosomes inhibiting bacterial growth (Dmitriev et al., 2020). Several eukaryotes form defensive symbiosis with polyketides producing bacteria, which protect them from predation, parasitism or infection (Beedessee et al., 2019; Engl et al., 2018; Piel, 2002; Stocker-Wörgötter, 2008; Storey et al., 2020).

Some groups of compounds are symbiont specific

The symbiotic bacteria are highly abundant in the gill tissues of deep-sea mussels (Szafranski et al., 2015). One could expect some lipid groups of bacterial origin to be restricted to the symbiotic tissue. We were indeed able to identify several groups of analogues compounds restricted to the gill tissue (***Supplementary Figure 1***). We could only identify gill-specific groups of lipids in positive ion mode data, no gill-specific groups were identified in the dataset acquired in negative ionization mode (**Supplementary Figure 2**). The *m/z* values of the gill-specific compounds are displayed in ***Supplementary Figure 3***, unfortunately none of those compounds were structurally identified.

While the presence of hopanoids, C_4-methyl-sterols or the new group of specialized metabolite described by Geier et al can all be used as biomarkers for the presence of MOX symbionts in the deep-sea mussels, so far no compounds specific to SOX symbionts were identified (Geier et al., 2020; Kellermann et al., 2012). Using our visualization approach we could identify several groups of SOX-specific lipids as well as a few MOX-specific lipids in both positive and negative ionization modes (***Supplementary Figure 4***, ***Supplementary Figure 6***). Only one of those group was structurally identified, a small group of triacyglycerol (***Figure 4***). This untargeted approach enabled us to identify several compounds linked to the symbiotic tissues or even directly to a specific symbiont. Investigating the spatial distribution of those compounds using metabolite imaging and determining the abundance of those compounds in the different species using MS1 data would allow us to gain more information.

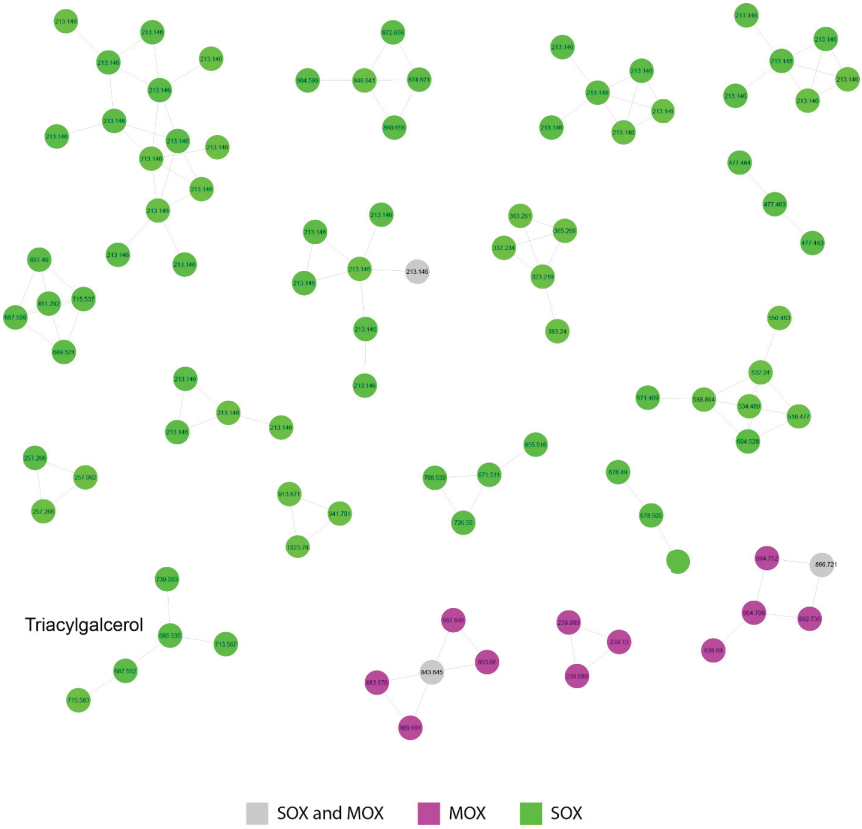

Figure 4 | Lipid groups which were linked to the presence of a specific symbiont. Subset of the molecular network representing the MS/MS data acquired in positive ionization mode. Many lipid groups were linked to the presence of SOX symbionts, but only one of those group was structurally identified (triacylglycerol). Only a few MOX-specific lipid groups were detected. The compounds are colored according to symbiont: magenta compounds are only present when MOX is present, green compounds are only present when SOX is present, grey compounds are present regardless of the symbiont composition. Each node is labeled with the m/z value of its parental ion.

Conclusion

We presented the analysis of the MS/MS data, which gave us an overview of the chemical landscape and enabled us to identify compounds. While many lipids remained unknown, the continuous annotation of deposited data and the growing popularity of the GNPS library might enable an improved identification in the near future. The annotation already pointed us toward

compounds that were not previously reported in deep-sea mussels such as polyketides, some specific prenols and steryl-glucosyls.

The results presented here are the first step of a more in-depth analysis. The analysis of the MS1 data will give us a more complete view of the lipid landscape of deep-sea mussels. We will be able to use the MS1 information to test which factor – species, symbionts, environment, tissue type – has the most influence on the lipid composition of deep-sea mussels, and to identify the compounds which create this difference.

The analysis of the molecular network revealed that some groups of compounds were linked to the presence of a specific symbiont. We found many compounds that were only detected in the presence of a SOX symbionts, unfortunately all but one of those groups remain of unknown identity. It is the first time potential biomoarkers for SOX symbionts are proposed and it would be worthwhile to investigate their structural identity and distribution further. Mei-Chen Liu is currently producing a metabolite imaging dataset of deep-sea mussels harboring only SOX symbionts and investigating the spatial distribution of those SOX-specific compounds. Determining their abundance in the different mussels' species and investing some effort in their structural identification might lead to a more comprehensive understanding of symbiotic interactions.

Material and methods

Sample collection

The mussels were collected using a remotely operated vehicle (ROV) and brought back to the surface in an insulated container to prevent temperature changes. Once on board, the gills were dissected from the mussel, snap-frozen in liquid nitrogen and stored at -80°C. For details on the species and sampling sites, see **Supplementary Table 1**.

Sample preparation

Lipids were extracted from small pieces of frozen mussels' tissues (50–100 mg). The tissues were placed in screw cap tubes containing silica beads (1.1-1.2 mm diameter, MS Lab) and 8 µL/mg tissue ice-cooled MeOH. The tissues were homogenized by two bursts (2x10 seconds burst at 6.5 m/s). The homogenized tissues were transferred into a 3 mL exetainer containing 8 µL/mg tissues of ice-cooled chloroform. The exetainers were vortexed for 15 seconds and placed on ice. HPLC grade water (7.2 µL/mg tissue) was added to each exetainer. The exetainers were vortexed for 30 sec and placed on ice for 10 minute to allow phase separation. The tissues debris were pelleted by a 10 minute centrifugation step (4 °C, 2500 x g). The tubes were then left to incubate

at room temperature for 10 minutes to achieve complete phase separation. Using a glass syringe, the lipid fraction (lower phase) was transferred in a HPLC-MS vial. Finally, the lipid fraction was evaporated to dryness under an N_2-flow. Store the dried extract at -80°C until further analysis.

Before analysis, the lipid fraction was resuspended in 500 µL of chloroform. The supernatant was then diluted 1:10 in ACN. 100 µL of the diluted extract was transferred to an HPLC-MS vials (1.5-HRSV 9mm Screw Thread Vials, Thermo Fisher™). 50 µL of each diluted samples were combined to form a quality control sample.

Solvents for LC–MS/MS.

All organic solvents were LC–MS grade, using acetonitrile (ACN; Honeywell, Honeywell Specialty Chemicals), isopropanol (IPA; BioSolve) and formic acid (FA; Sigma-Aldrich), methanol (MeOH, BioSolve). Water was deionized using the Astacus MembraPure system (MembraPure).

Data acquisition

The analysis was performed using a QExactive Plus Orbitrap (Thermo Fisher Scientific) equipped with a HESI probe and a Vanquish Horizon UHPLC system (Thermo Fisher Scientific). The lipids were separated on an Accucore C30 column (150 × 2.1 mm, 2.6 µm, Thermo Fisher Scientific), at 40 °C, using a solvent gradient. Buffer A (60/40 ACN/H2O, 10 mM ammonium formate, 0.1% FA) and buffer B (90/10 IPA/ACN, 10 mM ammonium formate, 0.1% FA) (Breitkopf et al., 2017) were used at a flow rate of 350 µl min−1. The lipids were eluted from the column with a gradient starting at 0% buffer B (***Table 1***).

Table 1 | Solvent gradient for high-resolution LC-MS/MS.

%B	Time [min]	Flow rate [µL min^{-1}]
0	-2 (pre-run equilibration)	350
0	2	350
16	5.5	350
45	9	350
52	12	350
58	14	350
66	16	350
70	18	350
75	22	350
97	25	350
97	32.5	350
15	33	350

0	34.4	350
0	36	350

*Buffer A (60/40 ACN/H_2O, 10 mM ammonium formate, 0.1% FA) and Buffer B (90/10 IPA/ACN, 10 mM ammonium formate, 0.1% FA) were used at a flow rate of 350 µl min^{-1}.

The injection volume was 10 µl. MS measurements were acquired in positive-ion and negative-ion mode, during two different runs, for a mass detection range of *m/z* = 150–1,500. Resolution of the mass analyzer was set to 70,000 for MS scans and 35,000 for MS/MS scans at *m/z* = 200. MS/MS scans of the eight most abundant precursor ions were acquired in positive-ion and negative-ion modes, excluding the 200 most abundant *m/z* detected in the extraction blank. Dynamic exclusion was enabled for 30 s and collision energy was set to 30 eV (for more information see ***Table 2***).

Table 2 | MS settings of Q Exactive Plus Orbitrap (Thermo Fisher Scientific) equippedwith a HESI probe and a Vanquish Horizon UHPLC System (Thermo Fisher Scientific).

MS^1	
Resolution	70'000
AGC target	5.00E+05
Max IT	65 ms
Scan range	150-1500 m/z
MS^2	
Resolution	35'000
AGC target	1.00E+06
Max IT	75 ms
Loop count	8
Dynamic exclusion	30 s
Isolation windows (pos.)	1 m/z
Isolation windows (neg.)	1 m/z
NCE	30

The .RAW files were converted to .mzXML using the msConvert software (ProteoWizard 3.0.20190) (Chambers et al., 2012).

Exploiting tandem mass spectrometry data: GNPS workflow

Classical Molecular Networking. To visualize the chemical space present in our MS/MS experiments, we created molecular networks. The networks were created using the METABOLOMICS-SNETS-V2 workflow (version release_28.2) on the GNPS website (http://gnps.ucsd.edu). The data was filtered by removing all MS/MS fragment ions within +/- 17 Da of the precursor m/z. MS/MS spectra were window filtered by choosing only the top 6 fragment ions in the +/- 50 Da window throughout the spectrum. The precursor ion mass tolerance was set

to 2 Da and a MS/MS fragment ion tolerance of 0.02 Da. The mass tolerance was set at 2 Da to ensure the inclusion of the libraries acquired in low mass resolution mode in the spectral matching search. The edges of the created network were only kept if they had a cosine score above 0.7 and more than 6 matched peaks. Furthermore, edges between two nodes were kept in the network if and only if each of the nodes appeared in each other's respective top 10 most similar nodes. Finally, the maximum size of a molecular family was set to 100, and the lowest scoring edges were removed from molecular families until the molecular family size was below this threshold. The spectra in the network were then searched against GNPS' spectral libraries (Wang et al., 2016). The library spectra were filtered in the same manner as the input data. All matches kept between network spectra and library spectra were required to have a score above 0.7 and at least 6 matched peaks.

Expanding annotation. We improved the annotation by feeding the resulting network in the DEREPLICATOR_PLUS (version 1.0.0) tool. Dereplicator+ expands the annotation of general metabolites and natural products such as polyketides and other lipids (Mohimani et al., 2018).

We used MS2LDA_MOTIFDB (version release_23.1), a tool which performs unsupervised substructure discovery (Rogers et al., 2019; van der Hooft et al., 2016, 2017; Wandy et al., 2018). It links characteristic fragmentation patterns (co-occurring mass fragment peaks and/or neutral losses) to chemical substructures specific to a class of compounds. It identifies the substructures present in our dataset based on a database of fragmentation pattern.

Integration of the results. Finally, we used the MOLNETENHANCER workflow (version release_22) (Ernst et al., 2019) which combined the outputs from molecular networking, MS2LDA and Dereplicator+. The integration of metabolome mining and annotation tools offers a more comprehensive chemical overview of metabolomics data. The results were then loaded in Cytoscape (version 3.8.2) for visualization and analysis (Shannon et al., 2003).

Acknowledgements

We would like to thank the crew and captains of the scientific vessels Meteor (M114-2 and M126), Nautilus (Na 58), Atlantis (AT21-02) and Sonne (Kermadec 2016), and their ROV pilots who helped us collect our extensive set of mussel species. We thank M. Weinhold, and J. Beckmann for support in the laboratory. This work was funded by the Max Planck Society, the DFG Cluster of Excellence 'The Ocean in the Earth System' at MARUM (University of Bremen), a Gordon and Betty Moore Foundation Marine Microbiology Initiative Investigator Award through grant GBMF3811 to Prof. N. Dubilier, and a European Research Council Advanced Grant (BathyBiome, grant 340535).

Code and data availability

The LC-MS/MS data will be made available on MetaboLights.

References

Abrajano, T. A., Murphy, D. E., Fang, J., Comet, P., & Brooks, J. M. (1994). 13C12c ratios in individual fatty acids of marine mytilids with and without bacterial symbionts. *Organic Geochemistry*, *21*(6), 611–617. https://doi.org/10.1016/0146-6380(94)90007-8

Allen, C. E., Tyler, P. A., & Van Dover, C. L. (2001). Lipid composition of the hydrothermal vent clam Calyptogena pacifica (Mollusca: Bivalvia) as a trophic indicator. *Journal of the Marine Biological Association of the United Kingdom*, *81*(5), 817–821.

Allen, P. E., & Martinez, J. J. (2020). Modulation of Host Lipid Pathways by Pathogenic Intracellular Bacteria. *Pathogens*, *9*(8), 614. https://doi.org/10.3390/pathogens9080614

Beedessee, G., Hisata, K., Roy, M. C., Van Dolah, F. M., Satoh, N., & Shoguchi, E. (2019). Diversified secondary metabolite biosynthesis gene repertoire revealed in symbiotic dinoflagellates. *Scientific Reports*, *9*(1), 1204. https://doi.org/10.1038/s41598-018-37792-0

Breitkopf, S., Ricoult, S., Yuan, M., Xu, Y., Peake, D., Manning, B., & Asara, J. (2017). A relative quantitative positive/negative ion switching method for untargeted lipidomics via high resolution LC-MS/MS from any biological source. *Metabolomics*, *13*. https://doi.org/10.1007/s11306-016-1157-8

Buczynski, M. W., Dumlao, D. S., & Dennis, E. A. (2009). Thematic Review Series: Proteomics. An integrated omics analysis of eicosanoid biology1[S]. *Journal of Lipid Research*, *50*(6), 1015–1038. https://doi.org/10.1194/jlr.R900004-JLR200

Cai, X.-H., Bao, M.-F., Zhang, Y., Zeng, C.-X., Liu, Y.-P., & Luo, X.-D. (2011). A new type of monoterpenoid indole alkaloid precursor from Alstonia rostrata. *Organic Letters*, *13*(14), 3568–3571. https://doi.org/10.1021/ol200996a

Chambers, M. C., Maclean, B., Burke, R., Amodei, D., Ruderman, D. L., Neumann, S., Gatto, L., Fischer, B., Pratt, B., Egertson, J., Hoff, K., Kessner, D., Tasman, N., Shulman, N., Frewen, B., Baker, T. A., Brusniak, M.-Y., Paulse, C., Creasy, D., … Mallick, P. (2012). A cross-platform toolkit for mass spectrometry and proteomics. *Nature Biotechnology*, *30*(10), 918–920. https://doi.org/10.1038/nbt.2377

Colaço, A., Prieto, C., Martins, A., Figueiredo, M., Lafon, V., Monteiro, M., & Bandarra, N. M. (2009). Seasonal variations in lipid composition of the hydrothermal vent mussel Bathymodiolus azoricus from the Menez Gwen vent field. *Marine Environmental Research*, *67*(3), 146–152. https://doi.org/10.1016/j.marenvres.2008.12.004

DeChaine, E. G., & Cavanaugh, C. M. (2006). Symbioses of Methanotrophs and Deep-Sea Mussels (Mytilidae: Bathymodiolinae). In J. Overmann (Ed.), *Molecular Basis of Symbiosis* (pp. 227–249). Springer. https://doi.org/10.1007/3-540-28221-1_11

Dmitriev, S. E., Vladimirov, D. O., & Lashkevich, K. A. (2020). A Quick Guide to Small-Molecule Inhibitors of Eukaryotic Protein Synthesis. *Biochemistry (Moscow)*, *85*(11), 1389–1421. https://doi.org/10.1134/S0006297920110097

Dowhan, W. (1997). MOLECULAR BASIS FOR MEMBRANE PHOSPHOLIPID DIVERSITY: Why Are There So Many Lipids? *Annual Review of Biochemistry*, *66*(1), 199–232. https://doi.org/10.1146/annurev.biochem.66.1.199

Duperron, S. (2010). The Diversity of Deep-Sea Mussels and Their Bacterial Symbioses. In S. Kiel (Ed.), *The Vent and Seep Biota: Aspects from Microbes to Ecosystems* (pp. 137–167). Springer Netherlands. https://doi.org/10.1007/978-90-481-9572-5_6

Engl, T., Kroiss, J., Kai, M., Nechitaylo, T. Y., Svatoš, A., & Kaltenpoth, M. (2018). Evolutionary stability of antibiotic protection in a defensive symbiosis. *Proceedings of the National Academy of Sciences*, *115*(9), E2020–E2029. https://doi.org/10.1073/pnas.1719797115

Ernst, M., Kang, K. B., Caraballo-Rodríguez, A. M., Nothias, L.-F., Wandy, J., Chen, C., Wang, M., Rogers, S., Medema, M. H., Dorrestein, P. C., & van der Hooft, J. J. J. (2019). MolNetEnhancer: Enhanced Molecular Networks by Integrating Metabolome Mining and Annotation Tools. *Metabolites*, *9*(7), 144. https://doi.org/10.3390/metabo9070144

Fahy, E., Sud, M., Cotter, D., & Subramaniam, S. (2007). LIPID MAPS online tools for lipid research. *Nucleic Acids Research*, *35*(suppl_2), W606–W612. https://doi.org/10.1093/nar/gkm324

Fang, J., Abrajano, T. A., Comet, P. A., Brooks, J. M., Sassen, R., & MacDonald, I. R. (1993). Gulf of Mexico hydrocarbon seep communities: XI. Carbon isotopic fractionation during fatty acid biosynthesis of seep organisms and its implication for chemosynthetic processes. *Chemical Geology*, *109*(1), 271–279. https://doi.org/10.1016/0009-2541(93)90074-S

Feng, Z., Liu, X., Zhu, H., & Yao, Q. (2020). Responses of Arbuscular Mycorrhizal Symbiosis to Abiotic Stress: A Lipid-Centric Perspective. *Frontiers in Plant Science*, *11*. https://doi.org/10.3389/fpls.2020.578919

Ferrer, R., & Moreno, J. J. (2010). Role of eicosanoids on intestinal epithelial homeostasis. *Biochemical Pharmacology*, *80*(4), 431–438. https://doi.org/10.1016/j.bcp.2010.04.033

Geier, B., Sogin, E. M., Michellod, D., Janda, M., Kompauer, M., Spengler, B., Dubilier, N., & Liebeke, M. (2020). Spatial metabolomics of in situ host–microbe interactions at the micrometre scale. *Nature Microbiology*, *5*(3), 498–510. https://doi.org/10.1038/s41564-019-0664-6

Gil, R., Latorre, A., & Moya, A. (2004). Bacterial endosymbionts of insects: Insights from comparative genomics. *Environmental Microbiology*, *6*(11), 1109–1122. https://doi.org/10.1111/j.1462-2920.2004.00691.x

Goebel, W., & Gross, R. (2001). Intracellular survival strategies of mutualistic and parasitic prokaryotes. *Trends in Microbiology*, *9*(6), 267–273. https://doi.org/10.1016/S0966-842X(01)02040-6

Grille, S., Zaslawski, A., Thiele, S., Plat, J., & Warnecke, D. (2010). The functions of steryl glycosides come to those who wait: Recent advances in plants, fungi, bacteria and animals. *Progress in Lipid Research*, *49*(3), 262–288. https://doi.org/10.1016/j.plipres.2010.02.001

Hannun, Y. A., & Obeid, L. M. (2018). Sphingolipids and their metabolism in physiology and disease. *Nature Reviews Molecular Cell Biology*, *19*(3), 175–191. https://doi.org/10.1038/nrm.2017.107

Heaver, S. L., Johnson, E. L., & Ley, R. E. (2018). Sphingolipids in host-microbial interactions. *Current Opinion in Microbiology*, *43*, 92–99. https://doi.org/10.1016/j.mib.2017.12.011

Hegazy, M. E. F., Mohamed, T. A., Alhammady, M. A., Shaheen, A. M., Reda, E. H., Elshamy, A. I., Aziz, M., & Paré, P. W. (2015). Molecular Architecture and Biomedical Leads of Terpenes from Red Sea Marine Invertebrates. *Marine Drugs*, *13*(5), 3154–3181. https://doi.org/10.3390/md13053154

Hentschel, U., Steinert, M., & Hacker, J. (2000). Common molecular mechanisms of symbiosis and pathogenesis. *Trends in Microbiology*, *8*(5), 226–231. https://doi.org/10.1016/S0966-842X(00)01758-3

Heung, L. J., Luberto, C., & Poeta, M. D. (2006). Role of Sphingolipids in Microbial Pathogenesis. *Infection and Immunity*, *74*(1), 28–39. https://doi.org/10.1128/IAI.74.1.28-39.2006

Jahnke, L. L., Summons, R. E., Dowling, L. M., & Zahiralis, K. D. (1995). Identification of methanotrophic lipid biomarkers in cold-seep mussel gills: Chemical and isotopic analysis. *Applied and Environmental Microbiology*, *61*(2), 576–582. https://doi.org/10.1128/aem.61.2.576-582.1995

Jiang, Y., Wang, W., Xie, Q., Liu, N., Liu, L., Wang, D., Zhang, X., Yang, C., Chen, X., Tang, D., & Wang, E. (2017). Plants transfer lipids to sustain colonization by mutualistic mycorrhizal and parasitic fungi. *Science*, *356*(6343), 1172–1175. https://doi.org/10.1126/science.aam9970

Kellermann, M. Y., Schubotz, F., Elvert, M., Lipp, J. S., Birgel, D., Prieto-Mollar, X., Dubilier, N., & Hinrichs, K.-U. (2012). Symbiont–host relationships in chemosynthetic mussels: A comprehensive lipid biomarker study. *Organic Geochemistry*, *43*, 112–124. https://doi.org/10.1016/j.orggeochem.2011.10.005

Kellogg, R. B., & Patton, J. S. (1983). Lipid droplets, medium of energy exchange in the symbiotic anemone Condylactis gigantea: A model coral polyp. *Marine Biology*, *75*(2), 137–149. https://doi.org/10.1007/BF00405996

Keymer, A., Pimprikar, P., Wewer, V., Huber, C., Brands, M., Bucerius, S. L., Delaux, P.-M., Klingl, V., Röpenack-Lahaye, E. von, Wang, T. L., Eisenreich, W., Dörmann, P., Parniske, M., & Gutjahr, C. (2017). Lipid transfer from plants to arbuscular mycorrhiza fungi. *ELife*, *6*, e29107. https://doi.org/10.7554/eLife.29107

Koelmel, J. P., Kroeger, N. M., Ulmer, C. Z., Bowden, J. A., Patterson, R. E., Cochran, J. A., Beecher, C. W. W., Garrett, T. J., & Yost, R. A. (2017). LipidMatch: An automated workflow for rule-based lipid identification using untargeted high-resolution tandem mass spectrometry data. *BMC Bioinformatics*, *18*(1), 331. https://doi.org/10.1186/s12859-017-1744-3

Mohammed, A. E., Abdul-Hameed, Z. H., Alotaibi, M. O., Bawakid, N. O., Sobahi, T. R., Abdel-Lateff, A., & Alarif, W. M. (2021). Chemical Diversity and Bioactivities of Monoterpene Indole Alkaloids (MIAs) from Six Apocynaceae Genera. *Molecules (Basel, Switzerland)*, *26*(2). https://doi.org/10.3390/molecules26020488

Mohimani, H., Gurevich, A., Shlemov, A., Mikheenko, A., Korobeynikov, A., Cao, L., Shcherbin, E., Nothias, L.-F., Dorrestein, P. C., & Pevzner, P. A. (2018). Dereplication of microbial metabolites through database search of mass spectra. *Nature Communications*, *9*(1), 4035. https://doi.org/10.1038/s41467-018-06082-8

Murphy, R. C., Fiedler, J., & Hevko, J. (2001). Analysis of Nonvolatile Lipids by Mass Spectrometry. *Chemical Reviews*, *101*(2), 479–526. https://doi.org/10.1021/cr9900883

Ourisson, G., Rohmer, M., & Poralla, K. (1987). Prokaryotic hopanoids and other polyterpenoid sterol surrogates. *Annual Review of Microbiology*, *41*, 301–333. https://doi.org/10.1146/annurev.mi.41.100187.001505

Patterson, R. L., Boehning, D., & Snyder, S. H. (2004). Inositol 1,4,5-Trisphosphate Receptors as Signal Integrators. *Annual Review of Biochemistry*, *73*(1), 437–465. https://doi.org/10.1146/annurev.biochem.73.071403.161303

Piel, J. (2002). A polyketide synthase-peptide synthetase gene cluster from an uncultured bacterial symbiont of Paederus beetles. *Proceedings of the National Academy of Sciences*, *99*(22), 14002–14007. https://doi.org/10.1073/pnas.222481399

Pond, D. W., Bell, M. V., Dixon, D. R., Fallick, A. E., Segonzac, M., & Sargent, J. R. (1998). Stable-Carbon-Isotope Composition of Fatty Acids in Hydrothermal Vent Mussels Containing Methanotrophic and Thiotrophic Bacterial Endosymbionts. *Applied and Environmental Microbiology*, *64*(1), 370–375. https://doi.org/10.1128/AEM.64.1.370-375.1998

Pranal, V., Fiala-Medioni, A., & Guezennec, J. (1997). Fatty acid characteristics in two symbiont-bearing mussels from deep-sea hydrothermal vents of the south-western Pacific. *Journal of the Marine Biological Association of the United Kingdom*, *77*(2), 473–492. https://doi.org/10.1017/S0025315400071812

Reue, K. (2011). A Thematic Review Series: Lipid droplet storage and metabolism: from yeast to man. *Journal of Lipid Research*, *52*(11), 1865–1868. https://doi.org/10.1194/jlr.E020602

Roeder, T. (1999). Octopamine in invertebrates. *Progress in Neurobiology*, *59*(5), 533–561. https://doi.org/10.1016/s0301-0082(99)00016-7

Rogers, S., Ong, C. W., Wandy, J., Ernst, M., Ridder, L., & van der Hooft, J. J. J. (2019). Deciphering complex metabolite mixtures by unsupervised and supervised substructure discovery and semi-automated annotation from MS/MS spectra. *Faraday Discussions*, *218*(0), 284–302. https://doi.org/10.1039/C8FD00235E

Roingeard, P., & Melo, R. C. N. (2017). Lipid droplet hijacking by intracellular pathogens. *Cellular Microbiology*, *19*(1). https://doi.org/10.1111/cmi.12688

Sachar, M., Anderson, K. E., & Ma, X. (2016). Protoporphyrin IX: The Good, the Bad, and the Ugly. *The Journal of Pharmacology and Experimental Therapeutics*, *356*(2), 267–275. https://doi.org/10.1124/jpet.115.228130

Sáenz, J. P., Grosser, D., Bradley, A. S., Lagny, T. J., Lavrynenko, O., Broda, M., & Simons, K. (2015). Hopanoids as functional analogues of cholesterol in bacterial membranes. *Proceedings of the National Academy of Sciences*, *112*(38), 11971–11976. https://doi.org/10.1073/pnas.1515607112

Schinnerl, J., Orlowska, E. A., Lorbeer, E., Berger, A., & Brecker, L. (2012). Alstrostines in Rubiaceae: Alstrostine A from Chassalia curviflora var. ophioxyloides and a novel derivative, rudgeifoline from Rudgea cornifolia. *Phytochemistry Letters*, *5*(3), 586–590. https://doi.org/10.1016/j.phytol.2012.05.019

Shannon, P., Markiel, A., Ozier, O., Baliga, N. S., Wang, J. T., Ramage, D., Amin, N., Schwikowski, B., & Ideker, T. (2003). Cytoscape: A software environment for integrated models of biomolecular interaction networks. *Genome Research*, *13*(11), 2498–2504. https://doi.org/10.1101/gr.1239303

Shimamura, M. (2020). Structure, metabolism and biological functions of steryl glycosides in mammals. *Biochemical Journal*, *477*(21), 4243–4261. https://doi.org/10.1042/BCJ20200532

Soltwisch, J., Heijs, B., Koch, A., Vens-Cappell, S., Höhndorf, J., & Dreisewerd, K. (2020). MALDI-2 on a Trapped Ion Mobility Quadrupole Time-of-Flight Instrument for Rapid Mass Spectrometry Imaging and Ion Mobility Separation of Complex Lipid Profiles. *Analytical Chemistry*, *92*(13), 8697–8703. https://doi.org/10.1021/acs.analchem.0c01747

Stanley, D. (2011). Eicosanoids: Progress towards manipulating insect immunity. *Journal of Applied Entomology*, *135*(7), 534–545. https://doi.org/10.1111/j.1439-0418.2010.01612.x

Stocker-Wörgötter, E. (2008). Metabolic diversity of lichen-forming ascomycetous fungi: Culturing, polyketide and shikimate metabolite production, and PKS genes. *Natural Product Reports*, *25*(1), 188–200. https://doi.org/10.1039/B606983P

Storey, M. A., Andreassend, S. K., Bracegirdle, J., Brown, A., Keyzers, R. A., Ackerley, D. F., Northcote, P. T., & Owen, J. G. (2020). Metagenomic Exploration of the Marine Sponge Mycale hentscheli Uncovers Multiple Polyketide-Producing Bacterial Symbionts. *MBio*, *11*(2). https://doi.org/10.1128/mBio.02997-19

Szafranski, K. M., Piquet, B., Shillito, B., Lallier, F. H., & Duperron, S. (2015). Relative abundances of methane- and sulfur-oxidizing symbionts in gills of the deep-sea hydrothermal vent mussel Bathymodiolus azoricus under pressure. *Deep Sea Research Part I: Oceanographic Research Papers*, *101*, 7–13. https://doi.org/10.1016/j.dsr.2015.03.003

Toledo, A., & Benach, J. L. (2015). Hijacking and Use of Host Lipids by Intracellular Pathogens. *Microbiology Spectrum*, *3*(6). https://doi.org/10.1128/microbiolspec.VMBF-0001-2014

van der Hooft, J. J. J., Wandy, J., Barrett, M. P., Burgess, K. E. V., & Rogers, S. (2016). Topic modeling for untargeted substructure exploration in metabolomics. *Proceedings of the National Academy of Sciences*, *113*(48), 13738–13743. https://doi.org/10.1073/pnas.1608041113

van der Hooft, J. J. J., Wandy, J., Young, F., Padmanabhan, S., Gerasimidis, K., Burgess, K. E. V., Barrett, M. P., & Rogers, S. (2017). Unsupervised Discovery and Comparison of Structural Families Across Multiple Samples in Untargeted Metabolomics. *Analytical Chemistry*, *89*(14), 7569–7577. https://doi.org/10.1021/acs.analchem.7b01391

Wandy, J., Zhu, Y., van der Hooft, J. J. J., Daly, R., Barrett, M. P., & Rogers, S. (2018). Ms2lda.org: Web-based topic modelling for substructure discovery in mass spectrometry. *Bioinformatics*, *34*(2), 317–318. https://doi.org/10.1093/bioinformatics/btx582

Wang, M., Carver, J. J., Phelan, V. V., Sanchez, L. M., Garg, N., Peng, Y., Nguyen, D. D., Watrous, J., Kapono, C. A., Luzzatto-Knaan, T., Porto, C., Bouslimani, A., Melnik, A. V., Meehan, M. J., Liu, W.-T., Crüsemann, M., Boudreau, P. D., Esquenazi, E., Sandoval-Calderón, M., … Bandeira, N. (2016). Sharing and community curation of mass spectrometry data with Global Natural Products Social Molecular Networking. *Nature Biotechnology*, *34*(8), 828–837. https://doi.org/10.1038/nbt.3597

Wenk, M. R. (2006). Lipidomics of host–pathogen interactions. *FEBS Letters*, *580*(23), 5541–5551. https://doi.org/10.1016/j.febslet.2006.07.007

Zhang, Y.-M., & Rock, C. O. (2008). Membrane lipid homeostasis in bacteria. *Nature Reviews. Microbiology*, *6*(3), 222–233. https://doi.org/10.1038/nrmicro1839

Supplementary Tables and Figures

Supplementary Table 1 | Information on the samples used in this study

MS_ID	Species	sampling_site	Tissue
MS70_01	*Bathymodiolus puteoserpentis*	MAR-Logatchev-Irina II	foot
MS70_02	*Bathymodiolus puteoserpentis*	MAR-Logatchev-Irina II	Gill
MS70_03	*Bathymodiolus puteoserpentis*	MAR-Logatchev-Irina II	rest
MS70_04	*Bathymodiolus puteoserpentis*	MAR-Logatchev-Irina II	foot
MS70_05	*Bathymodiolus puteoserpentis*	MAR-Logatchev-Irina II	Gill
MS70_06	*Bathymodiolus puteoserpentis*	MAR-Logatchev-Irina II	rest
MS70_07	*Bathymodiolus puteoserpentis*	MAR-Logatchev-Irina II	foot
MS70_08	*Bathymodiolus puteoserpentis*	MAR-Logatchev-Irina II	Gill
MS70_09	*Bathymodiolus puteoserpentis*	MAR-Logatchev-Irina II	rest
MS70_10	*Bathymodiolus puteoserpentis*	MAR-Logatchev-Irina II	foot
MS70_11	*Bathymodiolus puteoserpentis*	MAR-Logatchev-Irina II	Gill
MS70_12	*Bathymodiolus puteoserpentis*	MAR-Logatchev-Irina II	rest
MS70_13	*Bathymodiolus puteoserpentis*	MAR-Logatchev-Irina II	foot
MS70_14	*Bathymodiolus puteoserpentis*	MAR-Logatchev-Irina II	Gill
MS70_15	*Bathymodiolus puteoserpentis*	MAR-Logatchev-Irina II	rest
MS70_16	*Volcanidas insolatus*	Macauley cone	foot
MS70_17	*Volcanidas insolatus*	Macauley cone	gill
MS70_18	*Volcanidas insolatus*	Macauley cone	rest
MS70_19	*Volcanidas insolatus*	Macauley cone	foot
MS70_20	*Volcanidas insolatus*	Macauley cone	gill
MS70_21	*Volcanidas insolatus*	Macauley cone	rest
MS70_22	*Volcanidas insolatus*	Macauley cone	foot
MS70_23	*Volcanidas insolatus*	Macauley cone	gill
MS70_24	*Volcanidas insolatus*	Macauley cone	rest
MS70_25	*Volcanidas insolatus*	Macauley cone	foot
MS70_26	*Volcanidas insolatus*	Macauley cone	gill
MS70_27	*Volcanidas insolatus*	Macauley cone	rest
MS70_28	*Volcanidas insolatus*	Macauley cone	foot
MS70_29	*Volcanidas insolatus*	Macauley cone	gill
MS70_30	*Volcanidas insolatus*	Macauley cone	rest
MS70_31	*Bathymodiolus heckerae*	Chapopote	Foot
MS70_32	*Bathymodiolus heckerae*	Chapopote	rest
MS70_33	*Bathymodiolus heckerae*	Chapopote	Gill
MS70_34	*Bathymodiolus heckerae*	Chapopote	Foot
MS70_35	*Bathymodiolus heckerae*	Chapopote	rest
MS70_37	*Bathymodiolus heckerae*	Chapopote	Foot
MS70_38	*Bathymodiolus heckerae*	Chapopote	Gill
MS70_39	*Bathymodiolus heckerae*	Chapopote	rest

MS70_40	*Bathymodiolus heckerae*	Chapopote	Gill piece
MS70_41	*Bathymodiolus heckerae*	Chapopote	Foot
MS70_42	*Bathymodiolus heckerae*	Chapopote	Rest
MS70_43	*Bathymodiolus heckerae*	Chapopote	Foot
MS70_44	*Bathymodiolus heckerae*	Chapopote	Gill
MS70_45	*Bathymodiolus heckerae*	Chapopote	Gill
MS70_46	*Bathymodiolus heckerae*	Chapopote	Rest
MS70_47	*Gigantidas Childressi*	MC853	Foot
MS70_48	*Gigantidas Childressi*	MC853	Gill
MS70_49	*Gigantidas Childressi*	MC853	Mantle tissue
MS70_51	*Gigantidas Childressi*	MC853	Gill
MS70_52	*Gigantidas Childressi*	MC853	Mantle tissue
MS70_54	*Gigantidas Childressi*	MC853	Gill
MS70_55	*Gigantidas Childressi*	MC853	Mantle tissue
MS70_57	*Gigantidas Childressi*	MC853	Gill
MS70_58	*Gigantidas Childressi*	MC853	Mantle tissue
MS70_62	*Bathymodiolus thermophilus*	Tica vent field (East Pacific Rise)	Gill piece
MS70_63	*Bathymodiolus thermophilus*	Tica vent field (East Pacific Rise)	Foot
MS70_64	*Bathymodiolus thermophilus*	Tica vent field (East Pacific Rise)	Rest
MS70_65	*Bathymodiolus thermophilus*	Tica vent field (East Pacific Rise)	Gill piece
MS70_66	*Bathymodiolus thermophilus*	Tica vent field (East Pacific Rise)	Foot
MS70_67	*Bathymodiolus thermophilus*	Tica vent field (East Pacific Rise)	Rest
MS70_68	*Bathymodiolus thermophilus*	Tica vent field (East Pacific Rise)	Gill piece

Supplementary Table 2 | | Compounds identified by spectral library search in positive ion mode. Only matches to gold standard spectra are shown.

Compound_Name	Adduct	Precursor_MZ	MQScore	MZErrorPPM	SharedPeaks	MassDiff	LibMZ	SpecMZ	SpecCharge
Cer(d18:2/18:1)	M+H	561.512	0.786839	1793.3	8	1.00696	561.512	562.519	1
Cer(d18:2/20:1)	M+H	589.543	0.760367	2116.97	7	1.24805	589.543	588.295	1
DL-NORMETANEPHRINE	M+H	184.097	0.930551	5616.59	6	1.034	184.097	185.131	0
GalCer(d18:2/16:1)	M+H	695.534	0.818128	1444.94	11	1.005	695.534	696.539	1
NCGC00385123-01_C22H30O6	M+ACN+H	432.238	0.866486	2.32992	6	0.00100708	432.238	432.237	1
PC(14:0/20:4)	M+H	753.531	0.826957	173.824	6	0.130981	753.531	753.662	1
PC(15:0/18:3)	M+H	741.531	0.825661	2525.84	6	1.87299	741.531	743.404	1
PC(15:0/20:4)	M+H	767.547	0.834283	2141.86	6	1.64398	767.547	769.191	1
PC(16:1/17:1)	M+H	743.547	0.852592	174.844	6	742.8	743.547	743.677	2
PC(16:1/17:2)	M+H	741.531	0.838299	5.43244	7	740.516	741.531	741.527	2
PC(17:0/20:4)	M+H	795.578	0.815551	1250.66	6	0.994995	795.578	796.573	1
PC(17:0/22:6)	M+H	819.578	0.818229	822.388	6	0.674011	819.578	820.252	1
PC(17:1/18:1)	M+H	771.578	0.836209	2532.45	7	766.663	771.578	769.624	2
PC(18:0/22:4)	M+H	837.625	0.829436	192.223	6	0.161011	837.625	837.464	0
PC(18:1/22:1)	M+H	841.656	0.831812	1138.24	6	0.958008	841.656	840.698	1
PC(18:2/20:4)	M+H	805.562	0.723308	1446.17	10	1.16498	805.562	806.727	1
PC(19:0/20:4)	M+H	823.609	0.817338	1228.69	7	1.01196	823.609	824.621	1
PC(20:3/0:0)	M+H	545.348	0.802148	1846.45	7	1.00696	545.348	546.355	1
PC(O-16:0/20:4)	M+H	767.583	0.896121	1261.12	6	768.512	767.583	768.551	2
PC(O-18:0/22:5)	M+H	821.63	0.815303	598.815	6	0.492004	821.63	821.138	1
PC(P-16:0/16:1)	M+H	715.552	0.809042	1391.89	6	0.995972	715.552	716.548	1
PE(16:0/20:5)	M+H	737.5	0.732321	1362.72	8	1.005	737.5	738.505	1
PE(16:1/0:0)	M+H	451.27	0.710328	2231.52	7	1.00702	451.27	452.277	1
PE(18:0/20:4)	M+H	767.547	0.710975	1326.31	10	1.01801	767.547	768.565	1
PE(18:1/0:0)	M+H	479.301	0.731419	2101.02	7	1.00702	479.301	480.308	0
protoporphyrin IX	M+H	563.27	0.756514	10.7275	7	0.00604248	563.27	563.264	0
SM(d18:1/26:1)	M+H	840.708	0.794006	2224.31	6	1.87	840.708	842.578	1
TG(16:0/16:1/16:1)	M+NH4	802.705	0.703115	1253.24	13	1.00598	802.705	803.711	1

Supplementary Table 3 | Compounds identified by DEREPLICATOR+ in positive ion mode.

Name	Score	PeptideMass	SpectrumMass	MassDiff	Adduct	Charge	FDR
Coenzyme_Q_Coenzyme_Q8	18	726.559	727.564	0.00225	M+H	1	0
Î³-Tocotrienol_Î³-Tocotrienol	18	410.318	411.325	0.00027	M+H	1	0
TG(16:0/16:1(9Z)/22:5(7Z,10Z,13Z,16Z,19Z))	17	878.736	879.739	0.00427	M+H	1	0
TG(13:0/17:0/18:3(6Z,9Z,12Z))	17	800.689	801.695	0.00127	M+H	1	0
24,25-didehydrovitamin_D3	16	382.324	383.33	0.00129	M+H	1	0
TG(16:1(9Z)/18:4(6Z,9Z,12Z,15Z)/18:1(11Z))	14	850.705	851.711	0.00128	M+H	1	0
RK_397	14	636.387	637.394	0.0003	M+H	1	0
Milbemycin_E_Milbemycin_E	14	572.371	573.378	0.00029	M+H	1	0
nephthoside_monoacetate	14	570.356	571.362	0.00128	M+H	1	0
Ergosta-5,7,22-trien-3-ol_3-O-Î²-D-Galactopyranoside	14	558.392	559.396	0.00328	M+H	1	0
3-(4-Hydroxyphenyl)-2-propenoic_acid,_9CI_Hexacosyl_ester	14	528.454	529.461	0.00028	M+H	1	0
N/A	14	428.329	429.336	0.00028	M+H	1	0
Jaspic_acid_Jaspic_acid	14	410.282	411.292	-0.00271	M+H	1	0
Cholesta-5,8,22,24-tetraen-3beta-ol	14	380.308	381.315	0.00028	M+H	1	0
Albocycline,_9CI_11Î¾-Hydroxy	14	324.194	325.2	0.00127	M+H	1	0
3,13-Clerodadien-15-ol_(13Z)-form	14	290.261	291.265	0.00327	M+H	1	0
TG(18:4(6Z,9Z,12Z,15Z)/16:1(9Z)/20:4(8Z,11Z,14Z,17Z))	13	870.674	871.685	-0.00372	M+H	1	0
TG(14:0/16:1(9Z)/18:3(9Z,12Z,15Z))	13	798.674	799.679	0.00226	M+H	1	0
TG(12:0/12:0/18:4(6Z,9Z,12Z,15Z))	13	714.58	715.583	0.00427	M+H	1	0
DG(16:1(9Z)/20:3(8Z,11Z,14Z)/0:0)	13	616.507	617.518	-0.00373	M+H	1	0
DG(16:1(9Z)/20:4(8Z,11Z,14Z,17Z)/0:0)	13	614.491	615.496	0.00231	M+H	1	0
3,23-Dihydroxy-30-nor-12,20(29)-oleanadien-28-oic_acid_3-O-Î±-L-Arabinopyranoside	13	588.366	589.373	0.00029	M+H	1	0
Ergosta-3,5,24(28)-triene_Ergosta-3,5,24(28)-triene	13	380.344	381.351	0.00027	M+H	1	0
TG(15:0/18:3(6Z,9Z,12Z)/20:5(5Z,8Z,11Z,14Z,17Z))	12	860.689	861.692	0.00426	M+H	1	0
Pleuromutilin_1'-O-(9,12-Octadecadienoyl)	12	640.47	641.475	0.0023	M+H	1	0
Stigmasta-8,14,22-triene-3,5-diol_3-O-Î²-D-Xylopyranoside	12	558.392	559.398	0.00127	M+H	1	0

4-Methylcholesta-8,14,24-triene-3,23-diol	12	412.334	413.341	0.00028	M+H	1	0
calicoferol_D_(22E)-(8S)-3-hydroxy-22-methyl-9,10-seco-1,3,5(10),22-cholestatetraen-9-one	12	410.318	411.326	-0.00071	M+H	1	0
3-Deoxy-25-hydroxyvitamin_D3_(5Z,7E)-9,10-seco-5,7,10(19)-cholestatrien-25-ol	12	384.339	385.345	0.00128	M+H	1	0
24-Dehydroprevitamin_D3_(4E,6Z,8Z)-(1R)-4-methyl-9,10-seco-4(5),6,8,24-cholestatetraen-1-ol	12	382.324	383.33	0.00129	M+H	1	0
Ethyl_abietate	12	330.256	331.262	0.00129	M+H	1	0
Trisporic_acid_C_Trisporic_acid_C	12	306.183	307.187	0.00327	M+H	1	0
1,6,13-Xenicatrien-18,19-olide_1,6,13-Xenicatrien-18,19-olide	12	302.225	303.231	0.00129	M+H	1	0
Dicranenone_A_Dicranenone_A	12	288.173	289.179	0.00129	M+H	1	0
7,9-Octadecadiynoic_acid_7,9-Octadecadiynoic_acid	12	276.209	277.216	0.00028	M+H	1	0
Dihydro-5-(5-hydroxy-6-dodecenyl)-2(3H)-furanone_Dihydro-5-(5-hydroxy-6-dodecenyl)-2(3H)-furanone	12	268.204	269.211	0.00028	M+H	1	0

Supplementary Table 4 | Compounds identified by spectral library search in negative ion mode. Only matches to gold standard spectra are shown.

Compound_Name	Adduct	Precursor_MZ	Charge	MQScore	MZErrorPPM	SharedPeaks	MassDiff	LibMZ	SpecMZ	SpecCharge
Arachidonic acid	M-H	304.46	1	0.742165	0	6	0	304.46	303.232	1
PE(14:0/16:1)	M-H	661.468	1	0.819904	1699.29	8	1.12402	661.468	660.344	1
PE(15:1/16:1)	M-H	673.468	1	0.777667	1493.82	6	1.00604	673.468	672.462	1
PE(16:0/16:1)	M-H	689.5	1	0.920402	1460.51	9	1.00702	689.5	688.493	1
PE(16:0/18:1)	M-H	717.531	1	0.736122	443.177	7	0.317993	717.531	717.213	1
PE(16:1/0:0)	M-H	451.27	1	0.915587	2231.45	6	1.00699	451.27	450.263	1
PE(16:1/16:1)	M-H	687.484	1	0.83814	1522.94	7	1.047	687.484	686.437	1
PE(16:2/16:1)	M-H	685.468	1	0.913494	1467.67	10	1.00604	685.468	684.462	1

Supplementary Table 5 | Compounds identified by DEREPLICATOR+ in positive ion mode.

Name	Score	PeptideMass	MassDiff	Adduct	Charge	FDR
11,15-Dihydroxy-9-oxo-5,13,17-prostatrienoic_acid,_9CI_1,15-Lactone	16	332.199	-0.00072	M+H	1	0
Chalcolactone	15	350.209	0.00229	M+H	1	0
Amphidinolactone_A_Amphidinolactone_A	15	334.214	-0.00171	M+H	1	0
Microcarpalide_Microcarpalide	14	300.194	-0.00072	M+H	1	0
Attenol_A_Attenol_A	13	382.272	-0.00072	M+H	1	0
11,12-Epoxy-1,7-cembradiene-3,4,19-triol_19-Carboxylic_acid	13	352.225	-0.00072	M+H	1	0
10,20-Epoxy-2,10,12(20)-cembratriene-4,7,8-triol_10,20-Epoxy-2,10,12(20)-cembratriene-4,7,8-triol	13	336.23	-0.00073	M+H	1	0
2,16:7,8-Diepoxy-1(15),3,11-cembratrien-20-oic_acid_2,16:7,8-Diepoxy-1(15),3,11-cembratrien-20-oic_acid	13	332.199	0.00029	M+H	1	0
15-Hydroxy-6,9,12-octadecatrien-16-olide_15-Hydroxy-6,9,12-octadecatrien-16-olide	13	292.204	-0.00073	M+H	1	0
3-Oxo-2-(2-pentenyl)-1-cyclopentanehexanoic_acid_3-Oxo-2-(2-pentenyl)-1-cyclopentanehexanoic_acid	13	266.188	-0.00171	M+H	1	0
Foromacidin_A_Aglycone,_18-deoxo,_9-ketone	12	368.22	0.00328	M+H	1	0
Flavofungin,_8CI,_9CI_28,29-Dihydro,_23-deoxy,_24,29-dihydroxy	12	668.414	0.00058	M+2H	2	0
7,8-Epoxy-2-oxo-1(15),3,11-cembratrien-16-oic_acid_7,8-Epoxy-2-oxo-1(15),3,11-cembratrien-16-oic_acid	12	332.199	-0.00072	M+H	1	0
3,4,5,6,9,10-Hexahydro-4,6,9-trihydroxy-10-nonyl-2H-oxecin-2-one_3,4,5,6,9,10-Hexahydro-4,6,9-trihydroxy-10-nonyl-2H-oxecin-2-one	12	328.225	-0.00072	M+H	1	0
8(17)-Labdene-7,15-diol_15-Carboxylic_acid	12	322.251	-0.00072	M+H	1	0
15-Hydroxy-3,7,11-cembratrien-19-oic_acid_7,8-Dihydro	12	322.251	-0.00072	M+H	1	0
5,6-Dihydroxy-8,11,14-eicosatrienoic_acid_Î´-Lactone	12	320.235	-0.00073	M+H	1	0
Didemnilactone_(10E,14Z)-Isomer,_17,18-dihydro	12	318.219	-0.00071	M+H	1	0
13-Hydroxy-10-oxo-11-octadecenoic_acid_Lactone	12	294.219	-0.00071	M+H	1	0

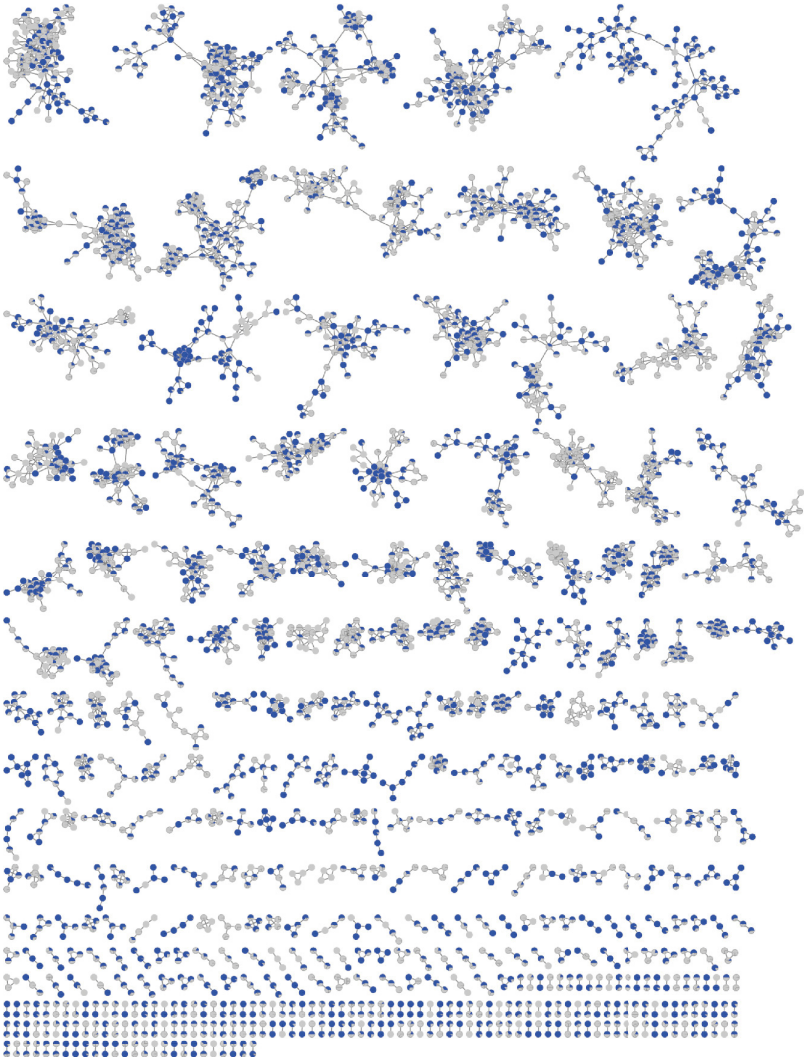

Supplementary Figure 1 | Several groups of lipid analogues were only detected in the gills and are likely of bacterial origin. Visualization of the distribution of the different lipids in symbiotic and non-symbiotic tissues (positive ionization mode). The compounds are colored according to the tissues in which they were detected: symbiotic tissue in blue and non-symbiotic tissue in grey. The compounds that were not related to any other were removed from this presentation.

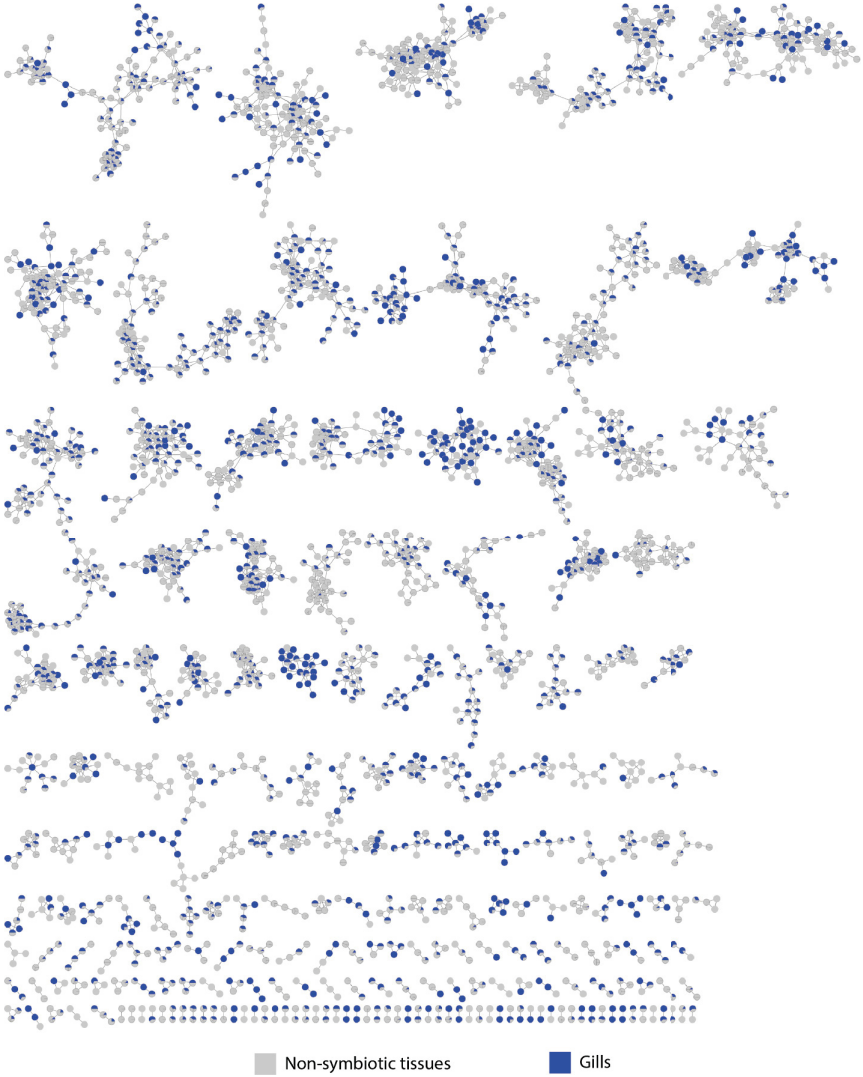

***Supplementary Figure 2* | No lipid group specific to the symbiotic tissue could be identified in the data acquired in negative ionization mode.** Visualization of the distribution of the different lipids in symbiotic and non-symbiotic tissues (negative ionization mode). The compounds are colored according to the tissues in which they were detected: symbiotic tissue in blue and non-symbiotic tissue in grey. The compounds that were not related to any other were removed from this presentation.

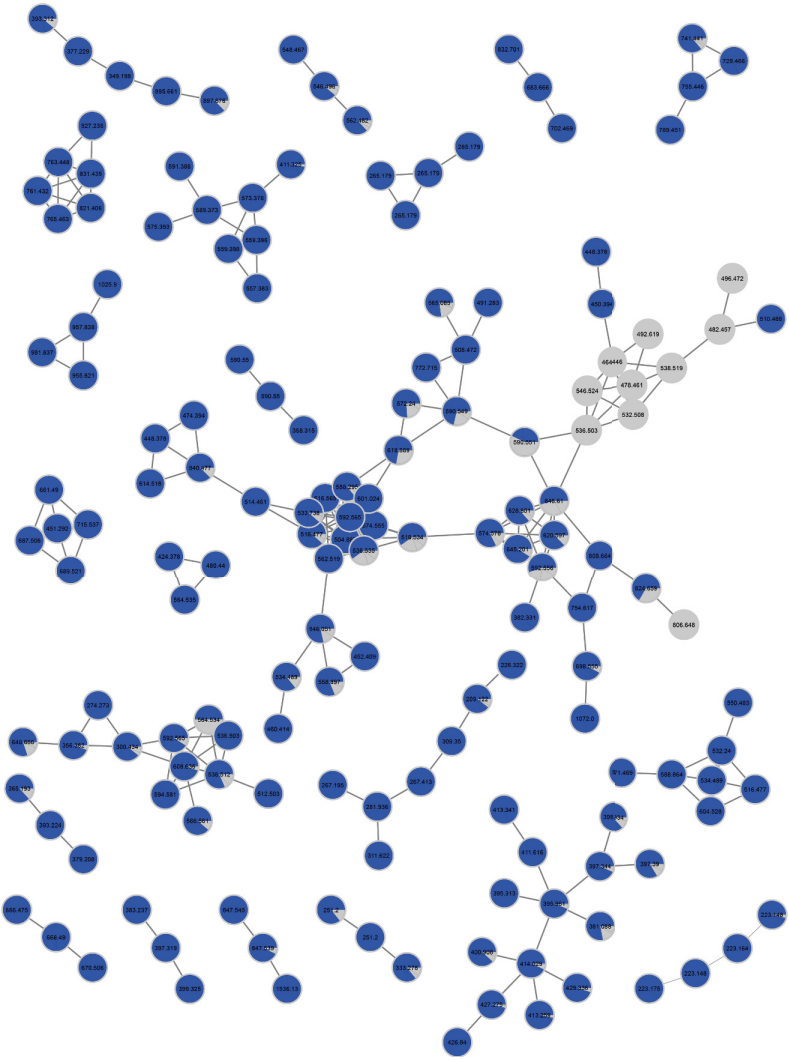

Supplementary Figure 3 | Lipid groups which were mainly or only present in the symbiotic tissues. Subset of the molecular network representing the MS/MS data acquired in positive ionization mode. The nodes are colored according to the tissues in which the compounds were detected: symbiotic tissue in blue and non-symbiotic tissue in grey. Each node is labeled with the m/z value of its parental ion.

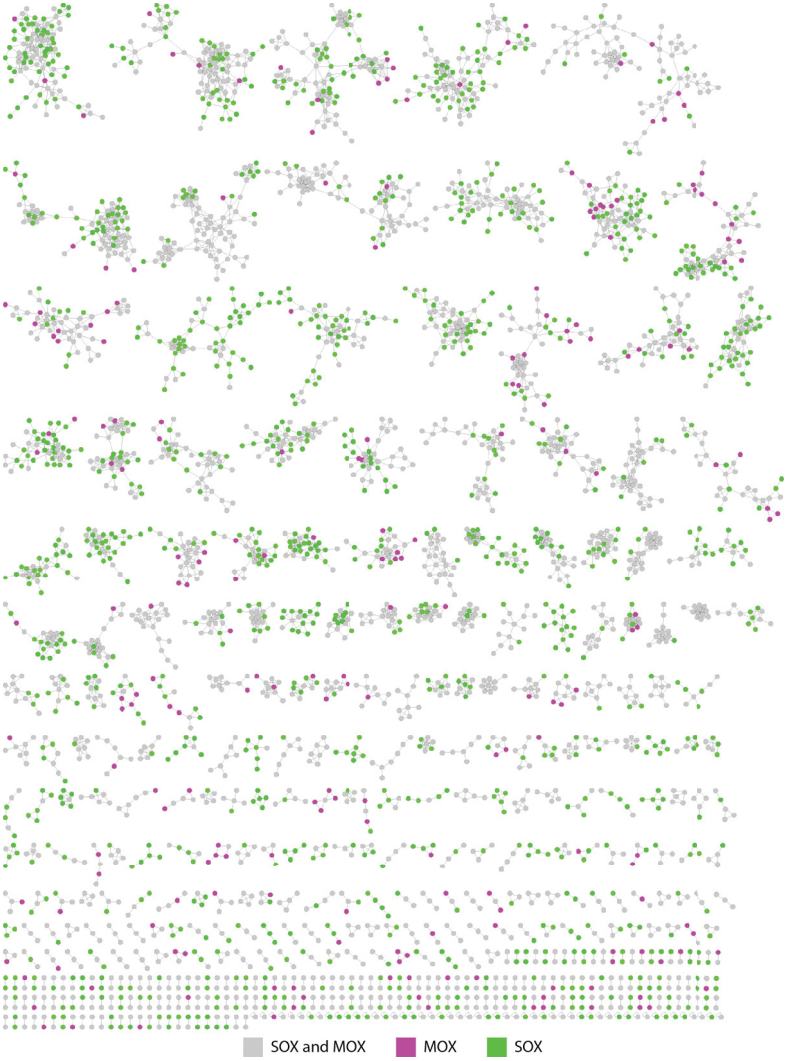

Supplementary Figure 4 | | Several groups of lipid analogues were linked to the presence of MOX or SOX symbionts. Visualization of the distribution of the different lipids according to the symbiont composition of the mussel species in which they were detected (positive ionization mode). The compounds are colored according to symbiont: magenta compounds are only present when MOX is present, green compounds are only present when SOX is present, grey compounds are present regardless of the symbiont composition. The compounds which were not related to any other were removed from this visualization.

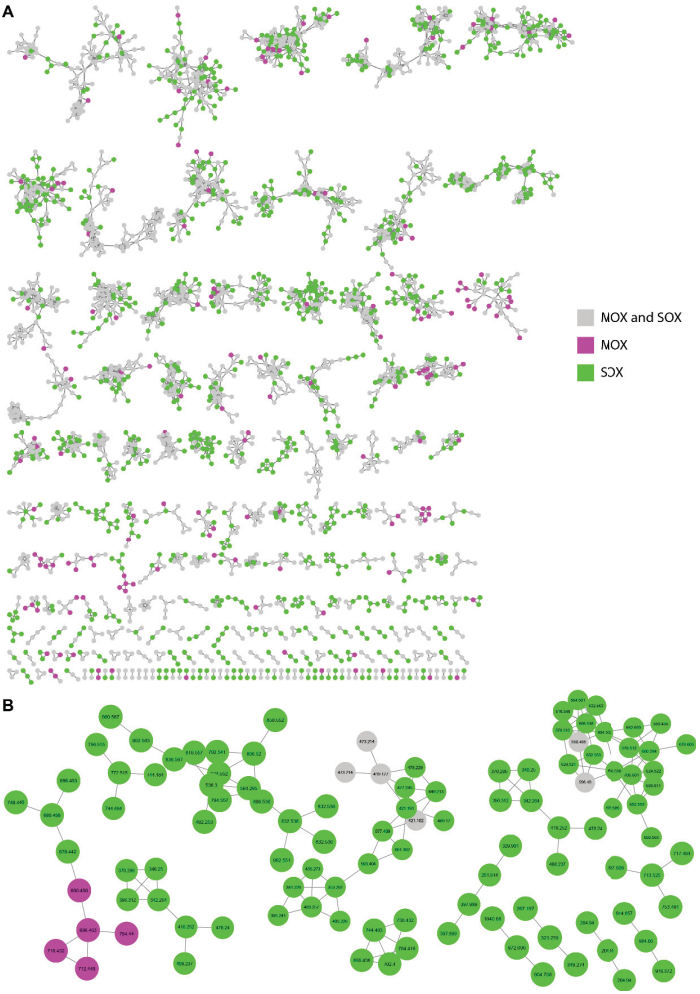

Supplementary Figure 5 | Several groups of lipid analogues were linked to the presence of MOX or SOX symbionts. A, Visualization of the distribution of the different lipids according to the symbiont composition of the mussel species in which they were detected (negative ionization mode). The compounds that were not related to any other were removed from this presentation. **B,** Subset of the molecular network representing the lipid groups linked to the presence of a specific symbiont. Each node is labeled with the m/z value of its parental ion. None of those compounds could be structurally identified. The nodes are colored according to symbiont: magenta compounds were only present when MOX was present, green compounds were only present when SOX was present, grey compounds were present regardless of the symbiont composition.

Chapter II

A new form of C_1-carrier discovered in deep-sea methanotrophic symbionts

A new form of C_1-carrier discovered in deep-sea methanotrophic symbionts

Dolma Michellod[1], Patric Bourceau[1], Jan Tebben[2,3], Benedikt Geier[1], Dennis Jakob[1], Maxim Rubin-Blum[4], Nicole Dubilier[1,5], Manuel Liebeke[1]

[1] Max Planck Institute for Marine Microbiology, Celsiusstraße 1, 28359 Bremen, Germany

[2] University of Bremen – UFT, Leobener Straße 6, 28359 Bremen, Germany

[3] Alfred Wegener Institute, Am Handelshafen 12, 27570 Bremerhaven, Germany

[4] Israel Limnology and Oceanography Research, Tel Shikmona, 3108000, Haifa, Israel

[5] MARUM, Center for Marine Environmental Sciences of the University of Bremen, 28359 Bremen, Germany

* *The manuscript is in preparation and has not been revised by all authors.*

* Author contribution: D.M, P.B and M.L conceived the study. D.M drafted the manuscript, with support from M.L, and contributions from B.G and P.B. D.M prepared the mussel samples, run the LC-MS/MS measurements and analyzed the data. P.B prepared the bacterial samples for additional MS/MS data and preliminary NRM data acquired by J.T. D.M, B.G and D.J collected the MALDI-MSI data. P.B ran blast searches. M.RB provided the phylogenetic tree. D.M analyzed the data.

Abstract

Many coenzymes are considered essential nutrients, which are required for physiological function, as they participate directly to numerous biochemical reactions and metabolic processes. In addition to a set of ubiquitous coenzymes, some organisms require unique coenzymes for their metabolism. Methanogens and methanotrophs, for example, have evolved a unique set of coenzymes, including tetrahydromethanopterin (H_4MPT). In this chapter, we studied in depth a specialized group of metabolites specific to methane-oxidizing bacteria and deep-sea mussel associations. Mass spectrometry enabled us to determine the structure of those specialized metabolites and identify them as a form of the coenzyme H_4MPT, and the esterified analogues of that coenzyme, described for the first time. The distribution of those specialized metabolites lead us to hypothesize potential functions for them in the symbiosis. Based on the abundance of the bacterial coenzyme in the host tissue we hypothesized that the host could use this bacterial coenzyme as an alternative to an essential coenzyme that animals need to obtain from their diet. In an extreme environment as the deep-sea, where resources are scarce, the host might need to adapt to the resources made available by its symbionts. The esterified analogues of the coenzyme co-localize with the methane-oxidizing symbionts and are likely to still be functional coenzymes. We hypothesized that fatty acids anchored the coenzyme to the cytoplasmic membrane of the bacteria. It would allow the oxidation of formaldehyde, a toxic intermediate of methane oxidation, to take place at the membrane surface rather than freely diffuse in the cytoplasm and would represent a new way for the symbiont to counteract the toxicity of formaldehyde.

Introduction

Coenzymes are small organic molecules which facilitate enzymatic reactions. Those small organic molecules can be prenol lipids, vitamins, vitamin-derivatives, or nucleotide derivatives. Coenzymes participate directly in numerous biochemical reactions and metabolic processes, such as cellular respiration. They carry chemical groups between enzymes, some mediate the transfer of functional groups, while others participate in oxidation-reduction reactions. Many coenzymes are considered essential nutrients, as

they are required for physiological function, although animals are not able to synthesize all of them and need to obtain some from their diet or their microbiome.

Coenzymes, such as ATP, NADH, and ubiquinone, are present in all living organisms and participate in core metabolic reactions. Some organisms require unique coenzymes for their metabolism. Methanogens, for example, have evolved a unique set of coenzymes, including: coenzyme F420, coenzyme B, coenzyme M, methanofuran, and tetrahydromethanopterin (H_4MPT) (DiMarco et al., 1990; Wolfe, 1985). H_4MPT, a coenzyme involved in the C_1-transfer reaction has been detected in aerobic methane oxidizing organisms (methanotrophs) (Chistoserdova et al., 1998a).

Here, we identified new forms of the H_4MPTcoenzyme in methane-oxidizing symbionts of deep-sea mussels. Using a spatial metabolomics method, a technique to visualize the distribution of individual metabolites in the tissue, Geier et al. detected specialized metabolites at the host-microbe interface in the deep-sea mussel *Bathymodiolus puteoserpentis* (Geier et al., 2020). In total, six related metabolites were detected but remained unidentified in their chemical structure. The screening of 11 other deep-sea mytilid species revealed that those metabolites were linked to the presence of methane-oxidizing (MOX) symbionts. Interestingly, a free-living relative of the MOX symbiont, *Methyloprofundus sediment* strain WF1, only contains traces of one of these specialized metabolites, the unknown metabolite (577 *m/z*). The identity of those specialized metabolites, their origin, and function in the symbiosis remains unknown.

Deep-sea mussels of the genus *Bathymodiolus* are associated with gammaproteobacterial sulfur-oxidizing (SOX) symbionts, MOX symbionts, or both (Duperron, 2010). The symbionts largely reside in specialized epithelial gill cells called bacteriocytes. Despite a functioning digestive system, these mussels depend on their chemosynthetic bacteria for nutrition ((DeChaine & Cavanaugh, 2006; Duperron, 2010). How carbon is transferred from symbionts to host is still under debate. Currently, lysosomal intracellular digestion and ‘leaking’ from intact symbiont cells to the host’s digestive system seem to play a role (Fiala-Médioni et al., 2002; Geier, 2020; Kádár et al., 2008; Streams et al., 1997).

Here, we identified the unknown metabolite group as esterified analogues of the coenzyme methenyl-tretrahydromethanopterin (methenyl-dH$_4$MPT) using liquid chromatography tandem mass spectrometry (LC-MS/MS), ultra-violet spectra and fluorescence information. We studied the diversity of the esterified analogues of the coenzyme in bathymodiolin symbioses by analyzing the metabolomics profile of six mussel species, belonging to three different genera and harboring either SOX and MOX or only MOX as primary symbionts (Figure 2A). Finally, using mass spectrometry imaging (MSI), we mapped the distribution of the different coenzyme analogues to gain better insight into their distribution and infer potential functions for this new group of metabolites. The presence of esterified analogues of the coenzyme methenyl-dH$_4$MPT in a wide range of mussel-MOX symbiotic associations, their absence in related free-living bacteria, and their distribution at the host-symbiont interface suggests that these specialized metabolites play an important role in the associations between MOX symbionts and deep-sea mussels.

Results and Discussion

We identified the unknown metabolite (577 *m/z*) as methenly-dH$_4$MPT and the other specialized metabolites as esterified analogues of methenyl-dH$_4$MPT. The structure and identity of the specialized metabolites remained elusive; manual and automated database searches did not return matches. We detected two variations of the specialized metabolites: with fatty acids and without. Compounds harboring fatty acid(s) are esterified structural analogues of an unknown metabolite (577 *m/z*). Representative tandem mass spectrometry (MS/SM) spectra of the two most abundant analogues (869 *m/z* and 813 *m/z*) can be seen in **Figure 1A** and **1B.** The MS/MS spectra show that the metabolites are composed of a core of 541 Da (unknown metabolite 577 *m/z* – 2H$_2$O) containing a pentose moiety and features one or two fatty acids. The pentose and the fatty acid moieties fragmented separately from the parental ion, indicating that the two moieties are not attached to each other. The fragment 255.09 *m/z* ($C_{12}H_{11}ON_6$, 255.0987 *m/z* ± 0.0007) indicated a core rich in nitrogen (**Figure 1A** and **1B**). The exact mass, fragmentation pattern, UV profile, and fluorescent spectra of the unknown metabolite (577 *m/z*) matched the description of methenyl-dephosphotetrahydromethanopterin (methenyl-dH$_4$MPT)

(DiMarco et al., 1990; Donnelly et al., 1985; Eikmanns & Thauer, 1985; van Beelen et al., 1984). This identification is supported by preliminary NMR data of methenyl-dH$_4$MPT isolated from a culture of *M. sedimenti*, a free-living relative of the MOX symbionts (Schwörer et al., 1993). Methenyl-dH$_4$MPT consists of a methylated pterin linked to an aminobenzoyl moiety, which is bound to a side chain made of a ribitol residue linked to a ribose. It contains two chromophoric groups, the pterin and the aminobenzoyl moiety, explaining the strong ultraviolet–visible (UV-Vis) spectra; the compound and its esterified analogues emit at 338 nm. In addition, methenly-dH$_4$MPT emits a fluorescence characteristic of 7-methylpterin, a methyl group which distinguishes methanopterin from all other pterin-containing natural products.

The unknown metabolite (577 *m/z*) was identified as methenyl-dH$_4$MPT. dH$_4$MPT Is the dephospho-form of the H$_4$MPT C$_1$-carrier, found in methanotrophic archaea and most methylotrophic bacteria (Chistoserdova et al., 1998b; Vorholt et al., 1999). H$_4$MPT-dependent C$_1$-transfer enzymes drive the oxidation of formaldehyde, a toxic intermediate of methylotrophy, into formate. Formate can then be used for energy production or be incorporated into biomass. Methenyl-dH$_4$MPT is one intermediate of this H$_4$MPT-dependent pathway (**Figure 1C**), the intermediate with the higher stability (Thauer et al., 1996). The MOX symbionts' genome encodes most of the enzymes described so far for dH$_4$MPT synthesis and the H$_4$MPT-dependent C$_1$ transfer (Ponnudurai et al., 2017). Methenyl-dH$_4$MPT is an intermediate of the energy metabolism of MOX symbionts and has been described in numerous methane oxidizing species. As stated previously, we detected two variations of the specialized metabolites: with fatty acids and without. Compounds harboring fatty acid(s) were esterified structural analogues of methenyl-dH$_4$MPT. This is the first time that methenyl-dH$_4$MPT's esterified analogues (methenyl-dH$_4$MPT(FA)) have been described.

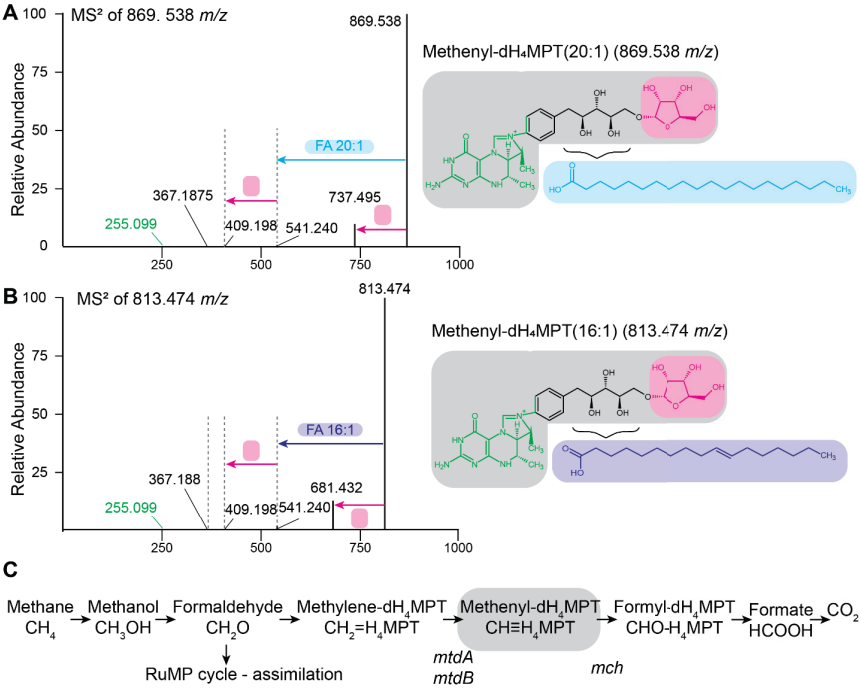

Figure 1 | Specialized metabolites identified as analogues of methenyl-dH4MPT decorated with fatty acids. **A, B,** Characteristic LC-MS/MS fragmentation pattern for *m/z* 869 and *m/z* 813, two of the most abundant analogues. One can observe the loss of a pentose (-132.0417 Da) and a fatty acids. The fragment ion *m/z* 541.2402 represents methenyl-dH4MPT (577 *m/z*) after the loss of two water molecules. **C,** General pathway of methane oxidation by aerobic methylotrophic bacteria. The enzymes names are in italic. Methenyl-dH4MPT is highlighted in grey. *mtdA, mtdB*, NAPD-dependent methylene-dH4MPT dehydrogenase; *mch*, methenyl-dH4MPT cyclohydrolase.

Diversity and abundances of dH4MPT analogues vary between mussel species; differences could not be explained by the habitat, the phylogeny of the MOX symbionts or the phylogeny of the host. Using MS1-based transformation identity networks, an approach that allows the simultaneous visualization of chemical relationships across all detected ions, we identified 23 different analogues in the six species of bathymodiolin mussels hosting MOX symbionts analyzed in this study (**Figure 2B**). The general chemical composition of all 23 metabolites was confirmed with LC-MS/MS. They all had a structure similar to the metabolites described previously (Geier et al., 2020): a core of 577 Da, containing a pentose moiety and decorated with one or two

fatty acids. The structure similarity was reflected in their fragmentation patterns and the clustering of the 12 most abundant metabolites within the same molecular network (**Figure 2C**).

The diversity and abundance of dH$_4$MPT analogues varied between host species (**Figure 2D** and **Supplementary Figure 1**). *Bathymodiolus heckerae* (19), *Bathymodiolus brooksi* (22) and *Bathymodiolus puteoserpentis* (21) displayed the highest diversity of metabolites, with up to 22 different metabolites detected in *B. brooksi*. *"Bathymodiolus" childressi* and *Gigantidas mauritanicus* showed the lowest abundance and diversity, only harboring six and five dH$_4$MPT analogues, respectively. *"B." childressi* and *G. mauritanicus* also differed from the other mussel species by containing nearly twice the levels of methenyl-dH$_4$MPT than its esterified analogues.

Although large differences in methane concentration were observed between hydrothermal vents and cold seeps, the mussels' habitat did not seem to impact the diversity and composition of the analogues (**Supplementary Figure 2**). The methane concentration measured at a vent site serves only as a proxy for the conditions experienced by the mussels. The mussels are found at diffuse flows sites, where methane concentrations were not measured. We cannot exclude, based on this observation, that methane concentration experienced by the mussels do not have an impact on the abundance and diversity of the methenyl-dH$_4$MPT and its esterified analogues.

The phylogenetic relationships between the MOX symbionts did neither affect the diversity nor the abundance of this new class of metabolites (**Supplementary Figure 1 and 3**). The MOX symbionts belong to a monophyletic group within Methylomonadanceae (Methylococcales), named Marine Methylotrophic Group I (MMG1). Most host species harbor only one type of MOX symbiont, but some hosts appear to be more flexible in bacterial partner selection. For example, *B. heckerae* hosts two lineages of MOX symbionts, belonging to two different subclades (M. Rubin, personal communication). The metabolites were detected in mussels that hosted MOX from subclade 1, MOX from subclade 2, or both. This suggests that the esterified analogues of methenyl-dH$_4$MPT are deeply rooted within the metabolism of the MG1 clade. MMG1 contains both symbiotic and free-living bacteria. To investigate a free-living member of MMG1, we screened

Methyloprofundus sedimenti strain WF1, the only current MMG1 member available in culture. We found methenyl-dH$_4$MPT in *M. sedimenti* extracts, but none of its esterified analogues, suggesting methenyl-dH$_4$MPT is synthesized by all members of MMG1 clade while the esterified analogues result from the interaction of the MOX symbionts and the mytilid hosts, and are specific to the symbiotic member of the MMG1 clade.

The fatty acid composition of the methenyl-dH$_4$MPT analogues reflects the fatty acid composition of the mussel's gills. The fatty acid moiety was the only variable part of the methenyl-dH$_4$MPT(FA)s, and varied in both, length and saturation. We identified 18 different fatty acids, ranging from C_{15} to C_{22}, both unsaturated and saturated (**Figure 2B** and **Supplementary Table 1**). Even through most fatty acids are widely distributed in the tree of life, a few fatty acids, as well as their relative abundance, can be used as biomarkers. The fatty acid composition of the methenyl-dH$_4$MPT(FA)s could reveal which partner produces and uses the esterified analogues. The fatty acid composition of the deep-sea bathymodiolin mussels reflects the contribution by the bacterial symbionts to their nutrition(Ben-Mlih et al., 1992; Kellermann et al., 2012; Phleger et al., 2005). In contrast to non-symbiotic, shallow water mussels, deep-sea mussels lack planktonic fatty acids (e.g., 16:4n-3, 18:4n-3 or 18:3n-3). Instead, deep-sea mussels are enriched in monounsaturated fatty acids (representing up to 69% of the fatty acids), recognized as bacterial biomarkers. The monounsaturated fatty acid 16:1 is the most abundant fatty acid (up to 56%) in the gills of several species of bathymodiolin mussels (Ben-Mlih et al., 1992; Kellermann et al., 2012; Phleger et al., 2005; Pond et al., 1998). The abundance of monounsaturated fatty acids in the gills of bathymodiolin mussels was reflected in the fatty acid composition of methenyl-dH$_4$MPT(FA)s, which was also dominated by monounsaturated fatty acids (**Figure 2C**). Methenyl-dH$_4$MPT(20:1) was present in all species and was often the most abundant. Methenyl-dH$_4$MPT(16:1), methenyl-dH$_4$MPT(18:1), methenyl-dH$_4$MPT(20:1), and methenyl-dH$_4$MPT(16:1/16:1) — when present — were the most abundant across all species. C:18 and C:20 polyunsaturated fatty acids are common in deep-sea mussels and are synthesized through chain elongation and unsaturation of the symbiont fatty acids (Kellermann et al., 2012; Pond et al., 1998). While the partner responsible for this transformation is unknown, higher concentration in the gill tissues compared to non-symbiotic tissues suggests that one of

the symbionts is responsible. However, most bacteria are unable of such transformations as they lack the necessary O_2-dependent fatty acids desaturases (Cronan, 2006; Mansilla & de Mendoza, 2005; Russell & Nichols, 1999; Zhu et al., 2006). The origin of the saturated fatty acid (16:0 and 18:0) present in other abundant metabolites (methenyl-dH$_4$MPT(16:0) and methenyl-dH$_4$MPT(18:0)) was harder to determine as they are abundantly present in both, animal and bacteria. Overall, the fatty acid composition of the specialized metabolites reflected the fatty acid composition of the gill tissue. We would expect to see similar methenyl-dH$_4$MPT(FA)s in the free-living *M. sedimenti* as its predominant fatty acids (16:0, 16:1ω9c, 16:1ω9t, 16:1ω8c and 16:2ω9,14) are similar to the fatty acids described in the mussel gills (Tavormina et al. 2015). However, we could not identify any esterified analogues in *M. sedimenti*. In the deep-sea mussels, most of the fatty acids attached to methenyl-dH$_4$MPT were of bacterial origin. However, due to the nutritional dependence of the host towards its symbionts and the absence of esterified analogues in the free-living relative, we cannot make a clear statement regarding the producer of the esterified analogues. Their biochemical origin and function remain unclear.

Methenyl-dH$_4$MPT is present in symbiont-free tissues, while its esterified analogues are most abundant in the tissue colonized by the symbionts. We used mass spectrometry imaging (MSI) to better understand the origin and possible role the methenyl-dH$_4$MPT(FA)s play in the symbiosis. Using meta-FISH, Geier et al. showed that in *B. puteoserpentis*, methenyl-dH$_4$MPT(20:1) was concentrated in bacteriocytes while methenyl-dH$_4$MPT was more abundant in the host tissue surrounding the bacteriocytes (Geier et al., 2020). We observed a similar distribution for methenyl-dH$_4$MPT(16:1) and methenyl-dH$_4$MPT in *B. puteosepentis*, *B. brooksi*, and *B. heckerae* (**Figure 3**). In *B. childressi* the metabolites were not abundant enough to recognize clear distributions (**Supplementary Figure 4**). All methenyl-dH$_4$MPT(FA)s displayed a similar distribution (**Supplementary Figure 5 to 10**). The identity of the fatty acids attached to methenyl-dH$_4$MPT did not have an impact on the broader distribution of the metabolite, suggesting that all esterified analogues have a similar function. Methenyl-dH$_4$MPT is more abundant in the symbiont-free region than in the part of the gills colonized by MOX symbionts, while

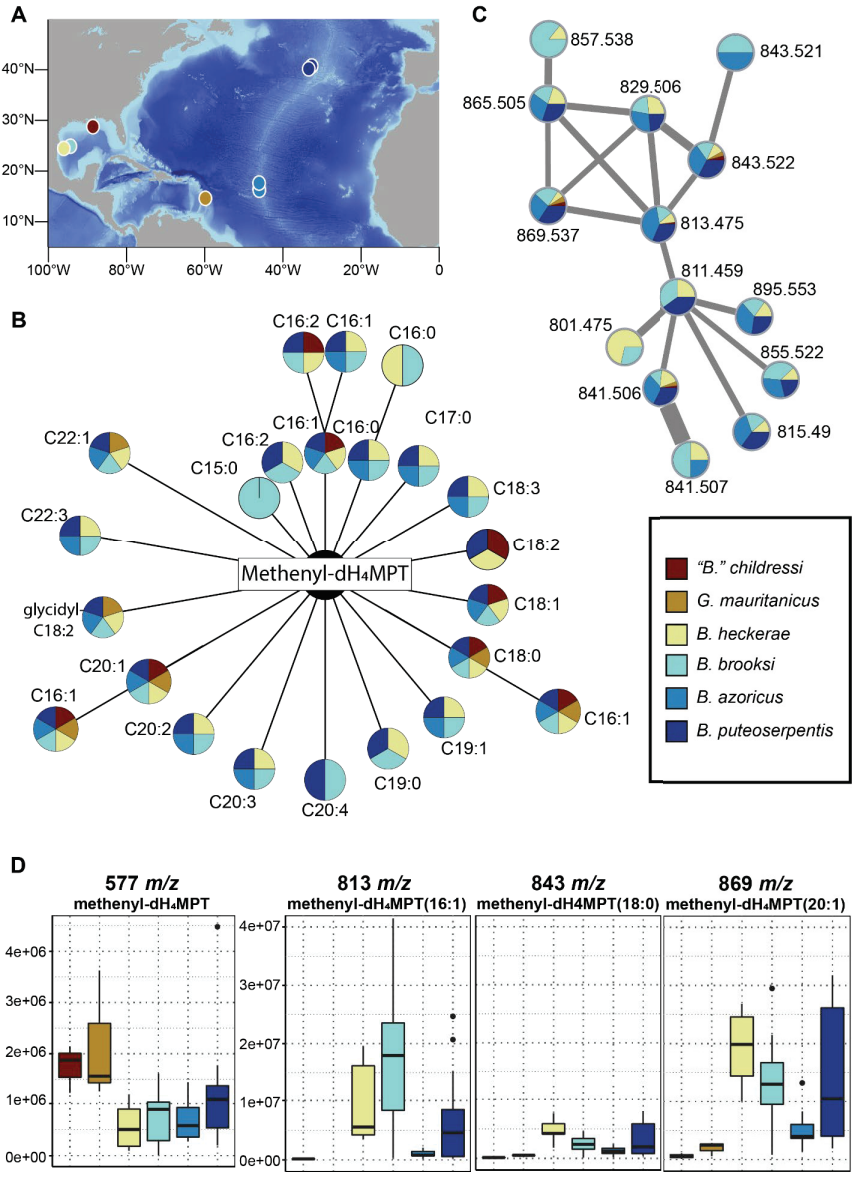
A
40°N
30°N
20°N
10°N
100°W
80°W
60°W
40°W
20°W
0
B
Methenyl-dH4MPT
C16:2
C16:1
C16:0
C17:0
C18:3
C18:2
C18:1
C18:0
C16:1
C19:1
C19:0
C20:4
C20:3
C20:2
C20:1
C16:1
glycidyl-C18:2
C22:3
C22:1
C15:0
C16:2
C16:1
C16:0
C
857.538
843.521
865.505
829.506
843.522
869.537
813.475
811.459
895.553
801.475
855.522
841.506
815.49
841.507
"B." childressi
G. mauritanicus
B. heckerae
B. brooksi
B. azoricus
B. puteoserpentis
D
577 m/z
methenyl-dH4MPT
813 m/z
methenyl-dH4MPT(16:1)
843 m/z
methenyl-dH4MPT(18:0)
869 m/z
methenyl-dH4MPT(20:1)
4e+06
3e+06
2e+06
1e+06
0e+00
4e+07
3e+07
2e+07
1e+07
0e+00

Figure 2: Diversity and biogeography of the symbiosis-associated analogues of methenyl-dH$_4$MPT. **A,** Sampling locations of the different mussels analyzed in this study. **B,** Network representation of the diversity of this metabolite class, the length of the edges represents the length of the fatty acids. The nodes are color coded by mussel species. **C**, MS^2 network of the new metabolite class generated from the LC-MS/MS data using GNPS and Cytoscape. The nodes are color coded according to the mussel species in which they were detected. The thickness of the edge represents the cosine (min cosine = 0.5). **D**, Relative abundance (wet weight normalized) of methenyl-dH$_4$MPT and of the three most abundant esterified analogues of methenyl-dH$_4$MPT.

methenyl-dH$_4$MPT(FA)s are more abundant in the symbiotic region. Those different distributions could indicate different functions.

The presence of methenyl-dH$_4$MPT in the non-symbiotic tissue of the host suggests that methenyl-dH$_4$MPT plays a role in the mussel's physiology. Why is methenyl-dH$_4$MPT, a metabolic intermediate of the MOX symbiont, more abundant in the host tissue? The accumulation of methenyl-dH$_4$MPT in the host tissue might be a result of the digestion of the symbiont by the host. The other intermediates of the H$_4$MPT C$_1$-transfer pathway (see **Figure 1**) are labile at low pH and would be degraded by lysosomal digestion. Methenyl-dH$_4$MPT is stabilized by the presence of the methenyl group and is intact after an overnight incubation at pH 2 (Beelen et al., 1984). However, it could easily be stripped of its more labile parts: the pentose, the ribitol, and the aminobenzoyl moiety. Why would the host neglect easily accessible sources of carbon?

The mussel might use dH$_4$MPT as an additional C$_1$-carrier. The presence of methenyl-dH$_4$MPT in the non-symbiotic tissues of the host suggests that the coenzyme might have a specific function in the host tissue (**Supplementary Figure 11**). The host might have found a way to use the coenzyme to its own advantage. C$_1$ metabolism in animals is essential to the synthesis of DNA, polyamines, amino acids, creatine, and phospholipids. The ability of an animal to methylate important cell components, such as lipids and proteins, depends on the presence of two coenzymes: colobamine (vitaminB12) and folate. Both, vitamin B12 and folate, are essential coenzymes that animals must obtain through their diet, as they cannot synthesize them. Folate, in its tetrahydrofolate form (H$_4$F), is not only used by animals, but by numerous bacteria as well. H$_4$F has an analogous structure to dH$_4$MPT (**Figure 4**) and, in methylotrophic bacteria, fulfils a similar function. A few bacteria, including the MOX symbionts, can produce both H$_4$F and dH$_4$MPT (Marx et al., 2003; Ponnudurai et al., 2017). Most enzymes involved in the bacterial C$_1$-transfer pathway are highly specific for H$_4$MPT or H$_4$F (Acharya 2005). One exception is *mtdA*, which can catalyze the formation of both methenyl-H$_4$F and methenyl-

dH_4MPT, although the catalytic efficiency is 20-fold lower for H_4F- than that of dH_4MPT-dependent reactions (Vorholt et al., 1999). In general, enzymes for those pathways catalyze analogous reactions but most of them seem to have evolved independently (Maden, 2000; Shima et al., 2002). To our knowledge, the specificity of animal enzymes involved in the C_1-transfer pathway for H_4F versus H_4MPT has never been tested. One could imagine that, over time, deep-sea mussels adapted to use both H_4F and H_4MPT as co-enzymes for C_1 transfer.

The esterified analogues of H_4MPT described in this study are different from other H_4MPT analogues described previously as their extension is not attached to the end of the coenzyme, but to the center of it. The methenyl-dH_4MPT(FA)s were only present in the symbiotic tissues (gills). The synthesis of dH_4MPT is costly, it requires at least 10 enzymes and would not be produced in abundance without a function. In the deep-sea mytilid symbioses, the esterified analogues of dH_4MPT are more abundant than dH_4MPT and only preset in the symbiotic tissue (gill). They were absent from the non-symbiotic tissues (mantel and foot) of the mussel. This suggests a strong association with the MOX symbionts. Those observations lead to two questions: (1) does the presence of fatty acids hinder the C_1-carrier function of dH_4MPT? (2) What advantages do the esterified coenzymes provide to the symbionts?

Several structural analogues of H_4MPT have been described in methanotrophic and methylotrophic bacteria (Maden, 2000) (**Figure 4B to D**). They all have an alternative terminal extension, which does not hinder their function as they are all functional analogues. The analogues described in this study are different as their extension is not attached to the end of the metabolite, but to the center of it. The MS/MS fragmentation patterns of the coenzyme analogues have indicated that one or two fatty acids were attached to the hydroxyl group of the ribitol moiety. We do not yet know the exact position of the fatty acid on the ribitol chain, it could be attached to any of the three hydroxyl groups as indicated in **Figure 3**. Ribitol in dH_4MPT has three hydroxyl groups (in 2c, 3c and 4c), which could potentially accept a fatty acid, however, we only found dH_4MPT analogues with one or two fatty acids attached.

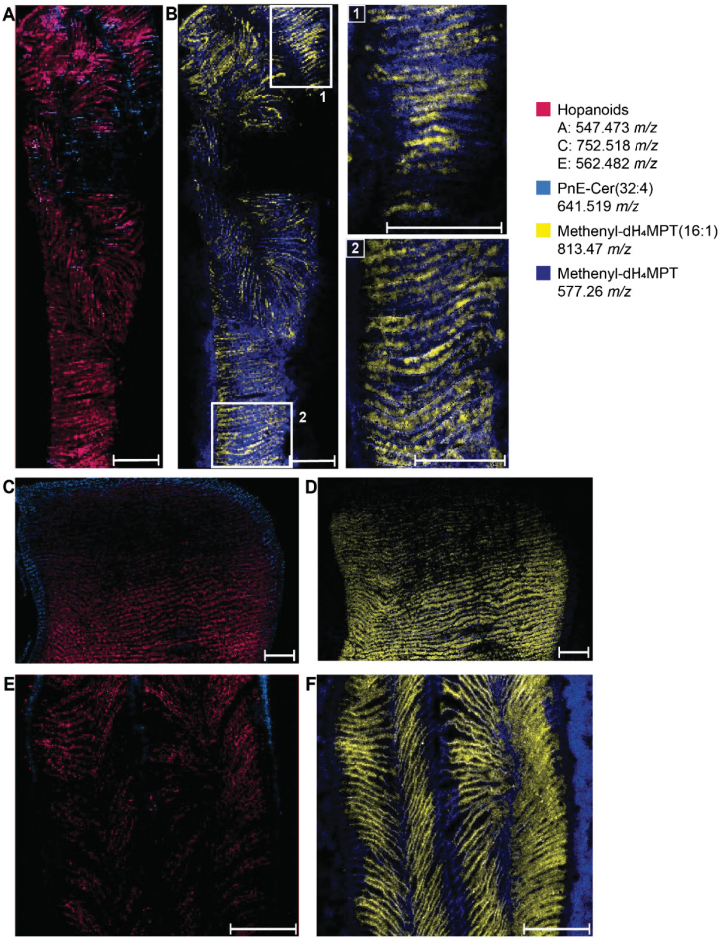

Figure 3: Methenyl-dH$_4$MPT and its analogues have different distributions in deep-sea mussel gills. Methenyl-dH$_4$MPT is more abundant in symbiont-free area while its esterified analogues are more abundant in the area colonized by MOX symbionts. **A, C and E,** Distribution of different metabolites partner specific in the gills of (A) *B. heckerae*, (B) *B. brooksi* and (C) *B. puteoserpentis*. phosphonoethanolamine ceramide PnE-Cer(32:4) (641.519 *m/z*, pale blue) is used to mark the symbiont-free area of the mussel gills, and different hopanoids (red) are used to mark the area colonized by the methane oxidizer symbionts: bacteriohopane-32,33,34,35-tetrol (547.473 *m/z*) is used for *B. heckerae*, 35-aminobacteriohopane-31,32,33,34-tetrol (562.482 *m/z*) is used for *B. puteoserpentis* and 752.518 *m/z* is used for

B. brooksi. **B, D and F,** Distribution of methenyl-dH$_4$MPT (577.262 *m/z*, dark blue) and one of its most abundant analogue, methenyl-dH$_4$MPT(16:1) (813.47 *m/z*, yellow). The scale bars represent 1 mm.

Preliminary results suggest that the presence of a fatty acid does not prevent interactions between the coenzyme and the different enzymes involved in formaldehyde oxidation. Two enzymes of the bacterial H$_4$MPT C$_1$-transfer pathway were crystalized, and their structure and interaction with the substrates were studied in details (Acharya et al., 2005; Ermler et al., 2002; Huang et al., 2020). Both enzymes were isolated from *Methhylorubrum extorquens* AM1 (Huang et al. 2020; Ermler et al. 2002; Acharya et al. 2005). We looked at the crystal structures of those two enzymes to assess how the addition of a fatty acid could impact the coenzyme-enzyme interaction. The first enzyme of the pathway, H$_4$MPT-dependent formaldehyde activating enzyme (*fae*), the ribitol and ribose group contribute only slightly to the binding, while most of the interactions occur between the enzyme and the coenzyme's pterin and aminobenzoyl groups, enclosed in the binding cleft (Acharya et al., 2005). With the second enzyme of the pathway, NADP-dependent methylene-H$_4$MPT dehydrogenase (*mtdA*), the coenzyme's pterin and aminobenzoyl group are also enclosed in a binding cleft. However, in this enzyme, the ribitol moiety contributes more strongly to the binding. The first hydroxyl group (in position 2c, see **Figure 4D**) of the ribitol contributes to the active conformation of the enzyme through strong interactions with the enzyme's residue (Huang et al., 2020) (**Supplementary Figure 12**). A fatty acid in the 2c position would prevent the attachment of the substrate to the enzyme. As long as the fatty acids are attached on the 3c or 4c positions, methenyl-dH$_4$MPT(FA) should still be able to interact with the enzymes. It should be noted that the crystal structures were obtained from *M. extorquens* AM1, an Alphaproteobacterium which is not closely related to our gammaproteobacterial symbionts. Even with an identity of 56 to 60% between the enzyme amino acid sequences, those observations should be treated with caution. Further work would be needed to see if the *mtdA* of the symbionts differs from the *mtdA* of their free-living relative, suggesting adaptation to accommodate the new analogues. Overall, these preliminary results indicate that the esterified form can fulfil the same function as dH$_4$MPT.

We hypothesized that the esterified analogues of dH_4MPT participate to confine the toxic formaldehyde near the membrane. If the esterified coenzymes fulfill the same function as the coenzyme, what advantages do they provide to the symbionts? At the moment we can only hypothesize. The identity of the fatty acids attached to the dH_4MPT broadly reflects the fatty acid composition of the gills. In addition, all analogues have a similar distribution, suggesting that the type of fatty acid attached to dH_4MPT does not have an impact on the function of the analogues. One could imagine that the fatty acid anchores the coenzyme to the cytoplasmic membrane of the bacteria. If the coenzyme is anchored to the membrane by one or two fatty acids attached to the ribitol (in c3 or c4 position), the pterin and aminobenzoyl group would still be free to interact with the enzymes. The symbionts oxidize methane to methanol through the monooxygenase complex (PmoCAB) and further to formaldehyde, using methanol dehydrogenase (XoxF). Those steps take place in the periplasm. The formaldehyde is transported into the symbiont's cytoplasm where it can be oxidized to formate, to generate electrons and reducing equivalents. This energy-generating step can be accomplished by the dH_4mPT-dependent C_1 transfer pathway. This step is essential as accumulation of formaldehyde is toxic for the cell. The enzymes involved in the formaldehyde oxidation pathway described so far are cytoplasmic proteins. However, one could imagine the advantages for the formaldehyde oxidation to take place at the membrane surface rather than freely diffusing in the cytoplasm. Tail-anchored membrane proteins are characterized by a single C-terminal transmembrane domain (TMD) that is responsible for both, targeting and anchoring the enzymes to the membrane. These tail-anchored membrane proteins are held in the cytoplasmic membrane by the TMD, while the entire functional N-terminus portion faces the cytosol. Lipid-anchored proteins, such as fatty acylated proteins or prenylated proteins are another type of membrane proteins, typically more difficult to identify by sequencing and would require experimental work such as western blot or proteomic analyses of the membrane fraction. Anchoring the enzymes involved in the dH_4MPT-dependent C_1-transfer pathway would represent a new way to counteract the toxicity of formaldehyde.

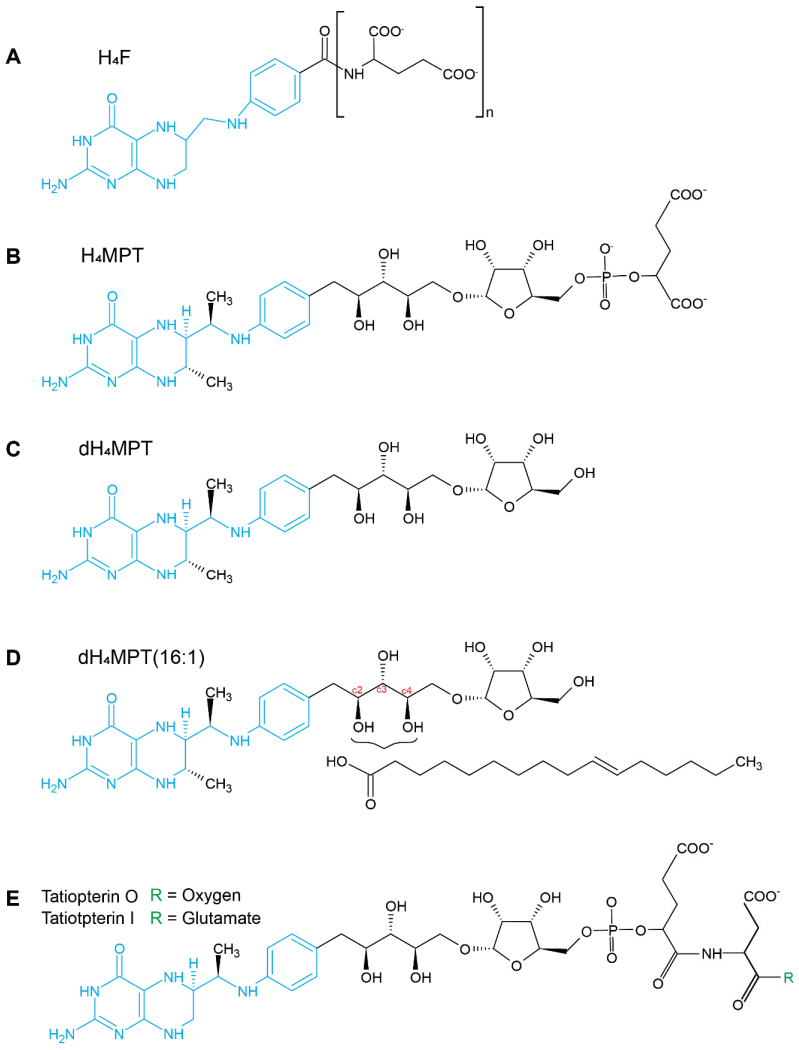

Figure 4: Structure of several pterins found in bacteria and archaea. **A**, Structure of tetrahydrofolate (H_4F), a coenzyme used by bacteria and animals. Structure of **B,** tetrahydromethanopterin (H_4MPT) and **C,** its dephospho form (dH_4MPT), those coenzymes have been described in archaea and bacteria. **D,** Example of an esterified dH_4MPT isolated from MOX symbionts of deep-sea mussels. **E,** Tatiopterin O and Tatiopterin I, coenzyme variations found in *Methanomicrobiaceae archaea*. The structure shared by all coenzymes are highlighted in blue. The carbon numbering of the ribitol group of $dH_4MPT(16:1)$ are indicated in red.

Conclusion

New techniques have led to the discovery of a previously unknown specialized metabolite, present only in methane-oxidizing bacteria living in symbiosis with deep-sea mytilid mussels (Geier et al., 2020). Our analyses revealed the broad diversity of the esterified analogues of dH_4MPT, a diversity not previously described in model organisms. The close association between invertebrates and bacterial symbionts turned out to not only impact secondary metabolism but primary metabolism as well. The specialized metabolites described here are analogues of a coenzyme involved in the energy metabolism of the symbiont.

Based on their abundance, diversity, and distribution, we hypothesized on their origin and function in the different partners. The presence of a bacterial coenzyme in the host tissues led us to hypothesize that the host could use dH_4MPT as an alternative coenzyme for C_1 transfer metabolism. Animals use folate as a coenzyme for C_1 transfer, and they need to obtain folate through their diet or via symbionts as they are not able to synthesize it themselves (Blatch et al., 2010; Salem et al., 2014). In an extreme environment like the deep-sea, where resources are scarce, the host might need to adapt to the resources made available by its symbionts. Folate transporters have consistently been shown to be higher expressed in deep-sea mussels than in their shallow water relatives (Zheng et al., 2017). A high expression of folate transporters has been linked to folate deficiency in some mammals and insects (Qiu et al., 2007; Salem et al., 2014; Zhao et al., 2011), suggesting that the host may lack folate. If folate is scarce, there is another coenzyme for C_1 transfer present in high abundance in the host tissue: dH_4MPT, the bacterial co-enzyme. Deep-sea mussels would be the first known animals to use dH_4MPT as a coenzyme, which so far has only been described in archaea and bacteria. While many examples of a host high-jacking a bacterial-derived compound to their own advantage have been described (Hughes & Sperandio, 2008), never has the host been observed to use a bacterial coenzyme as part of its own primary metabolism. We think this hypothesis deserves to be tested. The presence and location of dH_4MPT and dH_4MPT(FA) in other marine invertebrates hosting MOX symbionts could be determined using metabolomics imaging and LC-MS/MS. Furthermore, the dH_4MPT and H_4F content of *B. childressi*

mussels kept in aquaria could be analyzed under various nutrition conditions. These mussels were depleted from their symbionts and their diet complemented by filter feeding. Comparing the wild type to the starved mussels, and their respective transcriptomic changes would give us a good overview of C_1-transfer coenzymes in the symbiosis.

Many questions remain open including the cellular location and function of the dH_4MPT analogues. We might be able to answer some of them by comparing the cellular location of the enzymes of the dH_4MPT dependent pathways in the MOX symbionts and in the free-living *M. sedimenti*, lacking the esterified analogues. Finding the MOX symbionts' enzyme in the membrane fraction would support the idea of an anchoring of the coenzyme as a strategy to contain toxic formaldehyde to specific subcellular locations.

Material and Methods

Sample collection. Bathymodiolin mussels were collected along the Mid Atlantic ridge, the East Pacific rise, the Barbados Accretionary prism, the Tonga-Kermadec Ridge, and in the Gulf of Mexico. Seven species of the genus *Bathymodiolus* and three species of the genus *Gigantidas* were analyzed in this study. *"B." childressi* and *"B." mauritanicus* were considered as *Gigantidas* in this study following the classification from (Thubaut et al., 2013). For details on the species and sampling sites, see **Supplementary Table 2**. The mussels were collected using a remotely operated vehicle (ROV) and brought back to the surface in an insulated container to prevent temperature changes. Once on board, the gills were dissected from the mussel, snap-frozen in liquid nitrogen and stored at −80°C.

***Methyloprofundus sedimenti* cultivation.** The symbionts free-living relative, *M. sedimenti* strain WF1 was grown in 2L, 10L, and 20L Schott bottles filled to 50% with air as headspace. All cultures were kept at room temperature and agitated by slow stirring at around 100 rpm. Methanol was added to a concentration of 0.1% (vol) as the sole carbon and energy source. Modified nitrate mineral salts medium (NMS, ATCC 1306) was used, with a trace element solution with a formulation containing Cerium at a final concentration of 400 nM to support the function of the lanthanide dependent xoxF type methanol dehydrogenase. No vitamin solution was added to the medium which was

otherwise prepared as previously reported (see **Supplementary information**). When optical density ceased to increase, cells were harvested by centrifugation (4700g x 15 min) and stored at -20 °C until further processing. Before extraction, cells were thawed, resuspended in 500 ml MQ water and acidified to pH 2 with HCl. After overnight incubation cell debris was removed by centrifugation and the remaining supernatant extracted.

Solvents for LC–MS/MS. All organic solvents were LC–MS grade, using acetonitrile (ACN; Honeywell, Honeywell Specialty Chemicals), isopropanol (IPA; BioSolve) and formic acid (FA; Sigma-Aldrich), methanol (MeOH, BioSolve). Water was deionized using the Astacus MembraPure system (MembraPure).

Metabolite extraction for LC-MS. Lipids were extracted from small pieces of frozen gills (50–100 mg) using a mixture of ACN, MeOH and H_2O (2:2:1 v/v/v) and a stainless bead. The tissues were disrupted by one passage through a FastPrep (FastPrep24™, BM Biomedicals) for 40 seconds at 4 m/sec. The tissues were pelleted by centrifugation (1 min, 10,000 rpm, 4°C) and 750 µL of supernatant was transferred to HPLC-MS vials (1.5-HRSV 9mm Screw Thread Vials, Thermo Fisher™). Samples (50 µL each) were combined to form a quality control sample.

High-resolution LC–MS/MS. The analysis was performed using a QExactive Plus Orbitrap (Thermo Fisher Scientific), equipped with a HESI probe and a Vanquish Horizon UHPLC system (Thermo Fisher Scientific). The lipids were separated on an Accucore C30 column (150 × 2.1 mm, 2.6 µm, Thermo Fisher Scientific), at 40°C, using a solvent gradient. Buffer A (60/40 ACN/H2O, 10 mM ammonium formate, 0.1% FA) and buffer B (90/10 IPA/ACN, 10 mM ammonium formate, 0.1% FA) (Breitkopf et al., 2017) were used at a flow rate of 350 µl min^{-1}. The lipids were eluted from the column with a gradient starting at 0% buffer B (**Supplementary Table 3**). The injection volume was 10 µl. In the same run, MS measurements were acquired in positive-ion and negative-ion mode for a mass detection range of m/z = 150–1,500. Resolution of the mass analyzer was set to 70,000 for MS scans and 35,000 for MS/MS scans at m/z = 200. MS/MS scans of the eight most abundant precursor ions were acquired in positive-ion and negative-ion mode. Dynamic exclusion was enabled for 30 s and collision energy was set to 30 eV (for more information see **Supplementary Table 4**).

Tissue sectioning. The CMC-embedded gills were cross-sectioned at 10 µm thickness using a cryostat (Leica CM3050 S, Leica Biosystems) at a chamber temperature of −35°C and an object holder temperature of −22°C. Individual sections were thaw-mounted onto a coated Poly-L-lysine coated slide (Thermo scientific) and subsequently frozen in the cryostat chamber. Slides with tissue sections were stored in a vacuum desiccator (Duran) filled with silica granules (Carl Roth) to avoid condensation.

Matrix application. To assist ionization of the metabolites during AP-MALDI-MSI, a crystalline layer, called an ionization matrix, was applied to the sample surface.

DHAP matrix application. For matrix application, a total amount of 30 mg DHAP, dissolved in 1.5 mL acetone, was transferred in the brass pan of a home-built sublimation chamber. The reservoir was preheated to 130°C and, after solvent evaporation, the sample was placed on a water-cooled surface of 4°C directly over the pan with the sample facing downward. The whole setup was transferred to a vacuum of three millibar and the matrix was allowed to sublimate and redeposit for six minutes before the process was stopped by ventilation with N_2. After removing the sample slide from the apparatus, it was immediately transferred to the ion source of the mass analyzer. The six minute deposition resulted in a matrix coverage of 236 ± 34 µg/cm^2 as derived from weight measurements of clean glass slides before and after sublimation under the same conditions.

DHB matrix application. Before AP-MALDI matrix application, the sample was warmed to room temperature under a dry atmosphere in a sealed slide container (LockMailer microscope slide jar, Sigma-Aldrich) filled with silica granules (Carl Roth) to avoid condensation on the cold glass slide. In addition, optical images of the tissue section were acquired using a digital microscope (VHX-5000 Series, Keyence) before application of the matrix. To apply the matrix, we used an ultrafine pneumatic sprayer system with N_2 gas (SMALDIPrep, TransMIT) (Kompauer et al., 2017) to deliver 100 µl of a 30 mg ml^{-1} solution of 2,5-dihydroxybenzoic acid (S-DHB, 98% purity, Sigma-Aldrich) dissolved in 50% methanol:water with 0.1% trifluoroacetic acid (TFA). Spraying consisted of 10 layers at a flow rate of 10 µL min^{-1} (layer 1) and 15 µL min^{-1} (layers 2-10) resulting in a homogeneous layer of crystalline matrix with approximate grain sizes of one micron.

To locate the field of view and facilitate laser focusing, a red or blue marker was applied adjacent to the matrix-covered tissue section.

AP-MALDI-MSI measurements. MS-imaging measurements were carried out with an atmospheric pressure matrix-assisted laser desorption/ionization (AP MALDI) ion source ("AP-SMALDI10", TransMIT GmbH, Germany), coupled to a Fourier transform orbital trapping mass spectrometer (Q Exactive™ HF, Thermo Fisher Scientific GmbH, Germany). MS images were collected by scanning the matrix-covered tissue sections at different step sizes (5 µm, 10 µm or 30 µm) without overlapping of the laser spots. Mass spectra were acquired in positive-ion mode with a mass resolving power of 240,000 at *m/z* 200. For more details on each measurements details refer to **Supplementary Table 5.**

AP-MALDI-MSI data processing. After measurements, the Thermo *.raw files were centroided and converted to *.mzML with MSConvert GUI (ProteoWizard 3.0.9810) and then converted to *.imzML using the imzML Converter 1.3 (Race et al., 2012). The *imzML MALDI-MSI data were imported into SCiLS Lab (version 2021a Pro).

Molecular networking. Molecular networks were visualized in Cytoscape (v3.8.2) (Shannon et al., 2003), the AP-MALDI-MSI MS1 data were created using the MetaNetter 2 app (Burgess et al., 2017) and the LC-MS/MS data using GNPS (Wang et al., 2016).

To create the MS1 molecular network with MetaNetter 2 app, the MSI peak list was imported to create nodes. A list of major chemical transformations was used to calculate the mass differences as edges between the nodes. Adducts ($[Na]^+$, $[K]^+$ and $[NH_4]^+$) and isotopes were excluded from the network to reduce the redundancy of metabolite nodes and the complexity of the network. We used $[H]^+$ adducts to display the diversity of the measured metabolites. Nodes were then labelled based on the mussels' species in which they were detected. Coloring and reshaping of the nodes was performed in Cytoscape (3.8.2) using the cluster and annotation data.

A molecular network was created using the online workflow (https://ccms-ucsd.github.io/GNPSDocumentation/) on the GNPS website (http://gnps.ucsd.edu). The data were filtered by removing all MS/MS fragment ions within +/− 17 Da of the precursor *m/z*. MS/MS spectra were window filtered by choosing only the top 6 fragment ions in the

+/− 50 Da window throughout the spectrum. The precursor ion mass tolerance was set to 0.02 Da and a MS/MS fragment ion tolerance of 0.02 Da. A network was then created where edges were filtered to have a cosine score above 0.5 and more than six matched peaks. Furthermore, edges between two nodes were kept in the network if —and only if— each of the nodes appeared in each other's respective top 10 most similar nodes. Finally, the maximum size of a molecular family was set to 100, and the lowest scoring edges were removed from molecular families until the molecular family size was below this threshold. The spectra in the network were subsequently searched against GNPS' spectral libraries. The library spectra were filtered in the same manner as the input data. All matches kept between network spectra and library spectra were required to have a score above 0.7 and at least six matched peaks.

Acknowledgements

We would like to thank the crew and captains of the scientific vessels Meteor (M114-2 and M126), Nautilus (Na 58), Pourquoi pas? (BioBaz 2013) and Atlantis (AT21-02), and their ROV pilots who helped us collect our extensive set of mussel species. We thank A. Garsdal, M. Weinhold, and J. Beckmann for support in the laboratory. We thank T. Bien (University of Münster) for help with sample preparation. This work was funded by the Max Planck Society, the DFG Cluster of Excellence 'The Ocean in the Earth System' at MARUM (University of Bremen), a Gordon and Betty Moore Foundation Marine Microbiology Initiative Investigator Award through grant GBMF3811 to Prof. N. Dubilier, and a European Research Council Advanced Grant (BathyBiome, grant 340535).

Code and data availability

The LC-MS/MS data will be made available on MetaboLights. The MALDI-MSI data can be found on Metaspace (https://metaspace2020.eu/), see **Supplementary Table 2** for the Metaspace ID.

References

Acharya, P., Goenrich, M., Hagemeier, C. H., Demmer, U., Vorholt, J. A., Thauer, R. K., & Ermler, U. (2005). How an Enzyme Binds the C1 Carrier Tetrahydromethanopterin: STRUCTURE OF THE TETRAHYDROMETHANOPTERIN-DEPENDENT FORMALDEHYDE-ACTIVATING ENZYME (Fae) FROM METHYLOBACTERIUM EXTORQUENS AM1*. *Journal of Biological Chemistry*, *280*(14), 13712–13719. https://doi.org/10.1074/jbc.M412320200

Beelen, P. van, Labro, J. F. A., Keltjens, J. T., Geerts, W. J., Vogels, G. D., Laarhoven, W. H., Guijt, W., & Haasnoot, C. A. G. (1984). Derivatives of methanopterin, a coenzyme involved in methanogenesis. *European Journal of Biochemistry*, *139*(2), 359–365. https://doi.org/10.1111/j.1432-1033.1984.tb08014.x

Ben-Mlih, F., Marty, J. C., & Fiala-Médioni, A. (1992). Fatty acid composition in deep hydrothermal vent symbiotic bivalves. *Journal of Lipid Research*, *33*(12), 1797–1806. https://doi.org/10.1016/S0022-2275(20)41337-9

Blatch, S. A., Meyer, K. W., & Harrison, J. F. (2010). Effects of dietary folic acid level and symbiotic folate production on fitness and development in the fruit fly Drosophila melanogaster. *Fly*, *4*(4), 312–319. https://doi.org/10.4161/fly.4.4.13258

Breitkopf, S., Ricoult, S., Yuan, M., Xu, Y., Peake, D., Manning, B., & Asara, J. (2017). A relative quantitative positive/negative ion switching method for untargeted lipidomics via high resolution LC-MS/MS from any biological source. *Metabolomics*, *13*. https://doi.org/10.1007/s11306-016-1157-8

Burgess, K. E. V., Borutzki, Y., Rankin, N., Daly, R., & Jourdan, F. (2017). MetaNetter 2: A Cytoscape plugin for ab initio network analysis and metabolite feature classification. *Journal of Chromatography. B, Analytical Technologies in the Biomedical and Life Sciences*, *1071*, 68–74. https://doi.org/10.1016/j.jchromb.2017.08.015

Chistoserdova, L., Vorholt, J. A., Thauer, R. K., & Lidstrom, M. E. (1998a). C1 Transfer Enzymes and Coenzymes Linking Methylotrophic Bacteria and Methanogenic Archaea. *Science*, *281*(5373), 99–102. https://doi.org/10.1126/science.281.5373.99

Cronan, J. E. (2006). A bacterium that has three pathways to regulate membrane lipid fluidity. *Molecular Microbiology*, *60*(2), 256–259. https://doi.org/10.1111/j.1365-2958.2006.05107.x

DeChaine, E. G., & Cavanaugh, C. M. (2006). Symbioses of Methanotrophs and Deep-Sea Mussels (Mytilidae: Bathymodiolinae). In J. Overmann (Ed.), *Molecular Basis of Symbiosis* (pp. 227–249). Springer. https://doi.org/10.1007/3-540-28221-1_11

DiMarco, A. A., Bobik, T. A., & Wolfe, R. S. (1990). Unusual coenzymes of methanogenesis. *Annual Review of Biochemistry*, *59*(1), 355–394. https://doi.org/10.1146/annurev.bi.59.070190.002035

Donnelly, M. I., Escalante-Semerena, J. C., Rinehart, K. L., & Wolfe, R. S. (1985). Methenyl-tetrahydromethanopterin cyclohydrolase in cell extracts of Methanobacterium. *Archives of Biochemistry and Biophysics*, *242*(2), 430–439. https://doi.org/10.1016/0003-9861(85)90227-9

Duperron, S. (2010). The Diversity of Deep-Sea Mussels and Their Bacterial Symbioses. In S. Kiel (Ed.), *The Vent and Seep Biota: Aspects from Microbes to Ecosystems* (pp. 137–167). Springer Netherlands. https://doi.org/10.1007/978-90-481-9572-5_6

Eikmanns, B., & Thauer, R. K. (1985). Evidence for the involvement and role of a corrinoid enzyme in methane formation from acetate in Methanosarcina barkeri. *Archives of Microbiology*, *142*(2), 175–179. https://doi.org/10.1007/BF00447063

Ermler, U., Hagemeier, C. H., Roth, A., Demmer, U., Grabarse, W., Warkentin, E., & Vorholt, J. A. (2002). Structure of Methylene-Tetrahydromethanopterin Dehydrogenase from

Methylobacterium extorquens AM1. *Structure*, *10*(8), 1127–1137. https://doi.org/10.1016/S0969-2126(02)00802-X

Fiala-Médioni, A., McKiness, Z., Dando, P., Boulegue, J., Mariotti, A., Alayse-Danet, A., Robinson, J., & Cavanaugh, C. (2002). Ultrastructural, biochemical, and immunological characterization of two populations of the mytilid mussel Bathymodiolus azoricus from the Mid-Atlantic Ridge: Evidence for a dual symbiosis. *Marine Biology*, *141*(6), 1035–1043. https://doi.org/10.1007/s00227-002-0903-9

Geier, B. (2020). *Correlative mass spectrometry imaging of animal–microbe symbioses*. https://doi.org/10.26092/elib/73

Geier, B., Sogin, E. M., Michellod, D., Janda, M., Kompauer, M., Spengler, B., Dubilier, N., & Liebeke, M. (2020). Spatial metabolomics of in situ host–microbe interactions at the micrometre scale. *Nature Microbiology*, *5*(3), 498–510. https://doi.org/10.1038/s41564-019-0664-6

Huang, G., Wagner, T., Demmer, U., Warkentin, E., Ermler, U., & Shima, S. (2020). The Hydride Transfer Process in NADP-dependent Methylene-tetrahydromethanopterin Dehydrogenase. *Journal of Molecular Biology*, *432*(7), 2042–2054. https://doi.org/10.1016/j.jmb.2020.01.042

Hughes, D. T., & Sperandio, V. (2008). Inter-kingdom signalling: Communication between bacteria and their hosts. *Nature Reviews Microbiology*, *6*(2), 111–120. https://doi.org/10.1038/nrmicro1836

Kádár, E., Davis, S. A., & Lobo-da-Cunha, A. (2008). Cytoenzymatic investigation of intracellular digestion in the symbiont-bearing hydrothermal bivalve Bathymodiolus azoricus. *Marine Biology*, *153*(5), 995–1004. https://doi.org/10.1007/s00227-007-0872-0

Kellermann, M. Y., Schubotz, F., Elvert, M., Lipp, J. S., Birgel, D., Prieto-Mollar, X., Dubilier, N., & Hinrichs, K.-U. (2012). Symbiont–host relationships in chemosynthetic mussels: A comprehensive lipid biomarker study. *Organic Geochemistry*, *43*, 112–124. https://doi.org/10.1016/j.orggeochem.2011.10.005

Kompauer, M., Heiles, S., & Spengler, B. (2017). Atmospheric pressure MALDI mass spectrometry imaging of tissues and cells at 1.4-µm lateral resolution. *Nature Methods*, *14*(1), 90–96. https://doi.org/10.1038/nmeth.4071

Maden, B. E. H. (2000). *Tetrahydrofolate and tetrahydromethanopterin compared: Functionally distinct carriers in C1 metabolism*. 21.

Mansilla, M. C., & de Mendoza, D. (2005). The Bacillus subtilis desaturase: A model to understand phospholipid modification and temperature sensing. *Archives of Microbiology*, *183*(4), 229–235. https://doi.org/10.1007/s00203-005-0759-8

Marx, C. J., Chistoserdova, L., & Lidstrom, M. E. (2003). Formaldehyde-Detoxifying Role of theTetrahydromethanopterin-Linked Pathway in MethylobacteriumextorquensAM1. *Journal of Bacteriology*, *185*(24), 7160–7168. https://doi.org/10.1128/JB.185.23.7160-7168.2003

Phleger, C. F., Nelson, M. M., Groce, A. K., Cary, S. C., Coyne, K. J., & Nichols, P. D. (2005). Lipid composition of deep-sea hydrothermal vent tubeworm Riftia pachyptila, crabs Munidopsis subsquamosa and Bythograea thermydron, mussels Bathymodiolus sp. And limpets Lepetodrilus spp. *Comparative Biochemistry and Physiology Part B: Biochemistry and Molecular Biology*, *141*(2), 196–210. https://doi.org/10.1016/j.cbpc.2005.03.001

Pond, D. W., Bell, M. V., Dixon, D. R., Fallick, A. E., Segonzac, M., & Sargent, J. R. (1998). Stable-Carbon-Isotope Composition of Fatty Acids in Hydrothermal Vent Mussels Containing Methanotrophic and Thiotrophic Bacterial Endosymbionts. *Applied and Environmental Microbiology*, *64*(1), 370–375. https://doi.org/10.1128/AEM.64.1.370-375.1998

Ponnudurai, R., Kleiner, M., Sayavedra, L., Petersen, J. M., Moche, M., Otto, A., Becher, D., Takeuchi, T., Satoh, N., Dubilier, N., Schweder, T., & Markert, S. (2017). Metabolic and physiological interdependencies in the Bathymodiolus azoricus symbiosis. *The ISME Journal*, *11*(2), 463–477. https://doi.org/10.1038/ismej.2016.124

Qiu, A., Min, S. H., Jansen, M., Malhotra, U., Tsai, E., Cabelof, D. C., Matherly, L. H., Zhao, R., Akabas, M. H., & Goldman, I. D. (2007). Rodent intestinal folate transporters (SLC46A1): Secondary structure, functional properties, and response to dietary folate restriction. *American Journal of Physiology-Cell Physiology*, *293*(5), C1669–C1678. https://doi.org/10.1152/ajpcell.00202.2007

Race, A. M., Styles, I. B., & Bunch, J. (2012). Inclusive sharing of mass spectrometry imaging data requires a converter for all. *Journal of Proteomics*, *75*(16), 5111–5112. https://doi.org/10.1016/j.jprot.2012.05.035

Russell, N. J., & Nichols, D. S. (1999). Polyunsaturated fatty acids in marine bacteria—A dogma rewritten. *Microbiology (Reading, England)*, *145 (Pt 4)*, 767–779. https://doi.org/10.1099/13500872-145-4-767

Salem, H., Bauer, E., Strauss, A. S., Vogel, H., Marz, M., & Kaltenpoth, M. (2014). Vitamin supplementation by gut symbionts ensures metabolic homeostasis in an insect host. *Proceedings of the Royal Society B: Biological Sciences*, *281*(1796). https://doi.org/10.1098/rspb.2014.1838

Schwörer, B., Fernandez, V. M., Zirngibl, C., & Thauer, R. K. (1993). H2-forming N5,N10-methylenetetrahydromethanopterin dehydrogenase from Methanobacterium thermoautotrophicum. Studies of the catalytic mechanism of H2 formation using hydrogen isotopes. *European Journal of Biochemistry*, *212*(1), 255–261. https://doi.org/10.1111/j.1432-1033.1993.tb17657.x

Shannon, P., Markiel, A., Ozier, O., Baliga, N. S., Wang, J. T., Ramage, D., Amin, N., Schwikowski, B., & Ideker, T. (2003). Cytoscape: A software environment for integrated models of biomolecular interaction networks. *Genome Research*, *13*(11), 2498–2504. https://doi.org/10.1101/gr.1239303

Shima, S., Warkentin, E., Thauer, R. K., & Ermler, U. (2002). Structure and function of enzymes involved in the methanogenic pathway utilizing carbon dioxide and molecular hydrogen. *Journal of Bioscience and Bioengineering*, *93*(6), 519–530. https://doi.org/10.1016/S1389-1723(02)80232-8

Streams, M. E., Fisher, C. R., & Fiala-Médioni, A. (1997). Methanotrophic symbiont location and fate of carbon incorporated from methane in a hydrocarbon seep mussel. *Marine Biology*, *129*(3), 465–476. https://doi.org/10.1007/s002270050187

Thauer, R. K., Klein, A. R., & Hartmann, G. C. (1996). Reactions with Molecular Hydrogen in Microorganisms: Evidence for a Purely Organic Hydrogenation Catalyst. *Chemical Reviews*, *96*(7), 3031–3042. https://doi.org/10.1021/cr9500601

Thubaut, J., Puillandre, N., Faure, B., Cruaud, C., & Samadi, S. (2013). The contrasted evolutionary fates of deep-sea chemosynthetic mussels (Bivalvia, Bathymodiolinae). *Ecology and Evolution*, *3*(14), 4748–4766. https://doi.org/10.1002/ece3.749

van Beelen, P., Haasnoot, C. A. G., & Vogels, G. D. (1984). Structure and function of methanopterin. *Antonie van Leeuwenhoek*, *50*(1), 76–76. https://doi.org/10.1007/BF00404910

Vorholt, J. A., Chistoserdova, L., Stolyar, S. M., Thauer, R. K., & Lidstrom, M. E. (1999). Distribution of Tetrahydromethanopterin-Dependent Enzymes in Methylotrophic Bacteria and Phylogeny of Methenyl Tetrahydromethanopterin Cyclohydrolases. *Journal of Bacteriology*, *181*(18), 5750–5757. https://doi.org/10.1128/JB.181.18.5750-5757.1999

Wang, M., Carver, J. J., Phelan, V. V., Sanchez, L. M., Garg, N., Peng, Y., Nguyen, D. D., Watrous, J., Kapono, C. A., Luzzatto-Knaan, T., Porto, C., Bouslimani, A., Melnik, A. V., Meehan, M. J., Liu, W.-T., Crüsemann, M., Boudreau, P. D., Esquenazi, E., Sandoval-

Calderón, M., … Bandeira, N. (2016). Sharing and community curation of mass spectrometry data with Global Natural Products Social Molecular Networking. *Nature Biotechnology*, *34*(8), 828–837. https://doi.org/10.1038/nbt.3597

Wolfe, R. S. (1985). Unusual coenzymes of methanogenesis. *Trends in Biochemical Sciences*, *10*(10), 396–399. https://doi.org/10.1016/0968-0004(85)90068-4

Zhao, R., Diop-Bove, N., Visentin, M., & Goldman, I. D. (2011). Mechanisms of Membrane Transport of Folates into Cells and Across Epithelia. *Annual Review of Nutrition*, *31*. https://doi.org/10.1146/annurev-nutr-072610-145133

Zheng, P., Wang, M., Li, C., Sun, X., Wang, X., Sun, Y., & Sun, S. (2017). Insights into deep-sea adaptations and host–symbiont interactions: A comparative transcriptome study on Bathymodiolus mussels and their coastal relatives. *Molecular Ecology*, *26*(19), 5133–5148. https://doi.org/10.1111/mec.14160

Zhu, K., Choi, K.-H., Schweizer, H. P., Rock, C. O., & Zhang, Y.-M. (2006). Two aerobic pathways for the formation of unsaturated fatty acids in Pseudomonas aeruginosa. *Molecular Microbiology*, *60*(2), 260–273. https://doi.org/10.1111/j.1365-2958.2006.05088.x

Supplementary Tables and Figures

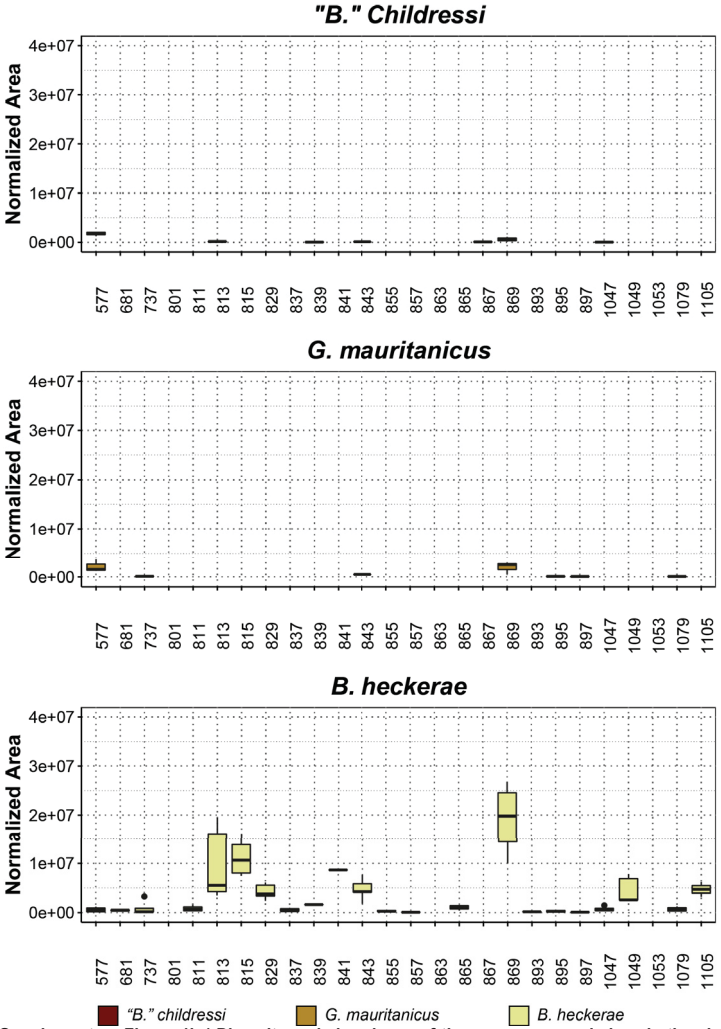

Supplementary Figure 1b | Diversity and abundance of the new compound class in the six species studied. The signal intensity was extracted from the LC-MS data using the Xcalibur quan software, the signal intensity was normalized using the gill wet weight

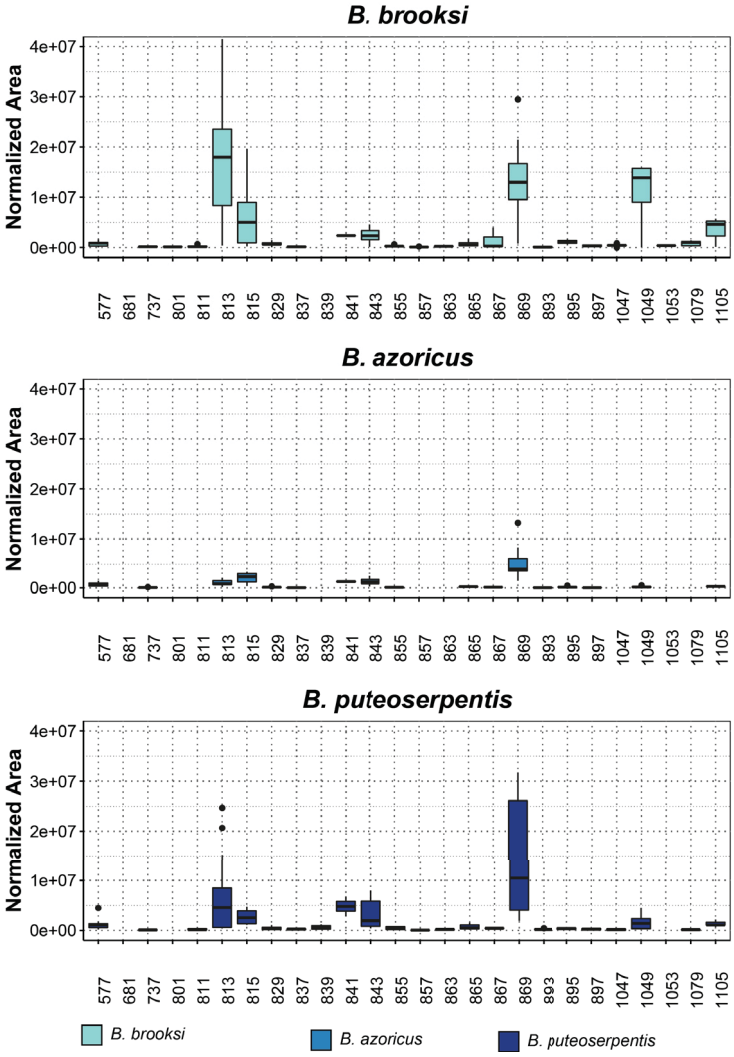

Supplementary Figure 2b | Diversity and abundance of the new compound class in the six species studied. The signal intensity was extracted from the LC-MS data using the Xcalibur quan software, the signal intensity was normalized using the gill wet weight

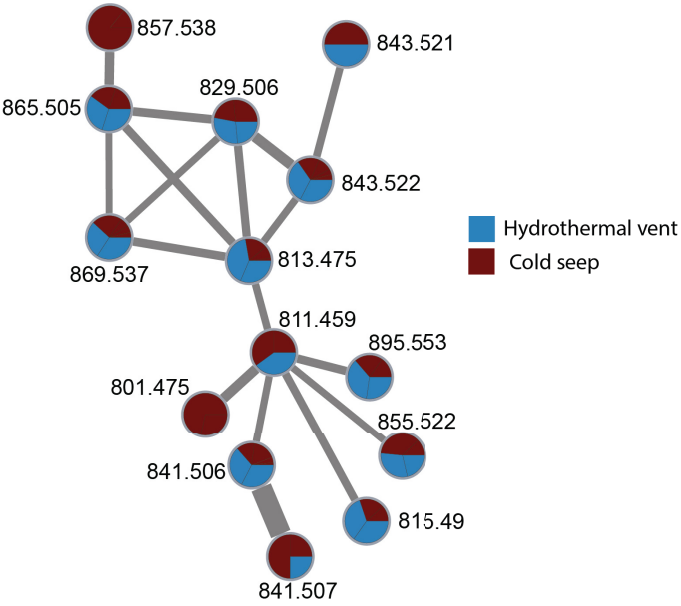

Supplementary Figure 3 | ***The diversity of the specialized metabolites was not linked to the environment of the host.***

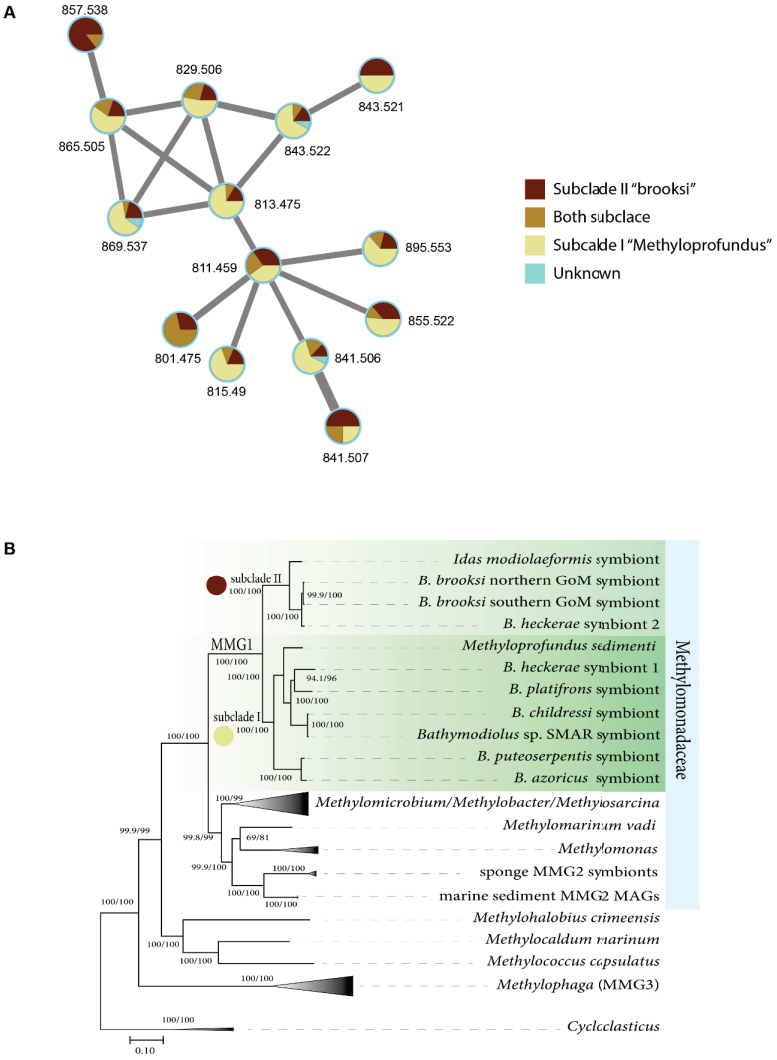

Supplementary Figure 4 | The distribution of the compound class was not linked to the MOX symbionts subclade hosted by the mussels. A, MS2 network of the compound class produced using GNPS and Cytoscape, the nodes are color coded according the MOX subclades hosted in the mussels gills. **B,** Phylogenomic tree of the Methylococcales clade, showing the evolutionary history of the Marine Methylotrophic Group 1 (MMG1, green) and related species. MMG1 clade includes the distinct subclades I and II. Tree courtesy to Maxim Rubin.

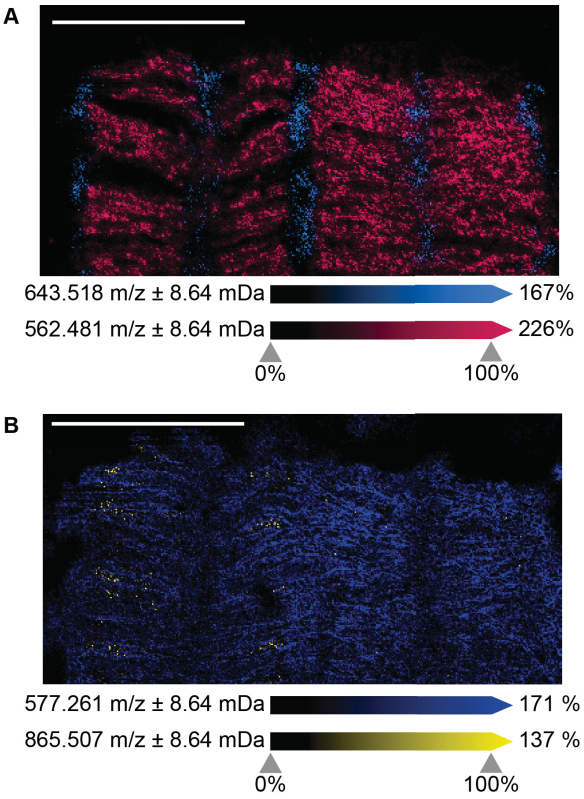

Supplementary Figure 5 | In *"B." Childressi* gills, methylene-dH$_4$MPT was also abundant in the area colonized by the symbionts, the analogues are rare and present in low abundance. A, Distribution of different partner-specific metabolites in the gills of *"B." childressi*. Phosphethanolamine ceramide PnE-Cer(32:4) (641.519 *m/z*, pale blue) is used to mark the symbiont-free area of the mussel gills and the hopanoid 35-aminobacteriohopane-31,32,33,34-tetrol (562.482 *m/z*) (red) is used to mark the area colonized by the methane oxidizer symbionts. **B,** Distribution of methenyl-dH$_4$MPT (577.261 m/z, dark blue) and of the only analogue detected in this MALDI dataset: methenyl-dH$_4$MPT-C$_{20:3}$ (865.507 *m/z*, yellow). The scale bars represent 1 mm.

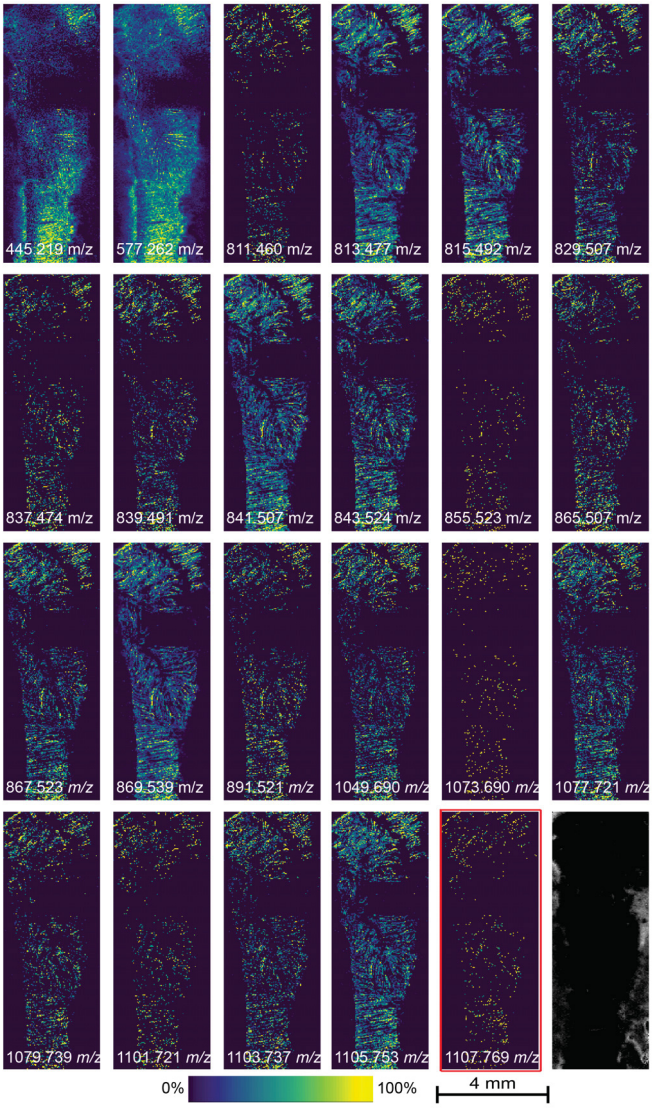

Supplementary Figure 6 | Distribution of methenyl-dH$_4$MPT and its analogues in the gills of *B. heckerae*. The data were acquired at a spatial resolution of 30 µm and were normalized by total ion chromatogram.

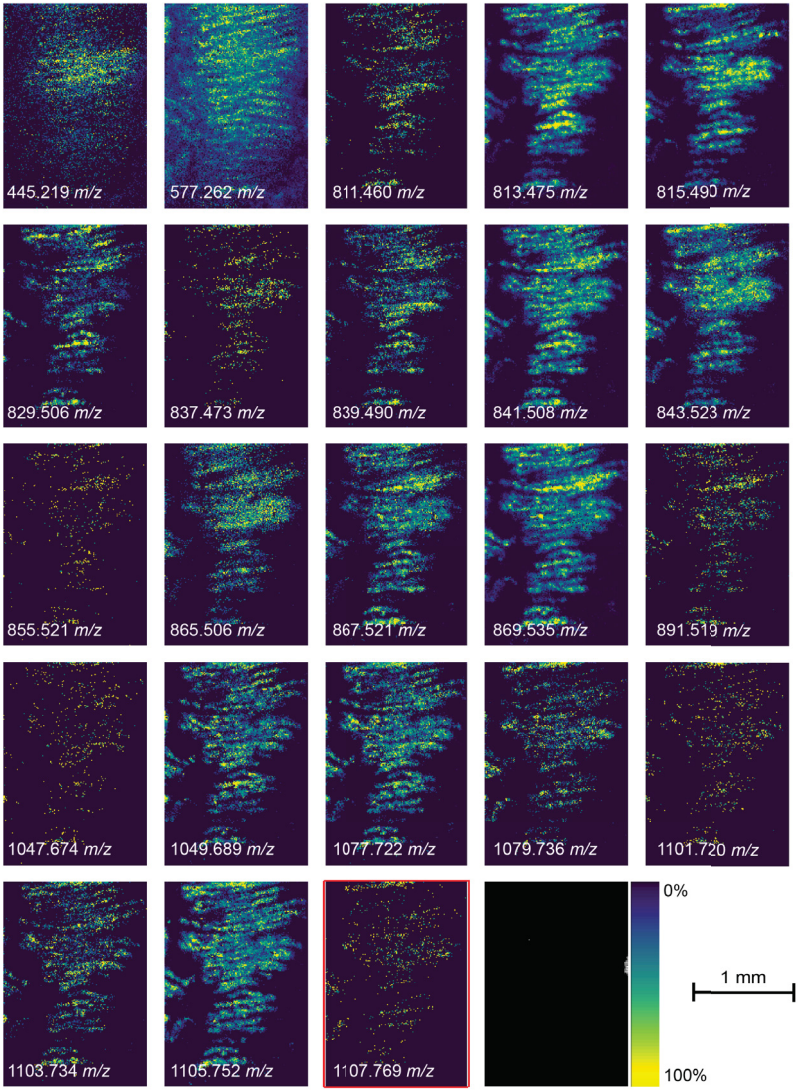

Supplementary Figure 7 | Distribution of methenyl-dH$_4$MPT and its analogues in the gills of *B. heckerae*. The data were acquired at a spatial resolution of 10 µm and were normalized by total ion chromatogram.

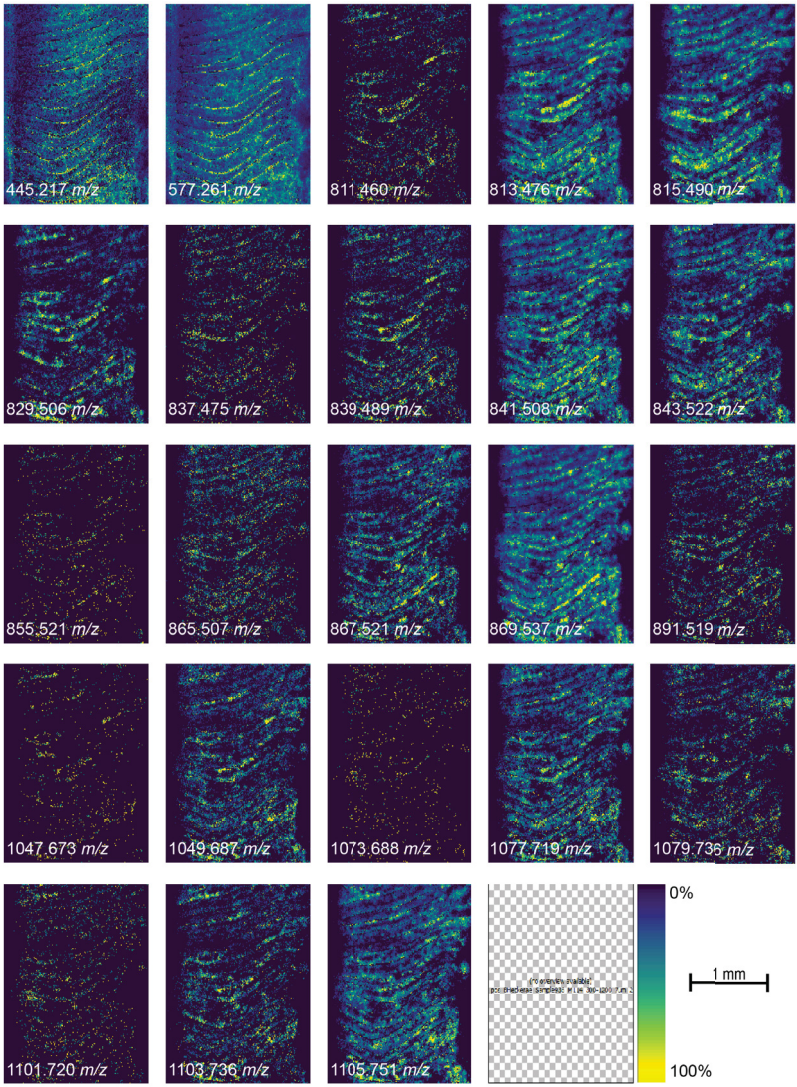

Supplementary Figure 8 | Distribution of methenyl-dH$_4$MPT and its analogues in the gills of *B. heckerae*. The data were acquired at a spatial resolution of 10 µm and were normalized by total ion chromatogram.

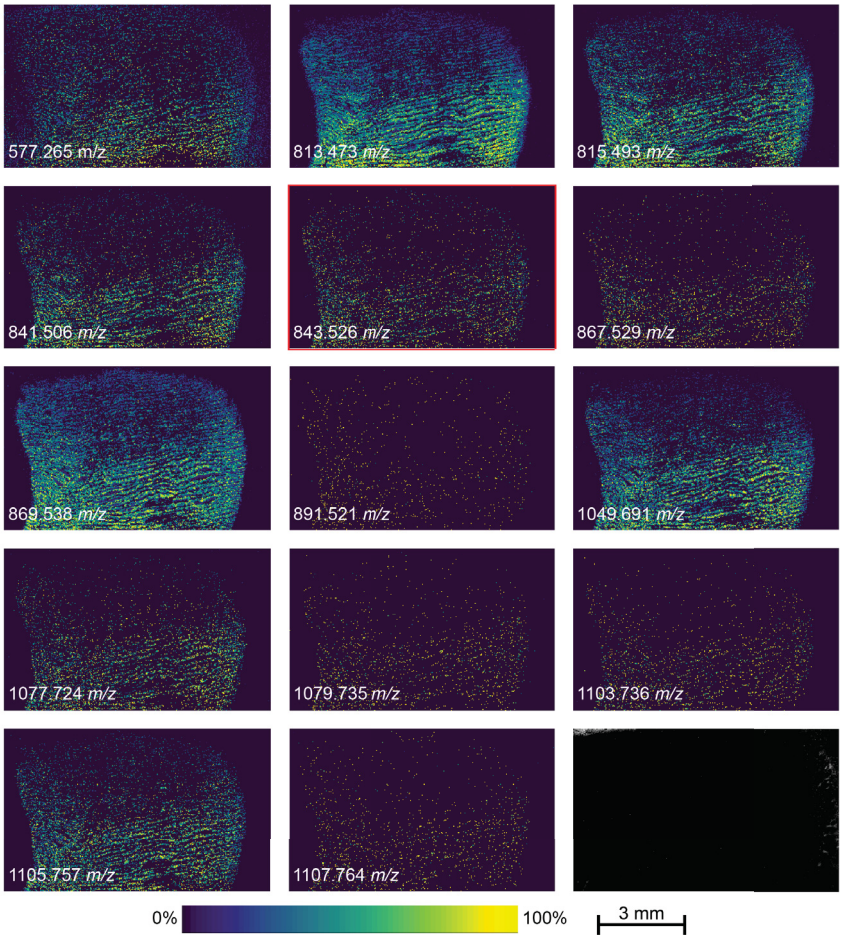

Supplementary Figure 9 | Distribution of methenyl-dH$_4$MPT and its analogues in the gills of *B. brooksi*. The data were acquired at a spatial resolution of 10 µm and normalized by total ion chromatogram.

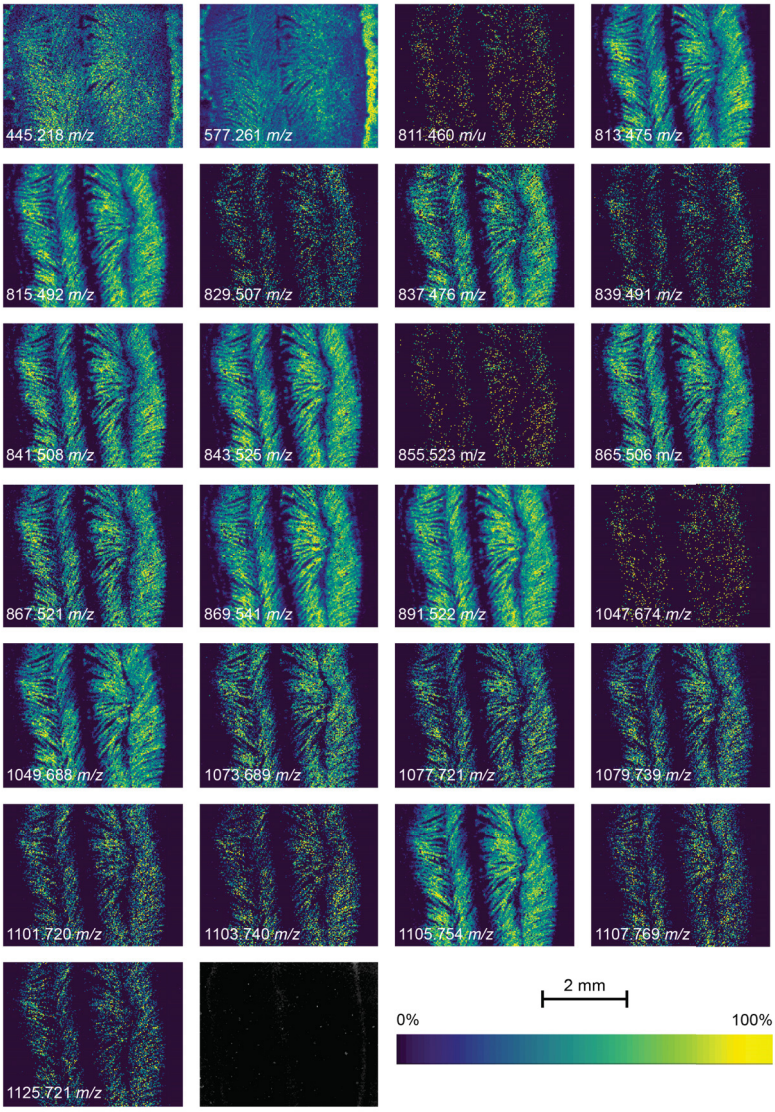

Supplementary Figure 10 | Distribution of methenyl-dH$_4$MPT and its analogues in the gills of *B. puteoserpentis*. The data were acquired at a spatial resolution of 10 µm and normalized by total ion chromatogram.

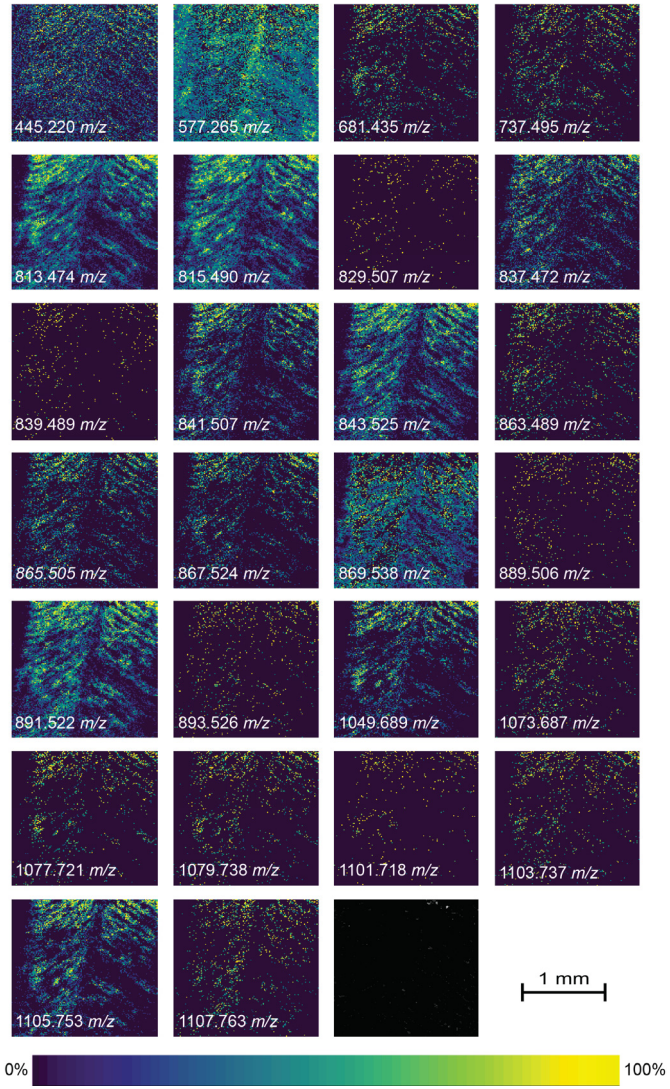

Supplementary Figure 11 | Distribution of methenyl-dH$_4$MPT and its analogues in the gills of *B. puteoserpentis*. The data were acquired at a spatial resolution of 5 µm and normalized by total ion chromatogram.

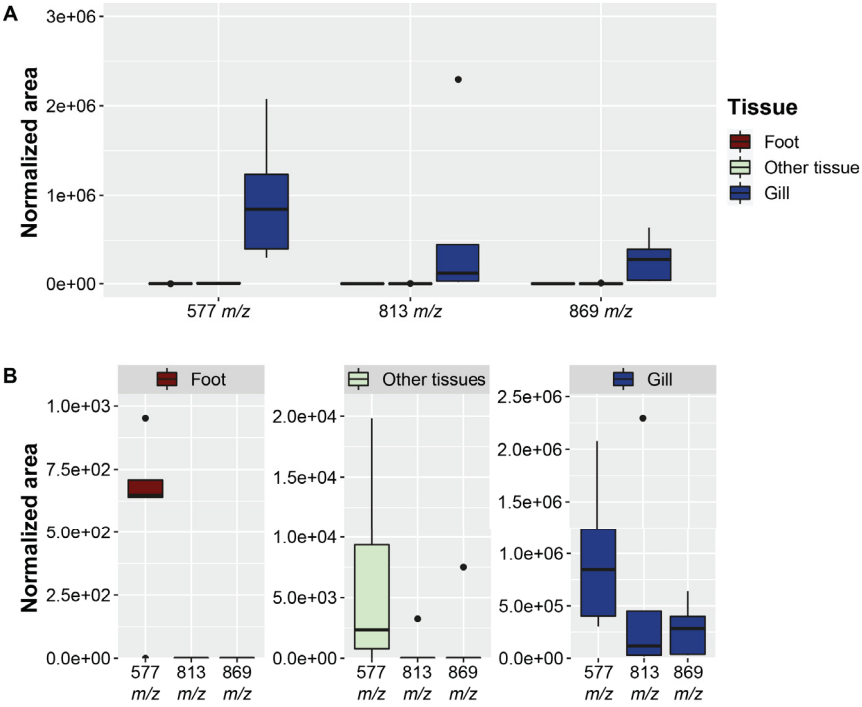

Supplementary Figure 12 | Methenyl-dH4MPT (577 *m/z*) was present in all the mussel tissues, while its esterified analogues (813 *m/z* and 869 *m/z*) were only present in the gills. A, All methanolite compounds were more abundant in the gill tissue than in non-symbiotic tissues (Foot and other tissues). **B,** Methenyl-dH4MPT was present but less abundant in the non-symbiotic tissues than in the gill tissues. The signal intensity (area) was normalized with the wet weight of each samples. We analyzed five samples of each tissue types. The 813 m/z and 869 m/z signals detected in "other tissues" originated from the same samples, the most likely explanation is tissue contamination. "Other tissues" represent all tissues leftover after the foot and gills were dissected. We were probably observing a contamination by gill tissues which were not properly dissected.

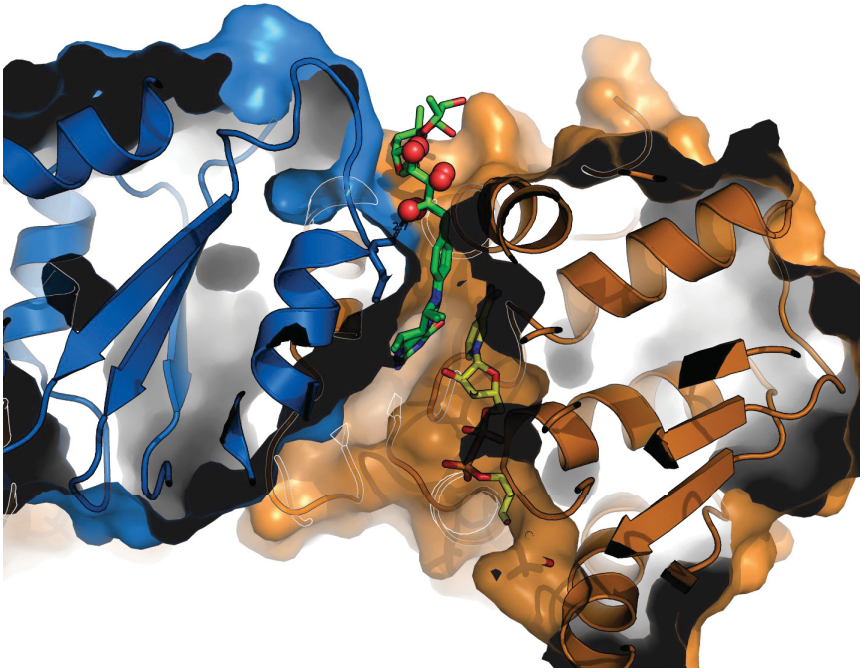

Supplementary Figure 13 | MtdA structure of *M. extorquens* modeled in closed conformation with both substrates attached. NADP is drawn in yellow while is dH4MPT is drawn in green. The pterin and benzamide groups sit in the cleft. The ribitol is at the opening, the three hydroxyl group of the ribitol are highlighted with red balls. In black, one can see the strong interaction between the first of the hydroxyl group and the protein. Figure courtesy to T. Wagner.

Supplementary Table 1 | List of the fatty acids attached to the different esterified analogues of dH_4MPT

Precursor	Fragment 1 methenyl-dH_4MPT - H_2O	Neutral loss	theorical *m/z*	Formula	ID	exp - theorical
801.4758	541.2399	260.2359	260.235145	C15H32O3	C15:0 (+H2O)	0.0008
811.4588	541.2402	270.2186	270.219495	C16H30O3	C16:2 (+H2O)	-0.0009
813.4747	541.2402	272.2345	272.235145	C16H32O3	C16:1 (+H2O)	-0.0006
815.4903	541.2405	274.2498	274.250795	C16H34O3	C16:0 (+H2O)	-0.0010
829.5052	541.2402	288.265	288.266445	C17H36O3	C17:0 (+H2O)	-0.0014
837.4744	541.2404	296.234	296.235145	C18H32O3	C18:3 (+H2O)	-0.0011
839.4905	541.2410	298.2495	298.250795	C18H34O3	C18:2 (+H2O)	-0.0013
841.5052	541.2399	300.2653	300.266445	C18H36O3	C18:1 (+H2O)	-0.0011
843.5215	541.2408	302.2807	302.282095	C18H38O3	C18:0 (+H2O)	-0.0014
855.5213	541.2398	314.2815	314.282095	C19H38O3	C19:1 (+H2O)	-0.0006
857.5375	541.2422	316.2953	316.297745	C19H40O3	C19:0 (+H2O)	-0.0024
863.4895	541.2407	322.2488	322.250795	C20H34O3	C20:4 (+H2O)	-0.0020
865.5054	541.2404	324.265	324.266445	C20H36O3	C20:3 (+H2O)	-0.0014
867.5219	541.2402	326.2817	326.282095	C20H38O3	C20:2 (+H2O)	-0.0004
869.5373	541.2405	328.2968	328.297745	C20H40O3	C20:1 (+H2O)	-0.0009
893.5369	541.2402	352.2967	352.297745	C22H40O3	C22:3 (+H2O)	-0.0010
895.5227	541.2402	354.2825	354.27701	C21H38O4	C18:2 - glycidyl (C_3H_5O) (+H2O)	0.0055
897.5676	541.2395	356.3281	356.329045	C22H44O3	C22:1 (+H2O)	-0.0009
1047.6729	813.4727	234.2002	234.198365	C16H26O	C16:2 (-H2O)	0.0018
1049.688	813.4737	236.2143	236.2140	C16H28O	C16:1 (-H2O)	0.0003
1053.7202	815.4891	238.2311	238.229665	C16H30O	C16:0 (-H2O)	0.0014
1079.7355	843.5178	236.2177	236.2140	C16H28O	C16:1 (-H2O)	0.0037
1105.7515	869.5387	236.2128	236.214015	C16H28O	C16:1 (-H2O)	-0.0012

Supplementary Table 2: Information on the samples measured with HPLC-MS. MAR = Mid-Atlantic Ridge, GoM = Gulf of Mexico, BAR = Barbados Accretionary Prism.

Sample name	Wet weight [mg]	Species	Cruise	Sampling field	Sampling site	Vent or seep
MS18_10	60	*Bathymodiolus brooksi*	M114-2 (2015)	GoM	Chapopote	seep
MS18_11	59	*Bathymodiolus brooksi*	M114-2 (2015)	GoM	Chapopote	seep
MS18_12	53	*Bathymodiolus brooksi*	M114-2 (2015)	GoM	Chapopote	seep
MS18_13	50	*Bathymodiolus brooksi*	M114-2 (2015)	GoM	Chapopote	seep
MS18_14	50	*Bathymodiolus brooksi*	M114-2 (2015)	GoM	Mictlan, Knoll 2201	seep
MS18_15	67	*Bathymodiolus brooksi*	M114-2 (2015)	GoM	Mictlan, Knoll 2201	seep
MS18_16	70	*Bathymodiolus brooksi*	M114-2 (2015)	GoM	Mictlan, Knoll 2201	seep
MS18_17	75	*Bathymodiolus brooksi*	M114-2 (2015)	GoM	Mictlan, Knoll 2201	seep
MS18_18	55/2	*Bathymodiolus heckerae*	M114-2 (2015)	GoM	Chapopote	seep
MS18_19	59/2	*Bathymodiolus heckerae*	M114-2 (2015)	GoM	Chapopote	seep
MS18_20	56/2	*Bathymodiolus heckerae*	M114-2 (2015)	GoM	Chapopote	seep
MS18_21	56/2	*Bathymodiolus heckerae*	M114-2 (2015)	GoM	Chapopote	seep
MS18_22	60/2	*Bathymodiolus heckerae*	M114-2 (2015)	GoM	Chapopote	seep
MS18_23	44	*Bathymodiolus azoricus*	BioBaz 2013	MAR	Menez Gwen, White Flames	vent
MS18_24	50	*Bathymodiolus azoricus*	BioBaz 2013	MAR	Menez Gwen, White Flames	vent
MS18_25	72	*Bathymodiolus azoricus*	BioBaz 2013	MAR	Menez Gwen, White Flames	vent
MS18_26	40	*Bathymodiolus azoricus*	BioBaz 2013	MAR	Menez Gwen, White Flames	vent
MS18_27	50	*Bathymodiolus azoricus*	BioBaz 2013	MAR	Menez Gwen, White Flames	vent
MS18_28	59	*Bathymodiolus azoricus*	BioBaz 2013	MAR	Menez Gwen, Woody	vent
MS18_29	70	*Bathymodiolus azoricus*	BioBaz 2013	MAR	Menez Gwen, Woody	vent
MS18_30	57	*Bathymodiolus azoricus*	BioBaz 2013	MAR	Menez Gwen, Woody	vent
MS18_31	70	*Bathymodiolus azoricus*	BioBaz 2013	MAR	Menez Gwen, Woody	vent
MS18_32	41	*Bathymodiolus azoricus*	BioBaz 2013	MAR	Menez Gwen, Woody	vent
MS18_33	52	*Bathymodiolus azoricus*	BioBaz 2013	MAR	Lucky Strike, Montségur	vent
MS18_34	60	*Bathymodiolus azoricus*	BioBaz 2013	MAR	Lucky Strike, Montségur	vent
MS18_35	53	*Bathymodiolus azoricus*	BioBaz 2013	MAR	Lucky Strike, Montségur	vent
MS18_36	67	*Bathymodiolus azoricus*	BioBaz 2013	MAR	Lucky Strike, Montségur	vent

MS18_37	65	*Bathymodiolus azoricus*	BioBaz 2013	MAR	Lucky Strike, Montségur	vent
MS18_38	84	*Bathymodiolus puteoserpentis*	BigMar 2016	MAR	Semenov-2, Ash lighthouse	vent
MS18_39	68	*Bathymodiolus puteoserpentis*	BigMar 2016	MAR	Semenov-2, Ash lighthouse	vent
MS18_40	52	*Bathymodiolus puteoserpentis*	BigMar 2016	MAR	Semenov-2, Ash lighthouse	vent
MS18_41	71	*Bathymodiolus puteoserpentis*	BigMar 2016	MAR	Semenov-2, Ash lighthouse	vent
MS18_42	52	*Bathymodiolus puteoserpentis*	BigMar 2016	MAR	Semenov-2, Ash lighthouse	vent
MS18_43	76	*Bathymodiolus puteoserpentis*	BigMar 2016	MAR	Irinovskoe	vent
MS18_44	53	*Bathymodiolus puteoserpentis*	BigMar 2016	MAR	Irinovskoe	vent
MS18_45	66	*Bathymodiolus puteoserpentis*	BigMar 2016	MAR	Irinovskoe	vent
MS18_46	42	*Bathymodiolus puteoserpentis*	BigMar 2016	MAR	Irinovskoe	vent
MS18_47	67	*Bathymodiolus puteoserpentis*	BigMar 2016	MAR	Irinovskoe	vent
MS18_48	45	*Bathymodiolus puteoserpentis*	BigMar 2016	MAR	Logatchev-Irina II	vent
MS18_49	50	*Bathymodiolus puteoserpentis*	BigMar 2016	MAR	Logatchev-Irina II	vent
MS18_50	52	*Bathymodiolus puteoserpentis*	BigMar 2016	MAR	Logatchev-Irina II	vent
MS18_51	52	*Bathymodiolus puteoserpentis*	BigMar 2016	MAR	Logatchev-Irina II	vent
MS18_52	65	*Bathymodiolus puteoserpentis*	BigMar 2016	MAR	Logatchev-Irina II	vent
MS18_53	50	*"Bathymodiolus" Childressi*	Nautilus GoM 2015 Na58	GoM	Mississipi Canyon block 853	seep
MS18_54	60	*"Bathymodiolus" Childressi*	Nautilus GoM 2015 Na58	GoM	Mississipi Canyon block 853	seep
MS18_55	52	*"Bathymodiolus" Childressi*	Nautilus GoM 2015 Na58	GoM	Mississipi Canyon block 853	seep
MS18_56	50	*"Bathymodiolus" Childressi*	Nautilus GoM 2015 Na58	GoM	Mississipi Canyon block 853	seep
MS18_68	45	*Gigantidas mauritanicus*	Atlantis 21-02	BAP	Milano seep area	seep
MS18_69	50	*Gigantidas mauritanicus*	Atlantis 21-02	BAP	Milano seep area	seep
MS18_70	45	*Gigantidas mauritanicus*	Atlantis 21-02	BAP	Milano seep area	seep

Supplementary Table 3 | Solvent gradient for high-resolution LC-MS/MS.

%B	Time [min]	Flow rate [µL min^{-1}]
0	-2 (pre-run equilibration)	350
0	2	350
16	5.5	350
45	9	350
52	12	350
58	14	350
66	16	350
70	18	350
75	22	350
97	25	350
97	32.5	350
15	33	350
0	34.4	350
0	36	350

*Buffer A (60/40 ACN/H_2O, 10 mM ammonium formate, 0.1% FA) and Buffer B (90/10 IPA/ACN, 10 mM ammonium formate, 0.1% FA) were used at a flow rate of 350 µl min^{-1}.

Supplementary Table 4 | MS settings of Q Exactive Plus Orbitrap (Thermo Fisher Scientific) equipped with a HESI probe and a Vanquish Horizon UHPLC System (Thermo Fisher Scientific).

MS^1	
Resolution	70'000
AGC target	5.00E+05
Max IT	65 ms
Scan range	150-1500 m/z
MS^2	
Resolution	35'000
AGC target	1.00E+06
Max IT	75 ms
Loop count	8
Dynamic exclusion	30 s
Isolation windows (pos.)	1 m/z
Isolation windows (neg.)	1 m/z
NCE	30

Supplementary Table 5 | Information on the samples measured with MALDI-MSI

species_sample	tissue	cruise	sampling site	matrix	polarity	mz_range	pixel_size [µm]	attenuator	Metaspace ID
"Bathymodiolus" childressi	gill	NA58	MC853	DHAP	pos	300 - 1300	7	28	MPIMM_166_QE_P_BC_CF
Bathymodiolus puteoserpentis	gill	MS126	Irina II	DHAP	pos	150 - 2000	10	27	MPIMM_141_QE_P_Bputeo
Bathymodiolus puteoserpentis	gill	MS126	Irina II	DHAP	pos	100 - 1500	5	31	MPIMM_142_QE_P_Bputeo
Bathymodiolus heckerae	gill	M114-2	Chapopote	SDHB	pos	300-1200	30	27	MPIMM_099_QE_P_BH_CF
Bathymodiolus heckerae	gill	M114-2	Chapopote	SDHB	pos	300-1200	7	33	
Bathymodiolus heckerae	gill	M114-2	Chapopote	SDHB	pos	300-1200	7	33	
Bathymodiolus brooksi	gill	M114-2	Mictlan, Knoll 2201	SDHB	pos	150-1500	15	27	MPIMM_225_QE_P_BB

Modified MNMS medium (1 L)

Solution 1 (Saltwater):

$MgSO_4$ x 7 H_2O	- 1 g
$CaCl_2$ x 2 H_2O	- 0.13 g
KNO_3	- 0.1 g (Do not add for tracer experiment)
NaCl	- 20 g

Dissolve in 500 ml of MQ water and make up final volume to 800 ml. Autoclave.

Solution 2 (Phosphate Buffer System):

KH_2PO_4	- 0.27 g
Na_2HPO_4 x 7 H_2O	- 0.544 g

Dissolve in 200 ml of MQ water and autoclave.

Note - Solution 1 and solution 2 should always be autoclaved separately; otherwise the medium precipitates!

After autoclaving and cooling down of the above two solutions, mix them both under sterile conditions. Add 1 ml of filter-sterilized trace element solution (TES), 1 ml filter-sterilized Iron-NTA (Fe-NTA) solution and filter-sterilized methanol or methane.

Inoculate with ~1% of preculture.

Use slight agitation by shaking or slow stirring for huge cultures.

Solution 3 (TES):

Nitrilotriacetic acid	- 30 g (Dissolve in 350 ml MQ and adjust to pH 8)
$MnCl_2$ x 4 H_2O	- 0.207 g
$CoCl_2$ x 6 H_2O	- 0.115 g
$ZnSO_4$ x 7 H_2O	- 0.25 g
$CuSO_4$ x 5 H_2O	- 1.5 g
$NaWo_4$ x 2 H_2O	- 0.036 g
$NaMoO_4$ x 2 H_2O	- 0.05 g
$NiCl_2$ x 6 H_2O	- 0.192 g
SeO_2	- 0.028 g
$CeCl_3$ x 7 H_2O	- 0.15 g
H_3BO_3	- 0.03g
MQ	- add 1000 ml

Solution 4 (FeNTA):

Nitrilotriacetic acid	- 10.32 g (Dissolve in 350 ml MQ and adjust to pH 8)
FeSO4 x 7 H_2O	- 8.64 g
MQ	- add 1000 ml

Chapter III

First animal capable of *de novo* phytosterol synthesis

First animal capable of *de novo* phytosterol synthesis

Dolma Michellod[1*], Tanja Bien[2], Daniel Birgel[3], Marlene Jensen[5], Manuel Kleiner[5], Sarah Fearn[4], Caroline Zeidler[1], Nicole Dubilier[1,6], Manuel Liebeke[1*]

[1] Max Planck Institute for Marine Microbiology, Celsiusstraße 1, 28359 Bremen, Germany

[2] Institute of Hygiene, University of Münster, Robert-Koch-Str. 41, 48149, Münster, Germany

[3] Institute for Geology, University of Hamburg, Bundesstraße 55, 20146 Hamburg, Germany

[4] Department of Materials, Imperial College London, London SW7 2AZ, United Kingdom

[5] Plant and Microbial Biology, NC State University, Raleigh, NC 27695, United States

[6] MARUM, Center for Marine Environmental Sciences, University of Bremen, 28359 Bremen, Germany

* *The manuscript is in preparation and has not been revised by all authors.*

* Author contribution: D.M, M.L and N.D conceived the study. D.M collected, processed and analyzed the metabolomics, metatranscriptomics and metagenomics samples. T.J and S.F collected mass spectrometry imaging data. D.B performed the GC-IRMS measurements. M.J and M.K. collected and analyzed the proteomics data. C.Z and D.M preformed the heterologous gene expression. D.M performed the enzyme assay and analyzed the data. D.M wrote the manuscript, with support from M.L, and contributions from T.B, D.B, M.K and C.Z.

Abstract

Sterols are essential for eukaryotic cell membrane functions. In addition to their structural role, sterols participate in signaling and are essential to lipid rafts assembly and function. While the last common ancestor of eukaryotes had the enzymatic machinery to produce diverse sterols - categorized today as animal, plant, or fungal sterols - animals are only able to synthesize cholesterol. Here we show an animal which retained the ability to synthesize sitosterol, a phytosterol that so far was thought to only be synthesized in plants. Using a multi-omics approach in combination with isotopic analysis, we found that marine gutless oligochaetes have the ability to synthesize cholesterol and sitosterol *de novo* using a novel sterol methyltransferase, an enzyme usually absent in animals and essential to sitosterol synthesis in plants. Heterologous gene expression and enzyme assays confirmed the sterol methyltransferase activity. The ability of the gutless oligochaetes to synthesize and incorporate sitosterol in their cell membrane shows that the demarcation of sterols by kingdom is not as strict as previously assumed. Our findings raise new questions on the role of sitosterol in animal membrane functioning and suggest that the evolution of sterol synthesis and sterol usage is more complex than suggested by studies on mice and humans.

Introduction

Sterols are essential lipids present in all eukaryotes. There are strong indications that all necessary enzymes for the biosynthesis of phytosterols, as well as cholesterol, were present in the last eukaryotic common ancestor (LECA) (Desmond & Gribaldo, 2009; Summons et al., 2006). Today, sterols are thought to be kingdom specific. Animals, with a few exceptions in sponges and corals, have cholesterol (C_{27}) as their major sterol. Fungi specialize in ergosterol (C_{28}) synthesis, while land plants harbor a mixture of phytosterols (C_{28} to C_{29}) dominated by sitosterol, stigmasterol and campesterol (Lagarda et al., 2006).

A few eukaryotes, such as insects and nematodes, have lost the ability to synthesize sterols (Desmond & Gribaldo, 2009) and need to fulfill their sterol requirement with their

diet. Most eukaryotes retained the ability of *de novo* sterol synthesis but are only able to synthesize a specific set of sterols. With the exception of sponges (Kanazawa, 2001), animals are limited to cholesterol synthesis; they cannot *de novo* synthesize other sterols like ergosterol and sitosterol.

Plants, including microalgae, synthesize a higher sterol diversity than animals and can contain non-negligible amounts of cholesterol in addition to their phytosterols (Behrman & Gopalan, 2005; Jäpelt & Jakobsen, 2013; Rampen et al., 2010; Volkman et al., 1998). Recently, the plant specific cholesterol synthesis pathway was elucidated (Sonawane et al., 2016). This pathway comprises 12 enzymes: half of those enzymes evolved through gene duplication and divergence from phytosterol biosynthetic enzymes, whereas others act reciprocally in both cholesterol and phytosterol biosynthesis (Sonawane et al., 2016). In contrast, sterol synthesis in animals is limited to cholesterol and an analogous animal phytosterol synthesis pathway has not been described.

Plant sterols differ from animal sterols by the presence of an extra methyl-(C_{28} sterols) or ethyl- (C_{29} sterols) group at C-24. Animals lack C-24 sterol methyltransferase (SMT), the enzyme that mediates the C-24 alkylation. SMTs have been described in a few marine sponges but despite wider search efforts, SMTs seem to be absent from higher animals (eumetazoans) (Haubrich et al., 2015; Volkman, 2005). As for most other sterol enzymes, an ancestral SMT was likely present in LECA but was lost in most of the animal phyla (Desmond & Gribaldo, 2009; Gold et al., 2016; Haubrich et al., 2015).

Here, we show the presence and active function of an animal specific SMT. We looked at the sterol profile of gutless oligochaetes, a group of small annelids living in marine sediment. They lack a digestive system and rely on obligatory bacterial endosymbionts for their nutrition (O Giere, 1981; Olav Giere, 1985; Kleiner et al., 2012; Woyke et al., 2006). It was reported that the *Olavius algarvensis* (Phallodrilinae) sterol profile was dominated by the plant sterol sitosterol. Using a multi-omics approach in combination with isotopic and imaging analyses, we studied the distribution of sterols in gutless oligochaetes and their ability to synthesize cholesterol and sitosterol *de novo*. This led to the first discovery of an SMT responsible for sitosterol biosynthesis in an animal.

Results and discussion

Sitosterol is the main sterol in marine gutless oligochaetes. Measurements of metabolites in single *Olavius algarvensis* worms with both gas chromatography-mass spectrometry (GC-MS) and high-performance liquid chromatography-mass spectrometry (HPLC-MS) revealed a total free sterol content of 3.44 ± 0.04 µg (n=12). Assuming an average wet weight of 1 mg per worm, sterols represented 0.34 % wet weight, a value similar to reported percentages for terrestrial and aquatic worms (Ballantine et al., 1978; McLaughlin, 1971; Voogt, 1973; Wilber & Bayors, 1947). Despite the amount of sterols being comparable to that of other worms, the sterol composition in *O. algarvensis* was different. Usually, cholesterol dominates the sterol pool in animals, often accounting for more than 90 % of the total sterol content (Goad, 1981; Sissener et al., 2018). In *O. algarvensis*, cholesterol (40%) was not the major sterol, instead sitosterol accounted for the majority of sterols detected (60%) (**Figure 1A**). Sitosterol is a phytosterol and is rarely abundantly present in animals. So far it has only been reported as abundant in a few phytoparasitic nematodes (David J. Chitwood et al., 1985, 1987; Cole & Krusberg, 1967) unable of *de novo* sterol synthesis (D. J. Chitwood, 1991). However, it is unclear if the abundance of sitosterol in phytoparasitic nematodes reflects the actual sterol composition of the nematodes or the sterol composition of their gut content. In the case of *O. algarvensis*, the absence of a gut excludes sterol contamination coming from organic matter in the digestive tract.

Sitosterol was not only the major sterol in *O. algarvensis* but in all the gutless oligochaete species analyzed in this study. We sampled in different locations in the Mediterranean Sea (Elba, Mallorca, Monaco) and in the Caribbean Sea (Bahamas, Belize), and all worms had a comparable lipid profile, with sitosterol as the major sterol. The sterol content was not influenced by sampling location, species (n=6), or genera (n=2). All gutless oligochaetes are in obligate nutritional symbiosis with chemosynthetic bacteria, which form a thick bacterial layer between the cuticle and the epidermis of the worm (**Figure 2B and 2F**). The composition of the symbiotic bacterial community did not have an impact on the sterol profile of the host. However, the presence of bacterial symbionts could

impact the sterol distribution in the host tissues, as reported for pathogenic and beneficial interactions (Bien et al., 2021; Geier et al., 2020; van der Meer-Janssen et al., 2010). The potential impact of the symbionts on the local sterol composition of the worm epidermis cannot be resolved by bulk measurements, but instead requires the use of metabolite imaging techniques.

Metabolite imaging shows homogeneous sitosterol and cholesterol distribution in the worm tissue. To localize the two sterols in the worms tissue, we used a high spatial-resolution method -Time-of-Flight Secondary Ion Mass Spectrometry (ToF-SIMS) - and a high mass-resolution imaging method -Matrix-Assisted Laser Desorption/Ionization combined with laser-induced post-ionization mass spectrometry imaging (MALDI-2-MSI) (Bien et al., 2021). High spatial-resolution imaging showed that sitosterol and cholesterol are uniformly distributed in the worm tissues (see **Figure 2G and 2H**). We could not identify any tissue specific distribution, and the presence of symbiont cells did not seem to modify the sterol profile of the proximate epithelial tissue. The high mass-resolution imaging of longitudinal worm sections confirmed the uniform sterol distributions throughout the animal (**Figure 2C, 2D and Supplementary Figure 15**) and, with accurate mass, the identity of the sterols (cholesterol $[M\text{-}H_2O+H]^+$ $C_{27}H_{45}$ *m/z* 369.352 ; sitosterol $[M\text{-}H_2O+H]^+$ $C_{29}H_{49}$ *m/z* 397.3756 (**Supplementary Table 1**)).

Sitosterol is present in the worm environment in concentrations sufficient to sustain the growth of small sterol auxotroph invertebrates. Chemical analysis of pore water profiles collected in the vicinity of seagrass meadows, the habitat of many gutless oligochaetes, revealed an irregular distribution of sterols. Some samples, such as the ones collected near *Posidonia oceanica* meadows off the island of Elba, had cholesterol and sitosterol present in the nano- to micro-molar range **(Supplementary Figure 1).** Samples collected in Belize, in the vicinity of other seagrasses like *Thalassia testudinum* and *Syringodium filiforme,* were devoid of detectable amounts of sitosterol or cholesterol. Seagrasses, like terrestrial plants, exude different organic compounds into their rhizosphere (Sogin et al., 2021; Vives-Peris et al., 2020). The sterol profile of *P. oceanica* roots was composed of sitosterol (69%), stigmasterol (11%) and campesterol (20%). *P. oceanica* could be the origin of the sitosterol in the porewater, but cannot be the source

of cholesterol as it was not present in its tissues. Cholesterol and sitosterol concentrations measured in the porewater environment (ranging from 25 nM to 3 µM) are in the range of reported minimal dietary sterol requirements for small sterol auxotroph invertebrates (Carvalho et al., 2010; Lu et al., 1977). The sterols in the porewater could pass through the cuticle of the worm as it is permeable to substances up to 70 kDa (Dubilier et al., 2006).

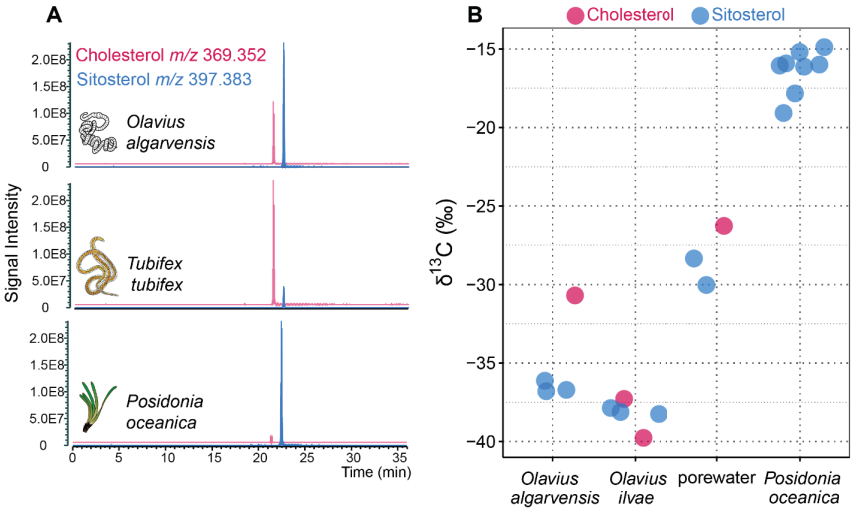

Figure 1 | *Olavius algarvensis* has an unusual sterol profile dominated by sitosterol, a plant sterol. A, Extracted-ion chromatograms (XIC) of cholesterol $[M\text{-}H_2O+H]^+$ *m/z* 369.52 (red) and sitosterol $[M\text{-}H_2O+H]^+$ *m/z* 397.383 (blue). The XICs were extracted from sterols extract from (from top to bottom): the marine gutless annelid *O. algarvensis*, the freshwater annelid *T. tubifex* and the seagrass *P. oceanica*. **B,** The ^{13}C isotopic composition of the sterols differ between gutless oligochaetes sterols and sterols present in the neighboring seagrass (*P. oceanica*) and the environment (porewater).

Worm sterols have an isotopic composition that is distinct from surrounding plants and environment. Isotopic composition is used to trace carbon origin and its path through the trophic chain with a passage from one trophic level to the next reflected by a change of 0.5 to 2 ‰ (McCutchan et al., 2003; Tiunov, 2007). Sitosterol present in seagrass tissue had isotopic values ranging from -16 to -15‰ (see **Figure 1B**). Those values are in accordance with *P. oceanica* bulk isotopic composition which ranges from -16.4 ‰ to -8.3 ‰ (Cooper & DeNiro, 1989; Jennings et al., 1997; Lepoint et al., 2004;

McMillan et al., 1980; Pinnegar & Polunin, 2000; Vizzini et al., 2010). They also match values previously reported specifically for sterols in other seagrasses (Canuel et al., 1997). The porewater sterols had carbon isotopic signature ($\delta^{13}C$) values of -30 to -28 ‰, about 12‰ lower than *P. oceanica* (see **Figure 1B**). Such differences between seagrass and sediment have been reported in the past for bulk $\delta^{13}C$ and sterol $\delta^{13}C$ (Canuel et al., 1997; Dauby, 1989; Fry et al., 1983; Thayer et al., 1978). Those differences reflect the mixed sources of the sterols present in the sediment, most of which are likely of planktonic origin. The sterols present in two worm species (*O. algarvensis* and *O. ilvae*) had the lowest $\delta^{13}C$ values, -39 to -36 ‰ for sitosterol and -40 to -31 ‰ for cholesterol (see **Figure 1B**). This unusual isotopic composition reflects the importance of the chemosynthetic symbionts in the nutrition of the host. In a previous study the bulk isotopic composition of *O. algarvensis* was determined by IRMS to be -30.6 ‰ (Kleiner et al., 2015). It is common for sterols to be ^{13}C-depleted relative to bulk biomass by 5 to 8 ‰ (Canuel et al., 1997; Hayes, 2018). This ^{13}C-depleted sterol signature led us to hypothesize that gutless oligochaetes synthesize both sterols *de novo*, using chemical building blocks provided by their chemosynthetic symbionts.

Homologues of all *de novo* sterol synthesis enzymes are encoded and expressed by *O. algarvensis*. We used metagenomics, metatranscriptomics and metaproteomics to search for enzymes specific to *de novo* sterol synthesis, screening both symbionts and host. The cholesterol biosynthesis pathway, starting with squalene, is a series of 10 connected enzymatic reactions encoded by 11 genes (**Figure 5** and **Supplementary Figure 2**). Our analysis showed that the symbionts, as with most bacteria, lacked the genetic machinery required for *de novo* sterol synthesis. The host, on the other hand, had the full enzymatic toolbox. Homologues of the 11 enzymes were present in the draft genome of *O. algarvensis* and *O. ilvae* (**Figure 5** and **Supplementary Table 2**). All enzymes were found to be transcribed (11 out of 11 enzymes) and most of the proteins where detected in the proteome (6 out of 11 proteins) of *O. algarvensis* (**Supplementary Table 2 and 3**), showing active expression of the pathway. Phylogenetic analysis allowed us to assign each homologue to an orthology group and thus a potential function (**Supplementary Figures 3 to 11**). Annelids have a limited ability for *de novo* sterol synthesis: polychaetes and some oligoachetes are capable of sterol synthesis, while

other oligochaetes such as *Lumbricus terrestris* are not (Voogt, 1973; Voogt et al., 1975; Walton & Pennock, 1972; Wootton & Wright, 1962). Here, we showed that *O. algarvensis* has all the enzymes required for *de novo* cholesterol synthesis, which in combination with the isotopic signature suggests that the worms are actively synthesizing cholesterol.

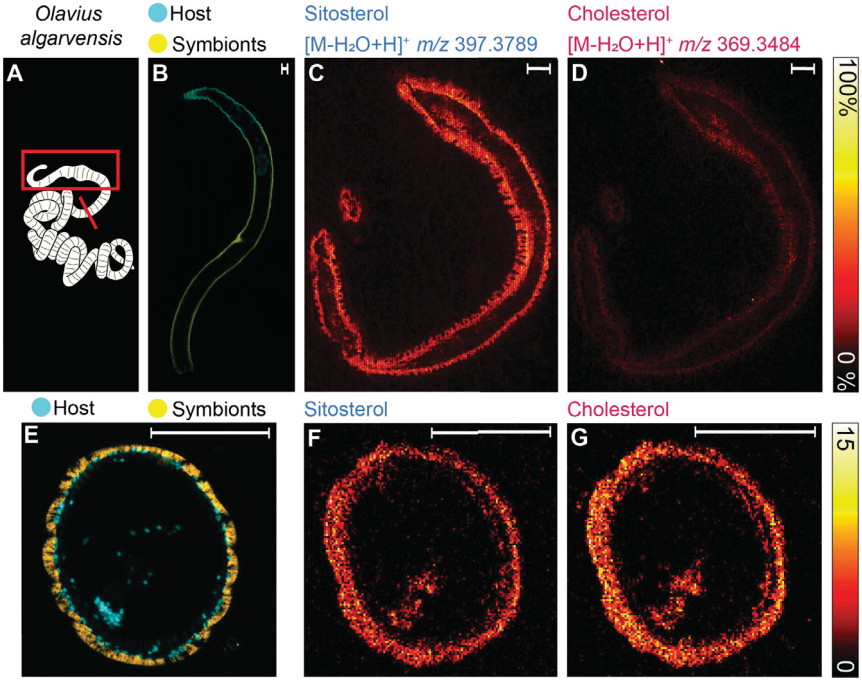

Figure 2 | Distribution of sitosterol and cholesterol in *Olavius algarvensis* measured by spatial metabolomics. **A,** Schematic representation of the worm, the red lines indicate the sectional planes. **B, E,** The chemosynthetic symbionts sit between the epidermis and cuticle of the worm. **B,** 16S rRNA targeted FISH images on whole mount worm (Image credit: Alex Gruhl). **E,** 16S rRNA targeted FISH images on cross section of the worms. The symbiont cells appear in yellow and host nuclei in blue. **C,** Distribution of *m/z* 397.3789 (sitosterol $[M\text{-}H_2O+H]^+$) as measured by MALDI-2-MSI. **D,** Distribution of *m/z* 369.3483 (cholesterol $[M\text{-}H_2O+H]^+$), measured with MALDI-2-MSI. **F,G,** Distribution of the sterol ions as imaged by ToF-SIMS. **F,** Summed intensity of sitosterol ions [*m/z*: 397.47, 383.37, 413.45]. **G,** Summed intensity of the cholesterol ions [*m/z* 369.38, 385.34, 401.35]. Scale bars represent 100 µm.

As described above, sterol synthesis does not follow one path in all kingdoms of life and, it is generally accepted that, animals are not capable of sitosterol synthesis. So how can one explain the presence of sitosterol and its ^{13}C composition pointing towards *de novo* synthesis in an animal? Even if we assume that, like in plants, gutless oligochaete enzymes can act reciprocally in both cholesterol and phytosterol biosynthesis, animals lack an essential enzyme dedicated to this pathway: C_{24}-sterol methyltransferase (SMT).

A homologue of SMT, an enzyme essential to sitosterol synthesis, is encoded and expressed in gutless oligochaetes. SMT catalyzes the transfer of a methyl group from S-Adenosyl-L-methionine (AdoMet) to the sterol side chain and is key for the biosynthesis of fungal and plant sterols. In the host draft genome, we found a putative SMT gene, 1071 bp long and organized as 4 exons with 3 introns (**Supplementary Figure 12**). The 1071 bp open reading frame (ORF) encoded a 356 amino-acid polypeptide. The amino acid sequence comparison against SwissProt SMTs resulted in similarity scores ranging from 25.75% to 42.58%, which is comparable to similarity scores observed between SMTs of different phyla (25.25% to 45.4%). The SMTs are evolutionary distant and only contain 63 completely conserved residues (about 20% of the protein); 25 of those residues are localized in the four conserved signature motifs and the other 38 can be found outside of those motifs (Bouvier-Navé et al., 1998; Jayasimha & Nes, 2008; Nes et al., 2004, 2008; Nes & Heupel, 1986; Schaller, 2004; Veeramachaneni, P. P., 2005). The four substrate binding regions are present in the gutless oligochaete SMT: Region II, which binds to AdoMet and Regions I, III and IV which interact with sterols (**Supplementary Figure 13**). All the C_{24}-SMT characteristics are present in the *O. algarvensis* homologue. We identified SMT homologues in the transcriptomes of nine other gutless oligochaete species. It is the first time a C^{24}-SMT is found in eumetazoans.

SMT homologues are present in two eumetazoan phyla, annelids and rotifers. To assess the presence of SMT homologues in other animals, we performed protein searches against NCBI (National Center for Biotechnology Information) databases (nr, tsa_nr, refseq_prot, env_nr and tsa; available from: https://www.ncbi.nlm.nih.gov/) as well as the proteomes predicted by Ensembl metazoan (Howe et al., 2020) and Compagen (Hemmrich & Bosch, 2008). Hits were found in four eumetazoan phyla (annelids,

mollusks, nematodes and rotifers), two insects, one crustacean, one fish and one fruit bat. The animal sequences and representative SMTs from different phyla (Desmond & Gribaldo, 2009; Gold et al., 2016) were used to build an amino acid sequence tree (**Supplementary Figure 14**). The sequences found in mollusks, insects, crustacean, fish and bats clustered together with plant or algae sequences and were likely to be contaminations from their gut content. The sequences isolated from nematodes belonged to the C_4-SMT group, a SMT specific to nematodes (D. J. Chitwood, 1991). Only the rotifer and annelid sequences did not cluster with plant or algae sequences (**Figure 3)**. The rotifer sequences grouped together forming a sister group to plant SMT1. Those rotifers were isolated from different environments and had access to different food resources, which suggest the sequences observed were not contamination. All annelid sequences fell in the C_{24}-SMT part of the tree. All the annelid sequences clustered together; with the exception of the leech *Hirudo verbena* (**Figure 3**). Annelid sequences formed their own group surrounded by sponge C_{24}-SMT and other C_{24}-SMTs. The annelid sequences clustered according to their taxonomic affiliation: marine polychaetes grouped together while terrestrial and aquatic oligochaetes formed a distinct group. These results suggest the existence of an animal SMT present in sponges, rotifers and annelids.

We detected SMTs in three animal phyla: sponges, annelids and rotifers. The presence of SMTs in some sponges has been reported previously and is essential for the synthesis of 24-isopropylcholesterol, a sponge biomarker (Gold et al., 2016). We report here the first SMT in annelids and rotifers. Sterol auxotrophy has been proposed for rotifers (Wacker & Martin-Creuzburg, 2012) and SMTs might play a different role in those organisms. SMTs were identified in 15 non-symbiotic annelid species belonging to the oligochaete and polychaete classes. We analyzed the sterol profile of *Capitella teleta* which exhibited a standard animal sterol profile dominated by cholesterol with only minute amounts of plant sterols. We could not find reports of annelid sterol profiles dominated by sitosterol or other plant sterols. Gutless oligochaetes are so far the only annelids shown to use SMT to synthesize sitosterol in abundance. In other annelids, sterols derived from SMT activity, even in low abundance, might play an important signaling role while cholesterol fulfills the bulk structural requirements. However one cannot exclude that, in

those annelids, SMT has overlapping functions that are not related to sitosterol synthesis, as suggested for some copies of plant SMTs (Carland et al., 2010).

Only one SMT isoform was encoded by the *O. algarvensis* genome, suggesting that *O. algarvensis* SMT is a bifunctional enzyme. In plants, C-24 and C-28 methylation are mediated by different enzyme isoforms, SMT1 and SMT2 (Bouvier-Navé et al., 1998; Hartmann, 2004; Neelakandan et al., 2009). However, many vascular plant and protozoan SMTs have bifunctional behavior: they can catalyze both C-24 and C-28 methylations in vitro (Bouvier-Navé et al., 1998; Neelakandan et al., 2009; Nes, 2003; Zhou et al., 2006). In addition, in basal plants such as green algae, a single SMT catalyzes both methylation steps, producing sterol with methylation at C-24 and ethylation at C-24 (Desmond & Gribaldo, 2009; Haubrich et al., 2015). Finally, sterol profiles and genome analyses suggest that sponge SMTs are bifunctional (Gold et al., 2016). It is therefore likely that the *O. algarvensis* SMT is able to produce sterols ethylated at C-24, specifically sitosterol with a single SMT isoform.

***O. algarvensis* SMT shows a sterol methyltransferase activity.** To confirm that the gutless oligochaete SMT corresponds to a functional SMT enzyme, we overexpressed SMTs from two species of gutless oligochaete in *Escherichia coli* cells and yielded a target protein migrating on SDS-PAGE with the expected size of ~40 kDa. The enzymes were not purified further as the purification steps have been shown to reduce the enzyme activity (Howard, 2016). To test the enzymatic activity, substrate preferences and products, we assayed crude protein extracts with AdoMet and different sterol substrates. The resulting products were analyzed using GC-MS. The SMTs from *O. algarvensis* and *O. clavatus* used zymosterol as substrate for the first C_1-transfer reaction. When incubated with zymosterol and AdoMet, both enzymes produced methylzymosterol (**Figure 4 and Supplementary Figure 16**). The mass spectra indicated that the methyl group was added to the zymosterol side chain, likely at the C_{24}-position (**Supplementary Figure 18**). This is the first time that the activity of an animal SMT is shown. We could determine the natural substrate of the first C_1-transfer reaction, zymosterol. However, sitosterol synthesis requires a second C_1-transfer. We did not detect products decorated with two methyl groups in our assay. We therefore hypothesize that in gutless

oligochaetes, like in plants, the two C_1-transfers happen at different stages of the biosynthetic pathway. The substrate of the second C_1-tranfer reaction remains unknown and its identification will require further testing.

The first part of the gutless oligochaete sitosterol synthesis pathway overlaps with cholesterol metabolism. The results of the enzymatic assay gave us information on the sitosterol synthesis pathway. Zymosterol, an intermediate of cholesterol synthesis, is produced in the second half of the pathway. This suggests that in gutless oligochaetes, cholesterol and sitosterol synthesis share a common trunk and only branched off towards the end of the pathway (**Figure 5**). The last five enzymatic reactions required for sitosterol synthesis are known but the order in which they occur still needs to be determined. We only identified one copy of the enzymes mediating those last five enzymatic reactions. This suggests that the same enzymes are acting in both the cholesterol and sitosterol pathways and that one sterol methyltransferase is responsible for both C_1-transfer reactions. This newly described animal sitosterol biosynthetic pathway is different from the known plant pathways and closely resembles known animal cholesterol metabolism.

Conclusion

While ubiquitous in plants and fungi, SMTs were mainly absent from animals (Haubrich et al., 2015; Volkman, 2005). So far, animal SMT sequences were only reported in a few sponges (the oldest multicellular animal) (Germer et al., 2017; Gold et al., 2016) and in *C. teleta* (Najle et al., 2016). It is hypothesized that an ancestral SMT was present in the last eukaryotic common ancestor (LECA) (Desmond & Gribaldo, 2009; Haubrich et al., 2015). The current hypothesis is that SMT was lost in the animal branch (Desmond & Gribaldo, 2009; Gold et al., 2016; Haubrich et al., 2015). Our results indicate that it was not lost in all phyla and seems to remain not only in porifera but also in annelids, rotifers and cnidaria. Those phyla are not closely related, live in different environments and have different lifestyles and sterol profiles. The absence of SMT in other animal phyla is puzzling; as more animal genomes are sequenced we might be able to identify new animal SMTs. All the animal sequences identified so far were found in the proteome and transcriptome, which indicates that the enzyme is actively used. The low abundance of

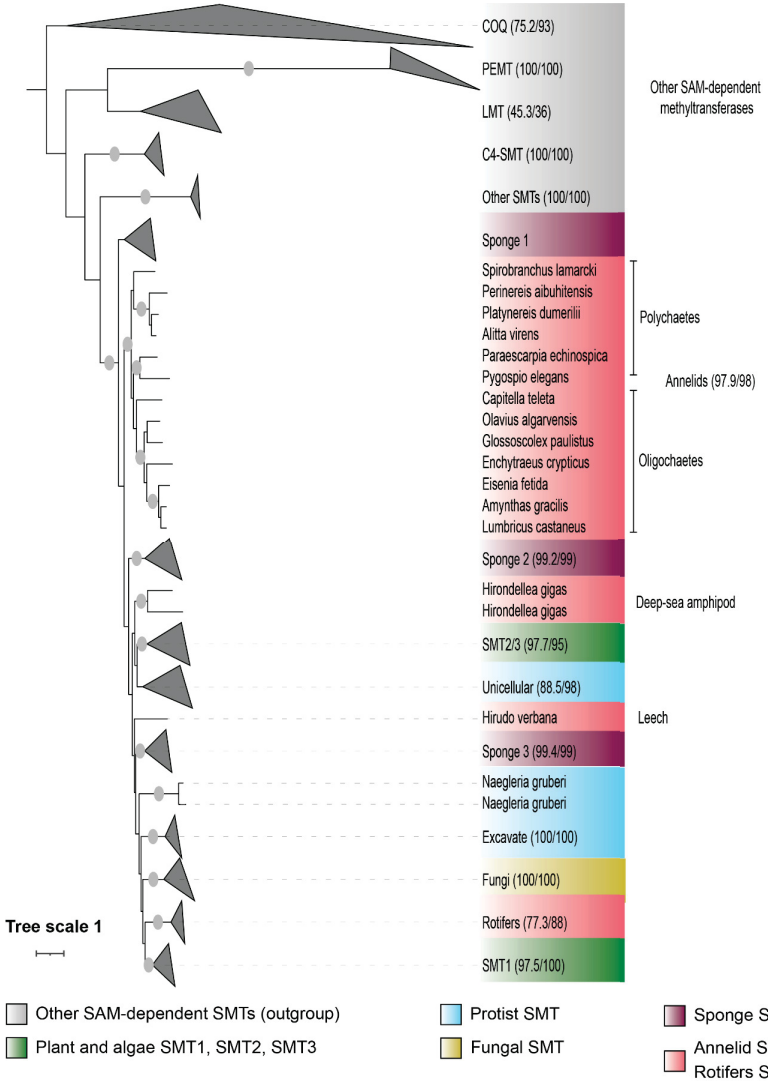

Figure 3 | Newly discovered annelid SMT sequences belonging to the C_{24}-SMT group. Maximum likelihood amino acid tree for eukaryotic SMTs, the sequences were clustered at 90% identity to make the tree more readable. Nodes with a bootstrap value > 90 are marked with grey circles. The tree is represented rooted at midpoint. Other SAM-dependent methyltransferases were used as outgroup. Ubiquinone biosynthesis O-methyltransferase (COQ),

Phosphoethanolamine N-methyltransferase (PEMT), Tocopherol O-methyltransferase (TMT), C4 sterol methyltransferase (C_4-SMT).

methyl groups in sterols in all non-symbiotic annelids analyzed so far (Ballantine et al., 1978; Cerbulis & Taylor, 1969; Marsh et al., 1990) suggests that the enzyme might play a different role in their metabolism. In gutless oligochaetes, the abundance and 13C isotopic composition of sitosterol suggest a novel biosynthetic pathway of sitosterol that is unlike the fungal or plant pathways and represents a new catalytically distinct type of sterol methyl transferase.

In all eukaryotes, free sterols reside predominantly in the plasma membrane. In mammalian and insect cells, phytosterols can replace cholesterol as structural component of the membrane but the cells still require a small amount of cholesterol for growth, as phytosterols cannot fulfill all the functions of cholesterol (Clark & Bloch, 1959; Rujanavech & Silbert, 1986; Stevenson & Brown, 2009; Xu et al., 2005). These studies are important because they showed that plant sterols could be taken up and utilized by animal plasma membranes. Studies on artificial membranes showed that cholesterol and plant sterols have different effects on the physical properties of the lipid bilayers. Gutless oligochaetes could replace part of the cholesterol in their plasma membrane by sitosterol, but this would have an impact on the physical properties of the cell membrane. As the worm has the ability to *de novo* synthesize both sitosterol and cholesterol, sitosterol likely has a unique role in gutless oligochaetes which cannot be fulfilled by cholesterol. Gutless oligochaetes represent an attractive novel system to study the impact of sterol composition on membrane properties *in vivo* and to further our understanding of the many roles sterols play in eukaryotic cells.

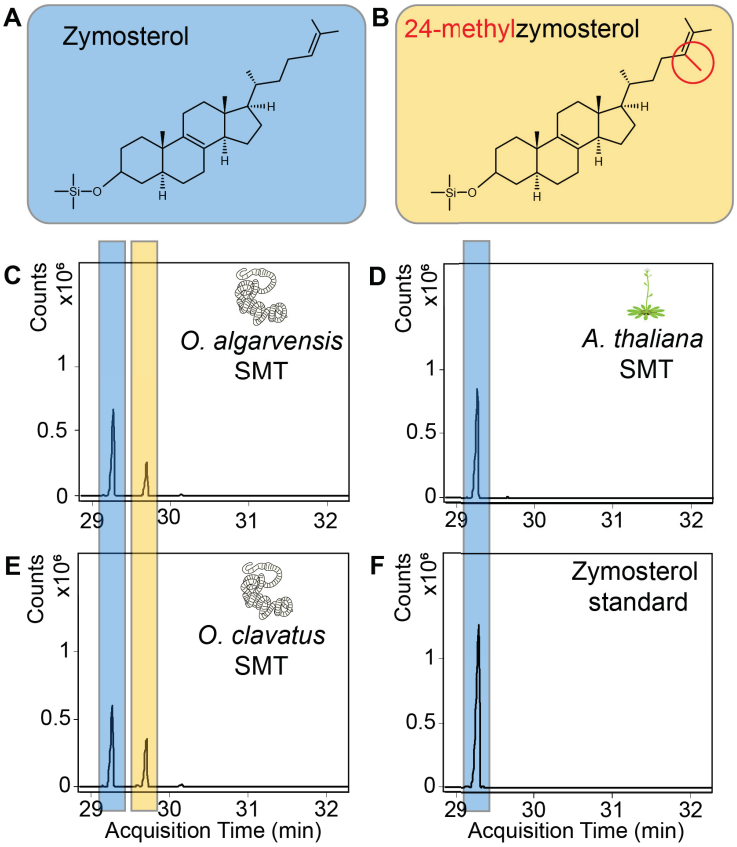

Figure 4 | The gutless oligochaete SMTs used zymosterol as substrate for the first C_1-transfer reaction. A,B, Structure of zymosterol and methyzymosterol, the substrate and product of the sterol methyltransferase assay. **C-F,** Chromatograms of the enzymatic assay performed with zymosterol as substrate. **C, E** The two gutless oligochaete SMTs added a methyl group to the side chain of zymosterol. **D,** Zymosterol was not the preferred substrate of *A. thaliana* SMT. F, The zymosterol used as substrate did not contain any trace of methylated zymosterol.

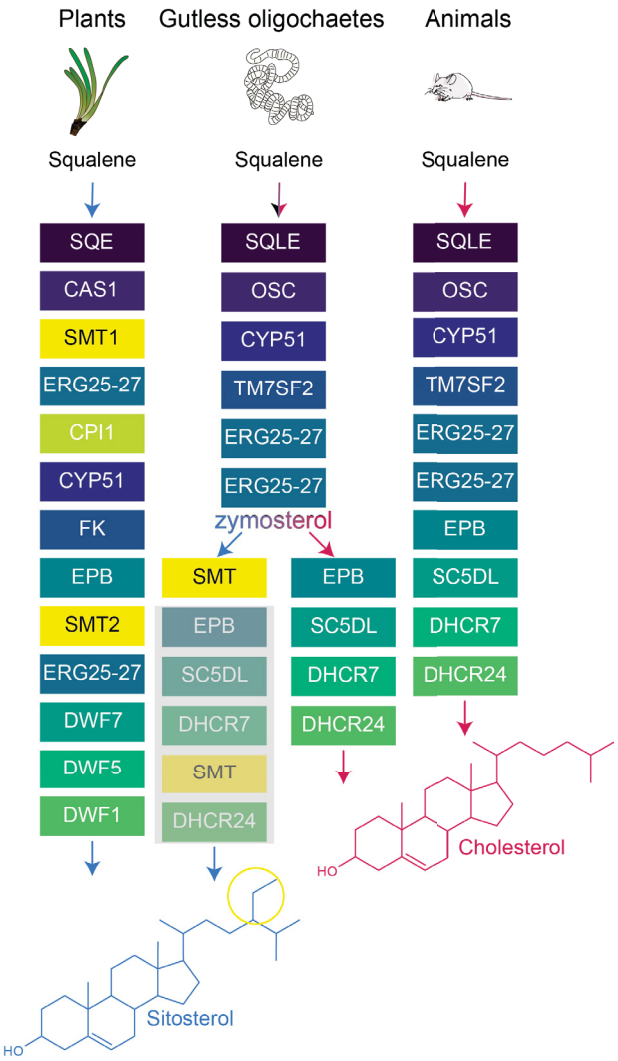

Figure 5 | Comparison of the proposed sterol synthesis pathway in gutless oligochaetes with the canonical cholesterol and sitosterol synthesis. A homologue of SMT, an enzyme usually absent from animals and essential to sitosterol synthesis, is present in *O. algarvensis*. We hypothesize that the first six steps are common to both cholesterol and sitosterol synthesis pathways. This trunk pathway branched off after the synthesis of zymosterol.

Zymosterol is the substrate used by SMT for the first C_1-transfer reaction. The order of the last steps in the sitosterol synthesis branch as well as the substrate of the second C_1-transfer reaction are unknown.

Materials and Methods

Reagents. All organic solvents were LC–MS grade: acetonitrile (ACN; Honeywell, Honeywell Specialty Chemicals), chloroform (Merck), isopropanol (IPA; BioSolve), methanol (MeOH; BioSolve), hexane (Sigma- Aldrich), acetone (Sigma-Aldrich), ethanol (EtOH, Sigma-Aldrich) and formic acid (FA; Sigma-Aldrich). Water was deionized using the Astacus MembraPure system (MembraPure). The pyridine (Pyridine dried (max. 0.0075 % H_2O) SeccoSolv®) was from Sigma-Aldrich. The reagents used for GC-MS derivatization were purchased at Chromatographie Service and Sigma Aldrich. The internal standards (5α-cholestane and Ribitol) used for GC-MS analysis were purchased at Sigma-Aldrich.

Sampling

Gutless oligochaetes. Sediments containing gutless oligochaetes were collected by scuba diving in the vicinity of seagrass meadows. Gutless oligochaete worms were extracted manually from the sediment and either directly fixed in MeOH or kept in aquaria with seagrass and sediment from the collection site for up to one year before usage in experiments. The worms were sampled in five different locations: in the bay of Sant'Andrea (Island of Elba, Italy) (42° 48'29.4588" N; 10° 8' 34.4436" E), in the bay of Magaluf (Mallorca, Spain) (39º 30' 14.814''N; 2º 32' 35.868''E), at Carrie Bow Cay (Belize) (16° 04' 59" N; 88° 04' 55" W),Twin Cayes (Belize) (16° 50' 3" N; 88° 6' 23" W), and in Okinawa (Japan) (26°29'33.4"N; 127°50'31.6"E).

Seagrass: Seagrass plants were collected by scuba diving in the bay of Sant'Andrea (Elba, Italy) (42° 48'29.4588" N; 10° 8' 34.4436" E). The leaves, roots and rhizomes were dissected using a razor blade, placed into individual bags and stored at -20°C.

Porewater: Porewater was collected from sediments for metabolomics analyses. We sampled in and nearby seagrass meadows in the Mediterranean in the bay of

Sant'Andrea (Elba, Italy) (42° 48'29.4588" N; 10° 8' 34.4436" E) and in the Caribbean at Carrie Bow Cay (Belize) (16° 04' 59" N; 88° 04' 55" W) and Twin Cayes (Belize) (16° 50' 3" N; 88° 6' 23" W). Using a steel lance (1 m long, 2 mm inner diameter) fitted with a wire mesh (63 µm) to prevent the intake of sediment and seagrass, porewater was slowly extracted from sediments into polypropylene syringes. A porewater profile consisted of top to bottom sampling of the sediments every 5 or 10 cm down to 30 cm. For metabolomics analysis, 10 mL samples were stored at -20°C until further processing. For DOC analysis, 20 mL of sample was filtered through pre-combusted (500 °C, 4 h) Whatman GF/F filters (0.7 µM) into 20 mL acid-washed and pre-combusted scintillation vials. Samples were acidified to pH 2 using 25 % hydrochloric acid and stored at 4 °C until analysis.

Metabolite extraction

Gutless oligochaetes: Metabolites were extracted from gutless oligochaetes using the following method for metabolite profiling: tissues from MeOH fixed worms were transferred to 2 mL screwcap tubes containing a mix of silica beads (Sigmund Linder). The residual methanol was added to the screw cap tube. The tubes were spiked with 100 µL of 5α-cholestane (1 mM) and 40 µL of ribitol (0.2 mg mL^{-1}). 0.5 mL of pre-cooled extraction solution (acetonitrile:MeOH:water (v:v:v) 2:2:1) was added to each tube.

Tissues were disrupted by bead beating: 2 cycles of 40 sec (4 m s^{-1}). The tissues were pelleted by centrifugation (10,000 rpm, 2 min), and the supernatants were transferred to new tubes. The pellets were extracted one more time with 1.5 mL of extraction solution. The supernatants were combined and evaporated to dryness in a vacuum concentrator without heating (approximately 1.5 h). The obtained aliquots were stored at -20 °C until metabolite derivatization.

Seagrass: The frozen plant tissues were ground to a fine powder in liquid nitrogen using a pestle and mortar. 70 mg of the powder was transferred to 2 mL screw cap tubes containing 1.2 mL methanol (pre-cooled at -20°C). The tubes were vortexed for 10 sec. The internal standards were added to the tubes: 40 µL ribitol (0.2 mg mL^{-1}) and 100 µL 5α-cholestane (1 mM), and the tubes were vortexed for another 10 sec. The tubes were

placed on a thermomixer and shaken for 10 min at 70°C at 950 rpm. The plant powder was pelleted by centrifugation (10 min, 11,000 x g, 4°C). The supernatant was transferred into a new 2 mL Eppendorf tube and evaporated to dryness using a Concentrator Plus (Eppendorf) (V-AL, 1.5 h, 45°C).

Porewater: Sterols were extracted using Superclean LC-18 SPE tubes (6 ml, 0.5 g, Supelco). The silica cartridge was equilibrated using a ultra-pure water(UPW):MeOH dilution series (0:1, 1:4, 1:1, 4:1, 1:0 [v/v]). The porewater samples were spiked with internal standard (100 µL 5α-cholestane (1mM)), before being loaded on the column. The impurities were removed by three successive ultra-pure water washes. Finally the sterols were eluted from the cartridge with 3 x 5 mL of methanol. The methanol fractions were collected and evaporated to dryness using a Concentrator Plus on V-AL mode with centrifugation at 30°C. Positive and negative controls were run in parallel. As negative control, sterols were extracted from 10 mL of artificial sea water (ASW). As positive control, 10 mL ASW spiked with 20, 40, or 80 nmol of cholesterol and β-sitosterol were analyzed.

GC-MS analysis

Derivatization: To remove condensation formed during extract storage, we further dried the extracts in a vacuum concentrator for 30 min prior sample preparation for GC-MS analysis.

Gutless oligochaete: Metabolite derivatization was performed by adding 80 µL of methoxyamine hydrochloride (MeOX) dissolved in pyridine (20 mg mL^{-1}) to the dried pellet and incubating for 90 min at 37 °C using a thermomixer (BioShake iQ, Analytik Jena) under constant rotation at 1350 rpm. Following the addition of 100 µL of N,O-Bis(trimethylsilyl)trifluoroacetamide (BSTFA) (Chromatographic Service), each extract was vortexed, and incubated for another 30 min at 37 °C on a thermomixer under constant rotation at 1350 rpm. After a short centrifugation, 100 µL of the supernatant was transferred to GC-MS vials for GC-MS data acquisition.

Seagrass: 80 µL of MeOX (20 mg mL^{-1} pyridine) was added to the dried extracts. The resuspended dried extract were vortexed for a few seconds and placed on a thermomixer (BioShake iQ, Analytik Jena) for 90 min (37°C, 1200 rpm). 80 µL of BSTFA was added to the tubes. They were vortexted for a few seconds and placed on a thermomixer (BioShake iQ, Analytik Jena) for 15 min (60°C, 1200 rpm). After a short centrifugation, 100 µL of the supernatant was transferred into GC-MS vials (Insert G27, sping S27 and Mikor-KH-Vial G1; Chromatographic Service) and analyzed by GC-MS.

Porewater: After complete evaporation, 80 µL of BSTFA was added to the tubes. The tubes were gently vortexed and placed on a thermomixer for 15 min (60°C, 950 rpm). After a short centrifugation (1 min, 9000 rpm), the supernatant was transferred into GC-MS vials and analyzed.

Data acquisition: The analysis of all metabolomics samples was conducted on a 7890B GC system (Agilent Technologies) coupled to a 5977A single quadrupole mass selective detector (Agilent Technologies). The gas chromatograph was equipped with a DB-5ms column (30 m × 0.25 mm, film thickness 0.25 µm; including 10 m DuraGuard column, Agilent Technologies) and a GC inlet liner (ultra inert, splitless, single taper, glass wool, Agilent). Helium was used as gas carrier at a constant flow (0.8 mL min^{-1}). An Agilent 7693 autosampler injected 1 µL of derivatized sample in splitless mode. The injector temperature was set at 290°C. The temperature program started at 60°C for 2 min, and then increased to 300°C at 10°C/min. Finally the temperature was held at 325°C for 7 min. Mass spectra were acquired in electron ionization mode at 70 eV across the mass range of 50–600 *m/z* and a scan rate of 2 scans s^{-1}. The retention time was locked using a standard mixture of fatty acid methyl esters (Sigma Aldrich). Sterol identification was based on NIST MS search hits and on comparison with standards.

Data analysis: Sterols were identified through comparison with standards using the Mass Hunter Suite and through comparison to the NIST database. Sterols were further quantified using the Mass Hunter Quantification Suite (Agilent).

HPLC-MS

High-resolution LC–MS/MS. The analysis was performed using a QExactive Plus Orbitrap (Thermo Fisher Scientific) equipped with a HESI probe and a Vanquish Horizon UHPLC system (Thermo Fisher Scientific). The lipids were separated on an Accucore C30 column (150 × 2.1 mm, 2.6 µm, Thermo Fisher Scientific), at 40°C, using a solvent gradient. Buffer A (60/40 ACN/H2O, 10 mM ammonium formate, 0.1% FA) and buffer B (90/10 IPA/ACN, 10 mM ammonium formate, 0.1% FA) (Breitkopf et al., 2017) were used at a flow rate of 350 µl min−1. The lipids were eluted from the column with a gradient starting at 0% buffer B (**Supplementary Table 4**). The injection volume was 10 µl. In the same run, MS measurements were acquired in positive-ion and negative-ion mode for a mass detection range of *m/z* = 150–1,500. Resolution of the mass analyzer was set to 70,000 for MS scans and 35,000 for MS/MS scans at *m/z* = 200. MS/MS scans of the eight most abundant precursor ions were acquired in positive-ion and negative-ion modes. Dynamic exclusion was enabled for 30 s and collision energy was set to 30 eV (for more details see **Supplementary Table 5**). The data was analyzed with *Thermo FreeStyle*™ (version 1.6) and Xcalibur *Quan* Browser Software v. 2.0.3 (Thermo).

GC-IRMS

Sample preparation: Sterols were extracted from the gutless worms *O. algarvensis* and *O. ilvae*, as well as from the rhizome and leaves of *Posidonia Oceanica*. All samples were extracted with dichloromethane:MeOH (2:1) three times. Then, the resulting total lipid extracts were separated by solid phase extraction with a Machery & Nagel aminopropyl modified silica gel column (500mg) into four fractions with increasing polarity (see (Birgel et al., 2008). For the sterols, the third fraction was used (dichloromethane:acetone 9:1). Prior to measurement on the GC-MS and GC-IRMS, the samples were silylated with BSTFA. The porewater samples were extracted as described above.

Data acquisition: The resulting sterols were identified on a Thermo Electron Trace DSQ II coupled gas-chromatograph-mass spectrometer (GC-MS) for identification. The GC-MS was equipped with a 30 m HP-5 MS UI fused silica capillary column (0.25 mm in

diameter, 0.25 µm film thickness). The carrier gas was helium. The GC temperature program used for both fractions was as follows: 60°C (1 min), from 60°C to 150°C at 10°C/min, from 150°C to 325°C at 4°C/min, 25 min isothermal. Identification of compounds was based on retention times and published mass spectral data. Compound-specific carbon stable isotope compositions of sterols were measured on a gas chromatograph (Agilent 6890) coupled with a Thermo Finnigan Combustion III interface to a Finnigan Delta Plus XL isotope ratio mass spectrometer (GC-IRMS). The GC conditions were identical to those mentioned above for GC-MS analyses. All sterols were corrected for their additional carbons introduced by derivatization with BSTFA. The standard deviation of the isotope measurements was < 0.8‰.

MALDI-2-MSI

Sample preparation: The worms were prepared following Kadesch et al. (2019) with a few modifications. Briefly, 20 µL of 6.7% glutaraldehyde solution in marine phosphate buffered saline were deposited on a glass slide. Gutless oligochaetes were transferred to the fixative using bended acupuncture needles. A coverslip was applied, and samples were frozen in liquid nitrogen and stored at −80°C until further processing.

A single worm was transferred using featherweight forceps onto the Sodium carboxymethyl cellulose (CMC; Sigma-Aldrich) stamp which was glued onto a cryostat specimen disc (Leica). A quantity of 10−20 µL of 8% gelatin solution (β= 80 g/L) were used to coat the worm. The specimen disc with the sample was transferred to the cryostat (Leica CM3050 S, Leica Biosystems) and kept for 30 min at -22°C before sectioning into specimens of 12 µm thickness (chamber temperature -22°C, object temperature -22°C). Sections were thaw-mounted on IntelliSlides (Bruker), and their quality was determined microscopically. Sections of sufficient quality were stored in a desiccator at room temperature (RT) until further analysis.

Matrix application: For matrix application, a total amount of 30 mg 2′,5′-Dihydroxyacetophenone (DHAP; Sigma-Aldrich) dissolved in 1.5 mL acetone was transferred to the brass pan of a home-built sublimation chamber. The reservoir was preheated to 130°C and, after solvent evaporation, the sample was placed on a water-

cooled surface of ~ 4°C directly over the pan with the sample pointing downward. The whole setup was then transferred to a vacuum of ~ 3 mbar and the matrix was allowed to sublimate and redeposit for 6 min before the process was stopped by ventilation with N_2. After removing the sample slide from the apparatus, it was immediately transferred to the ion source of the mass analyzer. The 6 min deposition resulted in a matrix coverage of 236 ± 34 µg/cm^2 as derived from weight measurements of neat glass slides before and after sublimation under the same conditions.

Data acquisition: MSI data were acquired on a modified timsTOF fleX instrument (Bruker Daltonik, Bremen, Germany) (Soltwisch et al., 2020). The mass resolving power of this hybrid QTOF-type instrument is about 40,000 (fwhm) in the investigated *m/z* range of 300–1500. Primary material ejection and ionization were achieved with a SmartBeam 3D laser (actively Q-switched, frequency-tripled diode-pumped solid-state laser; wavelength: 355 nm) followed by laser post-ionization (actively Q-switched, frequency-quadrupled Nd:YAG, NL 204-1k-FH, EKSPLA, Vilnius, Lithuania; wavelength: 266 nm). The distance of the primary ionization laser beam to the sample surface was set to about 500 µm and the delay between the two laser pulses, both operated at 1 kHz, was set to 8 µsec. For material ejection, a scan range of 1 µm of the laser spot on the target was used, resulting in an ablated area of 5 µm in diameter. The step size of the stage during the MSI run was set to 5 µm. The laser power was set to 40%, with 50 laser shots/pixel.

Data analysis: SCiLS lab (version 2021a) was used for data analysis and for the production of the ion images shown in the figures. The ion images represent the data without normalization and with hot spot removal.

TOF-SIMS

Sample preparation: *O. algarvensis specimens were fixed with 4%* paraformaldehyde (PFA) at 4°C for 4 h. The fixative was removed by 3 washes of marine phosphate buffer. The washed samples were then stored at -20°C in MeOH.

PFA fixed samples were embedded in paraffin. The MeOH was exchanged with pure EtOH by 3 successive incubations of 60 min in pure EtOH at RT. The samples were then

incubated in RothiHistol (30 min, 60 min, and overnight at RT). When the samples were infiltrated with paraffin at 60°C, they were placed in fresh paraffin after 30 min, then again after 60 min, and again after another 60 min and let to incubate overnight. For embedding, two-thirds of the embedding mold was filled with paraffin. The sample was placed in the mold and the mold was filled completely with paraffin. The sample was aligned and let to polymerize for a week. After polymerization, a microtome was used to cut 4 µm thin-sections. The sections were placed on Poly-L-lysine coated glass slides (Sigma-Aldrich), let to air dry overnight and baked at 60°C for 2 hours to improve adherence to the slide. Finally, the sections were de-waxed, first by three baths of 10 min in RothiHistol, followed by an EtOH series (96%, 80%, 70%, 50%), and finally the slides were dipped in ultra-pure water and let to air dry. Once dried they were wrapped in aluminum foil and stored in a desiccator (Roth, Desiccator ROTILABO® Glass, DN 250, 8.0 l) until ToF-SIMS analysis.

Data acquisition and analysis: SIMS data were acquired on an IONTOF ToF-SIMS 5 instrument (IONTOF GmbH). The analytical ion beam used was a 25keV Bi_3^+ LMIG. To obtain high resolution mass spectra, high current bunch mode was used with a beam current of ~1 pA. The analytical area was typically 100 μm^2. Secondary ion maps were collected using the Bi_3^+ LMIG in burst alignment mode for greater lateral resolving power. The samples were also sputter pre-cleaned using a 5keV Ar_{1000}^+ cluster ion beam. The data were analyzed in SurfaceLab 7 (IONTOF). We analyzed standards to determine the most abundant ions produced by each sterol: cholesterol ($C_{27}H_{45}$, 369.38 *m/z*; $C_{27}H_{45}O$, 385.34 *m/z*; $C_{27}H_{45}O_2$, 401.35 *m/z*) and sitosterol ($C_{29}H_{49}$, 397.47 *m/z*; $C_{28}H_{47}$, 383.37 *m/z*; $C_{29}H_{49}O$, 413.45 *m/z*). To determine the distribution of each sterol in *O. algarvensis* sections, the intensity of the three most abundant ions was combined.

Identification of genes involved in sterol biosynthesis

Transcriptomes generated in a previous study (Wippler et al., 2016) were analyzed more deeply in this study for sequence and expression information related to sterol biosynthesis. Protein sequences from humans, *A. thaliana* and Saccharomyces *cerevisiae* were used as query to search the transcriptomic assemblies with TBLASTN

(e-value 1e-10). The identity of the hits was confirmed by BLASTP search against the NCBI nr and swissprot database as well as by INTERPROSCAN domain prediction. *O. algarvensis* sequences were aligned with reference sequences (Desmond & Gribaldo, 2009) using Clutalw (Larkin et al., 2007), trimmed with trimAl (Capella-Gutiérrez et al., 2009). Those alignments were used to calculate maximum-likelihood trees with ultrafast bootstrap support values using IQ-TREE (Minh et al., 2020). The resulting trees were visualized and beautified using iTOL (Letunic & Bork, 2019). The trees can be found in **Supplementary Figures 3 to 11.**

Gutless oligochaete nucleic acid extraction, sequencing and analysis

Extraction and sequencing. Genomic DNA was extracted from fresh specimens of two gutless oligochaete species (*O. algarvensis* and *O. ilvae*, n=1). High molecular weight genomic DNA was isolated with the MagAttract HMW DNA Kit (Qiagen). Quality was assessed by the Agilent FEMTOpulse and DNA quantified by the Quantus dsDNA kit (Promega). DNA was processed to get a PacBio Sequencing-compatible library following the recommendations outlined in "Procedure & Checklist – Preparing HiFi Libraries from Low DNA Input Using SMRTbell Express Template Prep Kit 2.0". Libraries were sequenced on a Sequel II instance at the Max-Planck Genome-centre Cologne (MP-GC) with sequencing chemistry 2.0, binding kit 2.0 on one 8M SMRT cell for 30 h applying continuous long read (CLR) sequencing mode.

Assembly and identification of genes involved in sterol biosynthesis. The CLR reads were assembled using Flye (v 2.8) (Kolmogorov et al., 2019). The completeness of the assembly was assessed with QUAST (Gurevich et al., 2013) and BUSCO (Seppey et al., 2019). *O. algarvensis* SMT sequences were retrieved from the PacBio assembly using BLAT (Kent, 2002) and SCIPIO (Keller et al., 2008).

Metaproteomics

Extraction. We prepared tryptic peptides following the filter-aided sample preparation (FASP) protocol, adapted from Wiśniewski et al. (2009). We added 60 µL of SDT-lysis buffer to each worm and boiled samples at 95°C for 10 min. To minimize sample loss, we

omitted the 5 min centrifugation step at 21,000 x g described in the original protocol (Wiśniewski et al., 2009) and instead mixed the complete 60 µL of each lysate with 400 µL of UA solution in a 10 kDa MWCO 500 µL centrifugal filter unit. Next, we added 200 µL of UA solution and centrifuged again at 14,000 x g for 40 min. We added 100 µL of IAA solution (0.05 M iodoacetamide in UA solution) and then incubated samples at 22°C for 20 min in the dark. We removed the IAA solution by centrifugation followed by three wash steps with 100 µL of UA solution. Subsequently, we washed the filters three times with 100 µL of ABC buffer (50 mM ammonium bicarbonate). We added 0.54 µg of Pierce MS grade trypsin (Thermo Fisher Scientific) in 40 µL of ABC buffer to each filter. Filters were incubated overnight in a wet chamber at 37°C. The next day, we eluted the peptides by centrifugation at 14,000 x g for 20 min followed by the addition of 50 µL of 0.5 M NaCl and another centrifugation step. Peptides were quantified using the Pierce MicroBCA Kit (Thermo Fisher Scientific) following the instructions of the manufacturer.

One-dimensional liquid chromatography–tandem mass spectrometry (1D-LC-MS/MS). Samples were analyzed by one-dimensional liquid chromatography–tandem mass spectrometry using an alternating block-randomization to account for batch effects (Oberg & Vitek, 2009). For each run, 800 ng of peptide were loaded onto a 300 µm i.d. x 5 mm nano trap cartridge column packed with Acclaim PepMap100 C18, 5 µm, 100 Å (Thermo Fisher, 160454) using an UltiMate 3000 RSLCnano Liquid Chromatograph (Thermo Fisher Scientific). The pre-column was connected to a 75 µm x 75 cm analytical EASY-Spray column packed with PepMap RSLC C18, 2 µm material (Thermo Fisher Scientific), which was heated to 55°C via the integrated heating module. The analytical column was connected via an Easy-Spray source to a Q Exactive HF-X Hybrid Quadrupole-Orbitrap mass spectrometer (Thermo Fisher Scientific). Peptides were separated on the analytical column at a flow rate of 225 nl min^{-1} using a 260 min gradient going from buffer A (0.2% formic acid, 5% acetonitrile) to 31% buffer B (0.2% formic acid in acetonitrile) in 200 min, then from 31% to 50% buffer B in 40 min and ending with 20 min at 99% buffer B. Eluting peptides were ionized with electrospray ionization and analyzed in Q Exactive HF-X. Full scans were acquired in the Orbitrap mass spectrometer at 60,000 resolution. MS/MS scans of the 15 most abundant precursor ions were acquired in the Orbitrap mass spectrometer at 7,500 resolution. The mass (m/z) 445.12003 was

used as lock mass as described in Olsen et al. (2005). Singly charged ions were excluded from MS/MS analysis. Dynamic exclusion was set to 20 sec. An average of 145,350 MS/MS spectra were acquired per sample run.

Protein identification and quantification. We used a customized database containing 1,439,433 protein sequences including host and symbiont proteins as well as a cRAP protein sequence database (http://www.thegpm.org/crap/) of common laboratory contaminants. We performed searches of the MS/MS spectra against this database with the Sequest HT node in Proteome Discoverer version 2.3.0.523 (Thermo Fisher Scientific). The following parameters were used: trypsin (full), maximum two missed cleavages, 10 ppm precursor mass tolerance, 0.1 Da fragment mass tolerance and maximum of 3 equal dynamic modifications per peptide, namely: oxidation on M (+ 15.995 Da), carbamidomethyl on C (+ 57.021 Da) and acetyl on the protein N terminus (+ 42.011 Da). False discovery rates (FDRs) for peptide spectral matches (PSMs) were calculated and filtered using the Percolator Node in Proteome Discoverer (Spivak et al., 2009). Percolator was run with a maximum delta Cn 0.05, a strict target FDR of 0.01, a relaxed target FDR of 0.05 and validation based on q-value. We used the Protein FDR Validator Node in Proteome Discoverer to calculate q-values for inferred proteins based on the results from a search against a target-decoy database. Proteins with a q-value of <0.01 were categorized as high-confidence identifications and proteins with a q-value of 0.01–0.05 were categorized as medium-confidence identifications. We combined search results for all samples into a multi-consensus report in Proteome Discoverer and only proteins identified with medium or high confidence were retained, resulting in an overall protein-level FDR of 5%.

SMT distribution in animals

Gutless oligochaete search. Total RNA was extracted from nine different species of gutless oligochaete. RNA was quality and quantity assessed by capillary electrophoresis (Agilent Bioanalyser PicoChip) and then Illumina-compatible libraries were generated with the NEBNext® Single Cell/Low Input RNA Library Prep Kit for Illumina®. Libraries were again quality and quantity controlled followed by sequencing on a HiSeq 3000

device with 2 x 150 bp paired-end read mode. The raw reads were trimmed and corrected, the symbiont reads were mapped out and the host read assembled using Trinity. The resulting assemblies were screened for SMT homologues using the model SMTs as subject. Only the hits with e-values smaller than 1e-30 and spanning at least half the subject sequences were kept for further analysis.

Search in public databases. To assess the presence of SMT homologues in other animal, protein searches against NCBI (National Center for Biotechnology Information (NCBI), Available from: https://www.ncbi.nlm.nih.gov/) databases (nr, tsa_nr, refseq_prot, env_nr and tsa) as well as the proteomes predicted by Ensembl metazoan (Howe et al., 2020) and Compagen (Hemmrich & Bosch, 2008) were performed. The search was restricted to metazoan sequences to avoid hits from fungi and viridiplantae. Only hits with e-values smaller than 1e-10 and a coverage larger than 60% were retained for further analysis.

Phylogenetic tree. A phylogenetic tree was constructed from selected SMT protein sequences. Briefly, SMT sequences identified in (Desmond & Gribaldo, 2009; Gold et al., 2016) were downloaded from UniProt and jgi and used as reference. Other SAM-dependent methyltransferases (Ubiquinone biosynthesis O-methyltransferase, Phosphoethanolamine N-methyltransferase, Tocopherol O-methyltransferase and C4-sterol methyltransferase) were used as outgroup. Together with the animal SMT those sequences were clustered (90% ID), aligned using Clustalw (Larkin et al., 2007) and trimmed with TrimAl (Capella-Gutiérrez et al., 2009). IQ-TREE (Minh et al., 2020) was used to predict the best-fit models of evolution and to calculate a maximum-likelihood tree with ultrafast bootstrap support values from the concatenated alignment. The resulting tree was visualized and beautified using iTOL (Letunic & Bork, 2019).

SMT heterologous gene expression and enzyme assay

Heterologous gene expression. To determine the activity of the putative SMT enzymes, we overexpressed Oalg_SMT, OclaSMT and ArathSMT1 in *E.coli* and performed enzymatic assay. GenScript (Genscript®) generated pet28a(+) (NheI/XhoI) vectors

bearing the sequence of interest. For expression, the pet28(a)-OalgSMT and pet28(a)-OclaSMT vectors were transformed in Lemo21(DE3) *E. coli* competent cells (New England Biolabs (NEB)). The pet28(a)-ArathSMT1 vector was transformed in Overexpress C43(DE3) pLysS *E. coli* competent cells (Lucigen). A single colony of transformed cells was grown in 3 mL of lysogeny broth (LB) supplemented with the appropriate antibiotics for 8 h (37°C, 150 rpm). 1 mL of pre-culture was used to inoculate 1 L of ZYP-5052-Rich-Autoinduction-Medium (Studier, 2005) supplemented with antibiotics and 1500 µM rhamnose. The cultures were grown for 72 h at 20°C, with rotation at 150 rpm. After this incubation time, the cells were harvested by centrifugation at 4,500 x g for 25 min at 4°C. The supernatant was discarded. The resulting pellet was stored at -20°C until further use.

Protein extraction/cell lysis. The frozen pellets were thawed on ice. They were then resuspended in 15 mL sucrose solution (750 mM sucrose solution in 20 mM phosphate buffer at pH 7.5). Once the pellets were dissolved in the sucrose solution, 5 mg of lysozyme was added and the tubes were shaken for 10 min at RT. Cells were lysed by addition of 30 mL lysis buffer (100 mM NaCl, 15% glycerol, 3 mM EDTA in 20 mM phosphate buffer at pH 7.5), 0.2 mL MgSO4 stock solution (120 g/L) and 0.3 mL Triton X-100. The mix was vigorously shaken and incubated on ice until it reached a gelatinous consistency. The DNA was fragmented by addition of 2 mL DNase stock solution (50 mg DNase I in 35 mL IMAC buffer A and 15 mL glycerol). Finally, the cell fragments and inclusion bodies were pelleted by centrifugation (45min, 16,000 x g, 4°C). The supernatant, containing soluble protein, was aliquoted and stored at -80°C until further use.

Enzymatic assay. The assay was performed in 600 µL total volume. 100 µL of crude soluble protein extract was mixed with 400 µL phosphate buffer (20 mM, 5% glycerol, pH 7.5) in a 15 mL tube containing a sterol substrate (final concentration 100 µM) dispersed in Tween 80 (0.1% v/v). The reaction was initiated with 100 µL AdoMet working solution (0.6 mM). The reaction was performed in a water bath at 35°C for 16h. The reaction was terminated with 600 µL of 10% methanolic KOH. The products were extracted three times with 2.5 mL hexane and mixed on a vortex for 30 sec. The resulting organic layer was

evaporated to dryness in a concentrator at 30°C, V-AL for 1.5 h. Two internal standards, 5α-cholestane (100 µL, 1 mM solution) and ribitol (40 µL of 200 mg/L solution), were added to the tubes and evaporated to dryness. The samples were derivatized and analyzed on an Agilent GC-MS as described above.

Data availability

The metaproteomics mass spectrometry data have been deposited at the ProteomeXchange Consortium via the PRIDE partner repository (Vizcaíno et al., 2016) with the following dataset identifiers: PXD014881 (Review access at https://www.ebi.ac.uk/pride/login Username: reviewer07815@ebi.ac.uk, Password: d5MenBMF).

The rest of the data that support the findings of this study are available on request from the corresponding author, DM.

Acknowledgments

We thank Alfred Garsdal, Janine Beckmann, Marvin Weinhold, Martina Meyer, Silke Wetzel, Tora Gulstad, Kristopher Caspersen and Frantisek Fojt (Max Planck Institute for Marine Microbiology-MPI-MM) for support with data acquisition and sample preparation. We also thank Bruno Huettel (Max Planck Genome Center) for his support with sequencing. We are grateful for fruitful discussions colleagues in the Departments of Symbiosis (MPI-MM). We thank Miriam Weber, Christian Lott, and HYDRA staff for sample collections. We are grateful to the Max-Planck Society for financial support. This work is contribution *XXX* from the Carrie Bow Cay Laboratory, Caribbean Coral Reef Ecosystem Program, National Museum of Natural History, Washington DC.

References

Ballantine, J. A., Lavis, A., Roberts, J. C., Morris, R. J., Elsworth, J. F., & Cragg, G. M. L. (1978). Marine sterols—VII. The sterol compositions of oceanic and coastal marine annelida species. *Comparative Biochemistry and Physiology Part B: Comparative Biochemistry*, *61*(1), 43–47. https://doi.org/10.1016/0305-0491(78)90211-0

Behrman, E. J., & Gopalan, V. (2005, December 1). *Cholesterol and Plants* (world) [Research-article]. Division of Chemical Education. https://doi.org/10.1021/ed082p1791

Bien, T., Hambleton, E. A., Dreisewerd, K., & Soltwisch, J. (2021). Molecular insights into symbiosis—Mapping sterols in a marine flatworm-algae-system using high spatial resolution MALDI-2-MS imaging with ion mobility separation. *Analytical and Bioanalytical Chemistry*, *413*(10), 2767–2777. https://doi.org/10.1007/s00216-020-03070-0

Birgel, D., Elvert, M., Han, X., & Peckmann, J. (2008). 13C-depleted biphytanic diacids as tracers of past anaerobic oxidation of methane. *Organic Geochemistry*, *39*(1), 152–156. https://doi.org/10.1016/j.orggeochem.2007.08.013

Bouvier-Navé, P., Husselstein, T., & Benveniste, P. (1998). Two families of sterol methyltransferases are involved in the first and the second methylation steps of plant sterol biosynthesis. *European Journal of Biochemistry*, *256*(1), 88–96. https://doi.org/10.1046/j.1432-1327.1998.2560088.x

Breitkopf, S., Ricoult, S., Yuan, M., Xu, Y., Peake, D., Manning, B., & Asara, J. (2017). A relative quantitative positive/negative ion switching method for untargeted lipidomics via high resolution LC-MS/MS from any biological source. *Metabolomics*, *13*. https://doi.org/10.1007/s11306-016-1157-8

Canuel, E. A., Freeman, K. H., & Wakeham, S. G. (1997). Isotopic compositions of lipid biomarker compounds in estuarine plants and surface sediments. *Limnology and Oceanography*, *42*(7), 1570–1583. https://doi.org/10.4319/lo.1997.42.7.1570

Capella-Gutiérrez, S., Silla-Martínez, J. M., & Gabaldón, T. (2009). trimAl: A tool for automated alignment trimming in large-scale phylogenetic analyses. *Bioinformatics*, *25*(15), 1972–1973. https://doi.org/10.1093/bioinformatics/btp348

Carland, F., Fujioka, S., & Nelson, T. (2010). The Sterol Methyltransferases SMT1, SMT2, and SMT3 Influence Arabidopsis Development through Nonbrassinosteroid Products. *Plant Physiology*, *153*(2), 741–756. https://doi.org/10.1104/pp.109.152587

Carvalho, M., Schwudke, D., Sampaio, J. L., Palm, W., Riezman, I., Dey, G., Gupta, G. D., Mayor, S., Riezman, H., Shevchenko, A., Kurzchalia, T. V., & Eaton, S. (2010). Survival strategies of a sterol auxotroph. *Development*, *137*(21), 3675–3685. https://doi.org/10.1242/dev.044560

Cerbulis, J., & Taylor, M. W. (1969). Neutral lipid and fatty acid composition of earthworms (Lumbricus terrestris). *Lipids*, *4*(5), 363–368. https://doi.org/10.1007/BF02531007

Chitwood, D. J. (1991). Nematode sterol biochemistry. *Physiology and Biochemistry of Sterols.*, 257–293.

Chitwood, David J., Hutzell, P. A., & Lusby, W. R. (1985). Sterol Composition of the Corn Cyst Nematode, Heterodera zeae, and Corn Roots. *Journal of Nematology*, *17*(1), 64–68.

Chitwood, David J., McClure, M. A., Feldlaufer, M. F., Lusby, W. R., & Oliver, T. E. (1987). Sterol Composition and Ecdysteroid Content of Eggs of the Root-knot Nematodes Meloidogyne incognita and M. arenaria. *Journal of Nematology*, *19*(3), 352–360.

Clark, A. J., & Bloch, K. (1959). Function of Sterols in Dermestes vulpinus. *Journal of Biological Chemistry*, *234*(10), 2583–2588. https://doi.org/10.1016/S0021-9258(18)69742-X

Cole, R. J., & Krusberg, L. R. (1967). Sterol composition of the Nematodes Ditylenchus triformis and Ditylenchus dipsaci, and host tissues. *Experimental Parasitology*, *21*(2), 232–239. https://doi.org/10.1016/0014-4894(67)90085-9

Cooper, L., & DeNiro, M. (1989). Stable carbon isotope variability in the seagrass Posidonia oceanica: Evidence for light intensity effects. *Marine Ecology Progress Series*, *50*, 225–229. https://doi.org/10.3354/meps050225

Dauby, P. (1989). The stable carbon isotope ratios in benthic food webs of the gulf of Calvi, Corsica. *Continental Shelf Research*, *9*(2), 181–195. https://doi.org/10.1016/0278-4343(89)90091-5

Desmond, E., & Gribaldo, S. (2009). Phylogenomics of Sterol Synthesis: Insights into the Origin, Evolution, and Diversity of a Key Eukaryotic Feature. *Genome Biology and Evolution*, *1*, 364–381. https://doi.org/10.1093/gbe/evp036

Dubilier, N., Blazejak, A., & Rühland, C. (2006). Symbioses between Bacteria and Gutless Marine Oligochaetes. In J. Overmann (Ed.), *Molecular Basis of Symbiosis* (pp. 251–275). Springer. https://doi.org/10.1007/3-540-28221-1_12

Fry, B., Scalan, R. S., & Parker, P. L. (1983). 13C/12C ratios in marine food webs of the Torres Strait, Queensland. *Marine and Freshwater Research*, *34*(5), 707–715. https://doi.org/10.1071/mf9830707

Geier, B., Sogin, E. M., Michellod, D., Janda, M., Kompauer, M., Spengler, B., Dubilier, N., & Liebeke, M. (2020). Spatial metabolomics of in situ host–microbe interactions at the micrometre scale. *Nature Microbiology*, *5*(3), 498–510. https://doi.org/10.1038/s41564-019-0664-6

Germer, J., Cerveau, N., & Jackson, D. J. (2017). The Holo-Transcriptome of a Calcified Early Branching Metazoan. *Frontiers in Marine Science*, *4*. https://doi.org/10.3389/fmars.2017.00081

Giere, O. (1981). The Gutless Marine Oligochaete Phallodrilus leukodermatus. Structural Studies on an Aberrant Tubificid Associated with Bacteria. *Marine Ecology Progress Series*, *5*, 353–357. https://doi.org/10.3354/meps005353

Giere, Olav. (1985). The Gutless Marine Tubificid Phallodrilus planus, a Flattened Oligochaete with Symbiotic Bacteria. Results from Morphological and Ecological Studies. *Zoologica Scripta*, *14*(4), 279–286. https://doi.org/10.1111/j.1463-6409.1985.tb00198.x

Goad, L. J. (1981). Sterol biosynthesis and metabolism in marine invertebrates. *Pure and Applied Chemistry*, *53*(4), 837–852. https://doi.org/10.1351/pac198153040837

Gold, D. A., Grabenstatter, J., Mendoza, A. de, Riesgo, A., Ruiz-Trillo, I., & Summons, R. E. (2016). Sterol and genomic analyses validate the sponge biomarker hypothesis. *Proceedings of the National Academy of Sciences*, *113*(10), 2684–2689. https://doi.org/10.1073/pnas.1512614113

Gurevich, A., Saveliev, V., Vyahhi, N., & Tesler, G. (2013). QUAST: Quality assessment tool for genome assemblies. *Bioinformatics*, *29*(8), 1072–1075. https://doi.org/10.1093/bioinformatics/btt086

Hartmann, M.-A. (2004). 5 Sterol metabolism and functions in higher plants. In G. Daum (Ed.), *Lipid Metabolism and Membrane Biogenesis* (pp. 183–211). Springer. https://doi.org/10.1007/978-3-540-40999-1_6

Haubrich, B. A., Collins, E. K., Howard, A. L., Wang, Q., Snell, W. J., Miller, M. B., Thomas, C. D., Pleasant, S. K., & Nes, W. D. (2015). Characterization, mutagenesis and mechanistic analysis of an ancient algal sterol C24-methyltransferase: Implications for understanding sterol evolution in the green lineage. *Phytochemistry*, *113*, 64–72. https://doi.org/10.1016/j.phytochem.2014.07.019

Hayes, J. M. (2018). 3. Fractionation of Carbon and Hydrogen Isotopes in Biosynthetic Processes. In *Stable Isotope Geochemistry* (pp. 225–278). De Gruyter. https://www.degruyter.com/document/doi/10.1515/9781501508745-006/html

Hemmrich, G., & Bosch, T. C. G. (2008). Compagen, a comparative genomics platform for early branching metazoan animals, reveals early origins of genes regulating stem-cell differentiation. *BioEssays*, *30*(10), 1010–1018. https://doi.org/10.1002/bies.20813

Howard, A. L. (2016). *Characterization, Mutagenesis and Mechanistic Analysis of the Sterol C24-Methyltransferase: Implications for Understanding Active Site Requirements for Sterol Biosynthesis* [Doctoral thesis]. Texas Tech University.

Howe, K. L., Contreras-Moreira, B., De Silva, N., Maslen, G., Akanni, W., Allen, J., Alvarez-Jarreta, J., Barba, M., Bolser, D. M., Cambell, L., Carbajo, M., Chakiachvili, M., Christensen, M., Cummins, C., Cuzick, A., Davis, P., Fexova, S., Gall, A., George, N., … Flicek, P. (2020). Ensembl Genomes 2020—Enabling non-vertebrate genomic research. *Nucleic Acids Research*, *48*(D1), D689–D695. https://doi.org/10.1093/nar/gkz890

Jäpelt, R. B., & Jakobsen, J. (2013). Vitamin D in plants: A review of occurrence, analysis, and biosynthesis. *Frontiers in Plant Science*, *4*. https://doi.org/10.3389/fpls.2013.00136

Jayasimha, P., & Nes, W. D. (2008). Photoaffinity Labeling and Mutational Analysis of 24-C-Sterol Methyltransferase Defines the AdoMet Binding Site. *Lipids*, *43*(8), 681–693. https://doi.org/10.1007/s11745-008-3198-x

Jennings, S., Reñones, O., Morales-Nin, B., Polunin, N., Moranta, J., & Coll, J. (1997). Spatial variation in the 15N and 13C stable isotope composition of plants, invertebrates and fishes on Mediterranean reefs: Implications for the study of trophic pathways. *Marine Ecology Progress Series*, *146*, 109–116. https://doi.org/10.3354/meps146109

Kadesch, P., Quack, T., Gerbig, S., Grevelding, C. G., & Spengler, B. (2019). Lipid Topography in Schistosoma mansoni Cryosections, Revealed by Microembedding and High-Resolution Atmospheric-Pressure Matrix-Assisted Laser Desorption/Ionization (MALDI) Mass Spectrometry Imaging. *Analytical Chemistry*, *91*(7), 4520–4528. https://doi.org/10.1021/acs.analchem.8b05440

Kanazawa, A. (2001). Sterols in marine invertebrates. *Fisheries Science*, *67*(6), 997–1007. https://doi.org/10.1046/j.1444-2906.2001.00354.x

Keller, O., Odronitz, F., Stanke, M., Kollmar, M., & Waack, S. (2008). Scipio: Using protein sequences to determine the precise exon/intron structures of genes and their orthologs in closely related species. *BMC Bioinformatics*, *9*(1), 278. https://doi.org/10.1186/1471-2105-9-278

Kent, W. J. (2002). BLAT—The BLAST-Like Alignment Tool. *Genome Research*, *12*(4), 656–664. https://doi.org/10.1101/gr.229202

Kleiner, M., Wentrup, C., Holler, T., Lavik, G., Harder, J., Lott, C., Littmann, S., Kuypers, M. M. M., & Dubilier, N. (2015). Use of carbon monoxide and hydrogen by a bacteria–animal symbiosis from seagrass sediments. *Environmental Microbiology*, *17*(12), 5023–5035. https://doi.org/10.1111/1462-2920.12912

Kleiner, M., Wentrup, C., Lott, C., Teeling, H., Wetzel, S., Young, J., Chang, Y.-J., Shah, M., VerBerkmoes, N. C., Zarzycki, J., Fuchs, G., Markert, S., Hempel, K., Voigt, B., Becher, D., Liebeke, M., Lalk, M., Albrecht, D., Hecker, M., … Dubilier, N. (2012). Metaproteomics of a gutless marine worm and its symbiotic microbial community reveal unusual pathways for carbon and energy use. *Proceedings of the National Academy of Sciences*, *109*(19), E1173–E1182. https://doi.org/10.1073/pnas.1121198109

Kolmogorov, M., Yuan, J., Lin, Y., & Pevzner, P. A. (2019). Assembly of long, error-prone reads using repeat graphs. *Nature Biotechnology*, *37*(5), 540–546. https://doi.org/10.1038/s41587-019-0072-8

Lagarda, M. J., García-Llatas, G., & Farré, R. (2006). Analysis of phytosterols in foods. *Journal of Pharmaceutical and Biomedical Analysis*, *41*(5), 1486–1496. https://doi.org/10.1016/j.jpba.2006.02.052

Larkin, M. A., Blackshields, G., Brown, N. P., Chenna, R., McGettigan, P. A., McWilliam, H., Valentin, F., Wallace, I. M., Wilm, A., Lopez, R., Thompson, J. D., Gibson, T. J., & Higgins, D. G. (2007). Clustal W and Clustal X version 2.0. *Bioinformatics (Oxford, England)*, *23*(21), 2947–2948. https://doi.org/10.1093/bioinformatics/btm404

Lepoint, G., Dauby, P., & Gobert, S. (2004). Applications of C and N stable isotopes to ecological and environmental studies in seagrass ecosystems. *Marine Pollution Bulletin*, *49*(11), 887–891. https://doi.org/10.1016/j.marpolbul.2004.07.005

Letunic, I., & Bork, P. (2019). Interactive Tree Of Life (iTOL) v4: Recent updates and new developments. *Nucleic Acids Research*, *47*(W1), W256–W259. https://doi.org/10.1093/nar/gkz239

Lu, N. C., Newton, C., & Stokstad, E. L. R. (1977). The Requirement of Sterol and Various Sterol Precursors in Free-Living Nematodes. *Nematologica*, *23*(1), 57–61. https://doi.org/10.1163/187529277X00228

Marsh, A. G., Harvey, H. R., Grémare, A., & Tenore, K. R. (1990). Dietary effects on oocyte yolk-composition inCapitella sp. I (Annelida: Polychaeta): Fatty acids and sterols. *Marine Biology*, *106*(3), 369–374. https://doi.org/10.1007/BF01344314

McCutchan, J. H., Lewis, W. M., Kendall, C., & McGrath, C. C. (2003). Variation in trophic shift for stable isotope ratios of carbon, nitrogen, and sulfur. *Oikos*, *102*(2), 378–390. https://doi.org/10.1034/j.1600-0706.2003.12098.x

McLaughlin, J. (1971). Biochemical studies on Eisenia foetida (savigny, 1826), the brandling worm—I. Tissue lipids and sterols. *Comparative Biochemistry and Physiology Part B: Comparative Biochemistry*, *38*(1), 147–163. https://doi.org/10.1016/0305-0491(71)90294-X

McMillan, C., Parker, P. L., & Fry, B. (1980). 13C12C ratios in seagrasses. *Aquatic Botany*, *9*, 237–249. https://doi.org/10.1016/0304-3770(80)90025-X

Minh, B. Q., Schmidt, H. A., Chernomor, O., Schrempf, D., Woodhams, M. D., von Haeseler, A., & Lanfear, R. (2020). IQ-TREE 2: New Models and Efficient Methods for Phylogenetic Inference in the Genomic Era. *Molecular Biology and Evolution*, *37*(5), 1530–1534. https://doi.org/10.1093/molbev/msaa015

Najle, S. R., Molina, M. C., Ruiz-Trillo, I., & Uttaro, A. D. (2016). Sterol metabolism in the filasterean Capsaspora owczarzaki has features that resemble both fungi and animals. *Open Biology*, *6*(7), 160029. https://doi.org/10.1098/rsob.160029

Neelakandan, A. K., Song, Z., Wang, J., Richards, M. H., Wu, X., Valliyodan, B., Nguyen, H. T., & Nes, W. D. (2009). Cloning, functional expression and phylogenetic analysis of plant sterol 24C-methyltransferases involved in sitosterol biosynthesis. *Phytochemistry*, *70*(17), 1982–1998. https://doi.org/10.1016/j.phytochem.2009.09.003

Nes, W. D. (2003). Enzyme mechanisms for sterol C-methylations. *Phytochemistry*, *64*(1), 75–95. https://doi.org/10.1016/S0031-9422(03)00349-2

Nes, W. D., & Heupel, R. C. (1986). Physiological requirement for biosynthesis of multiple 24β-methyl sterols in Gibberella fujikuroi. *Archives of Biochemistry and Biophysics*, *244*(1), 211–217. https://doi.org/10.1016/0003-9861(86)90110-4

Nes, W. D., Jayasimha, P., & Song, Z. (2008). Yeast sterol C24-methyltransferase: Role of highly conserved tyrosine-81 in catalytic competence studied by site-directed mutagenesis and thermodynamic analysis. *Archives of Biochemistry and Biophysics*, *477*(2), 313–323. https://doi.org/10.1016/j.abb.2008.05.016

Nes, W. D., Jayasimha, P., Zhou, W., Kanagasabai, R., Jin, C., Jaradat, T. T., Shaw, R. W., & Bujnicki, J. M. (2004). Sterol Methyltransferase: Functional Analysis of Highly Conserved Residues by Site-Directed Mutagenesis. *Biochemistry*, *43*(2), 569–576. https://doi.org/10.1021/bi035257z

Oberg, A. L., & Vitek, O. (2009). Statistical Design of Quantitative Mass Spectrometry-Based Proteomic Experiments. *Journal of Proteome Research*, *8*(5), 2144–2156. https://doi.org/10.1021/pr8010099

Pinnegar, J. K., & Polunin, N. V. C. (2000). Contributions of stable-isotope data to elucidating food webs of Mediterranean rocky littoral fishes. *Oecologia*, *122*(3), 399–409. https://doi.org/10.1007/s004420050046

Rampen, S. W., Abbas, B. A., Schouten, S., & Damste, J. S. S. (2010). A comprehensive study of sterols in marine diatoms (Bacillariophyta): Implications for their use as tracers for diatom productivity. *Limnology and Oceanography*, *55*(1), 91–105. https://doi.org/10.4319/lo.2010.55.1.0091

Rujanavech, C., & Silbert, D. F. (1986). LM cell growth and membrane lipid adaptation to sterol structure. *The Journal of Biological Chemistry*, *261*(16), 7196–7203.

Schaller, H. (2004). New aspects of sterol biosynthesis in growth and development of higher plants. *Plant Physiology and Biochemistry*, *42*(6), 465–476. https://doi.org/10.1016/j.plaphy.2004.05.012

Seppey, M., Manni, M., & Zdobnov, E. M. (2019). BUSCO: Assessing Genome Assembly and Annotation Completeness. *Methods in Molecular Biology (Clifton, N.J.)*, *1962*, 227–245. https://doi.org/10.1007/978-1-4939-9173-0_14

Sissener, N. H., Rosenlund, G., Stubhaug, I., & Liland, N. S. (2018). Tissue sterol composition in Atlantic salmon (Salmo salar L.) depends on the dietary cholesterol content and on the dietary phytosterol:cholesterol ratio, but not on the dietary phytosterol content. *The British Journal of Nutrition*, *119*(6), 599–609. https://doi.org/10.1017/S0007114517003853

Sogin, E. M., Michellod, D., Gruber-Vodicka, H., Bourceau, P., Geier, B., Meier, D. V., Seidel, M., Ahmerkamp, S., Schorn, S., D'Angelo, G., Procaccini, G., Dubilier, N., & Liebeke, M. (2021). Sugars dominate the seagrass rhizosphere. *BioRxiv*, 797522. https://doi.org/10.1101/797522

Soltwisch, J., Heijs, B., Koch, A., Vens-Cappell, S., Höhndorf, J., & Dreisewerd, K. (2020). MALDI-2 on a Trapped Ion Mobility Quadrupole Time-of-Flight Instrument for Rapid Mass Spectrometry Imaging and Ion Mobility Separation of Complex Lipid Profiles. *Analytical Chemistry*, *92*(13), 8697–8703. https://doi.org/10.1021/acs.analchem.0c01747

Sonawane, P. D., Pollier, J., Panda, S., Szymanski, J., Massalha, H., Yona, M., Unger, T., Malitsky, S., Arendt, P., Pauwels, L., Almekias-Siegl, E., Rogachev, I., Meir, S., Cárdenas, P. D., Masri, A., Petrikov, M., Schaller, H., Schaffer, A. A., Kamble, A., … Aharoni, A. (2016). Plant cholesterol biosynthetic pathway overlaps with phytosterol metabolism. *Nature Plants*, *3*(1), 1–13. https://doi.org/10.1038/nplants.2016.205

Spivak, M., Weston, J., Bottou, L., Käll, L., & Noble, W. S. (2009). Improvements to the Percolator Algorithm for Peptide Identification from Shotgun Proteomics Data Sets. *Journal of Proteome Research*, *8*(7), 3737–3745. https://doi.org/10.1021/pr801109k

Stevenson, J., & Brown, A. J. (2009). How essential is cholesterol? *The Biochemical Journal*, *420*(2), e1-4. https://doi.org/10.1042/BJ20090445

Studier, F. W. (2005). Protein production by auto-induction in high-density shaking cultures. *Protein Expression and Purification*, *41*(1), 207–234. https://doi.org/10.1016/j.pep.2005.01.016

Summons, R. E., Bradley, A. S., Jahnke, L. L., & Waldbauer, J. R. (2006). Steroids, triterpenoids and molecular oxygen. *Philosophical Transactions of the Royal Society B: Biological Sciences*, *361*(1470), 951–968. https://doi.org/10.1098/rstb.2006.1837

Thayer, G. W., Parker, P. L., LaCroix, M. W., & Fry, B. (1978). The stable carbon isotope ratio of some components of an eelgrass, Zostera marina, bed. *Oecologia*, *35*(1), 1–12. https://doi.org/10.1007/BF00345537

Tiunov, A. V. (2007). Stable isotopes of carbon and nitrogen in soil ecological studies. *Biology Bulletin*, *34*(4), 395–407. https://doi.org/10.1134/S1062359007040127

van der Meer-Janssen, Y. P. M., van Galen, J., Batenburg, J. J., & Helms, J. B. (2010). Lipids in host–pathogen interactions: Pathogens exploit the complexity of the host cell lipidome. *Progress in Lipid Research*, *49*(1), 1–26. https://doi.org/10.1016/j.plipres.2009.07.003

Veeramachaneni, P. P. (2005). *Active site mapping of yeast recombinant sterol methyltransferase (Y81 W) from Saccharomyces cerevisiae and inhibition of ergosterol biosynthesis in Candida albicans.* [Master Thesis]. Texas Tech University Lubbock.

Vives-Peris, V., de Ollas, C., Gómez-Cadenas, A., & Pérez-Clemente, R. M. (2020). Root exudates: From plant to rhizosphere and beyond. *Plant Cell Reports*, *39*(1), 3–17. https://doi.org/10.1007/s00299-019-02447-5

Vizcaíno, J. A., Csordas, A., del-Toro, N., Dianes, J. A., Griss, J., Lavidas, I., Mayer, G., Perez-Riverol, Y., Reisinger, F., Ternent, T., Xu, Q.-W., Wang, R., & Hermjakob, H. (2016). 2016 update of the PRIDE database and its related tools. *Nucleic Acids Research*, *44*(D1), D447–D456. https://doi.org/10.1093/nar/gkv1145

Vizzini, S., Tomasello, A., Maida, G. D., Pirrotta, M., Mazzola, A., & Calvo, S. (2010). Effect of explosive shallow hydrothermal vents on δ13C and growth performance in the seagrass Posidonia oceanica. *Journal of Ecology*, *98*(6), 1284–1291. https://doi.org/10.1111/j.1365-2745.2010.01730.x

Volkman, J. K. (2005). Sterols and other triterpenoids: Source specificity and evolution of biosynthetic pathways. *Organic Geochemistry*, *36*(2), 139–159. https://doi.org/10.1016/j.orggeochem.2004.06.013

Volkman, J. K., Barrett, S. M., Blackburn, S. I., Mansour, M. P., Sikes, E. L., & Gelin, F. (1998). Microalgal biomarkers: A review of recent research developments. *Organic Geochemistry*, *29*(5), 1163–1179. https://doi.org/10.1016/S0146-6380(98)00062-X

Voogt, P. A. (1973). Biosynthesis and Composition of Sterols in Annelida. Ii. Investigations On Some Oligochaetes. *Netherlands Journal of Zoology*, *24*(4), 469–478. https://doi.org/10.1163/002829674X00200

Voogt, P. A., Rheenen, J. W. A. van, & Zandee, D. I. (1975). What about squalene in the earthworm Lumbricus terrestris? *Comparative Biochemistry and Physiology Part B: Biochemistry and Molecular Biology*, *50*(4), 511–513. https://doi.org/10.1016/0305-0491(75)90080-2

Wacker, A., & Martin-Creuzburg, D. (2012). Biochemical nutrient requirements of the rotifer Brachionus calyciflorus: Co-limitation by sterols and amino acids. *Functional Ecology*, *26*(5), 1135–1143. https://doi.org/10.1111/j.1365-2435.2012.02047.x

Walton, M. J., & Pennock, J. F. (1972). Some studies on the biosynthesis of ubiquinone, isoprenoid alcohols, squalene and sterols by marine invertebrates. *Biochemical Journal*, *127*(3), 471–479. https://doi.org/10.1042/bj1270471

Wilber, C. G., & Bayors, W. M. (1947). A comparative study of the lipids in some marine annelids. *The Biological Bulletin*, *93*(2), 99–101. https://doi.org/10.2307/1538280

Wippler, J., Kleiner, M., Lott, C., Gruhl, A., Abraham, P. E., Giannone, R. J., Young, J. C., Hettich, R. L., & Dubilier, N. (2016). Transcriptomic and proteomic insights into innate immunity and adaptations to a symbiotic lifestyle in the gutless marine worm Olavius algarvensis. *BMC Genomics*, *17*(1), 942. https://doi.org/10.1186/s12864-016-3293-y

Wiśniewski, J. R., Zougman, A., Nagaraj, N., & Mann, M. (2009). Universal sample preparation method for proteome analysis. *Nature Methods*, *6*(5), 359–362. https://doi.org/10.1038/nmeth.1322

Wootton, J. A. M., & Wright, L. D. (1962). A comparative study of sterol biosynthesis in Annelida. *Comparative Biochemistry and Physiology*, *5*(4), 253–264. https://doi.org/10.1016/0010-406X(62)90055-5

Woyke, T., Teeling, H., Ivanova, N. N., Huntemann, M., Richter, M., Gloeckner, F. O., Boffelli, D., Anderson, I. J., Barry, K. W., Shapiro, H. J., Szeto, E., Kyrpides, N. C., Mussmann, M., Amann, R., Bergin, C., Ruehland, C., Rubin, E. M., & Dubilier, N. (2006). Symbiosis insights through metagenomic analysis of a microbial consortium. *Nature*, *443*(7114), 950–955. https://doi.org/10.1038/nature05192

Xu, F., Rychnovsky, S. D., Belani, J. D., Hobbs, H. H., Cohen, J. C., & Rawson, R. B. (2005). Dual roles for cholesterol in mammalian cells. *Proceedings of the National Academy of Sciences of the United States of America*, *102*(41), 14551–14556. https://doi.org/10.1073/pnas.0503590102

Zhou, W., Lepesheva, G. I., Waterman, M. R., & Nes, W. D. (2006). Mechanistic Analysis of a Multiple Product Sterol Methyltransferase Implicated in Ergosterol Biosynthesis in Trypanosoma brucei*. *Journal of Biological Chemistry*, *281*(10), 6290–6296. https://doi.org/10.1074/jbc.M511749200

Supplementary Figures and Tables

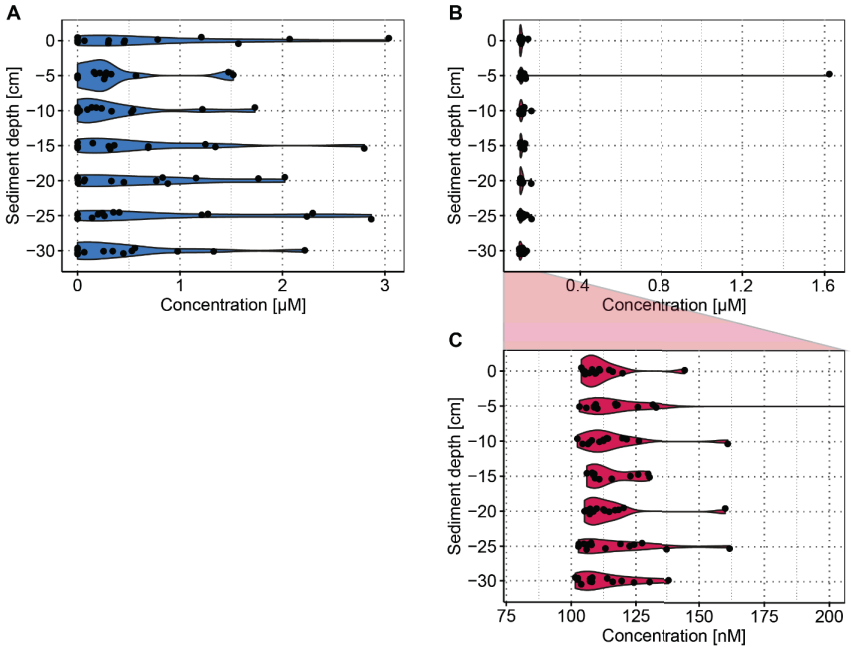

Supplementary Figure 1 | Sediment porewater underneath *P. oceanica* meadow (Elba, Italy) contains sitosterol and cholesterol. A, Sitosterol (blue) is present in the micromolar range under the seagrass bed. **B,** Cholesterol (red) is present in the nanomolar range under the seagrass bed. One measurement was in the micromolar range. **C,** Zoom of plot B to show the variation in cholesterol concentrations in the 100 to 200 nanomolar range.

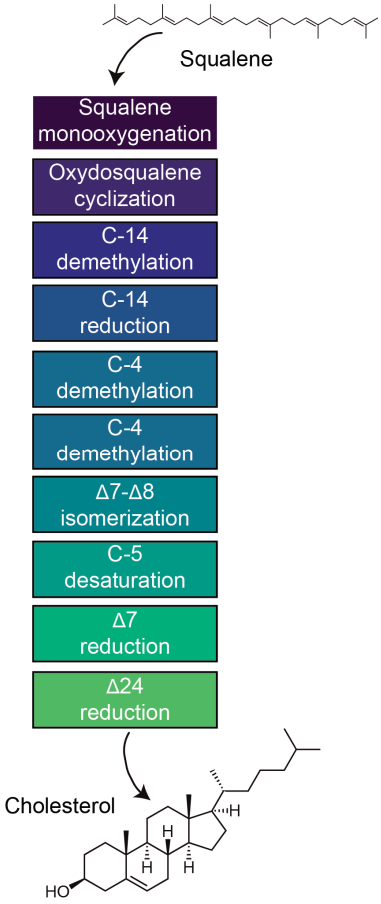

Supplementary Figure 2 | Canonical pathway of cholesterol synthesis.

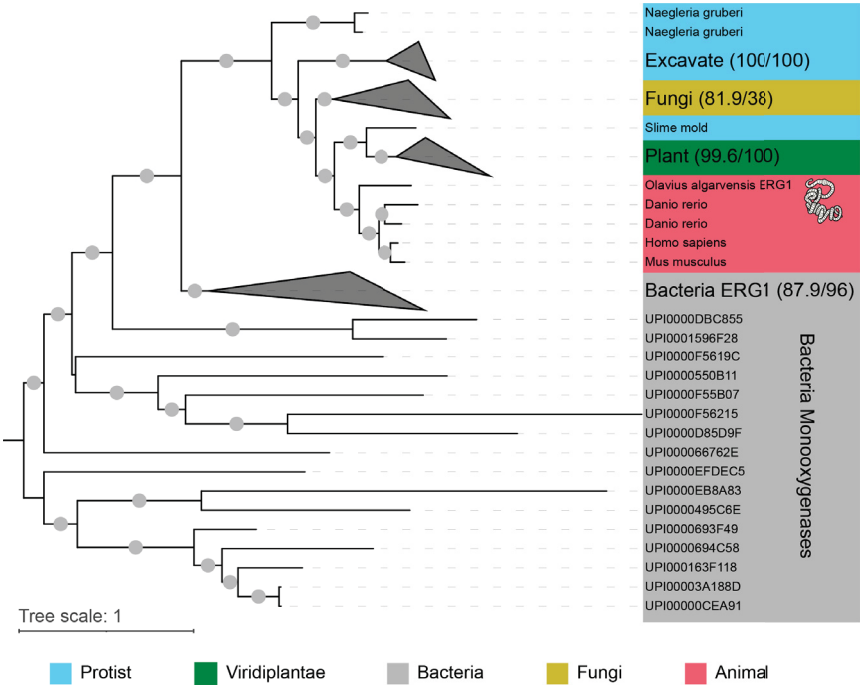

Supplementary Figure 3 | *Olavius algarvensis* squalene monooxygenase sequence clustered with the animal sequences. Maximum likelihood tree of ERG1 amino acid sequences. Bootstrap values ≥ 90% are marked with a grey circle. The bootstrap value and branch support value are indicated in brackets behind the collapsed groups. The tree was rooted at midpoint in iTOL.

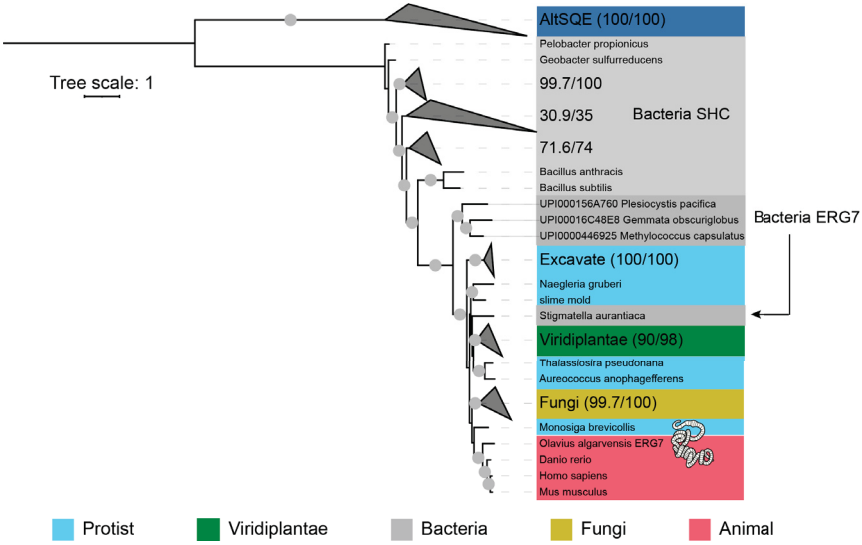

Supplementary Figure 4 | *Olavius algarvensis* lanosterol synthase sequence clustered with the animal sequences. Maximum likelihood tree of ERG7 amino acid sequences. Bootstrap values ≥ 90% are marked with a grey circle. The bootstrap value and branch support value are indicated in brackets behind the collapsed groups. The tree was rooted at midpoint in iTOL.

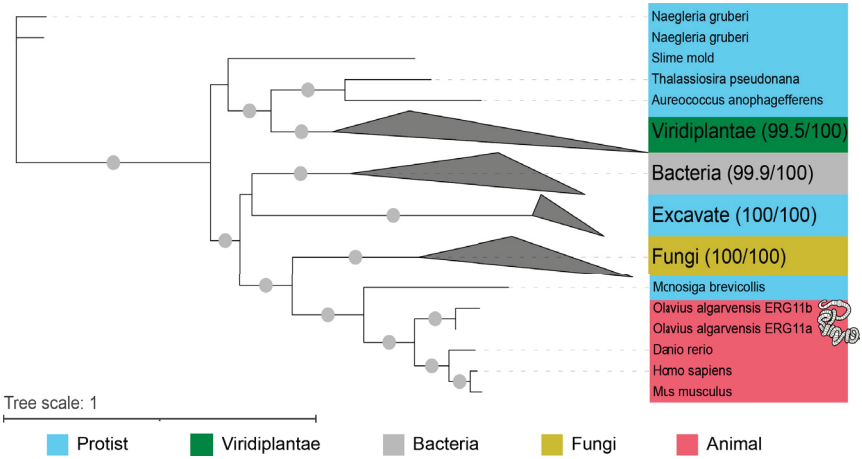

Supplementary Figure 5 | *Olavius algarvensis* sterol 14-demethylase sequences clustered with the animal sequences. Maximum likelihood tree of ERG11 amino acid sequences. Bootstrap values ≥ 90% are marked with a grey circle. The bootstrap value and branch support value are indicated in brackets behind the collapsed groups. The tree was rooted at midpoint in iTOL.

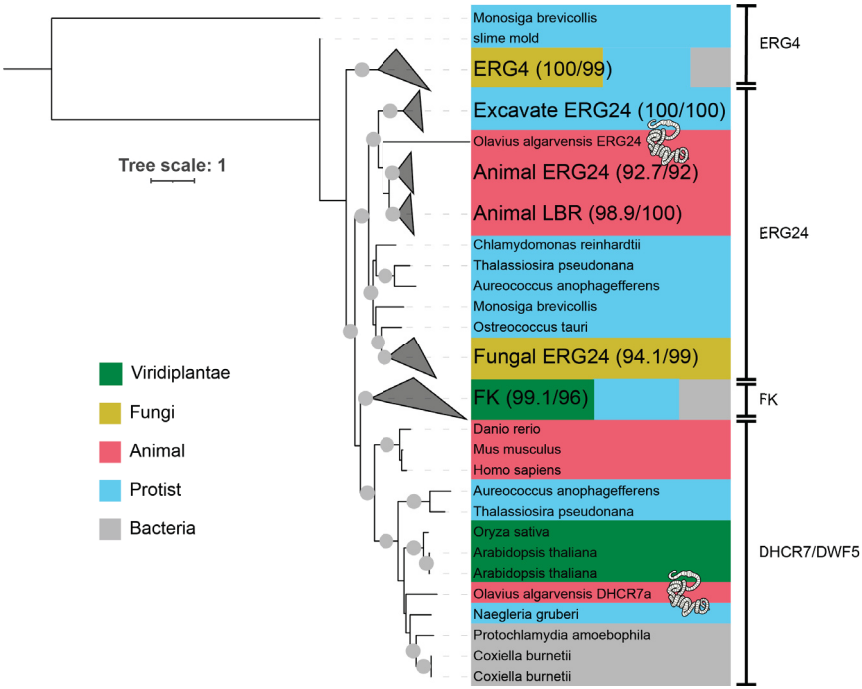

Supplementary Figure 6 | *Olavius algarvensis* delta(14)-sterol reductase sequence clustered with the animal sequences while the sterol 7-dehydrocholesterol reductase did not. The placement of *O. algarvensis* DHCR7 might indicate affinity for a different substrate than other animal. Maximum likelihood tree of the ERG4/ERG24 protein family. Bootstrap values ≥ 90% are marked with a grey circle. The bootstrap value and branch support value are indicated in brackets behind the collapsed groups. The tree was rooted at midpoint in iTOL.

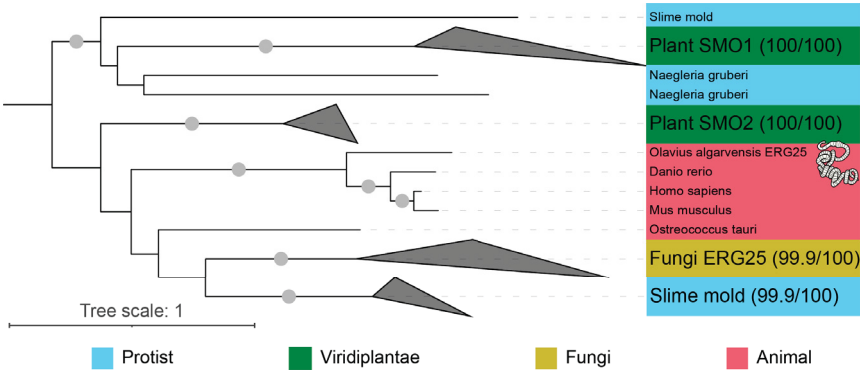

Supplementary Figure 7 | Olavius algarvensis methylsterol monooxygenase sequence clustered with the animal sequences. Maximum likelihood tree of the ERG25 amino acid sequences. Bootstrap values ≥ 90% are marked with a grey circle. The bootstrap value and branch support value are indicated in bracket behind the collapsed groups. The tree was rooted at midpoint in iTOL.

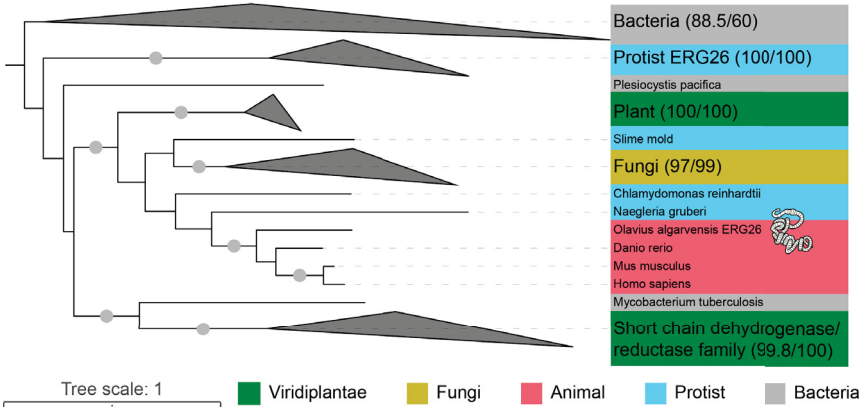

Supplementary Figure 8 | *Olavius algarvensis* Sterol-4-alpha-carboxylate 3-dehydrogenase, decarboxylating sequence clustered with the animal sequences. Maximum likelihood tree of the ERG26 amino acid sequences. Bootstrap values ≥ 90% are marked with a grey circle. The bootstrap value and branch support value are indicated in brackets behind the collapsed groups. The tree was rooted at midpoint in iTOL.

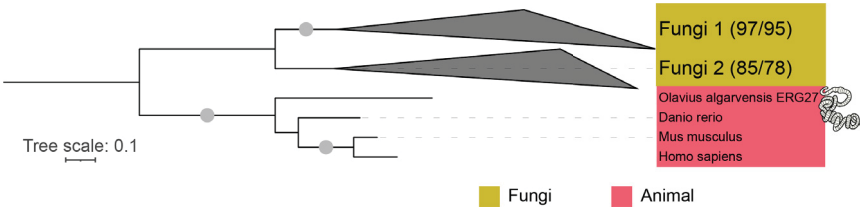

Supplementary Figure 9 | *Olavius algarvensis* 3-keto reductase sequence clustered with the animal sequences. Maximum likelihood tree of the ERG27 amino acid sequences. Bootstrap values ≥ 90% are marked with a grey circle. The bootstrap value and branch support value are indicated in bracket behind the collapsed groups. The tree was rooted at midpoint in iTOL. The gene performing C-3 ketoreduction in plant is still unknown, which explain the absence of plant sequences in this tree.

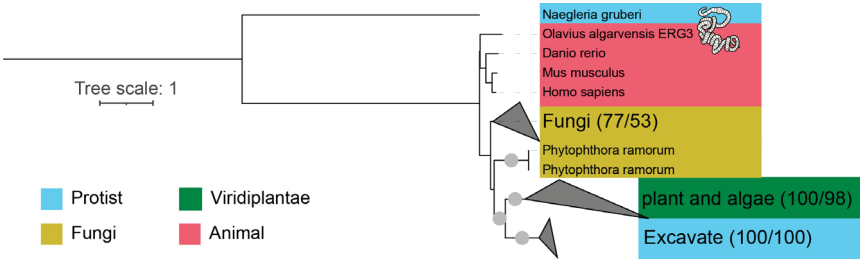

Supplementary Figure 10 | *Olavius algarvensis* sterol C-5 desaturase sequence clustered with the animal sequences. Maximum likelihood tree of the ERG3 amino acid sequences. Bootstrap values ≥ 90% are marked with a grey circle. The bootstrap value and branch support value are indicated in brackets behind the collapsed groups. The tree was rooted at midpoint in iTOL.

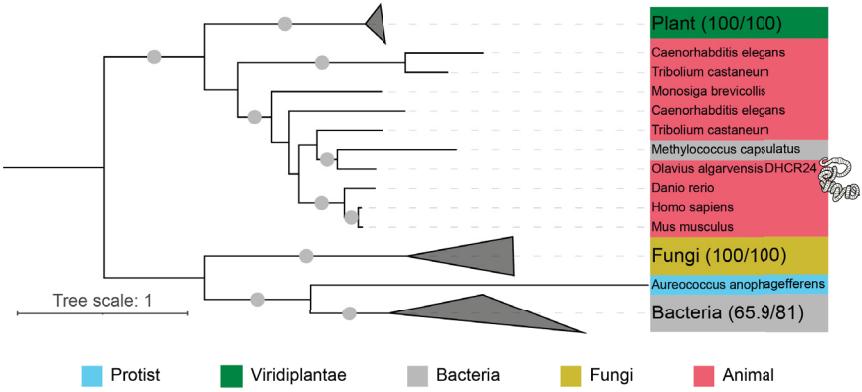

Supplementary Figure 11 | *Olavius algarvensis* sterol 24-dehydrocholesterol reductasesequence clustered with the animal sequences. Maximum likelihood tree of the DHCR24 amino acid sequences. Bootstrap values ≥ 90% are marked with a grey circle. The bootstrap value and branch support value are indicated in brackets behind the collapsed groups. The tree was rooted at midpoint in iTOL.

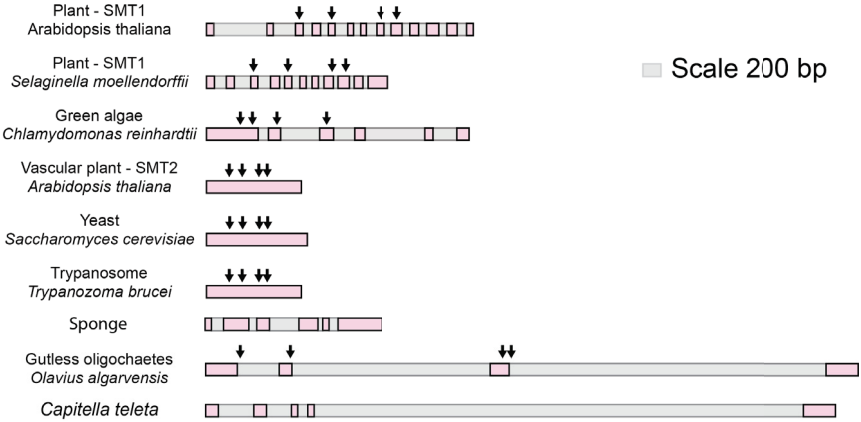

Supplementary Figure 12 | Genomic organization of representative SMT genes isolated from vascular plants, green algae, yeast, trypanosomes, sponges and annelids. The sterol and AdoMet binding sites are indicated by black arrows. The exons are presented in pink and the introns in grey.

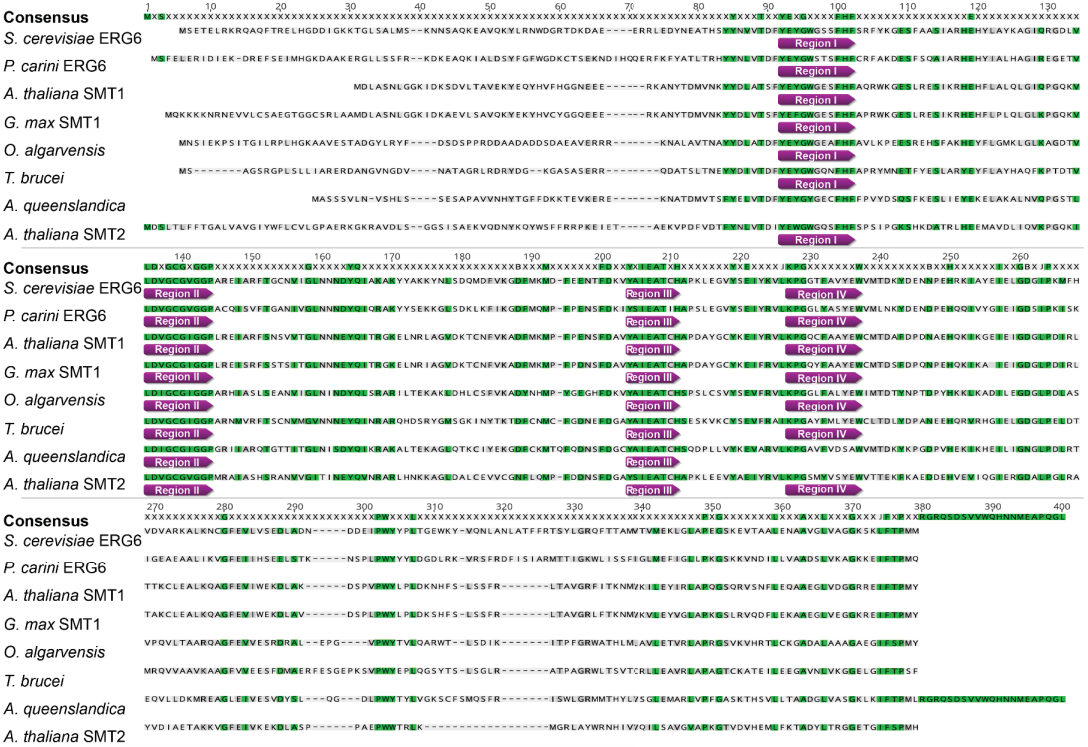

Supplementary Figure 13 | Alignments of sterol C24-methyltransferase amino acids sequences from: two fungi, *Saccharomyces cerevisiae* (P25087) and *Pneumocystis jirovecii* (Q96WX4); two plants: *Arabidopsis thaliana* SMT1 (Q9LM02) and SMT2 (Q39227) and *Glycine max* SMT1 (Q43445); one gutless oligochaete: *Olavius algarvensis* (this study); one excavate: *Trypanosoma brucei* (Q4FKJ2); and one sponge: *Amphimedon queenslandica* (A0A1X7ULF8). The sequences were aligned using clustlaw (Geneious). Sterol and AdoMet binding regions are indicated by purple shapes as Region I to IV.

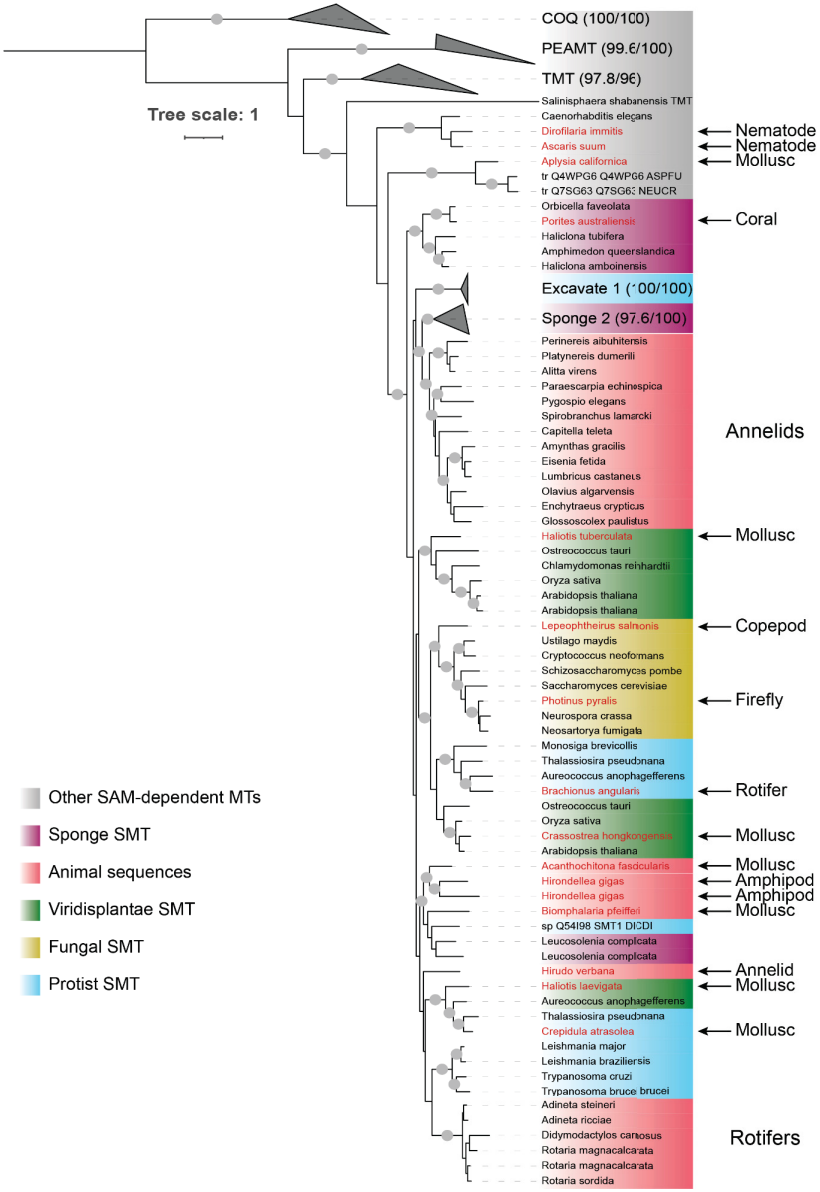
COQ (100/100)
PEAMT (99.6/100)
TMT (97.8/96)
Tree scale: 1
Salinisphaera shabanensis TMT
Caenorhabditis elegans
Dirofilaria immitis
Ascaris suum
Aplysia californica
tr Q4WPG6 Q4WPG6 ASPFU
tr Q7SG63 Q7SG63 NEUCR
Orbicella faveolata
Porites australiensis
Haliclona tubifera
Amphimedon queenslandica
Haliclona amboinensis
Excavate 1 (100/100)
Sponge 2 (97.6/100)
Perinereis aibuhitensis
Platynereis dumerili
Alitta virens
Paraescarpia echinospica
Pygospio elegans
Spirobranchus lamarcki
Capitella teleta
Amynthas gracilis
Eisenia fetida
Lumbricus castaneus
Olavius algarvensis
Enchytraeus crypticus
Glossoscolex paulistus
Haliotis tuberculata
Ostreococcus tauri
Chlamydomonas reinhardtii
Oryza sativa
Arabidopsis thaliana
Arabidopsis thaliana
Lepeophtheirus salmonis
Ustilago maydis
Cryptococcus neoformans
Schizosaccharomyces pombe
Saccharomyces cerevisiae
Photinus pyralis
Neurospora crassa
Neosartorya fumigata
Monosiga brevicollis
Thalassiosira pseudonana
Aureococcus anophagefferens
Brachionus angularis
Ostreococcus tauri
Oryza sativa
Crassostrea hongkongensis
Arabidopsis thaliana
Acanthochitona fascicularis
Hirondellea gigas
Hirondellea gigas
Biomphalaria pfeifferi
sp Q54I98 SMT1 DICDI
Leucosolenia complicata
Leucosolenia complicata
Hirudo verbana
Haliotis laevigata
Aureococcus anophagefferens
Thalassiosira pseudonana
Crepidula atrasolea
Leishmania major
Leishmania braziliensis
Trypanosoma cruzi
Trypanosoma brucei brucei
Adineta steineri
Adineta ricciae
Didymodactylos carnosus
Rotaria magnacalcarata
Rotaria magnacalcarata
Rotaria sordida
Nematode
Nematode
Mollusc
Coral
Annelids
Mollusc
Copepod
Firefly
Rotifer
Mollusc
Mollusc
Amphipod
Amphipod
Mollusc
Annelid
Mollusc
Mollusc
Rotifers
Other SAM-dependent MTs
Sponge SMT
Animal sequences
Viridisplantae SMT
Fungal SMT
Protist SMT

Supplementary Figure 14 | Most of the SMT homologues identified by blast were plant, protist and fungal contaminations or belonged to the C_4-SMT, a SMT specific to nematodes. Maximum likelihood amino acid tree of the SMTs and other SAM dependent methyltransferases used as outgroup. Bootstrap values ≥ 90% are marked with a grey circle. The bootstrap value and branch support value are indicated in brackets behind the collapsed groups. The animal sequences identified as contamination are highlighted in red, and black arrows point to them. The tree was rooted at midpoint in iTOL. Ubiquinone biosynthesis O-methyltransferase (COQ), Phosphoethanolamine N-methyltransferase (PEMT), Tocopherol O-methyltransferase (TMT), C4 sterol methyltransferase (C_4-SMT).

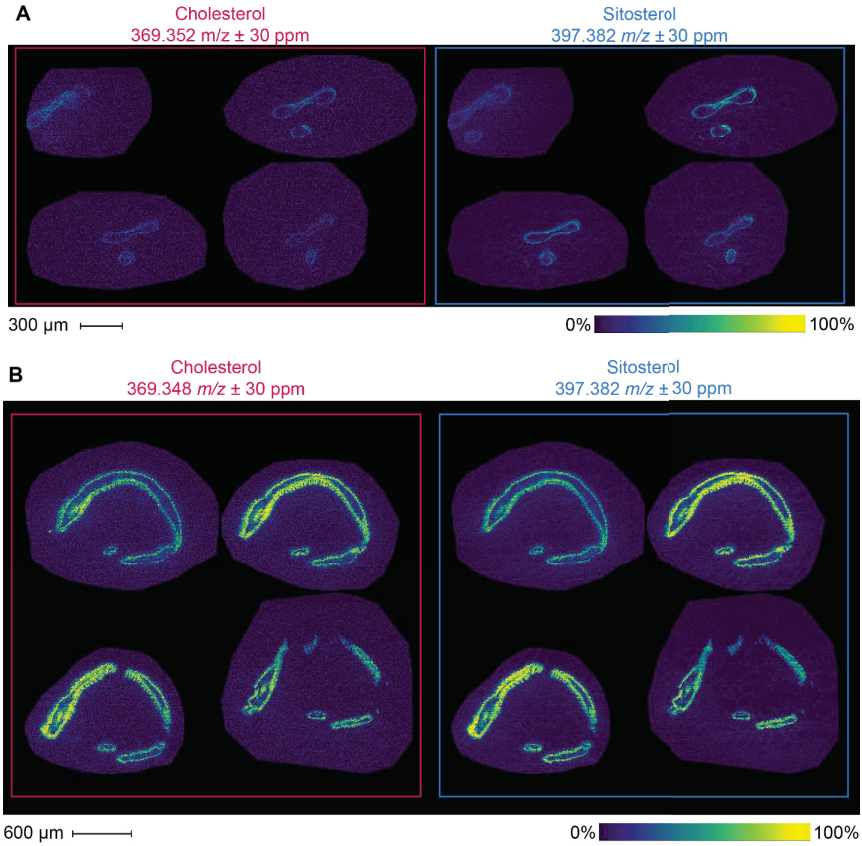

Supplementary Figure 15: Sitosterol and cholesterol are homogenously distributed in the *Olavius algarvensis* tissue. Cholesterol and sitosterol distribution in *O. algarvensis* cross section **(A)** and longitudinal section **(B).**

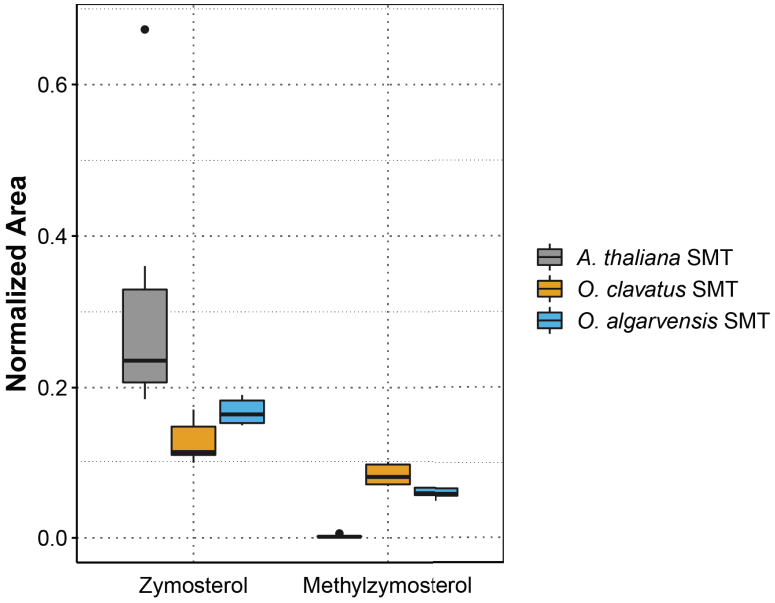

Supplementary Figure 16 | Gutless oligochaete sterol methyltransferases (SMT) use zymosterol as substrate. Sterol extract of the enzymatic assay. The abundance of the substrate (zymosterol) and the product (methylzymosterol) were quantified at the end of the enzymatic assay (n=5). The abundance was normalized with the ribitol intensity. *Arabidopsis thaliana* SMT did not use zymosterol as substrate. Both gutless oligochaete enzymes used zymosterol as substrate.

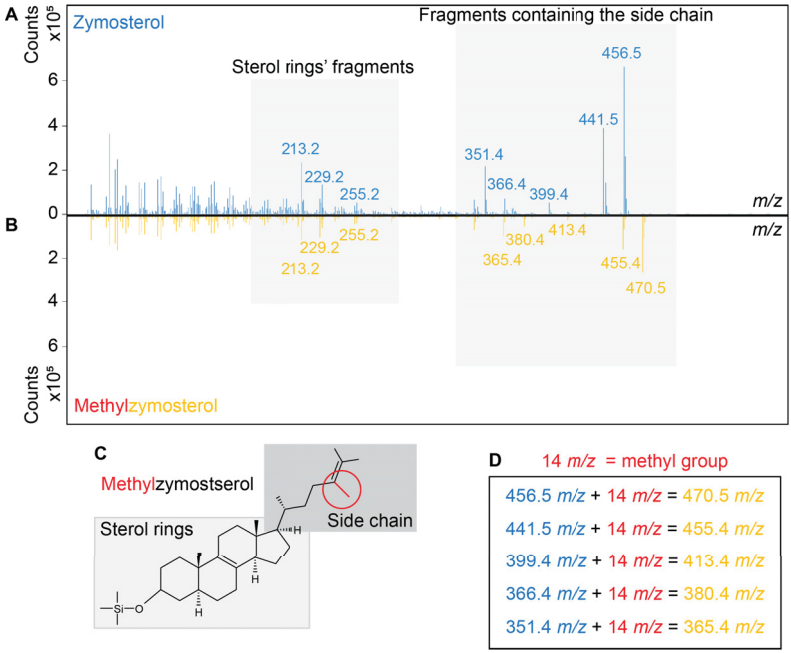

Supplementary Figure 17 | Gutless oligochaete sterol methyltransferases added a methyl group to the side chain of zymosterol. A, B, Representative mass spectra of zymosterol **(A)** and the compound identified as methylzymosterol **(B). C,** Structure of methylzymosterol, the methyl group is highlighted in red. **D,** The fragments containing the side chain are shifted by 14 m/z, a difference which represents the addition of a methyl group. No mass shift is observed in the sterol ring fragments. Those results indicate that the methyl group was added to the zymosterol side chain, likely at the C_{24} position.

Supplementary Table 1 | List of sterols detected by MALDI-2-MSI in *Olavius algarvensis*.

sterol	Formula	M	$[M\text{-}H_2O+H]^+$ (calc)	$[M\text{-}H_2O+H]^+$ (exp)
cholesterol	$C_{27}H_{46}O$	386.354865	369.3521	369.3453 ±117 ppm
sitosterol	$C_{29}H_{50}O$	414.386165	397.3834	397.3756 ± 117 ppm
stigmasterol	$C_{29}H_{48}O$	412.370515	395.3678	395.3640 ± 117 ppm

Supplementary Table 2 | Distribution of orthologues of enzymes of the sterol pathway in eukaryotic model organisms and in *Olavius algarvensis*. White indicates absence, G= genome, T= transcriptome, P= proteome.

Enzymatic Step		E.C number	fungi	plant	animal	G	T	P
Squalene monooxygenation (ERG1)		1.14.14.17						
Oxydosqualene cyclization (ERG7)		5.4.99.7 and 5.4.99.8						
C-14 demethylation (ERG11)		1.14.14.154						
C-14 reduction (ERG24)		1.3.1.70						
C-4 demethylation	C-4 methyl oxidation (ERG25)	1.14.18.9						
	C-3 dehydrogeneation/C-4 decaboxylation (ERG26)	1.1.1.170						
	C-3 ketoreduction (ERG27)	1.1.1.270						
Δ7-Δ8 isomerization (ERG2/EBP)		5.-.-.- and 5.3.3.5						
C-5 desaturation (ERG3)		1.14.19.20 and 1.14.21.6						
Δ7 reduction (DHCR7)		1.3.1.21						
Δ24 reduction (ERG4/DHCR24)		1.3.1.71 and 1.3.1.72						
C-22 desaturation (ERG5)		1.14.19.41						
C-24 methyaltion or C-28 methylation (ERG6)		2.1.1.41and 2.1.1.143						
Cyclopropylsterol isomerization (CPI1)		5.5.1.9						

Supplementary Table 3 | Detection of enzymes involved in sterol biosynthesis in the proteome of *Olavius algarvensis*. FDR = False discovery rate, # PSMs = number of peptide spectral matches, # of PUP = number of protein unique peptides.

Protein accession	Description	Found in proteome (filtered for 5% FDR)	Found in # of samples (out of 25)	q-value	#PSMs	#of PUP
ERG1_Host_330784_c8_seq1_40	squalene monooxygenase homologue	No	-	-	-	-
ERG2_Host_282622_c0_seq2_5	C-8 sterol isomerase homologue	Yes	4	0.008	4	0
ERG6_Host_316125_c3_seq1_6	sterol methyltransferase homologue	Yes	25	0	70	4
ERG7_Host_333294_c4_seq2_44	lanosterol synthase homologue	Yes	3	0	4	2
ERG11a_Host_334930_c0_seq4_30	sterol 14-demethylase homologue	Yes	25	0	50	1
ERG11b_Host_334930_c0_seq1_24	sterol 14-demethylase homologue	Yes	12	0	16	0
ERG24_Host_331074_c0_seq1_34	delta(14)-sterol reductase homologue	Yes	25	0	123	5
ERG25_Host_335885_c4_seq2_8	methylsterol monooxygenase homologue	No	-	-	-	-
ERG26a_Host_330893_c3_seq7_9	Sterol-4-alpha-carboxylate 3-dehydrogenase, decarboxylating homologue	Yes	17	0	25	1
ERG27_Host_329156_c0_seq5_38	3-keto reductase homologue	No	-	-	-	-
ERG3_Host_326988_c0_seq1_35	sterol C-5 desaturase homologue	No	-	-	-	-

DHCR24_4731_Verc3_concensus	24-dehydrocholesterol reductase homologue	No	-	-	-	-
DHCR7a_4731_TRINITY_DN28908_c0_g1_i1 - ORF 2	7-dehydrocholesterol reductase homologue	No	-	-	-	-

Supplementary Table 4: Solvent gradient for high-resolution LC-MS/MS.

%B	Time [min]	Flow rate [µL min^{-1}]
0	-2 (pre-run equilibration)	350
0	2	350
16	5.5	350
45	9	350
52	12	350
58	14	350
66	16	350
70	18	350
75	22	350
97	25	350
97	32.5	350
15	33	350
0	34.4	350
0	36	350

Buffer A (60/40 ACN/H_2O, 10 mM ammonium formate, 0.1% FA) and Buffer B (90/10 IPA/ACN, 10 mM ammonium formate, 0.1% FA) were used at a flow rate of 350 µl min^{-1}.

Supplementary Table 5: MS settings of Q Exactive Plus Orbitrap (Thermo Fisher Scientific) equipped with a HESI probe and a Vanquish Horizon UHPLC System (Thermo Fisher Scientific).

MS[1]	
Resolution	70,000
AGC target	5.00E+05
Max IT	65 ms
Scan range	150-1500 m/z
MS[2]	
Resolution	35,000
AGC target	1.00E+06
Max IT	75 ms
Loop count	8
Dynamic exclusion	30 s
Isolation windows (pos.)	1 m/z
Isolation windows (neg.)	1 m/z
NCE	30

Discussion

Discussion

During my studies, I described the chemical landscape of deep-sea mussels living in close association with chemoautotrophic bacteria (*Chapter I*) and determined the structural identity, distribution and potential functions of a metabolite group specific to the association between deep-sea mussels and methane-oxidizing symbionts (*Chapter II*). This research was expanded to shallow water symbioses formed by gutless annelids and chemoautotrophic bacteria and the study of the unusual sterol profile of the host (Chapter III).

The studies focusing on deep-sea mussels provided a general overview of their lipid composition and revealed a new form of C_1 carrier, specific to symbiotic methane-oxidizing bacteria. The study of gutless oligochaete's sterol profile led to the description of the first animal sitosterol biosynthesis pathway, which relies on an enzyme previously believed to be lost in animals. The major finding of this thesis are presented and discussed in the different chapters. Here, I will discuss more in depth questions and hypotheses mentioned in those chapters and provide suggestions on how to test these hypotheses in the future.

Potential roles of the C_1 carrier dH_4MPT and its esterified analogues

A recent study combining metabolic imaging and fluorescence in situ hybridization (FISH) microscopy identified a new group of unknown metabolites at the host-symbiont interface in the gills of *Bathymodiolus puteoserpentis* (Geier et al., 2020). Using a combination of mass spectrometry and spectroscopy approaches we identified those compounds as (1) dephospho-tetrahydromethanopterin (dH_4MPT), a C_1 carrier specific to methanotrophic bacteria and (2) the esterified analogues of this C_1 carrier, described here for the first time.

The use of bacterial coenzyme as adaptation to the symbiotic lifestyle in deep-sea mussels

The dH_4MPT C_1 carrier is present in methane-oxidizing (MOX) symbionts as well in free-living methanotrophic bacteria. It is one of the two coenzymes which can carry the C_1 group during the oxidation of the toxic formaldehyde. The presence of this bacterial C_1 carrier in the host tissues, even outside of the symbiotic organ, suggests that it might play a role in the C_1 metabolism of the eukaryotic host.

C_1 metabolism is essential to nucleotide synthesis, amino acid homeostasis and methylation of DNA, RNA, proteins and phospholipids (Wagner, 2001). In eukaryotes and bacteria, C_1 metabolism is mediated by the folate coenzyme, under the form of tetrahydrofolate (H_4F) (Wagner, 2001). While plants, fungi and some bacteria can synthesize H_4F, animals lack key enzymes of the H_4F biosynthetic pathway and consequently must obtain it either through their diet or their symbiotic bacteria (Akman et al., 2002; Blatch et al., 2010; Hunter et al., 2015; Snyder & Rio, 2015).

Due to the nutritional dependency of the host on its symbionts, deep-sea mussels are likely to rely on their symbionts to obtain H_4F. The MOX symbionts are able to synthesize both C_1 carriers: H_4F and dH_4MPT (Marx et al., 2003; Ponnudurai et al., 2017) while the SOX symbionts can synthesize H_4F (Sayavedra, 2016). Proteomics data indicates that dH_4MPT is the preferred energy generation pathway in MOX symbionts (Ponnudurai et al., 2017), suggesting that H_4MPT is more abundant than H_4F in the MOX symbionts. We speculate that in the presence of the MOX symbionts, the host use dH_4MPT as an alternative C_1 carrier for its C_1 metabolism.

In order to test this hypothesis, one would need to quantify the H_4F and dH_4MPT in the host tissues. Two set of samples would be especially indicated for this analysis. The first set would be composed of mussel species harboring only SOX symbionts and mussel species harboring MOX symbionts. The quantification of the two C_1 carriers would tell us if part of the H_4F provided by the SOX symbionts in SOX only symbiosis is preplaced by dH_4MPT when MOX symbionts are present. The second set of samples are *"B". childressi* mussels kept in aquaria for an extended period of time during which they lost most of their symbionts and relied on filter feeding. The comparison of the C_1 carrier identity and abundance in wild type and in aquaria mussels would provide another indication of C_1 carrier used by the host in the presence and absence of MOX symbionts. In addition, the

transcriptomics data of this second set of samples are available and would give a context to our observations.

The next step would be to test the specificity of enzymes involved in the C_1 metabolism of animals for H_4F versus dH_4MPT. The dH_4MPT coenzyme could be extracted from *Methyloprofundus sediment* strain WF1 (WF1), a culturable free-living relative of the MOX symbionts, using established protocols (Keltjens et al., 1986). The purified coenzyme could then be assayed with mussels enzymes involved in the C_1 metabolisms to assess if they can use dH_4MPT as an alternative to H_4F.

The use of a bacterial coenzyme by a eukaryotic host would be a new and unique way in which deep-sea mussels adapted to their symbiotic lifestyle. It would be interesting to know if other marine invertebrates associated with methanotrophic symbionts (Goffredi et al., 2020; Rubin-Blum et al., 2019) developed similar adaptation.

Esterified C_1 carrier as a new way to counteract the toxicity of formaldehyde?

The esterified analogues of the C_1 carrier dH_4MPT were present in all deep-sea mussels harboring MOX symbionts. Those compounds were exclusively detected in the symbiotic tissues. In most cases they were more abundant than their un-esterified analogue. Their prevalence and abundance suggest that they play a role in the physiology of the MOX symbiont.

Many bacteria possess an extensive intracytoplasmic membranes (ICM) (Shively, 2006). This is the case for type I methanotrophs such as the MOX symbionts (**Figure *1***). These ICMs mediate important biogeochemical functions such as methane oxidation. The ICMs increase the membrane surface area for energy transduction and enhance local control over proton gradients and metabolites concentrations. In methanotrophs, the ICMs are packed with particulate methane monooxygenase (pMMO) which can represent up to 50% of the total membrane protein (Collins et al., 1991).

The pMMO, an enzyme specific to methanotrophs, mediates the first step of methane oxidation: the oxidation of methane to methanol. Methane monooxygenase (MMO) exists under two forms: soluble MMO (sMMO) and pMMO. The MOX symbionts as all type I methanotrophs, encode the pMMO. The pMMO is membrane bound and associated with

the ICM (Brantner et al., 2002; Davies & Whittenbury, 1970; Prior & Dalton, 1985; Stanley et al., 1983). The ICM is believed to play a role in structuring the enzyme or concentrating methane.

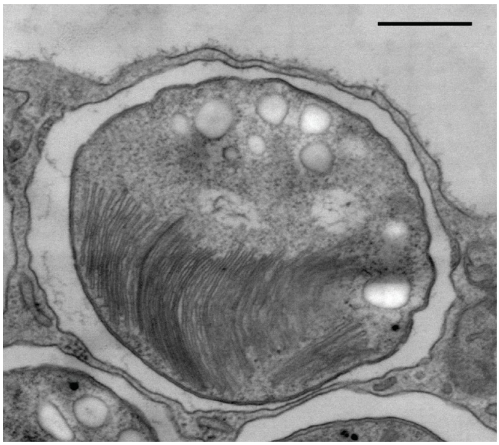

Figure 1 | Transmission electron microscopy image of the methane-oxidizing symbiont of a deep-sea mussel showing the intracytoplasmic membrane (ICM) structure. Scale bar = 500 nm; Image courtesy of N. Leisch.

In the symbionts, the methanol is further oxidize to formaldehyde, using the XoxF methanol dehydrogenase (MDH). MDH is a periplasmic enzyme which has been shown to be associated with the ICM (Brantner et al., 2002; Whiddon et al., 2019). The localization of the MDH in the intra-ICM space would be consistent with different lines of evidence suggesting that, in type I methanotrophs, the ICM exists as invagination of the cytoplasmic membranes (Brantner et al., 2000, 2002; Whiddon et al., 2019; Whittenbury et al., 1970).

The newly produced formaldehyde is then transported into the symbiont's cytoplasm where it can be oxidized to formate, to generate electrons and reducing equivalents. This energy-generating step can be accomplished by the dH_4mPT-dependent C_1 transfer pathway. The formaldehyde oxidation is essential as accumulation of formaldehyde is toxic for the cell. In the MOX symbionts we found esterified analogues of dH_4MPT. We speculated that the fatty acids attached to the coenzyme anchor the coenzyme in the membrane of the bacteria. This bacterial membrane could be ICM. The oxidation of

methane to formate would take place in a restricted environment. The presence of dH_4MPT in the membrane would ensure that no formaldehyde diffuse freely in the cytoplasm (**Figure 2**).

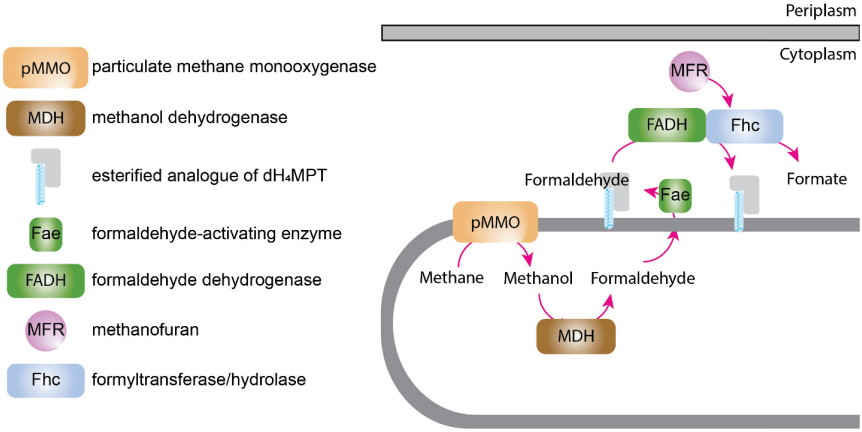

Figure 2 | Schematic representation of the methane oxidation and proposed location of esterified analogues of dH_4MPT.

The enzymes involved in the oxidation of formaldehyde to formate described so far are cytoplasmic proteins. So from this stage on, two scenarios can be envisioned: (1) the fatty acid is cleaved and the rest of the pathway takes place in the cytoplasm or (2) the rest of the pathway takes place at the surface of ICM. We know that the first hypothesis is unlikely to take place as we detected esterified forms of methenyl-dH_4MPT in our analysis. Methenyl-dH_4MPT is an intermediate in the oxidation of formaldehyde to formate. Based on our current data, scenario number two is more likely. In addition a preliminary analysis suggests that the presence of a fatty acid should not disturb the interactions between the coenzyme and the enzymes of the formaldehyde oxidation pathway.

The dH_4MPT is not the only coenzyme involved in the dH_4MPT-dependent oxidation of formaldehyde, methanofuran (MFR) is required for the last step of the pathway (**Figure 2**). The presence of an esterified form of the MFR coenzyme would provide further

evidence that in MOX symbionts the oxidation of methane to formate likely takes place at the membrane.

A method was developed to isolate ICM from type I methanotrophs and was used as line of evidence to show that the pMMO is localize in the ICM membrane (Brantner et al., 2000). We could use this protocol to localize the enzymes of the formaldehyde oxidation pathway. In addition, the natural fluorescence of dH_4MPT might be used to determine the exact localization of the dH_4MPT in the bacteriocyte and in the surrounding tissues.

Anchoring the dH_4MPT coenzyme in the ICM would be an efficient way to prevent the presence of free formaldehyde in the cytoplasm. So far we only detected the esterified form of dH_4MPT in symbiotic bacteria, it was absent in closely related free-living bacteria. At the moment it is unclear if the esterification of the coenzyme is an adaptation specific to the symbiotic lifestyle or if its absence in free-living bacteria is linked to the cultivation conditions.

Discussing the unusual sterol profile of gutless oligochaetes

In chapter 3 we showed that gutless oligochaetes synthesized both cholesterol and sitosterol. They harbored a stable sterol composition dominated by sitosterol (60%). Cholesterol, usually the major sterol in animal only accounted for 40% of the total sterol. Why do gutless oligochaetes harbor a mixture of sterols in their membrane?

Why two sterols?

Sterols are structural constituents of the lipid bilayer. They interact with the fatty acyls of the phospholipids and by doing so modulate the fluidity and permeability of the lipid bilayer by restricting the movement of the fatty acyls. To be able to fulfill their structural function sterols need to feature: a free 3-hydroxygroup, a planar tetracyclic skeleton and an aliphatic side chain with 8-10 carbon atoms (Bloch, 1983). Both cholesterol and sitosterol possess those attributes. In mammalian and insect cells, fungal and plant sterols, including sitosterol, can replace cholesterol as structural component of the membrane (Clark & Bloch, 1959; Rujanavech & Silbert, 1986; Stevenson & Brown, 2009; Xu et al.,

2005) which suggests that sitosterol could be the main structural component of gutless oligochaetes cell membrane. So why keep cholesterol?

Beyond its role in membrane structure, cholesterol plays a role in membrane function. It forms dynamic microdomains involved in the modulation of membrane trafficking, signal transduction and host–pathogen interactions (Sezgin et al., 2017).

Outside of the membrane environment cholesterol serves as precursor to oxysterols, bile acids, vitamin D and steroid hormones (Berg et al., 2002). All those cholesterol derivatives are engaged in a variety of biological processes. Oxysterols for examples are involved in the regulation of cholesterol homeostasis, in embryonic signaling pathways and act as activators of several transcription factors (Edwards & Ericsson, 1999; Luu et al., 2016). Because of the important roles cholesterol and its derivatives play in cell physiology, cholesterol homeostasis is tightly regulated (Luo et al., 2020). It is likely that sitosterol cannot fulfill all cholesterol functions in gutless oligochaetes. Which leads us to the second question: why do gutless oligochaetes synthesize and incorporate sitosterol in their tissues?

What is the function of sitosterol in gutless oligochaetes?

Sitosterol is usually absent from animal cells. Even when present in the diet, phytosterol is not as readily absorbed as cholesterol and the little that is absorbed is pumped back into the intestinal lumen by specialized transporters (Wang & Cohen, 2009). Plant-feeding insects transform the phytosterol obtain from their diet into cholesterol (Ikekawa et al., 1993; Svoboda & Feldlaufer, 1991). This active exclusion and transformation of plant sterols in animals suggest that the small difference in their structural architecture lead to different cellular functions.

Although in vivo studies showed that phytosterols can be incorporated into animal cell membranes, they did not investigate the influence of plant sterols on membrane properties or on the cell physiology (Clark & Bloch, 1959; Rujanavech & Silbert, 1986; Stevenson & Brown, 2009; Xu et al., 2005). Studying the effects of phytosterol on animal membrane is challenging. Model membranes can be used but they represent an oversimplified version of the cellular membrane and do not account for the interplay between the sterol, the membrane lipids and the membrane proteins. All those

membranes components coevolved and will differ from one organism to the next. Here we have a unique animal system that can be used to investigate the role of sitosterol in animal membranes. To study the functions of the sitosterol in animals we could modify the sterol balance of *Olavius algarvensis* by inhibiting sitosterol synthesis.

Sterol methyltransferase (SMT) inhibitors were developed as anti-amoeba and anti-fungal drugs (Kidane et al., 2017; Nes, 2000). They inhibit the activity of SMT and consequently the synthesis of sitosterol. Those inhibitors do not interfere with cholesterol synthesis in animals. Their specificity varies from one SMT to the others. Thanks to the successful transformation of *Olavius algarvensis* SMT (Oalg_SMT) *in E. coli*, we could assay Oalg_SMT with different inhibitors and identify the most suitable. We could then observe the effect of sitosterol synthesis inhibition on the worm survival, metabolomics and transcriptomic profile. This would give us a unique insight into the roles of sitosterol in an animal system.

SMT homologues were also identified in the transcriptomes of non-symbiotic annelids. Surprisingly, those annelids had a classic animal sterol composition dominated by cholesterol. Sitosterol was absent or present in minute amount. This suggest that SMT might have a different function in those non-symbiotic annelids. Using the SMT inhibitors on those organisms could give us insight into other potential roles SMT might be playing in animals.

Concluding remarks

Symbiotic partners coevolved a unique language to communicate and interact with each other. The biosynthetic pathway encoded by each partners represent the words of this molecular language. Lipids are an essential part of these inter-kingdom cross-talks. For example, it was recently shown that lipid exchange was essential to the successful colonization of land by the plant (Rich et al., 2021).

Studying lipid in symbiosis comes with its own challenges: most of the compounds from environmental samples are unknown and it is often difficult to trace the origin of the lipid with mass spectrometry alone. However, we are now uniquely equipped to rise to those challenges. Powerful data analysis tools such as public spectral libraries and LC-MS/MS

molecular networking have been developed to help identify and interpret the diversity behind unknown new compounds. Advances in the spatial resolution of metabolite imaging help to interpret and guide those untargeted approaches. Finally, metagenomics and transcriptomic data enable us to contextualize the presence of those new compounds. During my PhD, the study of such unusual metabolites enabled me to identify a new form of the C_1 carrier methanopterin and speculate on potential use of a bacterial enzyme by a eukaryotic host as an adaptation to the symbiotic lifestyle. My study also revealed a new animal sitosterol biosynthetic pathway. This finding raises new questions on the role of sitosterol in animal membrane functioning and suggests that the evolution of sterol synthesis and sterol usage is more complex than suggested by studies on mice and humans. These findings were based on only two groups of compounds and you have seen in Chapter 1 how many unknown compounds are still to be characterized. I for one cannot wait to see the wealth of new pathways, adaptations and interactions hidden behind those unknown compounds.

References

Akman, L., Yamashita, A., Watanabe, H., Oshima, K., Shiba, T., Hattori, M., & Aksoy, S. (2002). Genome sequence of the endocellular obligate symbiont of tsetse flies, Wigglesworthia glossinidia. *Nature Genetics*, *32*(3), 402–407. https://doi.org/10.1038/ng986

Berg, J. M., Tymoczko, J. L., & Stryer, L. (2002). Important Derivatives of Cholesterol Include Bile Salts and Steroid Hormones. *Biochemistry. 5th Edition*. https://www.ncbi.nlm.nih.gov/books/NBK22339/

Blatch, S. A., Meyer, K. W., & Harrison, J. F. (2010). Effects of dietary folic acid level and symbiotic folate production on fitness and development in the fruit fly Drosophila melanogaster. *Fly*, *4*(4), 312–319. https://doi.org/10.4161/fly.4.4.13258

Bloch, K. E. (1983). Sterol structure and membrane function. *CRC Critical Reviews in Biochemistry*, *14*(1), 47–92. https://doi.org/10.3109/10409238309102790

Brantner, C. A., Buchholz, L. A., Remsen, C. C., & Collins, M. L. P. (2000). Isolation of Intracytoplasmic Membrane from the Methanotrophic Bacterium Methylomicrobium album BG8. *Current Microbiology*, *40*(2), 132–134. https://doi.org/10.1007/s002849910026

Brantner, C. A., Remsen, C. C., Owen, H. A., Buchholz, L. A., & Collins, M. (2002). Intracellular localization of the particulate methane monooxygenase and methanol dehydrogenase in Methylomicrobium album BG8. *Archives of Microbiology*, *178*(1), 59–64. https://doi.org/10.1007/s00203-002-0426-2

Clark, A. J., & Bloch, K. (1959). Function of Sterols in Dermestes vulpinus. *Journal of Biological Chemistry*, *234*(10), 2583–2588. https://doi.org/10.1016/S0021-9258(18)69742-X

Collins, M. L. P., Buchholz, L. A., & Remsen, C. C. (1991). Effect of Copper on Methylomonas albus BG8. *Applied and Environmental Microbiology*, *57*(4), 1261–1264.

Davies, S. L., & Whittenbury, R. Y. 1970. (1970). Fine Structure of Methane and Other Hydrocarbon-utilizing Bacteria. *Microbiology*, *61*(2), 227–232. https://doi.org/10.1099/00221287-61-2-227

Edwards, P. A., & Ericsson, J. (1999). Sterols and Isoprenoids: Signaling Molecules Derived from the Cholesterol Biosynthetic Pathway. *Annual Review of Biochemistry*, *68*(1), 157–185. https://doi.org/10.1146/annurev.biochem.68.1.157

Geier, B., Sogin, E. M., Michellod, D., Janda, M., Kompauer, M., Spengler, B., Dubilier, N., & Liebeke, M. (2020). Spatial metabolomics of in situ host–microbe interactions at the micrometre scale. *Nature Microbiology*, *5*(3), 498–510. https://doi.org/10.1038/s41564-019-0664-6

Goffredi, S. K., Tilic, E., Mullin, S. W., Dawson, K. S., Keller, A., Lee, R. W., Wu, F., Levin, L. A., Rouse, G. W., Cordes, E. E., & Orphan, V. J. (2020). Methanotrophic bacterial symbionts fuel dense populations of deep-sea feather duster worms (Sabellida, Annelida) and extend the spatial influence of methane seepage. *Science Advances*, *6*(14), eaay8562. https://doi.org/10.1126/sciadv.aay8562

Hunter, D. J., Torkelson, J. L., Bodnar, J., Mortazavi, B., Laurent, T., Deason, J., Thephavongsa, K., & Zhong, J. (2015). The Rickettsia Endosymbiont of Ixodes pacificus Contains All the Genes of De Novo Folate Biosynthesis. *PLOS ONE*, *10*(12), e0144552. https://doi.org/10.1371/journal.pone.0144552

Ikekawa, N., Morisaki, M., & Fujimoto, Y. (1993). Sterol metabolism in insects: Dealkylation of phytosterol to cholesterol. *Accounts of Chemical Research*, *26*(4), 139–146. https://doi.org/10.1021/ar00028a002

Kawakubo, M., Ito, Y., Okimura, Y., Kobayashi, M., Sakura, K., Kasama, S., Fukuda, M. N., Fukuda, M., Katsuyama, T., & Nakayama, J. (2004). Natural Antibiotic Function of a Human Gastric Mucin Against Helicobacter pylori Infection. *Science*, *305*(5686), 1003–1006. https://doi.org/10.1126/science.1099250

Keltjens, J. T., Caerteling, G. C., & Vogels, G. D. (1986). [63] Methanopterin and tetrahydromethanopterin derivatives: Isolation, synthesis, and identification by high-performance liquid chromatography. In *Methods in Enzymology* (Vol. 122, pp. 412–425). Academic Press. https://doi.org/10.1016/0076-6879(86)22201-6

Kidane, M. E., Vanderloop, B. H., Zhou, W., Thomas, C. D., Ramos, E., Singha, U., Chaudhuri, M., & Nes, W. D. (2017). Sterol methyltransferase a target for anti-amoeba therapy: Towards transition state analog and suicide substrate drug design. *Journal of Lipid Research*, *58*(12), 2310–2323. https://doi.org/10.1194/jlr.M079418

Lee, H., Wang, P., Hoshino, H., Ito, Y., Kobayashi, M., Nakayama, J., Seeberger, P. H., & Fukuda, M. (2008). A1,4GlcNAc-capped mucin-type O-glycan inhibits cholesterol α-glucosyltransferase from Helicobacter pylori and suppresses H. pylori growth. *Glycobiology*, *18*(7), 549–558. https://doi.org/10.1093/glycob/cwn037

Luo, J., Yang, H., & Song, B.-L. (2020). Mechanisms and regulation of cholesterol homeostasis. *Nature Reviews Molecular Cell Biology*, *21*(4), 225–245. https://doi.org/10.1038/s41580-019-0190-7

Luu, W., Sharpe, L. J., Capell-Hattam, I., Gelissen, I. C., & Brown, A. J. (2016). Oxysterols: Old Tale, New Twists. *Annual Review of Pharmacology and Toxicology*, *56*(1), 447–467. https://doi.org/10.1146/annurev-pharmtox-010715-103233

Marriott, H., Mitchell, T., & Dockrell, D. (2008). Pneumolysin: A Double-Edged Sword During the Host-Pathogen Interaction. *Current Molecular Medicine*, *8*, 497–509. https://doi.org/10.2174/156652408785747924

Marx, C. J., Chistoserdova, L., & Lidstrom, M. E. (2003). Formaldehyde-Detoxifying Role of theTetrahydromethanopterin-Linked Pathway in MethylobacteriumextorquensAM1. *Journal of Bacteriology*, *185*(24), 7160–7168. https://doi.org/10.1128/JB.185.23.7160-7168.2003

Nes, W. D. (2000). Sterol methyl transferase: Enzymology and inhibition. *Biochimica Et Biophysica Acta*, *1529*(1–3), 63–88. https://doi.org/10.1016/s1388-1981(00)00138-4

Ponnudurai, R., Kleiner, M., Sayavedra, L., Petersen, J. M., Moche, M., Otto, A., Becher, D., Takeuchi, T., Satoh, N., Dubilier, N., Schweder, T., & Markert, S. (2017). Metabolic and physiological interdependencies in the Bathymodiolus azoricus symbiosis. *The ISME Journal*, *11*(2), 463–477. https://doi.org/10.1038/ismej.2016.124

Prior, S. D., & Dalton, H. (1985). The Effect of Copper Ions on Membrane Content and Methane Monooxygenase Activity in Methanol-grown Cells of Methylococcus capsulatus (Bath). *Microbiology*, *131*(1), 155–163. https://doi.org/10.1099/00221287-131-1-155

Rich, M. K., Vigneron, N., Libourel, C., Keller, J., Xue, L., Hajheidari, M., Radhakrishnan, G. V., Ru, A. L., Diop, S. I., Potente, G., Conti, E., Duijsings, D., Batut, A., Faouder, P. L., Kodama, K., Kyozuka, J., Sallet, E., Bécard, G., Rodriguez-Franco, M., … Delaux, P.-M. (2021). Lipid exchanges drove the evolution of mutualism during plant terrestrialization. *Science*, *372*(6544), 864–868. https://doi.org/10.1126/science.abg0929

Rubin-Blum, M., Antony, C. P., Sayavedra, L., Martínez-Pérez, C., Birgel, D., Peckmann, J., Wu, Y.-C., Cardenas, P., MacDonald, I., Marcon, Y., Sahling, H., Hentschel, U., & Dubilier, N. (2019). Fueled by methane: Deep-sea sponges from asphalt seeps gain their nutrition from methane-oxidizing symbionts. *The ISME Journal*, *13*(5), 1209–1225. https://doi.org/10.1038/s41396-019-0346-7

Rujanavech, C., & Silbert, D. F. (1986). LM cell growth and membrane lipid adaptation to sterol structure. *The Journal of Biological Chemistry*, *261*(16), 7196–7203.

Sayavedra, L. (2016). *Host-symbiont interactions and metabolism of chemosynthetic symbiosis in deep-sea Bathymodiolus mussels* [University of Bremen Bremen]. https://pure.mpg.de/pubman/faces/ViewItemOverviewPage.jsp?itemId=item_2484177

Sezgin, E., Levental, I., Mayor, S., & Eggeling, C. (2017). The mystery of membrane organization: Composition, regulation and roles of lipid rafts. *Nature Reviews Molecular Cell Biology*, *18*(6), 361–374. https://doi.org/10.1038/nrm.2017.16

Shively, J. M. (2006). *Complex Intracellular Structures in Prokaryotes*. Springer Science & Business Media.

Snyder, A. K., & Rio, R. V. M. (2015). "Wigglesworthia morsitans" Folate (Vitamin B9) Biosynthesis Contributes to Tsetse Host Fitness. *Applied and Environmental Microbiology*, *81*(16), 5375–5386. https://doi.org/10.1128/AEM.00553-15

Stanley, S. H., Prior, S. D., Leak, D. J., & Dalton, H. (1983). Copper stress underlies the fundamental change in intracellular location of methane mono-oxygenase in methane-oxidizing organisms: Studies in batch and continuous cultures. *Biotechnology Letters*, *5*(7), 487–492. https://doi.org/10.1007/BF00132233

Stevenson, J., & Brown, A. J. (2009). How essential is cholesterol? *The Biochemical Journal*, *420*(2), e1-4. https://doi.org/10.1042/BJ20090445

Svoboda, J. A., & Feldlaufer, M. F. (1991). Neutral sterol metabolism in insects. *Lipids*, *26*(8), 614–618. https://doi.org/10.1007/BF02536425

Wagner, C. (2001). Biochemical Role of Folate in Cellular Metabolism*. *Clinical Research and Regulatory Affairs*, *18*(3), 161–180. https://doi.org/10.1081/CRP-100108171

Wang, D. Q.-H., & Cohen, D. E. (2009). CHAPTER 3—Absorption and Excretion of Cholesterol and Other Sterols. In C. M. Ballantyne (Ed.), *Clinical Lipidology* (pp. 26–44). W.B. Saunders. https://doi.org/10.1016/B978-141605469-6.50007-X

Whiddon, K. T., Gudneppanavar, R., Hammer, T. J., West, D. A., & Konopka, M. C. (2019). Fluorescence-based analysis of the intracytoplasmic membranes of type I methanotrophs. *Microbial Biotechnology*, *12*(5), 1024–1033. https://doi.org/10.1111/1751-7915.13458

Whittenbury, R., Phillips, K. C., & Wilkinson, J. F. Y. 1970. (1970). Enrichment, Isolation and Some Properties of Methane-utilizing Bacteria. *Microbiology*, *61*(2), 205–218. https://doi.org/10.1099/00221287-61-2-205

Xu, F., Rychnovsky, S. D., Belani, J. D., Hobbs, H. H., Cohen, J. C., & Rawson, R. B. (2005). Dual roles for cholesterol in mammalian cells. *Proceedings of the National Academy of Sciences of the United States of America*, *102*(41), 14551–14556. https://doi.org/10.1073/pnas.0503590102

Acknowledgements

This thesis would not have been possible without the support, love and laughter from my family, friends and colleagues over the past few years.

I would like to start by thanking **Prof. Dr. Nicole Dubilie**r. Thank you for offering me the opportunity to work in your Department, for your support along the way, for giving me the chance to go on field trips and cruises and for reviewing my thesis.

Dr. Manuel Liebeke, thank you for your supervision over the years, for introducing me to the wonderful world of mass spectrometry and for all the interesting discussions, we had along the way.

Many thanks also to **Dr. Elizabeth Hambleton** for sharing my love of sterols, reviewing my thesis and making the time to join the examination committee.

I would also like to thank **Prof. Dr. Marcel Kuypers**, **Prof. Dr. Tilmann Harder** and **Carlotta Lück** for joining the examination committee.

I would like to thank **Christiane Glöckner** and **Anita Tingberg** for making my experience in Germany so easy and for your support during my MarMic time. I would also like to thank **Susanne Krüger, Ulrike Tietjen** and **Martina Patze** for arranging my field trips and business travels.

I would like to thanks every past and present members of the **Symbiosis Department** for always making me feel welcome and supported. Special thanks to my office mates: **Wiebke, Max** and **Jan**. We have not see much of each other in the last year, looking forward to a full office again.

Special thanks for the technicians of the symbiosis department, **Martina, Miriam**, **Wiebke** and **Silke** for your help in the lab throughout my PhD.

I would like to thank the **Metabolic interactions group** for their support, ideas and exciting discussion. I would especially like to thanks **Janine** and **Marvin** who helped me in my battle against our moody HPLC-MS. As well as **Erik, Tora, Kristoffer** and **Alfred** for their support with the GC-MS measurements.

Max, I really enjoyed sharing an office you. It always makes for interesting conversations and one gets to see beautiful pictures passing by, never lose your excitement.

Anna, thanks for the many coffee breaks, the doppelkopf evenings and our Belizean adventures.

Miguel, thanks for bringing us all together with the international lunches. You have a special talent for bringing people together around food.

Benedikt, thank you for being my “academic older brother”, you contagious enthusiasm and your love of small things.

Niko, thank you for being a great climbing partner and sharing my addiction to series, love for gin and passion for the things we cannot change.

Alex, thank you for sharing your knowledge of Olavius with me. I still haven’t found a question you cannot answer.

Yui, thank you for your calm presence, our long coffee break discussions and the smocked beer.

Caro, thank you for being a partner in crime when it comes to studying the strange things *Olavius algarvensis* does.

Brandon, I remember fondly our time at H.-H.-Meier Allee 7. I miss your shenanigans.

I would like to thank **NAYA** for the sundowners, the cookies and an amazing field trip.

I would like to thank **Miriam Weber, Christian Lott** and the **HYDRA-team,** for making the impossible possible during our field trips to Elba. I would like to thank **Kat** the expert worm sorter, it was great to have you on Elba with us! The start of a nice friendship.

I would also like to thank the great people who enjoy bad movies, good barbecues and excellent rum, you lighten up my years in Bremen.

Doritos class, this would have been a very different adventure without you. Special thanks to **Candice, Clara, Greta, Andi** and **Alex**. You made Bremen feel like home. I am pretty sure we haven’t see the end of each other.

Merci, **papa** et **maman**, pour avoir toujours cru en moi et m’avoir donné la confiance de croire que tout est possible. Merci à **Marion** et **Baptiste** pour les mille et un memes, pour être toujours là même lorsque l’on vit dans des pays différents et pour votre soutien. Merci à toi, petit **Jean,** qui a toujours soutenu mon rêve de poissonnerie, et à toutes les tribus Michellod et Fournier.

Cyrille, merci de t’être engagé dans cette aventure en Allemagne du Nord avec moi. Je me réjouis de décider de nos prochaines aventures ensembles.

Contributions to manuscripts and co-authorships

First author manuscripts

Chapter I, „Investigating the lipid profile of deep-sea mussel symbioses“

Manuscript in preparation

Contribution

Conceptual design: 90%

Data acquisition and experiments: 100%

Analysis and interpretation of results: 100%

Preparation of figures and tables: 100%

Writing the manuscript: 95%

Chapter II, “A new form of C_1-carrier discovered in deep-sea methanotrophic symbionts”

Manuscript in preparation

Contribution

Conceptual design: 60%

Data acquisition and experiments: 70%

Analysis and interpretation of results: 90%

Preparation of figures and tables: 90%

Writing the manuscript: 90%

Chapter III, “First animal capable of de novo phytosterol synthesis”

Manuscript in preparation

Contribution

Conceptual design: 80%

Data acquisition and experiments: 80%

Analysis and interpretation of results: 90%

Preparation of figures and tables: 90%

Writing the manuscript: 90%

Coauthorships

Berg, J.S., **Michellod, D.**, Pjevac, P., Martinez-Perez, C., Buckner, C.R., Hach, P.F., Schubert, C.J., Milucka, J. and Kuypers, M.M., 2016. Intensive cryptic microbial iron cycling in the low iron water column of the meromictic Lake Cadagno. *Environmental microbiology*, *18*(12), pp.5288-5302.

Contribution: Isotope labelling experiments, iron measurements and mass spectrometry isotope uptake sample preparation and measurements.

Geier, B., Sogin, E.M., **Michellod, D.**, Janda, M., Kompauer, M., Spengler, B., Dubilier, N. and Liebeke, M., 2020. Spatial metabolomics of in situ host–microbe interactions at the micrometre scale. *Nature microbiology*, *5*(3), pp.498-510.

Contribution: Acquisition and analysis of LC-MS/MS data

Sogin, E.M., **Michellod, D.**, Gruber-Vodicka, H., Bourceau, P., Geier, B., Meier, D.V., Seidel, M., Ahmerkamp, S., Schorn, S., D'Angelo, G. and Procaccini, G., 2021. Sugars dominate the seagrass rhizosphere. *bioRxiv*, p.797522.

Manuscript under revision at *Nature*; preprint available at *bioRviv* https://doi.org/10.1101/797522

Contribution: Contribution to collection, preparation, and analysis of primary samples for dissolved organic matter, metabolomics, and sequencing analyses.

Universität Bremen

Ort, Datum: _____

Bremen, 3. Juni 2021

Versicherung an Eides Statt

Ich, Dolma Michellod
Matrikelnummer: 2987268

versichere an Eides Statt durch meine Unterschrift, dass ich die vorstehende Arbeit selbständig und ohne fremde Hilfe angefertigt und alle Stellen, die ich wörtlich dem Sinne nach aus Veröffentlichungen entnommen habe, als solche kenntlich gemacht habe, mich auch keiner anderen als der angegebenen Literatur oder sonstiger Hilfsmittel bedient habe.
Ich versichere an Eides Statt, dass ich die vorgenannten Angaben nach bestem Wissen und Gewissen gemacht habe und dass die Angaben der Wahrheit entsprechen und ich nichts verschwiegen habe.
Die Strafbarkeit einer falschen eidesstattlichen Versicherung ist mir bekannt, namentlich die Strafandrohung gemäß § 156 StGB bis zu drei Jahren Freiheitsstrafe oder Geldstrafe bei vorsätzlicher Begehung der Tat bzw. gemäß § 161 Abs. 1 StGB bis zu einem Jahr Freiheitsstrafe oder Geldstrafe bei fahrlässiger Begehung.

_____
Bremen, 3. Juni 2021, Dolma Michellod